Universidade de Aveiro Departamento de Biologia
Ano 2018

Fernanda de Oliveira Esteves Rosário

Revelando as vias de cito e genotoxicidade de AgNP em células de pulmão e osso: abordagem *in vitro* e *in vivo*

Unraveling pathways of cyto and genotoxicity of AgNP in lung and bone cells: *in vitro* and *in vivo* approach

Universidade de Aveiro Departamento de Biologia
Ano 2018

Fernanda de Oliveira Esteves Rosário

Revelando as vias de cito e genotoxicidade de AgNP em células de pulmão e osso: abordagem *in vitro* e *in vivo*

Unraveling pathways of cyto and genotoxicity of AgNP in lung cells: *in vitro* and *in vivo* approach

Tese apresentada à Universidade de Aveiro para cumprimento dos requisitos necessários à obtenção do grau de Doutor em Biologia, realizada sob a orientação científica da Doutora Maria da Conceição Santos, Professora Catedrática do Departamento de Biologia da Faculdade de Ciências da Universidade do Porto e co-orientação científica da Doutora Helena Cristina Correia de Oliveira, Investigadora em Pós-doutoramento do Departamento de Biologia e do Centro de Estudos do Ambiente e do Mar da Universidade de Aveiro e do Professor Doutor Peter Herman Maria Hoet, professor catedrático na Faculdade de Medicina da Universidade Católica de Leuven (KU Leuven) e investigador no Laboratory of Pneumology - Research Unit of Lung Toxicology no Department of Public Health and Primary Care Centre for Environment and Health.

Apoio financeiro da Fundação para a Ciência e Tecnologia (FCT) – bolsa de investigação FCT SFRH/BD/91270/2012. Este trabalho foi ainda financiado pelo Fundo Europeu de Desenvolvimento Regional (FEDER) e Programa Operacional Fatores de Competitividade (COMPETE) (PTDC/AAC-AMB/113649) e CESAM (FCT UID/AMB/50017/2013).

FCT Fundação para a Ciência e a Tecnologia
MINISTÉRIO DA CIÊNCIA, TECNOLOGIA E ENSINO SUPERIOR Portugal

COMPETE

“A wizard is never late. Nor is he early. He arrives precisely when he means to!” Gandalf

o júri

presidente

Prof. Doutor Nelson Fernando Pacheco da Rocha
Professor Catedrático, Universidade de Aveiro

Doutor Carlos Manuel Marques Palmeira
Professor Catedrático, Universidade de Coimbra

Doutora Isabel O' Neill de Mascarenhas Gaivão
Professora Auxiliar, Universidade de Trás-Os-Montes e Alto Douro

Doutora Verónica Isabel Correia Bastos
Investigadora, Universidade do Porto

Doutora Iola Melissa Fernandes Duarte
Equiparada a Investigadora Principal, Universidade de Aveiro

Orientadora

Doutora Helena Cristina Correia de Oliveira
Investigadora em Pós-Doutoramento, Universidade de Aveiro (Coorientadora)

agradecimentos

Não tenho o dom da palavra, mas gostaria de agradecer, em primeiro lugar, às minhas orientadoras. À Professora Doutora Conceição Santos ser capaz de me fazer querer ir mais longe e acreditar que tudo é possível. E à Doutora Helena Oliveira agradeço por todo este caminho percorrido. Todo o apoio, todo o trabalho em me manter com os pés assentes no chão quando queria voar mais alto do que seria realmente possível, por todo o carinho e por toda a dedicação.

To Dr. Peter Hoet for receiving me so well in your group. I've never felt so welcome, guided and inspired by someone. Despite, the few months that I was in Leuven I'll always be grateful for your orientation and kind words when I doubted myself.

Às minha eternas amigas Filipa Domingues e Daniela Ramos, por gostarem de mim como eu sou. Por todos os anos de amizade e noite incríveis.

Às minhas fiéis companheiras de laboratório, Jenny Costa, Catarina Remédios, Bárbara Correia, Cláudia Jesus, Joana Amaral, Diana Sousa, pelo apoio, gargalhadas, amizade e cervejas nestes 4 anos de trabalho. Amizade que irá permanecer.

Às minhas recentes companheiras de laboratório, Catarina Menezes, Ana Costa, Joana Santos e Inês Macário. O pouco tempo que foi, numa altura quase final, foi repleto de gargalhas, cafés e partilhas de frustrações. Obrigada pelo carinho meninas.

To my dearest Lab fellows in the Laboratory of Pneumology, Sofie Van Den Broucke and Hanne Vriens. Your help, suggestions and great Ice cream were very important to me.

To my beloved friend Satyajeet Bhonsale! You were more than a friend, you were like a brother to me. You made my stay in Leuven a pleasant journey. Thank you for being by my side all along.

Aos meus pais, por me fazerem acreditar que tenho superpoderes e que tudo o que quero, posso alcançar! Por cuidarem sempre de mim com um amor incondicional. Acima de tudo, por fazerem da minha vida uma alegria na qual vou querer sempre estar.

To my person, a minha irmã Natasha. Por toda felicidade que é partilhar a vida contigo, por todo o amor, por acreditares em mim e por seres uma fonte de inspiração. Para além disso, obrigado por seres especialmente picuinhas com a formatação da minha tese.

Ao meu amado namorado Nuno. Obrigada por teres partilhado estes anos comigo e por te arriscares a partilhar muito mais. Obrigada também, por me mostrares o que é o amor.

Por último e não menos importante, agradeço a mim! Por não desistir quando senti que o queria fazer. Por ser corajosa e acreditar que o futuro vai ser incrível.

palavras-chave

AgNPs, A549, MG-63, citotoxicidade, genotoxicidade, instilação, distribuição, excreção, *in vivo, in vitro*, RMN.

resumo

As nanopartículas de prata (AgNPs) têm sido amplamente utilizadas devido às suas propriedades antimicrobianas e anti-inflamatórias. Em virtude das suas propriedades únicas, as AgNPs têm vindo a ser incorporadas numa vasta gama de setores, tais como, na ciência, na medicina, na indústria e em diversos produtos de consumo, presentes no nosso dia-a-dia. Esta ubiquidade conduz à possibilidade de exposição através de várias vias, sobretudo, pela via inalatória, oral e dérmica. Embora existam diversos estudos que reportam os efeitos das AgNPs, ainda não é claro se a sua toxicidade é intrínseca ou originada pela libertação de iões de prata. Assim, neste estudo são propostas duas hipóteses: A) pequenas diferenças no tamanho das AgNPs são suficientes para induzir diferentes perfis de toxicidade em células de pulmão (linha celular A549) e osso (linha celular MG-63) *in vitro*; B) a toxicidade, distribuição e excreção das AgNPs é condicionada pelo tamanho, após-instilação *in vivo* em ratinhos. Nos estudos *in vitro*, as linhas celulares foram expostas a AgNPs com 10nm (AgNP10) e 20nm (AgNP20) (até 100 µg/mL), bem como à prata iónica (na forma de $AgNO_3$). Após exposição foram estudados diferentes parâmetros, tais como, a internalização das AgNPs pelas linhas celulares, a viabilidade celular e proliferação, alterações na dinâmica do ciclo celular, indução de micronúcleos e a morte celular por apoptose e/ou necrose. Além disso, estudou-se a contribuição da prata iónica na toxicidade das AgNPs nas células. Os resultados da linha celular A549 mostraram que as AgNP20 reduziram a actividade metabólica para doses <5 µg/mL, enquanto que as AgNP10 induziram toxicidade metabólica a doses > 50 µg/mL. Também para doses > 50 µg/mL, AgNP10 induziu dano severo no DNA (cometa classe 3-4), paragem do ciclo celular em G_2 e indução de apoptose tardia. AgNP20 induziu paragem na fase S e aumentou a % sub-G_1 após 24h de exposição, efeito que se manteve após 48h de exposição. Este tamanho induziu também apoptose tardia/necrose nas células A549. Os resultados de MG-63 mostraram que as AgNP20 induziram a paragem do ciclo celular em G_0/G_1 e diminuição da proliferação celular, enquanto que as AgNP10 induziram um dano severo no DNA, levando a morte por necrose.

Combinando os resultados de A549 e MG-63, concluíu-se que a linha celular A549 é mais sensível às AgNPs e que a toxicidade foi dependente do tamanho e da concentração utilizadas. Concluiu-se, ainda que, uma pequena diferença no tamanho de AgNPs foi suficiente para induzir diferentes respostas em ambas as linhas celulares, mas não foi suficiente para influenciar a taxa de internalização. O $AgNO_3$ induziu maior toxicidade do que as AgNPs em curtas exposições (48h), contudo, a longo prazo, observou-se que, as AgNPs se tornaram mais tóxicas, inibindo completamente o crescimento de ambas linhas celulares.

Nos estudos *in vivo*, avaliou-se a toxicidade, distribuição e excreção de prata de dois tamanhos diferentes de AgNPs (5 e 50nm) e prata iónica ($AgNO_3$) em ratinhos. Foram realizados dois ensaios:

resumo (cont.)

A) exposição aguda - após 1 ou 2 instilações intratraqueais (IT) e recuperação durante 7 dias; B) exposição crónica - após repetidas ITs, administradas uma vez por semana durante 5 semanas. Neste ensaio, os animais recuperaram por 1, 2, 7, 14, 21 ou 28 dias após a última instilação (dpi). No final de ambos os estudos, foram recolhidas amostras de sangue para hematologia, e respetivos órgãos (cérebro, pulmão, fígado, coração, baço e rim), assim como, urina e fezes para avaliação da concentração de prata por ICP-MS. Tecidos de pulmão e fígado foram recolhidos para análises de GSH/GSSG. No estudo agudo, tecidos de pulmão foram ainda recolhidos para avaliar os efeitos no perfil metabólico por RMN e no estudo crónico, os dados recolhidos foram utilizados para construir um modelo farmacocinético baseado na fisiologia (PBPK).

Em geral, no estudo agudo, os efeitos das AgNP instiladas mostraram ser dependentes do tamanho e do número de instilações. Sendo que as AgNP5 induziram um efeito inflamatório semelhante a $AgNO_3$, enquanto que as AgNP50 mostraram ter maior influência no sistema imunitário inato.

Quanto aos resultados da biodistribuição, a maior concentração de prata foi obtida nos pulmões, seguida de sangue, baço, rins e fígado. Mais especificamente, a AgNP5 mostrou uma distribuição mais rápida, mas também uma maior taxa de acumulação. Enquanto que as AgNP50 permaneceram maioritariamente no sangue com apenas uma pequena percentagem de prata distribuída para os órgãos, apesar disso, a quantidade de prata distribuída para os órgãos, apresentou uma alta taxa de excreção.

Após 2 IT de AgNPs ou $AgNO_3$, o estado redox do pulmão sugere uma resposta a stress oxidativo, correlacionada com o aumento de prata no pulmão. A GSH no fígado aumentou após 1 IT de AgNP50 e $AgNO_3$, podendo estar relacionado à excreção biliar de prata como complexo Ag-GSH. O perfil metabólico dos tecidos pulmonares revelou uma série de alterações induzidas por Ag em metabolitos envolvidos em diferentes vias, como, glicólise, metabolismo do ciclo de Krebs, metabolismo de fosfolípidos e defesa antioxidante. Notavelmente, a maioria das alterações metabólicas observadas após 1 TI foram recuperadas ou alteradas nos animais submetidos a 2 IT, sugerindo mecanismos de adaptação para lidar com o insulto inicial e recuperar a homeostase. Adicionalmente, a exposição a $AgNO_3$ não mostrou alterações significativas após 2 IT.

Para o estudo crónico, os resultados da hematologia mostraram que as AgNP5 induziram uma toxicidade mais severa e por um maior período de tempo, comparado com AgNP50 e $AgNO_3$. Em geral, após exposição crónica, o estado redox do pulmão e fígado mostrou indução de stress oxidativo que poderá estar relacionado com a exposição a prata. Os níveis de prata diminuíram ao longo do tempo nos órgãos dos animais tratados com AgNP50 e $AgNO_3$, enquanto que nos ratinhos expostos a AgNP5, os níveis de prata apresentaram-se mais altos a 28 dpi, no pulmão, baço, rim, fígado e sangue. A principal via de excreção pareceu ser através da urina, especialmente para AgNP50 e $AgNO_3$. Uma alta concentração de AgNP5 também foi verificada nas fezes. O modelo PBPK não se mostrou eficiente na previsão da distribuição de AgNPs com tamanho entre 5-50 nm. Para os 7 tecidos avaliados, os resultados do PBPK foram concordantes com os dados *in vivo* apenas para o coração e fígado.

Em geral, este estudo sugere que pequenas diferenças no tamanho entre AgNPs são suficientes para induzir diferentes efeitos em linhas celulares humanas. Contudo, ao comparar diferenças de tamanhos maiores, para além do tamanho, o número de exposições parece desempenhar um papel nos efeitos, distribuição e eliminação das AgNPs.

Keywords

AgNPs, A549, MG-63, cytotoxicity, genotoxicity, instillation, distribution, excretion, *in vivo, in vitro*, NMR.

abstract

Silver nanoparticles (AgNPs) have been extensively used due to their antimicrobial and anti-inflammatory properties. The unique properties have been exploited in a wide range of fields, such as, medical, scientific, industrial, and in consumer products allowing the exposure through various routes including inhalation, ingestion and dermal. Although, there are many studies reporting the effects of AgNPs, is still not clear whether their toxicity is attributed to AgNPs intrinsic toxicity and/or from the released ions. Therefore, this study was sub-divided in two main hypotheses: A) small differences on AgNPs size enough to induce different toxicity profiles in lung (cell line A549) and bone cells (cell line MG-63) grown *in vitro*; B) the toxicity, distribution and excretion kinetics AgNPs upon instilled mice *in vivo* is size dependent. Therefore, in the *in vitro* studies, A549 and MG-63 cell lines were exposed to AgNPs with 10 nm (AgNP10) and 20 nm (AgNP20) (up to 100µg/mL), as well as ionic silver (as $AgNO_3$). The effects on cell viability, proliferation, induced apoptosis, DNA damage and cell cycle dynamics were assessed. Also, the contribution of ionic silver (due to AgNP dissociation) on the toxicity of AgNPs was determined.

Results for A549 cell line showed that for concentrations <5µg/mL, AgNP20 induced higher mortality, while AgNP10 showed higher toxicity at doses >50µg/mL. Also, for doses >50µg/mL, AgNP10 induced severe DNA damage (comet class 3-4), cell cycle arrest at G_2 and induction of late-apoptosis. AgNP20 induced arrest at S phase and increase in the % sub-G_1, that was not recovered after 48h. AgNP20 also induced late-apoptosis/necrosis. MG-63 results showed that AgNP20 induced cell cycle arrest at G_0/G_1 and decrease in cell proliferation, while AgNP10 induced severe DNA damage which lead to death by necrosis. Finally, combining both A549 and MG-63 results, we concluded that A549 are more sensitive to AgNPs and the toxicity was highly dependent on size and concentration. Additionally, a small difference in AgNP size is enough to induce a size-dependent toxicity in both cell lines, but it was not enough to influence the uptake rate by both cell lines. $AgNO_3$ in short exposure (48h) is more toxic compared to AgNPs, however, for longer exposures AgNPs shown higher toxicity completely inhibiting cell growth. Silver toxicity, distribution and excretion of two different sizes of AgNPs (5 and 50nm) and ionic silver ($AgNO_3$) were assessed *in vivo* in mice.

abstract (cont.)

Two experiments were performed: A) acute exposure - endpoint evaluation after 1 or 2 intratracheal instillation (IT) and recovery for 7 days; B) chronic exposure - endpoint evaluation after repeated ITs, once a week for 5 weeks. Mice were allowed to recover for 1, 2, 7, 14, 21 or 28 days after the last instillation (dpi). At the end of both studies, blood samples were collected for hematology, and the organs (brain, lung, liver, heart, spleen and kidney), urine and feces were collected to evaluate the silver concentration by ICP-MS. Lung and liver tissues were collected to GSH analysis. For the acute study only, lung tissues were collected to study the effects on the metabolic profile by NMR and for the chronic study, data was gathered to build a Physiologically based pharmacokinetic (PBPK) model. Overall, for the acute study the effects of the instilled AgNPs were dependent on size and number of instillations. The AgNP5 shared a similar inflammatory effect with $AgNO_3$, while AgNP50, seemed to have higher influence on the innate immune system.
Regarding the biodistribution results, the highest concentration of silver obtained was in the lungs, followed by blood, spleen, kidneys and liver. AgNP5 showed a faster and higher distribution to all organs but with a high rate of accumulation. The AgNP50 remained mostly in the blood with only a small fraction of silver detected in the organs, although, the small concentration of silver distributed to the organs, presented a high rate of excretion. After 2 IT of AgNPs or $AgNO_3$, the redox state of the lungs suggested an oxidative stress response correlated to higher amounts of silver. In the liver, there was an increase in GSH for AgNP50 or $AgNO_3$, which could be related to biliary excretion of silver as Ag-GSH complex. NMR profiling of lung tissues revealed several Ag-induced alterations in metabolites involved in different pathways, such as glycolysis and TCA cycle amino acid metabolism, phospholipid metabolism and antioxidant defense. Notably, most of the metabolic changes observed after 1 IT were reversed in animals subjected to 2 IT of AgNPs, suggesting adaptation mechanisms to recover homeostasis. Additionally, $AgNO_3$ showed no significant alterations after 2 IT.
For the chronic study, hematology results showed that AgNP5 induced major and longer lasting toxicity compared to AgNP50 and $AgNO_3$. The redox state of both lung and liver, overall, showed an oxidative stress response which could be related to the silver exposure. The major route for excretion seems to be through the urine, especially for AgNP50 and $AgNO_3$. Also, a high concentration of AgNP5 was also found in feces. The PBPK model was not successful predicting the real distribution of particles from 5 – 50nm. From the 7 specific tissues, the modelled data for the heart and liver were in line with the *in vivo* data.
Overall, this study suggests that even small differences on AgNPs size are enough to induce different outcomes and effects in human cell lines. Additionally, when comparing bigger sizes differences, along with the size, the number of exposures seems to play a role in the AgNPs effects, distribution and elimination from the body.

Most results presented in this thesis are part (integrated the main work) of the following papers:

- Rosário F., Hoet P., Santos C., Oliveira H, (2016). Death and cell cycle progression are differently conditioned by the AgNP size in osteoblast-like cells. Toxicology. 368, 103-115. doi: 10.1016/j.tox.2016.08.020

- Rosário F., Hoet P., Nogueira AJA., Santos C., Oliveira H, (2018). Differential pulmonary *in vitro* toxicity of two small-sized polyvinylpyrrolidone-coated silver nanoparticles. Journal of Toxicology and Environmental Health, Part A. https://doi.org/10.1080/15287394.2018.1468837

- Rosário F., Creylman J., Verheyen G., Van Miert S., Santos C., Hoet P., Oliveira H, (2018). Impact of particle size on toxicity, tissue distribution and excretion kinetics of chronic intratracheal instilled silver nanoparticles in mice

- Rosário F., Duarte I., Santos C., Hoet P., Oliveira H, (2018). Biodistribution and pulmonary metabolic effects of silver nanoparticles in mice following acute intratracheal instillations

Index

List of abbreviations and symbols

3R’s – Replacement, Reduction and Refinement

ADME – Absorption, distribution, metabolism and excretion

AgNP10 – 10 nm silver nanoparticles

AgNP20 – 20 nm silver nanoparticles

AgNP5 – 5 nm silver nanoparticles

AgNP50 – 50nm silver nanoparticles

AgNPs – Silver nanoparticles

APS – 3-(aminopropyl) trimethoxysilane

BBB – Blood-brain barrier

Bw – Body weight

CBMN – Cytochalasin B-blocked micronucleus

CCVs – Clathrin coated vesicles

CME – Clathrin-mediated endocytosis

CvME – Caveolin-mediated endocytosis

DLS – Dynamic light scattering

DMSO – Dimethyl sulfoxide

Dpi – Post the last instillation

ENPs – Engineered nanoparticles

ES – Effect size

FBS – Fetal bovine serum

GI – Gastrointestinal tract

GSH – Reduced glutathione

GSSG – Oxidized glutathione

HGB – Hemoglobin concentration

IC50 – 50% inhibition concentration

IT – Intratracheal instillation

LOAEC – Low observable adverse effect concentration

MCV – Mean corpuscular volume

MN – Micronuclei

MPS – Mononuclear phagocyte systems

NDCI – Nuclear division cytotoxicity index

NIOSH – National Institute of Occupational Safety and Health NIOSH

NMR – Nuclear Magnetic Resonance

NMs – Nanomaterials

NPBs – Presence of nucleoplasmic bridges

NPs – Nanoparticles

OSHA – Occupational Safety and Health Administration

PBPK – Physiologically based pharmacokinetic model

PCA – Principal Component Analysis

PE – Plating efficiency

PEG – Polyethylene glycol

PLT – Platelet

PQN – Probabilistic quotient normalization

PVP – Poly(vinylpyrrolidone)

RBC – Red blood cells

ROS – Reactive oxygen species

SD – Standard deviations

SEM – Scanning electron microscopy

SF – Surviving factor

SOD – Superoxide dismutase

SS – Side-scatter signal

TEM – Transmission electron microscopy

VEGF – Vascular endothelial growth factor

WBC – White blood cells

Chapter I: Introduction

Part of this chapter was already published as:

Remédios, C., Rosário, F., Bastos, V., 2012. Environmental Nanoparticles Interactions with Plants: Morphological, Physiological, and Genotoxic Aspects. J. Bot. 2012, 1–8. doi:10.1155/2012/751686

1. Historical overview

The first mention of the term nanotechnology was in 1959 in a lecture by Richard Feynman, a professor of Californian Institute of Technology. The lecture was called “There’s plenty room at the *bottom*” and for the first time it was considered the use of atoms as building particles to create nanosized products.

Later, in 1974 the actual word "Nanotechnology" was used and introduced to the scientific world. Taniguchi (1974) used the word to describe the creation of nano-sized mechanisms, reporting "Nano-technology mainly consists of the processing of separation, consolidation, and deformation of materials by one atom or by one molecule".

In 1986, the ideas of Feynman were developed by Drexler in his book “Vehicles of creation: the arrival of the nanotechnology era”. Since then there was an increase in important discoveries, inventions, organizations, researches and publications which created an essential impact on the development of nanotechnology.

From 1996-1998, the first survey newsletter on the development and achievements of nanotechnology development was published by the committee of the American Center for Global Technology Assessment. Consequently, in 1999 the session of the interbranch group on nanoscience, nanoengineering and nanotechnology (IWHG), set up a group of conclusions and recommendation which lead to the approval of the National Nanotechnological Initiative of the USA (NNI), by the Presidential council on Science and Technology. The NNI was approved in 2001 with the purpose of "prioritizing nanotechnology development, which should become a basis for the economy and national security of the USA in the first half of the 21st century".

The creation of NNI was a massive mark in the nanotechnology development. Remarkably, after this, the US President Clinton assign 500 million dollars for the state of nanotechnology initiative. President Clinton quote "... to diagnose cancer in a few affected cells and to achieve other amazing results. The initiative being offered is for at least twenty years and promises to lead to important practical results"(Tolochko, 2009). Another leader of nanotechnological development is Japan. In 2000, the Japanese Economic Association organized a special department on nanotechnology and in 2001 it was created a Framework Plan to organize effective cooperation between industrial, state and scientific department and organizations in

the research field. By the beginning of XX century, increasing attention is given to nanotechnology development, within the frame work of national programs in western Europe countries, China, South Korea and CIS (Commonwealth of Independent States). Nowadays, nanotechnology is a revolutionary science, with predicted evolution within the next decades that may have equivalence with the ones observed for other industries, as the one of computers during the second half of the last century or earlier with the automobile industry. This nanoparticles industry will keep on contributing to diverse products and services, and to serve multiple consumers' purposes (Fig.1).

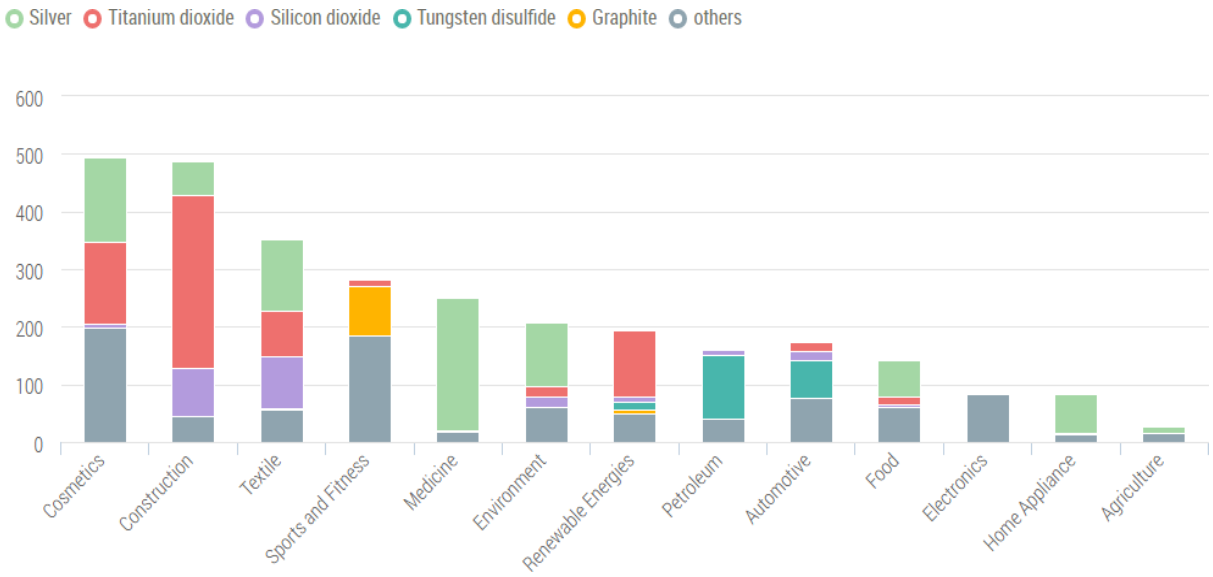

Figure 1 – Representation of the nanomaterials used in Products by industrial divisions. Data gathered until 2015. Adapted from http://statnano.com/.

2. Nanoparticle Classification

The unit nanometer derived from the Greek "nano" which means "dwarf", since nanometers are referred to particles smaller than 100 nm or 1 µm (Buzea et al., 2007). The European Union adopted a definition of nanomaterial in 2011 recommended by the European Commission, which according to it a nanomaterial is "*A natural, incidental or manufactured material containing particles, in an unbound state or as an aggregate or as an agglomerate and where, for 50 % or more of the particles in the number size distribution, one or more external*

dimensions is in the size range 1 nm - 100 nm" (Fig.2).

However, NPs are considered the building blocks of nanotechnology (Stern and McNeil, 2008), with at least in one of three measurements by nanometer scale concerning both the sample of a material, which provides a high surface/volume ratio, leading to high reactivity (Farré et al., 2011). These factors act together and can change or enhance properties of NPs, such as strength, electrical properties, and optical characteristics (Farré et al., 2011). Moreover, their small size and large surface area can determine the harmful potential of NPs (Donaldson et al., 2004).

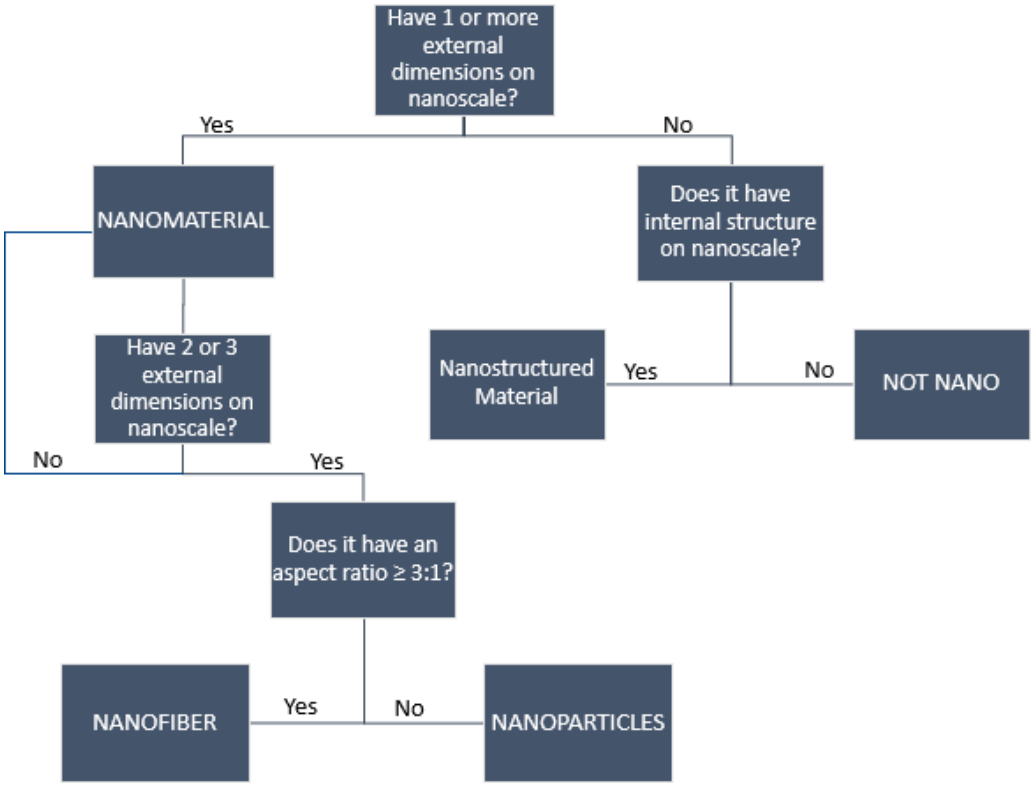

Figure 2 – Nanotechnology terms chart. Adapted from Quantum dot tetrapod: Mike Wong, Rice University; Nanofiber: DOI: 10.1002/adma.200803174.

There is a lot of controversy around the NPs classification. NPs can be classified according to generic trait bases, structure, production and release source, and for last, according to its composition. According to their source's classification, NPs can derive from natural and anthropogenic sources (engineered and unwanted or incidental) (Biswas and Wu, 2005; Nowack and Bucheli, 2007; Tervonen et al., 2009).

- **Natural** processes that produce NPs are derived from natural phenomena rather than a factory or research lab: Among the most abundant natural nanoparticles are soil colloids, volcanic eruptions, forest fires, simple erosion, sand storms, and by plants and animals (shedding of skin and hair) (Buzea et al., 2007).
- **Unwanted or incidental NPs** from: by-products of simple combustion, food cooking, and chemical manufacturing; welding or refining and smelting; combustion in vehicle and airplane engines; combustion of treated pulverized sewage sludge; and combustion of coal and fuel oil for (power generation).
- **Engineered NPs** intentionally designed to be in the nanoscale (studied or used commercially because of their novel properties): classified as carbon NPs, metal oxide NPs, zero-valence metal NPs, Quantum dots (QDs) and Dendrimers (Farré et al., 2011);

ENPs can be classified regarding their dimensionality, morphology, composition, uniformity, and agglomeration (Buzea et al., 2007), since "*they can be spherical, tubular, irregularly shaped and can also exist in fused, aggregated or agglomerated forms*" (Nowack and Bucheli, 2007). Dimensionality refers to their shape or morphology which can classifythem on their number of dimensions, such as one-dimensional (1D), two-dimensional (2D) and three-dimensional (3D) NPs.

The characteristics to be taken relatively to NPs morphology are flatness, sphericity and aspect ratio. NPs can be composed of single material or several materials; in nature composites of various agglomerated materials are found, although single-composites can be easily synthesized today. In respect to uniformity and agglomeration, NPs can exist as dispersed aerosols, suspensions/colloids, or in agglomerate state, due to their different chemistry and electromagnetic properties.

According to their composition, ENPs can be general divide in the following classes:

1) Carbon-based materials (e.g., C60 fullerene, single-walled carbon nanotubes (SWCNT) and multiwalled carbon nanotubes (MWCNT);
2) Metal-based NPs (e.g., Metal, metal oxide and binary oxide NPs)
3) Dendrimers (Nanosized polymers consisting of branched units);
4) Quantum dots (e.g., CdSe, CdTe, ZnSe, ZnS);
5) Nanocomposites (e.g., Ceramic matrix, Metal matrix, Polymer matrix and Integrated Nanocomposite Particles)

Carbon based: The first carbon-based NPs produced was the fullerene (60C hollow sphere). C60 was synthesized in 1985 at Rice University (Kroto et al., 1985; Matorin et al., 2010). After that, a fullerene derivative MWCNT was synthesized under defined conditions and finally, the SWCNT, offering excellent thermal and electrical conductivity as well as tensile strength, which is 460 times that of steel (Matorin et al., 2010; Nitin et al., 2002). Carbon nanotubes are made from rolled up sheets of graphene and are classified as SWCNTs or MWCNTs depending on the constituent numbers of graphene layers. Due to characteristics like tensile strength and thermal conductivity, are applied in automotive industries and aircrafts, in battery, electronics, electrodes, sensors, adhesives, water purification systems (Kausar et al., 2017; Kingston et al., 2014; Nitin et al., 2002; Sathyanarayana and Hübner, 2013).

Metal based: These nanoparticles can be divided in zero-valent metal NPs, ionic metal NPs and metal oxides NPs. Zero-valent and ionic metal NPs can be synthesized chemically as well as biologically through the reduction of metal salts by a reducing agent (Klaine et al., 2008). AgNPs can be used in wound dressings to prevent bacterial infections and zero-valent iron NPs are applied in soil, water and sediments remediation (Fabrega et al., 2011; Fong and Wood, 2006). Metal oxides NPs like TiO_2, ZnO, Bi_2O_3, CeO_2 or CrO_2 can be synthesized by top- down approach through several physical, chemical and biological methods. Titanium dioxide (TiO_2), zinc oxide (ZnO) have applications in paint industry, in solar cells, sunscreens and cosmetics, due to their unique property to block ultra-violet radiations (Smijs and Pavel, 2011).

Dendrimers: Dendrimers are multifunctional nanosized polymers built from branched units, with controlled size, flexibility, topology and molecular weight. These features will allow their use in different field like biology, catalysis, surface modifications. Due to their modifications, dendrimers can be used as colored glasses, chemical sensors and in biological fields like DNA transfecting agents, hydrogels, DNA chips and as therapeutic agents for prion diseases, drug delivery (Klaine et al., 2008; Phogat et al., 2016).

Quantum dot: Used for being a semiconductor nanostructure made of any semiconductor material, such as, silicon, cadmium selenide, cadmium sulfide, or indium arsenide (Peralta-Videa et al., 2011). This confines to quantum dots the motion of conduction band electrons, valence band holes, or excitons, in all three spatial directions. They range between 2 to 10 nanometers in diameter, which is equivalent to 50 atoms (Alivisatos et al., 2005; Andergassen et al., 2010). QDs have important applications in industrial sector and great biological and biomedical utility like cellular imaging/labeling being an excellent alternative to conventional fluorescent dyes used in imaging (Phogat et al., 2016).

Nanocomposites: These are hybrid materials that incorporate nanosized particles into a matrix of standard material (Okpala, 2013). The effectiveness of the nanoparticles is such that the amount of material added is normally only between 0.5 and 5% by weight. This potentiates improved properties as include mechanical strength, toughness and electrical or thermal conductivity, along with new applications in many fields Nanocomposites are divided in Ceramic Matrix Nanocomposites (e.g., Al_2O_3/TiO_2, Al_2O_3/SiO_2, Al_2O_3/CNT); Metal Matrix Nanocomposites (e.g., Co/Cr, Fe-Cr/ Al_2O_3); Polymer Matrix Nanocomposites (polyester/TiO_2, polymer/CNT) and Integrated Nanocomposite Particles (which combines specific functions of each material, for instance, liposome–polymer nanocomposite) (Okpala, 2013; Phogat et al., 2016).

From their multiple conformation, composition, and nature, NPs present multiple functions and almost infinite applications. Nanotechnology has, therefore, gained a place as an emerging science with a recent rise in interest of NPs, mostly due to our increasing ability to synthesize and manipulate such particles.

3. Nanotoxicology – Introduction, distribution and behavior in the environment Primary geogenic NPs may form as aerosols from, for example, sprays of salts and sulfates mostly from the sea, or as sulfate aerosols from volcanic emissions, or even as forest fires (soot and/or polycyclic aromatic hydrocarbons). Moreover, NPs may be introduced in the environment by anthropic reasons, being introduced, for example, intentionally to remediate groundwater and contaminated soil (Flahaut, 2010; Klaine et al., 2008), or also unintentionally by several sources, as research and clinical settings and solid or liquid waste streams production facilities (Ray et al., 2009). The biggest risk of release of this material may occur during transportation to good manufacturers and by intentional releases for environmental application (Flahaut, 2010; Ray et al., 2009). The toxicity and degradation of these compounds in the environment cannot be accurately assessed yet because it depends on the NPs type, physicochemical properties, and on the environment media and the respective conditions. Also, since these materials half-lives may be months to possibly years, NPs are expected to be accumulated and transformed over time by local conditions, enlarging the possibility to keep increasing the concentrations of anthropic substances in the environment (Flahaut, 2010; Hardman, 2006). Because of the extensive use and massive production, the global market value of nanotechnology was estimated ~ $1.5 trillion U.S.D. by 2015, ENPs are currently considered as an emerging class of environmental contaminants. Recent research advances have (I) improved analytical capabilities for detecting them in different environmental media, (II) increased availability of related toxicity data, and (III) increased public awareness. Nevertheless, there are still many open questions that need to be answered to fully understand their origin, fate, and toxicity. ENPs pose risk to human health and the environment via oral, inhalation, and dermal exposure routes (Biskos and Schmidt-Ott, 2012; Lam et al., 2006; Morimoto et al., 2010). To estimate the environmental and human health risks associated with ENM exposure, information about their size, shape, and the dose-response relation is required (Kuempel et al., 2006; Kumar et al., 2014). The standard United States National Research Council suggested four steps to assess environmental and human health risk of chemicals and metals (EHHRA): (I) hazard identification, (II) exposure assessment, (III) dose-response assessment, and (IV) risk characterization. A few studies have attempted to apply some of these steps for estimating risks of exposure to ENPs. However, very few studies have carried out an exhaustive risk assessment process for ENPs, probably due to the lack of required

information on their fate, exposure, and toxicity. The current knowledge about NPs and the challenges of nanotoxicity assessment lead to a lack of effective regulation of NPs use. Some governmental entities, as EPA, have been conducting efforts to, not only comprehend the properties of NPs and their potential risks for human health and the environment, but also to regulate the use, storage, and disposal of these materials to allow a safe and sustainable nanotechnology development (Fig.3). Although there are no specific environmental laws, NPs cut across some existing EPA regulations. For example, several NPs are considered chemical substances under the Toxic Substances Control Act, and pesticides containing nanotechnology products are regulated under the Federal Insecticide, Fungicide, and Rodenticide Act (see http://www.epa.gov/nanoscience/). Still, a recent report from EPA's Office of Inspector General stated that "…*EPA does not currently have sufficient information or processes to effectively manage the human health and environmental risks of nanomaterials*..." and that "... *EPA has the statutory authority to regulate nanomaterials but currently lacks the environmental and human health exposure and toxicological data to do so effectively*" (U.S. EPA, 2011). According to this report, some proposed policies have failed, and others that await approval are facing significant barriers to their effectiveness (U.S. EPA, 2011).

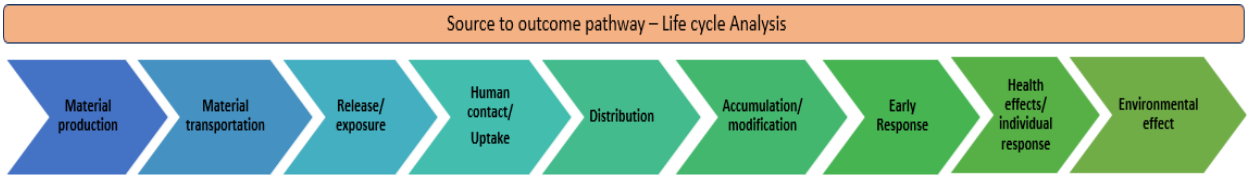

Figure 3 – Illustration of the steps of the life cycle analysis for ENM risk assessment.

3.1. Transport and interactions

Transport and partition of NPs through environment is the most critical parameter to evaluate NPs impact, being expected high mobility of NPs that are designed to be released into the environment (Wang and Zhang, 1997). Transport and, therefore, NPs mobility are determined by forces, such as London-van der Waals and double-layer forces that are responsible for attachment. This phenomenon is called Brownian motion (diffusion). Gravity and fluid motion are also factors that influence transport of NPs (Biswas and Wu, 2005; Handy et al., 2008a,

2008b). NPs are predicted to have high efficiency of transport to collector surfaces due to Brownian diffusion and their potential mobility may be predicted by knowing the exact surface properties of NPs. The surface properties of engineered NPs are of essential importance for their aggregation behavior, and thus for their mobility in aquatic and terrestrial systems and interactions with algae, plants, and fungi (Auffan et al., 2010; Klaine et al., 2008; Navarro et al., 2008).

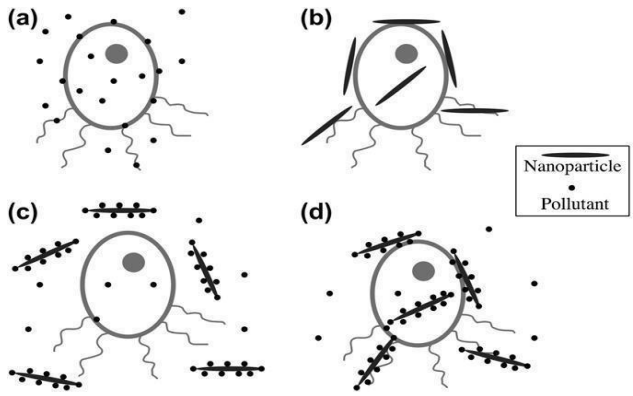

Figure 4 – Scheme of nanoparticles interactions, according to Nowack and Bucheli, (2007). (a) Adsorption and uptake of pollutant, (b) adsorption and uptake of nanoparticle, (c) adsorption (or absorption) of pollutants onto NP and reduction in pollutant uptake by organisms and (d) adsorption of NP with adsorbed (or absorbed) pollutant and possible uptake of pollutant-NP.

NPs can interact with toxic compounds and it can both amplify the toxic effect and have a positive role in the environment, alleviating the toxicity of the compounds. There are two scenarios of possible NP-Pollutant-Cell interactions: NPs may adsorb or absorb the pollutant and decrease the free concentration, resulting in a reduction of pollutant uptake by organisms, and there's also the possibility of NP-pollutant uptake (adsorbed) by the organisms, in which the toxic effect could be caused either by NPs, pollutant or the synergistic way by both together (Nowack and Bucheli, 2007). In Fig.4 are summarized some of the potential interactions of NPs.

4. Silver Nanoparticles

4.1. Silver nanoparticles features and usage

Silver nanoparticles (AgNPs) or nanosilver are one of the promising products in the nanotechnology industry. The most fundamental entity of silver is the Ag cation (Ag^+), which makes it highly reactive. Indeed, Ag ion (~0.1 nm of ionic radius) is persistent, cannot be destroyed and can associate with other ions. In contrast, AgNP is made of metallic silver ions in clusters (size 1-100 nm) and/or of silver compounds engineered into a particle of nanoscale size which is not necessarily persistent, since particles can dissolve or disaggregate (Balogh et al., 2000).

During the last two decades, an extensive number of methods have been reported for the synthesis of AgNPs by several physical, chemical and biological methods from metallic silver and their specific physicochemical properties may differ from those of the bulk substance or from particles of larger size. This advances in their manufacturing techniques attracted the attention of many industries wanting to exploit the unique properties of silver NPs for beneficial use.

Recently, "green" productions of AgNPs have recently been introduced to the industry. Mohan Kumar et al. (2012) reported a rapid biogenic synthesis of AgNPs using *Terminalia chebula*. Also, Philip (2010) reported a rapid and cost-effective production of AgNPs, of various shapes, using the leaf extract of *Hibiscus rosa sinensis.*

AgNPs small size made possible the passage through biological membranes (Oberdörster et al., 2005a). Also, they present a large surface to volume ratio providing unique optical and physical properties that are not present in bulk silver, and which are claimed to have great potential for many industries applications.

The major reason for AgNP disseminated use is its strong antibacterial effect for a wide array of organisms. AgNP is an effective killing agent against a broad spectrum of Gram-positive (*Enterococcus, Listeria, Staphylococcus, and Streptococcus*) and Gram-negative (*Escherichia, Pseudomonas, Salmonella*) bacteria (Wijnhoven et al., 2009; Yin et al., 1999) and, to antibiotic-resistant strains (*Staphylococcus aureus*) (Percival et al., 2007; Wright et al., 1999). Their antimicrobial activity has been shown to be size-dependent and shape-dependent (Morones et

al., 2005; Pal et al., 2007; Panacek et al., 2006). Small nanoparticles with a large surface area to volume ratio provides a more efficient means for antibacterial activity even at very low concentrations (Sanford and Venkatapathy, 2010). While the shape "Truncated triangular" silver nanoplates display the strongest antibacterial activity (Wijnhoven et al., 2009).

Antifungal and antiviral properties are also a valuable advantage of AgNPs. These particles are effective fungicides against a broad spectrum of common fungi, including (*Aspergillus*, *Candida*, and *Saccharomyces*) (Kim et al., 2007; Wright et al., 1999) but their mode of action is still not clear neither well studied regarding their antibacterial mode of action. Also, AgNPs inhibit HIV-1 virus replication in 86%, but this effect is exclusively within the range of 1-10nm (Sun et al., 2005).

Another biological property of AgNPs is the anti-inflammatory effect, which was proven *in vivo*, *in vitro* and in clinic (Ge et al., 2014). Yilma et al. (2013) demonstrated that PVP-coated AgNPs mediated its anti-inflammatory effect in macrophages infected with *C. trachomatis* by regulating various upstream surface receptors and downstream inflammatory pathway genes. In a porcine model with contact-dermatitis, the anti-inflammatory properties of AgNPs showed a return near to normal after 72h, compared to $AgNO_3$ and saline solution (Nadworny et al., 2010). For these particularities, AgNP can be found in personal-grooming kits and cosmetics like, lotions, creams, toothpastes, soaps, female-hygiene products, laundry detergents and cleansers (Luoma, 2008). AgNPs spray mist products are used to sterilize and deodorize surfaces in kitchens and hospitals, bathrooms and baby clothes. Consumer electronics (e.g., cell phone covers), shoe insoles, slippers and shoe liners brooms, food storage containers are also AgNP containing. AgNP is also, widely incorporated in textiles and fabrics such as outerwear, sportswear, underwear, socks, and bedding materials such as comforters, sheets and mattress covers (Luoma, 2008; Tolaymat et al., 2010). Additionally, AgNP can significantly inhibit biofilm and glycoprotein film formations. Therefore, to protect and prevent from infections, these nanoparticles have been receiving much interest in the field of orthopedics, used as coating for implantable devices, (e.g., catheters, joint replacement prostheses) (Furno et al., 2004; Necula, 2013; Sibbald et al., 2001; Wilcox et al., 1998), as coating of surgical instruments (Eby et al., 2009) and as additive compound in bone cement (Joseph et al., 2003). After a device implantation, the surface of an implantable device become coated with patient-derived

glycoproteins from tissue and/or blood plasma, which leads to microorganism's biofilm formation. The use of AgNPs as additives in bone cements or prostheses has reduced the biofilm formation, the infection rates, and the initial mortality (2.7%-18%) rate in joint replacement (Ahlberg et al., 1978).

AgNPs are used as coating in medical devices such as medical tools and materials used in the areas of surgery, anesthesiology, cardiology and urology, pacemakers, catheters, and vascular prostheses (Lansdown, 2007). By using wound dressings containing AgNP, doctors found that not only did silver inhibit the growth of bacteria, the wounds healed more quickly (DiRienzo, 2006). Also, colloidal silver is used in diet supplements by millions of people on daily bases (http://www.silver-colloids.com/Tables/ Experiment.PDF).

While AgNPs are widely used in various medical, food or consumer products and, several toxic effects for AgNPs were reported, no data on concentrations of AgNP in commercially products, amount of release Ag or even the size and form in which it is present, are (or hardly) available. Additionally, the information available about silver containing products is mainly focused on the US market (Wijnhoven et al., 2009). A similar public European database is unavailable.

4.2. Exposure routes

4.2.1. Lung exposure

Due to the lung large surface area, the lung is the major and primary entry for inhaled AgNPs and other nanoparticles. Since their entrance, it could deposit into the entire respiratory tract, first at the nose, pharynx, and finally at the lungs. Particle size can determine AgNPs fate in the human system. Particles of 5 nm can be retained in the lung in a percentage of 90% and then deposit relatively uniformly in the three regions. Particles of 20nm decrease this retained percentage to 80%, which means that 20% of the inhaled particles penetrate the lung but leave it upon exhaling (Oberdörster, 2005).

In the alveolar region, inhaled fine particles (> 100 nm) are readily phagocytized by alveolar macrophages. Consequently, alveolar macrophages play a key role in the fate of such particles.

Three major processes are involved in the elimination of nanoparticles in the alveolar region: chemical dissolution for soluble particles, elimination through the tracheobronchial tree with subsequent ingestion into gastrointestinal tract (GI) and excretion with the feces and physical translocation into lymph nodes. This elimination mechanism will depend on particle size and solubility. By translocation, the low solubility or insoluble particles deposited in the pulmonary tree are eliminated from the respiratory system. The larger particles are normally deposited in the upper sections of the lungs, being eliminated by the tracheobronchial mucous towards the digestive system (Ostiguy et al., 2006). Normally this is an efficient mechanism that eliminates particles, even ultrafine particles, in less than 24hours (Kreyling et al., 2002). At the alveolar level, nanoparticles will be *phagocytosed* by macrophages and subsequently either be removed from the alveolar region or released onto the alveolar surface upon necrosis of the alveolar macrophages. The phagocytosis process may lead to chemotactic activities which trigger the complement system cascade and the inflammatory cell response to the site of AgNPs. According to Oberdorster et al. (2005a) the effect of the inflammatory and the complement cascade may take up to two month 10 days in rat and roughly two years in humans to be cleared. The ineffective nanoparticles removal by macrophages can lead to accumulation, interaction of these particles with the alveolar epithelial cells and distribution from the epithelium to interstitial tissues (Oberdörster, 2005; Oberdörster et al., 2005a).

The two main mechanisms of distribution after lung translocation are: via the bloodstream or along the axons of the sensitive nerves to the central nervous system (Oberdörster, 2005; Oberdörster et al., 2005a). The translocation of inhaled ultrafine particles into the bloodstream could affect the endothelial function and promote thrombosis and other circulatory system problems, including increased blood coagulation (Elder et al., 2000; Elder et al., 2002; Nemmar et al., 2002). Takenaka. (2001) observed AgNPs in lung and blood immediately after mice exposure to 10nm AgNP inhalation by inhalation. Other study on inhalation exposure to different sized AgNPs showed neither significant changes in body weight nor hematological changes, although, AgNPs were found in all investigated organs (liver, kidney and brain) (Ji et al., 2008).

4.2.2. Dermal absorption

The skin is the largest organ of the body and the barrier against external environment. Therefore, the skin can be exposed to AgNPs within the air and sprays, clothing and wound dressings that are already on the market. Dermal penetration by AgNPs it is controversial, since some studies show that nanoparticles are able to penetrate the stratum corneum (strongly keratinized – 10μm), while others claim that nanoparticles enter through hair follicles, sweat glands, broken and flexed skin (Borm et al., 2006; Buzea et al., 2007; Teow et al., 2011; Toll et al., 2004). Findings by Tinkle et al. (2003) and Wright et al. (2012) have shown that AgNPs penetrate only in the superficial layers of the stratum corneum and only NPs less than 1 μm in diameter may penetrate skin mechanically. Also, parameters such as clothing, age, type of skin and dose and size of the AgNPs.

The clinical proven anti-inflammatory property and control of wound infection made AgNPs-based dressings and surgical sutures to have approval for clinical application. Although, their dermal toxicity is still a topic of scientific debate and concern. Despite laboratory and clinical studies confirming the dermal biocompatibility of AgNPs-based dressings (Chen et al., 2006; Muangman et al., 2006; Wright et al., 2012) several other researchers have demonstrated the cytotoxicity of these materials. Dermal application of AgNP-coated dressing in human burns patient show reversible silver toxicity and transient discoloration of skin (argyria-like) (Trop et al., 2006; Vlachou et al., 2007). One week after treatments, a high level of silver was found in urine and plasma (Trop et al., 2006). It remains unclear whether silver ions or AgNPs were transported into the body. However, absorption through intact skin is low (<1 ppm) since much of the free ion is precipitated as Ag sulfide in the superficial layers of the stratum corneum. Oberdorster et al. (2005b) demonstrated penetration of a variety of nanoparticles in the dermis and translocation to the systemic vasculature via lymphatic system and regional lymph. Paddle-Ledinek et al. (2006) exposed cultured keratinocytes to extracts of several types of silver containing dressings. Of these, extracts of nanocrystalline silver coated dressings were most cytotoxic. Similar observations were also reported by Lam et al. (2004). Additionally, inhalation and dermal absorption of AgNPs could lead to the uptake of these particles via nervous system (brain, spinal cord and nerves). Tang et al. (2009; 2010) showed blood brain barrier (BBB) destruction and neuronal degeneration in rats after AgNP exposure.

4.2.3. Gastrointestinal tract

As seen above, at this moment, many food supplements/products and drugs available on the markers, contain AgNPs. Although, GI exposure can also happen either unintentional from hand to mouth transfer or from traditional materials. In addition, inhaled particles cleared by mucociliary escalator, can be ingested into the GI (Buzea et al., 2007; Teow et al., 2011).

Size, surface charge or coating and attachments to ligands, are some of the characteristics that control the site-specific target of different regions of the GI (Hillyer and Albrecht, 2001). Once in GI, AgNPs could undergo chemical changes (e.g., pH). Mwilu et al. (2013) showed changes in AgNPs exposed to human synthetic stomach fluid, which may trigger agglomeration. Agglomeration may lead either to fast transit, followed by excretion by feces and urine or, bigger agglomerates may obstruct the GI and lead to death (Buzea et al., 2007; Teow et al., 2011).

The bioavailability of orally administered AgNP, was investigated in Male SD rats treated by a single oral or intravenous administration. The bioavailability was based on the values of AUC_{oral}/AUC_{iv}, which was 1.2% in the group treated with 1 mg/kg AgNPs and 4.2% in the group treated with 10 mg/kg AgNPs, respectively (Park et al., 2011). Most AgNPs were found in feces after oral administration, and blood levels were low. It was suggested that absorption of AgNP through the GI was poor, which may explain the low toxicity noted for AgNP after oral administration. The transport or absorption mechanisms of AgNP in GI remain unknown and more investigations are needed to understand this aspect.

4.3. Uptake

The uptake of AgNPs, once inside the organism, should be performed with non-agglomerated state and the rate of agglomeration should be studied prior to *in vitro* uptake studies in the correspondent medium, like dynamic light scattering (DLS) (Kettiger et al., 2013). Although, assess the uptake of AgNPs is not that linear, since AgNPs are reactive particles and have the potential to modulate biological interaction between particles, target cells and biological media (Nel et al., 2009). The uptake and intracellular trafficking of AgNPs is mostly determined by NP physicochemical properties, concentration, exposure period and specific transport

mechanisms. The main physicochemical properties of AgNPs affecting NP cellular uptake include NP surface charge and chemistry, shape, size and aggregation state.

Because of AgNP range size, they are able to interact with the cellular machinery in a similar way to macromolecules (Aggarwal et al., 2009; Nel et al., 2009; Salvati et al., 2011). The phospholipid membrane regulates the transport of molecules into the cells, acting as a barrier protecting the intracellular structures. Direct penetration of AgNP has been reported in THP-1 monocytic leukemia cells exposed to 20 nm citrate-coated AgNPs, as observed by TEM (Haase et al., 2011).

Although, apart from the direct penetration there are two main actively entry ways for AgNPs are via endocytic pathways, divided in phagocytosis and pinocytosis, this last one is, divided in macropinocytosis, clathrin-mediated endocytosis (CME), caveolae-mediated endocytosis (CvME) and alternative routes (Lühmann et al., 2008; Mailänder and Landfester, 2009).

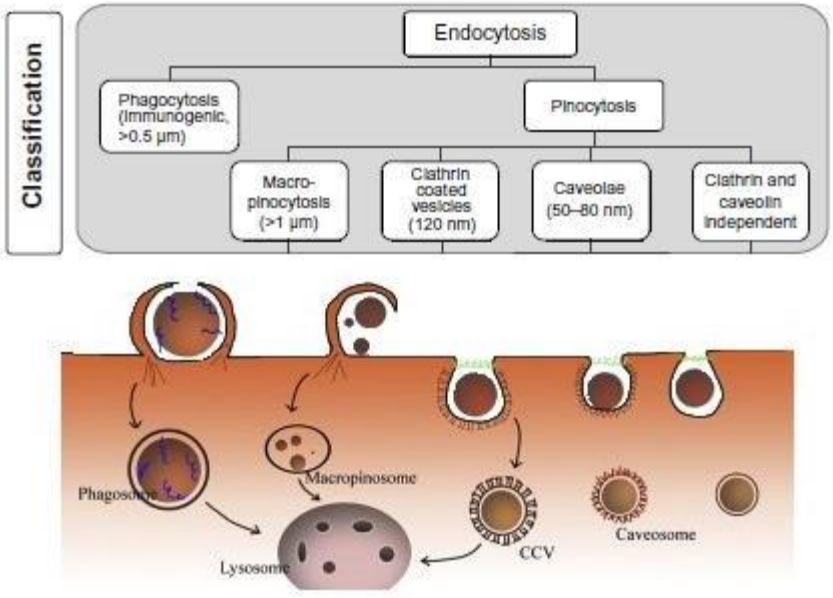

Figure 5 – Nanoparticles internalization pathways in mammalian cells. The picture briefly shows the classification of endocytic trafficking and different mechanisms of endocytosis. Abbreviation is: CCV, clathrin coated vesicle. Adapted from Kettiger et al. (2013) and Kou et al. (2013).

❖ Phagocytosis is performed predominantly by specialized cells of the immune system (i.e., macrophages, monocytes, neutrophils, and dendritic cells), to remove particles larger than 500 nm from the organism, mainly through the mode of a receptor-mediated process (Fig.5)

(Aderem and Underhill, 1999; Hillaireau and Couvreur, 2009; Kittler et al., 2010; Kou et al., 2013). Although, recent reports document the phagocytic uptake of considerably smaller particles (França et al., 2011; Lunov et al., 2011).

In this process particles are recognized by small proteins and promotes the binding of protein-coated particles to internalizing receptors on the cell plasma membrane, depending on the cell line (as scavenger receptor) (Wang et al., 2012). The receptor-ligand interaction triggers a signal cascade in the target cell resulting in action assembly and formation of a cell surface extension that zippers around the particles, engulfing it in an intracellular vesicle, phagosomes (Hillaireau and Couvreur, 2009). Internalized particles are subsequently degraded, and the receptors are cycled back to the cell surface. The rate of these successive events depends greatly on the ingested particle and typically lasts from 30 minutes to several hours (Dobrovolskaia and McNeil, 2007). AgNPs taken up as agglomerate tend to be less easily degraded by the host as they can be detected in macrophages for several months, thus bearing a risk of long-term toxicity (Wang et al., 2011; Zhu et al., 2009).

❖ Pinocytosis is the route for the cells to drink fluid, solutes and suspensions containing small particles ranging from a few nanometers to several hundred nanometers (Kou et al., 2013). This route can be divided in four modes (Conner and Schmid, 2003): (I) Macropinocytosis, (II) Clathrin-mediated endocytosis, (III) Caveolin-mediated endocytosis, or (IV) alternative routes. The capacity of this uptake pathway for AgNPs is very high, suggesting a possibility for pharmaceutical delivery.

I. Macropinocytosis contributes to the internalization of larger AgNPs with a size of >1 μm are taken up nonspecifically and in the specific case of phagocytosis up to 5 μm. (Kettiger et al., 2013). Past studies suggest that in some systems, macropinocytosis is the dominant mechanism of AgNP internalization. This is stimulated by e.g., growth factors that interact with receptor tyrosine kinases activating the signaling cascade results in the formation of actin-driven circular membrane protrusions that collapse onto the membrane and fuse with it engulfing larger particles (Conner and Schmid, 2003; Mercer and Helenius, 2009). Unlike other endocytic processes, macropinocytosis is largely inhibited by the presence of inhibitors of Na^+/H^+ exchange, such as amiloride. Luther et al. (2011), reported in astrocytes exposed to PVP-coated

AgNPs a 30% uptake decrease after incubation with amiloride.

II. Clathrin-mediated endocytosis (CME) is the best characterized route of cellular entry, present in all mammalian cells. By this route particles with a size of 120–150 nm (max. 200nm) are internalized within clathrin-coated vesicles entering the endosomal/lysosomal trafficking route, whereas the transport could either be adsorptive or receptor-mediated (Chithrani et al., 2006; Harush-Frenkel et al., 2008; Rejman et al., 2004). Cationic particles or proteins bind nonspecifically to the negatively charged cell surface triggering the adsorptive CME, while the receptor-mediated process in highly selective and specific (e.g., transferrin, growth factor and insulin) (Hervé et al., 2008; Lesniak et al., 2010; Thomsen et al., 2012). After NPs interact with receptors on the cytomembrane, a cytosolic protein named clathrin-1 polymerizes on the cytosolic side of the plasma where the cargo is internalized (Rappoport, 2008). After wrapping the nanoparticles inside, the vesicle is pinched off through the GTPase activity of dynamin, forming a clathrin coated vesicles (CCVs) (Pucadyil and Schmid, 2009). CCVs move towards inside the cells. Inhibition of clathrin-dependent endocytosis is most commonly achieved by potassium depletion or incubation with chlorpromazine. In human glioblastoma U251 cells exposed to potato starch coated AgNPs, potassium depletion resulted in decreased AgNP uptake, confirming clathrin-dependent endocytosis of the studied AgNPs (AshaRani et al., 2009).

III. Caveolin-mediated endocytosis (CvME) is a common cellular entry pathway (Kou et al., 2013). This is an important uptake route for AgNPs located on the basolateral side of most cells. The caveolae are vesicles with a diameter of 50-80 nm, coated with a protein called caveolin, that invaginated and are cut off from the membrane with the help of dynamin from hydrophobic membrane domains (Kettiger et al., 2013). There are three isoforms of caveolin in mammalian cells. Caveolin-3 is muscle specific, while caveolin-1 and -2 are abundant in most non-muscle cells (such as endothelial cells, fibroblasts and adipocytes) and absent in neurons and leukocytes (Benmerah and Lamaze, 2007). The caveolae vesicles traffic to fuse with caveosomes. The caveosomes containing nanoparticles e move along to the endoplasmic

reticulum, where they can penetrate into the cytosol, and then enter nuclear via the nuclear pore complex (Kasamatsu and Nakanishi, 1998; Khalil et al., 2006; Pelkmans et al., 2002). AgNPs with small size seem to be transported more efficiently up to 40nm, while larger particles (>500nm) appear to be taken up only in exceptional case (Rejman et al., 2004; Wang et al., 2009). Additionally, with this route pathogens and AgNPs can bypass lysosomes avoiding lysosomal degradation (Benmerah and Lamaze, 2007; Medina-Kauwe, 2007).

IV. Recently, several endocytic routes emerged that do not fit into those categories, which are both clathrin and caveolin-independent (Kettiger et al., 2013; Kou et al., 2013). Data suggest that particles large than 100nm are internalized via these routes (Mayor and Pagano, 2007). These routes rely on GTPases, cholesterol and requires specific lipid compositions and depend on specific regulation by proteins such as Arf6-dependent, division control protein Cdc42-dependent and Rhoa-dependent (Howes et al., 2010). This field draws more and more attentions, but unfortunately, it is still far away from deep understanding and need further research.

4.4. Toxicity assessment

4.4.1. *In vitro* studies

The use of AgNPs has increased along the years, and since these NPs are widely used there is few information on the AgNPs interaction with human organs, tissues and cells, regarding the health implications, occupational risks and hazards.

A crossed research in PubMed showed that 12712 AgNPs papers have been published since 1996, from which 1187 are AgNPs *in vitro* studies (Fig.6 - B). *In vitro* studies have shown that silver NPs can induce toxic effects such as, induction of apoptosis, inflammation, DNA-strand breaks, point mutations, oxidative DNA adducts, free radical production and membrane damage (Ahamed et al., 2008; AshaRani et al., 2009; Foldbjerg et al., 2011; Gopinath et al., 2008; Ye et al., 2011).

The primary mechanisms that mediate the AgNP cytotoxicity to the cells are oxidative stress and release of Ag^+, which lead to damaging consequences such as membrane disruption, inflammation, DNA damage and cell death. Released Ag^+ interact with thiol groups of

antioxidants such as reduced glutathione (GSH), superoxide dismutase (SOD) and thioredoxin. Lysosomal rupture which ultimately end up in lysosome-mediated apoptosis were proved by electron spin resonance studies. These studies showed that dissolution of Ag^+ induced hydroxyl and other free radical production in lysosomes (Arora et al., 2012; He et al., 2012; Yang et al., 2012; Zhang et al., 2014).

Once in the mitochondria, AgNPs potentiate mitochondrial membrane collapse, disruption of the respiratory chain with subsequent oxidative stress, inhibition of ATP synthesis and apoptosis or DNA damage (Piao et al., 2011).

AgNP <10nm has been shown to diffuse through nuclear pores into the nucleus of human fibroblasts and glioblastoma cells, instigating ROS production, DNA damage, cell cycle arrest and genotoxicity (AshaRani et al., 2009). Inflammatory and immunological responses are also triggered by AgNPs. Yang et al. (2012) showed that AgNP induced inflammasome formation and IL-1β in human blood monocytes (Almofti et al., 2003; Asharani et al., 2009; Trickler et al., 2010). AgNP can also act as anti-angiogenesis agent by targeting the activation of PI3/Akt signaling pathways and caspase-3 activation or in habiting vascular endothelial growth factor (VEGF) and as anti-cancer agent against leukemia, breast cancer, liver and lung cancer cells (Gurunathan et al., 2013, 2009; H. R. Kim et al., 2011; Kim et al., 2009).

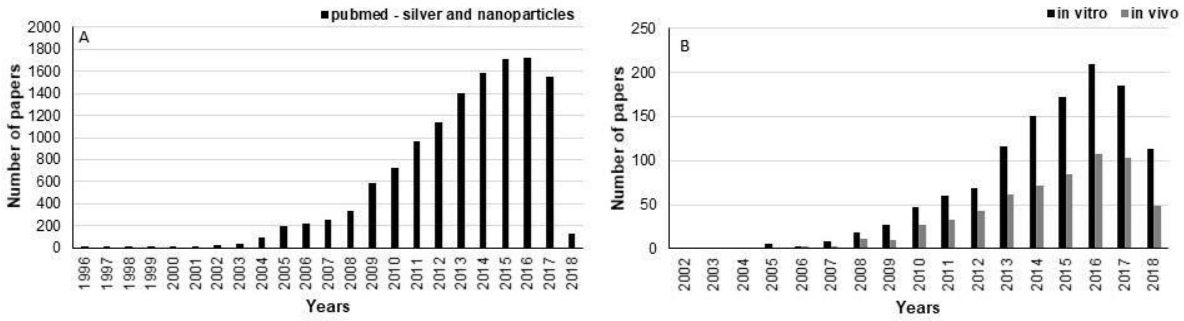

Figure 6 – Number of publications on AgNPs (A); and *in vitro* or *in vivo* AgNPs toxicity assessment (B), over the years. Research obtained by PubMed**.**

4.4.1.1. Physicochemical characteristics and their relevance for *in vitro* toxicity

Due to AgNPs unique properties, their effective toxicity can be complex to assess, as there are several factors, which can interfere (e.g., Size, shape, silver ion dissolution and release,

agglomeration, surface coating). These important physical and chemical properties could be crucial to cytotoxicity determination, since these may lead to an over/underestimation of the real toxicity of AgNPs (Bae et al., 2011; El Badawy et al., 2012; Kittler et al., 2010; Liu and Hurt, 2010; Wijnhoven et al., 2009). Physicochemical characteristics also affect their biodurability, which in turn influence the long-term toxicity, pathogenicity and biological activity of the particles and fiber (Gliga et al., 2014). Therefore, is crucial to toxicity assessment to characterize the physicochemical properties of the AgNPs in order to address properly their effects.

❖ Size

Particle size is the primary and most investigated characteristic of AgNP and most of the studies conclude that the particle size can mediate various biological effects, such as oxidative stress, DNA damage, mitochondrial dysfunction, cellular uptake, and permeabilization across biological barriers. Despite some controversy results, the majority of the studies indicate that the size of the AgNPs has an inverse relation between the induced toxicity. The high surface area to volume ratio, facilitates their interaction with the surrounding media (cells, proteins and/or organelles) as well as the release of Ag^+ ions leading to elevated toxicity and inhibition of metabolic activity in cells. Also, below their postulated critical size (<30nm) AgNPs could present a high surface energy and therefore became less stable, resulting in increased surface reactivity (Auffan et al., 2010; Luyts et al., 2013). Gliga et al. (2014) assessed the toxicity of citrate coated AgNP 10, 40 and 75 nm and PVP-coated AgNP 10nm in lung epithelial BEAS-2B. These authors reported that both PVP and citrated coated 10nm AgNP showed the same cytotoxicity pattern, inhibiting mitochondrial activity and cell membrane integrity. However, there were no observed effects for the larger particles (40 and 75nm).

Braydich-Stolle et al. (2010) reported that from several polysaccharide-coated AgNP sizes tested (10, 25-30, 80nm), only the smallest AgNP size induced apoptosis and ROS. Carlson et al. (2008) exposed rat alveolar cell line macrophages (NR8383) to AgNP 15, 30 and 55nm and showed that the smaller particles induced dose dependent toxicity via ROS after 24h, while 30nm show toxicity absence of ROS and 55nm induced little toxicity even to higher does and no ROS. Yen et al. (2009) exposed J774A macrophages to ~3, 6 and 24nm AgNP for 24h, 48h and 72h and showed that after 24h the smallest AgNP inhibited cell proliferation with a low

observable adverse effect concentration (LOAEC) of 10µg/mL, while the larger particles cause no effects. After 48h and 72h of exposure, the cell proliferation inhibition was decreased for 10µg/mL, irrespective of AgNP size. Kim et al. (2012), also assessed size related toxicity of ~10, 50 and 100nm AgNP and reported that after 24h of exposure, 100nm AgNP were the most cytotoxic with a LOAEC of 10µg/mL, while 10 and 50 AgNP had LOAEC of 80 and 40µg/mL, respectively. After 48h of exposure, all particles induce apoptosis at 10µg/mL or more, but only 10nm AgNP induced a higher membrane damage and ROS production. Therefore, some studies indicate that size toxicity can also be time-dependent.

Overall, smaller particles seem to induce higher ROS production and higher toxicity when compared to larger ones. These particles can pass though the plasma membrane easily and with a higher surface area/volume ratio can amplify the interaction with cellular compounds. This size effect can also be related with time and Ag^+ release, which is directly correlated with the surface area, giving to the smaller sizes of AgNP a higher rate of Ag^+ release into cells.

Size can also influence the AgNP uptake by cells leading to intracellular accumulation (AshaRani et al., 2009; Gliga et al., 2014; Liu et al., 2010; Martínez-Gutierrez et al., 2012; Shavandi et al., 2011). Liu et al. (2010) assessed the toxicity of 5, 20 and 50nm AgNPs and found a size-dependent toxicity to HepG2 cells, due to a greater cell uptake and Ag^+ dissolution from 5nm AgNP, when compared to the larger particles. The smaller AgNP induced a depletion of SOD and glutathione antioxidant system, leading to ROS production, mitochondrial membrane permeabilization, cell cycle arrest and apoptosis. In murine adrenal medullary chromaffin cells, cellular uptake of citrate-coated AgNPs as determined by ICP-OES showed that exposure to smallest NPs resulted in the highest number of internalized NPs (Love et al., 2012). Chen et al. (2015) also reported a size-dependent uptake 15, 50 and 100nm AgNP by red blood cells. AgNP 50nm showed the higher rate of cell uptake and adsorption, suggesting an optimal size of ~50 nm for passive uptake by RBC. Although, the smallest size AgNP 15nm displayed a greater ability to induce hemolysis and membrane damage. Unfortunately, studies elucidating the effect of AgNPs size on uptake were conducted primarily on immortalized cell lines and each cell type possesses a unique phenotype, optimal nanoparticle uptake size may depend on the cell being assayed.

❖ Shape

AgNPs shape can also impact the cytotoxicity degree and effects, although it is a less studied feature. Frequently utilized silver nanostructures in the biomedical field include silver spherical nanoparticles, nanowires, nanorods, nanoplates, and nanocubes. Primary and agglomerated nanoparticles occur in forms such as spheres, rods, fibers, wires, belts, triangles, and platelets. Shapes with a high aspect ratio, like fibers, have an aerodynamic size that is about three times their actual diameter and are easier to deposit and cause direct physical damage.

Pal et al. (2007) investigated the antibacterial properties of differently shaped AgNPs against the gram-negative bacterium *Escherichia coli*. They found that Truncated triangular silver nanoplates with a {111} lattice plane as the basal plane displayed the strongest biocidal action, compared with spherical and rod-shaped nanoparticles and with Ag^+ (in the form of $AgNO_3$). Helmlinger et al. (2016) also studied the toxicity of differently shaped AgNPs, spheres (diameter 40–80 and 120–180nm; two different samples), platelets (20–60nm), cubes (140–180nm), and rods (diameter 80–120nm, length > 1000 nm), towards human mesenchymal stem cells and *S. aureus* (DSMZ 1104). The authors found a toxic effect to the cells at concentrations > 12.5 μg mL^{-1}, but no shape dependence. Although, particles shape influenced their dissolution kinetics and this characteristic influenced the toxicity towards bacteria. Particles with shapes that present higher specific surface area were more toxic for bacteria than particles with smaller specific surface areas. Shape also has an important role in their immunological effects. Stoehr et al. (2011) investigated the toxic and immunotoxic effects of silver wires (length: 1.5- 25μm; diameter 100-160nm), spherical AgNPs (30nm) and silver microparticles (<45μm) on alveolar epithelial cells (A549). The authors found a stronger toxicity for silver wires by reduction of viability and LDH release, whereas spherical silver particles had no effect. Although no immunotoxicity was found for silver wires neither silver particles, the authors state that the increased toxicity and the absence of specific immunotoxic responses could imply that the toxicity of the silver wires is caused mechanically by the needle-like structure. It also should be noticed that the large length of the wires, when compared to the nanoparticles, does not allow complete entry and this induces cell membrane damage. In a study by Zhang et al. (2012), polystyrene nanospheres were taken up by HeLa cells (human epithelioid cervix carcinoma), while nanodisks of approximately identical diameter were not internalized. It is also known, that some shapes could only be taken up by the

cells in a specific orientation, what will ultimately dictate their effects toward the cell (Champion and Mitragotri, 2006).

❖ Silver ion release

Dissolution is another property that needs to be addressed and it can depend on size, shape, coating, pH, time and/or oxidation. In the presence of oxygen, AgNPs of all shapes dissolve in pure water. The dissolution kinetics were correlated to the estimated specific surface area of the particles, where particles with a higher specific surface area dissolve faster than particles with a smaller one. The dissolution of AgNPs implies an oxidation reaction at the NP surface, from the elemental Ag (0) to Ag^+, according to the general scheme: Ag (0) + oxidant (oxygen or reactive oxygen species) $\rightarrow$ Ag^+ + $(oxidant)^-$. Furthermore, the size of AgNPs affects the extent and kinetics of AgNP dissolution, with the smallest NPs being dissolved faster and to a larger extent (Marques et al., 2011; Reidy et al., 2013). The nature of the coating however, appears to be less significant than the size effect (Marques et al., 2011). AgNP dissolution is expected to significantly depend on pH and to be more efficient at low pH (Liu and Hurt, 2010). However, pH in gastric fluids may be as low as pH 1.6 (human gastric fluid) (Marques et al., 2011) and pH 0.8 in fish guts (Bakke et al., 2010)., therefore an extensive and rapid AgNP dissolution would be expected at this low ph.

Gliga et al. (2014) observed that small AgNPs (10nm) were more cytotoxic for human lung cells and that the toxicity observed was associated with the rate of intracellular Ag^+ release, in a so-called 'Trojan horse' effect, when compared to 40 and 75nm. "Trojan horse hypothesis", which suggests that the particulate structure of AgNPs may facilitate increased cellular uptake (by endocytosis) and subsequent intracellular release of the Ag^+ ions; thus, leading to a greater intracellular bioavailability of the ions (Cronholm et al., 2013; Gliga et al., 2014; Hsiao et al., 2015; Milić et al., 2015). Yang et al. (2012) found a linear correlation between silver nanoparticle toxicity and the amount of dissolved silver. Also, oxidative dissolution was limited (maximally 15% in 24h), but still crucial for the toxicity of all studied AgNPs. The less soluble particles induced oxidative stress, an effect specific to nanoparticulate silver, was observed. Xiu et al. (2012) demonstrated that the toxicity of several AgNPs (PEG or PVP-coated, of three different sizes each) accurately followed a dose-dependent response pattern of E. coli exposed

to Ag^+ in form of $AgNO_3$. The authors found that AgNPs were very sensitive to the presence of air which allowed the oxidative dissolution of AgNP to release Ag^+. Also, they suggested that the AgNP morphological properties, known to affect antimicrobial activity, are indirect effectors that primarily influence Ag^+ release. Grosse et al. (2013) studied the effects of citrate-coated AgNP 10, 50 and 100nm and Ag^+ in the form of $AgNO_3$ and found that the AgNP release more Ag^+ and induce higher cell membrane damage in rat brain endothelial cells (RBE4), when compared to inhibitory effects of 30µM Ag^+. Colony formation, as an indicator of proliferation ability, was completely inhibited by AgNPs at concentrations higher than 1 µg/mL, while Ag^+ had less effect on the colony formation of RBE4 cells than AgNPs. Also, the aging seems to influence the silver ion release and therefore the AgNP toxicity. Kittler et al. (2010) demonstrated that "aged" AgNP were 20-times more toxic to mesenchymal stem cells than freshly prepared AgNPs due to the increased release of Ag^+. The authors also demonstrated that the dissolution was size, coating and temperature dependent. Additionally, He et al. (2013) construct an aggregation−dissolution model, in which the proportion of accessible reactive sites on primary particles as well as the aggregate size. The authors found a decrease in the dissolution rate of AgNPs over time for different concentrations of NaCl, has a response to an aggregation mechanism.

❖ Coating, agglomeration and charge

Uncoated NPs tend to become more reactive mostly due to their superficial charge and tend to have high profiles of aggregation and sedimentation, increasing the local organisms and cells more prone to high exposure (Fabrega et al., 2011, 2009; Navarro et al., 2008). A strategy to overcome these characteristics and increase NPs stabilization is to use a coating. The most frequently used capping agents are, citrate, 3-(aminopropyl) trimethoxysilane (APS), poly(vinylpyrrolidone) (PVP) and polyethylene glycol (PEG) and these agents can prevent AgNPs aggregation, ion dissolution, increase AgNPs mobility and make it less unstable.

Nguyen et al. (2013) compared the toxic effects of uncoated (20, 40, 60 and 80nm) and citrate or PVP coated AgNPs (10, 50, and 75nm) in macrophage and epithelial cells. The authors showed that uncoated AgNPs are more toxic than coated AgNPs. While uncoated AgNPs appear to suppress inflammatory responses, and enhance oxidative stress in the test cells, coated AgNPs

induce toxic effects through up-regulation of cytokines. While, another study reported that the surface coating of AgNPs influenced their toxicity by differently regulating cell-cycle and cell death mechanisms in human keratinocytes (HaCaT) (Bastos et al., 2016). In this study, citrate-coated AgNPs induced apoptotic death and a drastic cell cycle downregulation at G_2, while cells exposed to PEG-coated AgNPs appeared to be at an earlier phase of apoptosis. Moreover, Ag^+ release and ROS production were similar for both AgNP types, but uptake data showed that PEG-coated AgNPs were taken up by cells to a lower extent than citrate-coated AgNPs. Gliga et al. (2014) reported an increased aggregation and sedimentation of citrate- coated AgNPs and less stability in biological media, when compared to PVP-coated with the same size. Despite that, the toxic effect of both particles was similar in BEAS-2B cells. A similar observation was made by Lankoff et al. (2012), where THP1, HepG2 and A549 cells where exposed to silver (20 and 200nm) and titanium dioxide (21nm) NPs. In this study, all particles were efficiently taken up by the cells with decreasing metabolic activation and increasing cell death, but the least agglomerated particles were the most toxic. Cells have more capacity to uptake NPs when they are in a suspension than when they are agglomerated or sediment (Albanese and Chan, 2011; Lankoff et al., 2012). The reduction in toxicity upon aggregation phenomenon may be attributed to the decrease in surface area seen when AgNP form aggregates (Lankoff et al., 2012).

Coating agents can modify AgNPs surface charge, what can ultimately protect against surrounding medium absorption. For example, a well-known example on how AgNPs can change their biological identity and eventually their toxicity is the “corona”. The corona is a shell of proteins (and other biomolecules such as lipids and sugars) that arises on the surface of AgNPs, even the ones designed to avoid its formation. Miclăuş et al. (2014) suggested that nanoparticle-protein interaction is dynamic over time and can occur over long periods of hours (forming hard corona – inner layer) or short time scales of seconds or minutes (forming soft corona – outer layer). This shell resides on the AgNP surface for sufficient timescale to influence it properties and confers a new biological identity to the NPs such that they can engage with cellular machinery (Walczyk et al., 2010). It has been suggested that this protein corona is more significant in determining the biological response (i.e., immunogenicity) than the bare material properties of the particle itself (Khang et al., 2014; Linse et al., 2007; Walczyk et al., 2010). A study by Kittler et al. (2010), examined the cytotoxicity of spherical PVP and citrate coated

AgNPs (diameter of 50±20 nm) dispersed in cell culture media (media containing 10% BSA or 10% fetal calf serum). The authors found that the formation of Ag-protein coronas with BSA and fetal calf serum reduced the cytotoxicity of human mesenchymal stem cells (hMSCs) by inhibiting the release of free Ag^+ from the AgNPs.

The surface charge of AgNPs is most often negative at neutral pH, if weak acids are used as coatings and is strongly pH-dependent. If the surface charge of AgNPs is neutralized as a function of pH, agglomeration occurs, as shown for example for carbonate-coated AgNPs and for citrate-coated AgNPs at low pH (El Badawy et al., 2010; Tejamaya et al., 2012). PVP-coated AgNPs, seems to be more stable as a function of pH and of media composition, as they are sterically stabilized (Huynh and Chen, 2011; Tejamaya et al., 2012). The zeta potential is another important parameter which can be altered AgNP coatings and gives information on the particle's stability in solution. Linking zeta-potential to particle toxicity is more difficult, but in general, higher toxicity has been noticed with positively charged AgNPs as compared to negative or neutral charged AgNPs. This difference may be due to the higher affinity of the positively charged NPs to the negatively charged cell membranes, promoting internalization and intracellular bioavailability of these particles (Cho et al., 2009; Suresh et al., 2012). Kaur and Tikoo, (2013) synthetized two negatively charged AgNP, one more stable and the other more agglomerated, by reduction with tannic acid (TSNPs) and sodium borohydride nanoparticles (BSNPs), with highest and lowest surface potential, respectively. The authors exposed skin epithelial A431, A549 and murine macrophages RAW264.7 cells to AgNPs and showed that the less agglomerated TSNPs AgNP exhibited a higher negative zeta-potential and, also higher toxicity. Higher toxicity of TSNPs was attested by dose-dependent increase in cellular disruption and ROS generation. BSNPs showed cytotoxic effect up to the concentration of 50 µg/mL and thereafter the cytotoxic effect attenuated.

In vitro studies are a fastest, less expensive and less ethically ambiguous way to evaluate the toxicity, of a wide range of compounds. Respecting the principle of 3R's (Replacement, Reduction and Refinement), it is possible to mimic the *in vivo* or environmental conditions. The control of culture conditions such as, pH, temperature, nutrient and waste concentrations, is crucial to ensure that the toxicity is from the compound and not because of unstable culturing

conditions. In this work both MG-63 and A549 cell line were used to evaluate the *in vitro* toxicity of AgNPs.

❖ A549 cell line – Human lung adenocarcinoma

Since the increase in the industrial production of manufactured nanoparticles, the general population may be extremely more exposed to these particles present in the air. Therefore, the most common and important route of exposure to AgNPs is via occupational inhalation, of airborne particles or powders, possible leading to negative pulmonary effects (Elder et al., 2002; Semmler et al., 2004).

Inhalation, or ingestion, of Ag in large quantities and over a long period of time can cause a disease called "argyria", which leads to a blue or grey discoloration of the skin and other organs (Drake and Hazelwood, 2005). Additionally, the lung is considered to be the least protected organ and the main portal entry of inhaled NPs that can gain access to the alveoli, the deepest part of the respiratory tract where they can be translocated to other tissues (Nel et al., 2006; Oberdörster et al., 2005b). The system inhalation is the most common route of exposure to NPs in the workplaces. Once inhaled, these materials are carried by electrostatic force of the air from the upper to the lower respiratory tract (Cross et al., 2007; Oberdörster et al., 2005). The Occupational Safety and Health Administration (OSHA) and the National Institute of Occupational Safety and Health (NIOSH) limits silver in workplace air to 0.01 mg/m^3 and limits the time of exposure to 40h per week (Drake and Hazelwood, 2005), however data on the levels of exposure of humans to AgNPs on real scenarios (e.g., concentrations and routes) is still lacking.

Much research has been done with AgNPs toxicity of the respiratory tract, from 95 research papers found in A549, 47 of them address AgNPs toxicity. However, many questions concerning the specific interactions of AgNPs with organisms after inhalation remain open. AgNPs released into the environment (such as for instance air or water, experimental media or biological fluids) are subject to a number of processes (such as aggregation and oxidation with the formation of Ag^+) that alter their physicochemical characteristics. These possible processes influence the mode of transport, fate and possible toxicity of AgNPs (Levard et al., 2012).

Therefore, more toxicological assessment in AgNPs toxicity toward the respiratory systems, as well as, real exposure scenario should be conducted. A549 cells, derived from human lung adenocarcinoma, are well-characterized and thus suitable for *in vitro* toxicity tests (Foster et al., 1998; Lieber et al., 1976). When cultured *in vitro*, these cells grow as an adherent monolayer, and show multilamellar cytoplasmic inclusions bodies, that are typical from type II alveolar epithelial cells of the lung. Altogether, A549 cells are suitable to serve as an *in vitro* model of human adenocarcinoma cells (Lieber et al., 1976).

❖ MG-63 Cell line – Human osteosarcoma

The bone is extensively exposed to NPs, by medical devices, bone cement and bone implants. The major challenge of tissue engineering is to find appropriate materials that could control infection and also allow bone regeneration without toxicity.

Until the 1970s, most patients that suffered with malignant bone tumor, were treated with amputation, but today most patients, undergo implantation of endoprostheses (Mittermayer et al., 2001). However, the placement of endoprostheses as a limb-saving treatment is accompanied by a high rate of late complications such as loosening, mechanical failure, and periprosthetic infection (Mittermayer et al., 2001). Capanna et al. (1994) recorded an infection rate of 43% after surgery for tumor endoprostheses, while Hardes et al. (2010) found and infection rate reduced from 17.6% in uncoated the titanium mega prostheses and to 5.9% for silver-coated prosthesis. Post-operative infections remain the most devastating complication, following total joint-replacement infection, with mortality rates between 2.7 % and 18%. With a view to decreasing post-operative infections in orthopedic surgeries, bone cements have added NPs to their composition in order to decrease or avoid biofilm formation. In this way AgNPs poly (methyl methacrylate) cement has shown potent antibacterial action against methicillin-resistant *Staphylococcus epidermidis* and *S. aureus* (Alt et al., 2004). Similar results were obtained for bone cement modified with Ag–tiopronin NPs that displayed high antimicrobial efficacy against MRSA (Prokopovich et al., 2013). Slane et al. (2015) incorporated AgNPs in acrylic bone cement a quantified the antimicrobial activity. The authors found that the properties of the AgNP-loaded cement were similar to the standard cement, but the AgNP-loaded cement had no antimicrobial effect on planktonic *S. aureus* and *S. epidermidis*, with only a significantly

reduced biofilm formation on the surface of the cement (Slane et al., 2015). It has been pointed out that the AgNP concentration must be as low as 0.1% w/w in order not to modify the mechanical properties (Prokopovich et al., 2013) and to prevent cytotoxicity in osteoblasts and osteoclasts (Albers et al., 2013). Although, there is a lack of information on the amount silver ions (Ag^+) released from the products, which means that there can be times when not enough silver ions to control infection are being released, and times when more than enough Ag^+ is being released from the implant. Therefore, researchers have yet to figure out a way to accurately control the release of silver ions from the silver-coated implants and to assess if their toxicity is attributed to NPs intrinsic toxicity and/or from the released ions (Kawata et al., 2009; Navarro et al., 2008). However, from the almost 200 papers published on new surgical and dentistry materials coated with AgNP, few of them addressed AgNP cytotoxicity in bone cells. Jegatheeswaran et al. (2016) and Nayak et al. (2016) investigated the antibacterial activity and cytotoxicity of biomimetic f-HAp/PVP/Ag nanocomposite and a green synthetized AgNPs, respectively, and both found reduction of the biofilm forming bacteria and antiproliferative effects on MG-63. Also, Pishbin et al. (2013) assessed the effects of chitosan, chitosan/glass and chitosan/Bioglass/AgNP, and found a lower release of Ag ions (<2.5ppm) which efficiently decreased the viability of *S. aureus* up to 10 days. Although chitosan and chitosan/Bioglass® coating supported proliferation of MG-63 cells chitosan/Bioglass®/AgNP coatings containing 342µg of AgNP showed cytotoxic effects. The authors attributed to the relatively high concentration of AgNP to the cytotoxic effect. Additionally, (Cao et al., 2011; De Giglio et al., 2013; Ye et al., 2011) used embedded AgNPs, which therefore masks the putative toxicities due to AgNPs alone, as well as the effective release of Ag^+ from these NPs. In this study, we use MG-63 cell line, which is derived from malignant bone tumor (human osteosarcoma) to investigate the toxic effects of AgNPs. These cells exhibit characteristics from osteoblastic-like cells including fibroblast morphology, high levels of alkaline phosphatase activity and osteoblast-like regulated synthesis of osteocalcin and collagen type I (Bilbe et al., 1996; Pautke et al., 2004). Although, these cells share osteoblastic features, their chromosomal alterations lead to abnormal molecular and cellular functions, with multiple triploidy (Di Palma et al., 2003). MG-63 is a continuous cell line with infinite growth potential, for a long period of time, relatively easy to culture (grows on an adherent monolayer) and has a high rate of proliferation.

These characteristics made MG-63 cell line suitable for this type of *in vitro* tests (Di Palma et al., 2003).

4.4.2. *In vivo* studies

In vitro studies are the first way to assess toxicity since it offers benefits in terms of ethical considerations and reduce costs, although *in vivo* studies can correspond to actual conditions within a living organism providing more relevant information, allowing to detect interactions hat arise *in vivo* and allow investigation of long-term effects of AgNP exposure.

The respiratory system is a major portal and least protected of entry for AgNPs. Due to their small size, AgNP can deeply penetrate the lungs and diffuse o the high lung surface area. Several inhalation or intratracheal instillation (IT) in rats have demonstrated that AgNP can distribute among the organs. Braakhuis et al. (2014) assessed the particle size deposition in rat lungs after exposure to AgNP 15 and 410nm for 6h/day, for four days. Only AgNP 15nm induced toxic effects, including the increase in neutrophils, in cytokines, and in glutathione in the lungs 24h post-exposure, all of which disappeared after 7 days. Also, the internal alveolar mass dose of the AgNP 15nm was 3.5 times higher compared to the AgNP 410nm. A short-term inhalation of AgNP by Roberts et al. (2013) showed no apparent marked acute toxicity in rats after inhalation of a low-concentration (100 $\mu g/m^3$) and a high-concentration (1000 $\mu g/m^3$) of AgNP for 5h. Changes in pulmonary or cardiovascular parameters were absent or non-significant at 1 or 7 days post-exposure with the exceptions of increased blood monocytes 1 day after high-dose Ag exposure.

According to previous toxicity studies, the acute inhalation toxicity LC50 for AgNPs has been suggested at higher than 3.1×10^6 particles/cm^3 (750 $\mu g/m^3$) (Sung et al., 2011), although a 28-day AgNP inhalation toxicity study showed no significant toxicity up to 1.32×10^6 particles/cm^3 (61 $\mu g/m^3$) (Ji et al., 2008). In a previous sub-chronic inhalation study by Sung et al. (2009), male and female rats were exposed to AgNP (~19nm) for 6 h/day, 5 days/week, for 13 weeks in a whole-body inhalation chamber. It was found a bile-duct hyperplasia in the liver increased dose dependently in both the male and female rats and a dose-dependent increase in mixed inflammatory cell infiltrates, chronic alveolar inflammation, and small granulomatous lesions

in lungs and liver. Also, Kim et al. (2011) exposed male and female rats to AgNP 18nm for 6 h/day 90 days ($0{,}7x10^6$, $1.4x10^6$ and $2.9x10^6$ particles/cm^3) and found a dose-dependent deposition of AgNP in the blood, stomach, brain, liver, kidneys, lungs, and testes but no genotoxicity in male and female rat bone marrow. Cho et al. (2013) showed a significant increase in the level of DNA damage after inhalation of AgNP for 12 weeks, 6h/day, although no dose-dependent results were observed.

Another major route of exposure is the skin. Ag compounds have long been used in wound dressings, the incorporation of AgNPs into wound dressings is on the rise. Although there is a lack of animal studies on nanocrystalline silver the available literature reviewed suggested that nanocrystalline silver has a role in altering the inflammatory events in wounds and facilitate the early phase of wound healing.

Wright et al. (2012) examined early healing events and the efficacy of 20 and 50nm AgNP in a porcine model of contaminated wounds. They found the AgNP product promoted rapid wound healing in the first few days post injury and that the cellular apoptosis occurred at a higher rate in non-AgNP treated wounds, suggesting that AgNP silver has a role in altering the inflammatory events in wounds and facilitate the early phase of wound healing. Lu et al. (2013) assessed the *in vitro* antibacterial activity and *in vivo* wound healing capacity of the nanofibers in rabbits and rats' skin. A mixture of poly(vinyl alcohol) (PVA) and chitosan oligosaccharides (COS) with AgNPs demonstrated superior wound healing compared with gauze and the PVA/COS/$AgNO_3$ and caused no skin irritation after single or multiple applications.

Ingestion is one of the primary routes for entry for Ag compounds, colloidal Ag, and AgNPs. AgNPs are routinely ingested as dietary supplements for the homeopathic treatment of allergies, diabetes, tuberculosis and gastrointestinal distress. Normal dietary intake of Ag from drinking water and trace amounts in foods is estimated at 70–90 mg/day. After oral exposure for 28 days to AgNP and silver acetate (AgAc), it was shown in rats that the organ distribution of silver was similar when AgNPs or AgAc were administered orally to rats (Loeschner et al., 2011). Park et al. (2010) treated, for 14 days, mice with 1mg/kg of AgNPs (22nm, 42nm, and 71nm) and large-sized AgNPs (323nm) by oral administration. These authors found that small-sized AgNPs were distributed to the organs including brain, lung, liver, kidney, and testis while large-sized were not detected in those tissues. The levels of TGF-β in serum and B cells distribution were

significantly increased in the treated group of small-sized AgNPs but not in large-sized AgNPs. Blood levels, tissue distributions, and excretion of Ag were measured in male Sprague-Dawley rats after 24h of a single oral administration of AgNP and silver ions (Ag^+) were assessed by Park, (2013). The author found a decrease in red blood cell counts, hematocrit, and hemoglobin in the Ag^+-treated groups and an increase in platelet counts and mean platelet volume for the AgNP-treated rats. Also, that the AgNP were excreted through feces, suggesting low bioavailability.

Munger et al. (2014) evaluated the effect of AgNP oral exposure to 60 healthy volunteers through several time-length exposures and reported no significant changes in pulmonary ROS or pro-inflammatory cytokine generation. This result was attributed to poor absorption of AgNPs in the gut and poor translocation of these particles to the respiratory system from the gastrointestinal route.

Animals and humans differ in structure and function and extrapolations of findings from animal models to the human environment must be done with caution. Therefore, further studies are necessary better understand possible silver nanoscale particle toxicity risks on the human system from different delivery systems.

4.5. Distribution to organs and tissues (Liver, Spleen, Kidneys)

Once the barrier is passed (i.e. skin, lung epithelia, intestinal lining) nanoparticles may be within systemic circulation. After reach the systemic circulation, distribution through the entire body followed by uptake by the organs could be expected.

The first-pass metabolism site, after the translocation through systemic circulation, is the liver, which is able to remove compounds from the blood and transform into chemicals easier to be excreted.

For therapeutic applications of AgNP targeted to brain disorders, AgNP must be able to cross the blood-brain barrier (BBB) without harming the integrity of the brain. Several studies have been conducted using murine models and have shown localized edema to the brain 24h after AgNP systemic exposure, indicating the need for further research (Arvizo et al., 2012). Many studies showed deposition of AgNP in liver, kidneys, blood, brain and tests after either oral,

inhaled or intravenous exposure (Cha et al., 2008; Ebabe et al., 2013; Ji et al., 2008; Kim et al., 2011; Kim et al., 2008; Paluri, 2011; Park et al., 2011; Takenaka, 2001). Although, more research is required to determine the effects of long-term deposition of AgNPs in various organs. AgNPs may enter human and animal bodies for several routes of exposure, such as ingestion, inhalation, dermal contact and it could be intentionally administered intravenously (i.v)**.** After the entry in the body the main target organs are the skin, lungs, liver, spleens, brain, kidneys, adrenals and testes. AgNPs could also pass through blood vessels walls and lymphatic system which allow them to be transported all over the body.

Generally, the degree of bioaccumulation will be determined by a balance between the rate of uptake of AgNP (depends on bioavailability) and the rate of loss and dilution by growth and it varies with, a) the time of exposure, b) bioavailable concentration, c) nature of the environment, d) route of exposure and, e) biology and ecology of the organism. Hereupon, this is an important process to understand when evaluating hazard and risks from AgNPs.

4.5.1. Physiologically based pharmacokinetic models

The Human body is a complex system and adding up all possible routes for human exposure, it is difficult to assess particle concentrations or transformations, so in order to have a realistic idea of the effects of a particle, besides the external exposure, it is very important, to evaluate the internal exposure. This can be defined as the amount of external exposure that is absorbed and reaches the systemic circulation. One approach that can be used to correlate relationships between an external dose and internal organ, blood or excretion dose with pharmacokinetics and target organ dosimetry, there by establishing a dose-response relationship for AgNPs, is physiologically based pharmacokinetic (PBPK) modeling. PBPK model is a computational technique that simulates the kinetics of a particle after exposure, which is normally measured by four processes ADME (absorption, distribution, metabolism, and excretion). The PBPK could be a good method to structure the available information and data, put them into context (Bachler and Hungerbühler, 2013).

With these models it is possible to mimic a variety of scenarios of risk assessments and to incorporate nanoparticle-specific mechanistic information more accurately. This is particularly important for nanoparticles because the pharmacokinetics of nanoparticles could be affected by

multiple factors, including size, surface coating, surface charge, protein binding, exposure route, dose, and species. Currently, there are two PBPK models for AgNPs (Bachler and Hungerbühler, 2013; Lankveld et al., 2010).

Lankveld et al. (2010) developed the first PBPK model for 20, 80, and 110nm AgNPs in rats following daily i.v. injections for 5 days. The model was composed of five compartments (blood, liver, spleen, kidneys and remaining tissues). Distribution of AgNPs in the liver, kidney, and spleen was described by two state variables: one is freely available for exchange between tissues and blood, and the other is irreversibly bound to tissues.

Bachler and Hungerbühler, (2013) developed and validated a model structure for both silver forms by reproducing exposure conditions (dermal, oral, and inhalation) of *in vivo* experiments and comparing simulated and experimentally assessed organ concentrations in 12 compartments (blood, brain, spleen, bone marrow, testes, muscles, heart, lungs, liver, skin, kidneys, and intestines). The established compartments were calibrated with empirical data from available TK studies from intravenous studies available on the disposition of Ag^+ and AgNPs within rat and human.

To reduce the complexity of the models, transfer functions have been developed for the uptake rates of (nano)silver from the blood to the organs. These were based on organ-specific characteristics (i.e., glutathione concentration, capillary wall type, phagocytosis efficiency). For the transport from the organ to the blood, the same release rate for all organs was used. Once the model structure was set up, the distribution, metabolism and excretion rates were calibrated with *in vivo* kinetic data for intravenously injected AgNP. TK data for extravascular administrated (nano)silver (e.g., oral, subcutaneous) was not considered. The authors used data from Klaassen, (1979) and Lankveld et al. (2010) for the Ag^+ and AgNPs rat model, respectively. For example, to determine the absorption of particles from the inhalation it was used a sophisticated model from the International Commission on Radiological Protection (ICRP) which consider a size-dependent deposition in five different lung compartments, as well as movement/clearance processes between these compartments and the GI. The movement/clearance rates were determined from an *in vivo* study on rats for silver NPs. Notably, for all the exposure routes they could successfully predict the biodistribution of Ag^+ and 15–150 nm AgNPs and successfully extrapolated from rats to humans. The predicted results were

shown to be helpful for exposure and risk assessment of AgNPs in humans.

Also, the authors referred that more experimental studies are needing to further increase the reliability of the obtained models: (1) *in vitro* determination of the pulmonary and intestinal absorption fraction of Ag^+ and AgNPs of different sizes, coatings and concentrations; (2) investigations into the disposition of AgNPs that could not be recovered in the *in vivo* studies; (3) the storage kinetics of Ag^+ and AgNPs, including the influence of macrophages; (4) the transport efficiency of AgNPs of rat blood capillaries compared to human blood capillaries; and, (5) the TKs of silver NPs that are smaller than 15 nm.

4.6. Metabolomics and NMR Principles

The omics revolution in systems biology has provided an unprecedented level of understanding of how organisms respond to environmental factors such as diet, aging, and disease. Metabolomics is the study of small molecules (<1500 Da) in living systems, which provides information with a high potential for accurately describing the physiological state of an organism. External stimuli activate different responses from a living organism which trigger the activation of distinct biological pathways, swapping metabolites between reactions. Thanks to technical advances in NMR spectroscopy, mass spectrometry and compound separation, it is now possible to identify and quantify hundreds of metabolites and determine the metabolic state of an organism (i.e. the metabolome). The Human Metabolome Database lists 42000 metabolites and the number of lipid variants is on the order of 100 000. Of this vast number of metabolites, only 1500 may be identified from global profiling, 200–500 from targeted profiling, and far fewer are routinely subjected to quantitative analysis (Wishart et al., 2009).

The introduction of high-resolution magic angle spinning, Nuclear Magnetic Resonance (NMR), has made it possible to analyze the metabolite compounds in from many types of biological samples, intact tissues or cells to avoid sample destruction in relatively short order.

NMR technique is based in phenomenon that occurs based in the principle that many nuclei have spin and are electrically charge. Therefore, when nuclei are placed in a magnetic field, as

they absorb they reemit electromagnetic waves. An energy transfer is possible between the base energy to a higher energy level (generally a single energy gap). The energy transfer takes place at a wavelength that corresponds to radio frequencies and when the spin returns to its base level, energy is emitted at the same frequency. The signal that matches this transfer is measured in many ways and processed in order to yield an NMR spectrum for the nucleus concerned. Therefore, using stable isotope«, NMR can be used to elucidate the dynamics and mechanisms of metabolite transformations and to explore the compartmentalization of metabolic pathways. The most commonly used isotopes in biomolecular NMR studies are ^{1}H (proton), ^{13}C, ^{15}N, and ^{31}P. Of these, ^{1}H is the most sensitive followed by ^{31}P, both are present at near 100% natural abundance with a large number of materials into which they are incorporated (Markley et al., 2017). One-dimensional (1D) ^{1}H NMR is the most widely used NMR approach in metabolomics. Signals are either binned and then analyzed or fitted to patterns of signals corresponding to the metabolites expected to be present in the mixture (Markley et al., 2017). ^{13}C NMR signals cover a 200-ppm range compared with 10 ppm for ^{1}H and as a consequence are better resolved; however, the low sensitivity of ^{13}C (less by a factor of 8 or more) is compounded by its low natural abundance (1.1%). If 1D ^{1}H NMR peaks from a compound are well resolved with acceptable signal-to-noise, their intensities correlate linearly with its relative concentration (Markley et al., 2017). To determine absolute concentrations, one adds a standard of known concentration. Proton NMR is commonly applied in determining and validating the structure of organic and biological compounds. There are three main pieces of information that can be derived from each spectrum: (I) the position of a peak indicates the chemical shift (reflecting the electronic environment), (II) the area under a peak is proportional to the number of nuclei in that environment (reflecting concentration), and, (III) the peak splitting indicates the coupling with neighboring NMR-active protons (Bingol et al., 2016; Fan and Lane, 2016). Protons that are in the same chemical environment are said to be "chemically equivalent" and will resonate at the exact same frequency without coupling; benzene, for example has six chemically equivalent hydrogen, resulting in a single peak with a shift of 7.5 ppm and 6-fold intensity (Fan and Lane, 2016; Ian A. Lewis et al., 2007).

In complex mixtures, as the case of biological samples typically analyzed through metabolomics, the proton spectrum comprises a large multitude of signals, requiring the use of

bidimensional (2D) experiments to assign those signals to specific metabolites. These 2D methods include ^{1}H-^{1}H COSY (correlated spectroscopy), ^{1}H–^{1}H TOCSY (total correlation spectroscopy), and ^{1}H–^{1}3C HSQC (heteronuclear single-quantum correlation) (Fan and Lane, 2016).

Applications of metabolomics include disease diagnosis, monitoring the effects of medical interventions including drugs, detection of adulteration of food, and analysis of biochemical pathways and their perturbations resulting from mutations, aging, diet, exercise, or life style. Metabolomics and NMR are used regularly in drug discovery programs to uncover the efficacy, specificity, or toxicity of lead compounds and to provide information on the *in vivo* mechanism of action and to eliminate compounds likely to cause problems with side effects. Recent studies have utilized metabolomics to search for biomarkers for colon cancer and multiple sclerosis (C. Chen et al., 2015; Forgue et al., 2006; Powers, 2014). The properties of AgNPs can also change the cellular metabolism and response which can be detected by NMR. HaCaT cell line was exposed to citrate-coated AgNPs of 10, 30 or 60 nm diameter and to 30 nm AgNPs coated either with citrate (CIT), polyethylene glycol (PEG) or bovine serum albumin (BSA), to assess the influence of NP size and surface chemistry. Overall, CIT-coated 60 nm and PEG-coated 30 nmAgNPs had the least impact on cell viability and metabolism.

The role of Ag^{+} and reactive oxygen species (ROS)-mediated effects was also studied, in comparison to CIT-coated 30 nm particles and Ag^{+}. Ag^{+} produced a change in the metabolic profile that was remarkably similar to that seen for AgNPs, the main difference being the lesser impact on the Krebs cycle and energy metabolism. Finally, this study reported that while down- regulated glycolysis and disruption of energy production were common to AgNPs and H_2O_2, the impact on some metabolic pathways (GSH synthesis and the Krebs cycle) was independent of ROS-mediated mechanisms. Jarak et al. (2017) have used NMR metabolomics and with conventional clinical chemistry and histological examination, to characterize multi-organ and systemic metabolic responses to AgNPs intravenously administered to mice at 8 mg/kg body. They found in particular that the liver of dosed mice was found to switch from glycogenolysis and lipid storage, at 6 h post-

injection, to glycogenesis and lipolysis, at subsequent times up to 48 h. Moreover, metabolites related to antioxidative defense, immunoregulation and detoxification seemed to play a crucial role in avoiding major hepatic damage. The spleen showed several early changes, including depletion of several amino acids. The heart showed the metabolic shift towards TCA cycle intensification and increased ATP production reflecting a beneficial adaptation to the presence of AgNPs, while in the lung the TCA cycle was down regulated which showed signs of inflammation.

5. Aims and outline of this work

The general aim of this thesis was to evaluate the effects of particle size on AgNPs induced cytotoxicity and genotoxicity, along with their biodistribution and excretion kinetics. To achieve our goal, the specific aims were:

In vitro:

- To evaluate the effects of AgNPs on cell morphology, cell viability, cell cycle unbalances and clastogenicity,
- To differentiate the short-term effects and long-term effects of AgNPs exposure,
- To evaluate genotoxic potential of AgNPs measuring DNA damage, chromosome breakage, cytostasis and cytotoxicity,
- To compare the total AgNPs induced effects, with the corresponding amount of Ag^+,
- To assess the cell death induced by AgNPs.

In vivo:

- To analyze the effect of silver particle size on mice tissue distribution after one single IT or 2 IT,
- To analyze the effect of silver particle size on mice tissue distribution after repeated IT,
- To determine the accumulation of AgNPs in potential mice target organs,
- To examine the blood inflammatory effects,
- To analyze the GSH/GSSG content in the mice liver and lung,
- To examine the excretion of AgNPs by urine and feces,
- To gather the obtained data in a PBPK model, and finally,
- To analyze the metabolic profile of mice lungs after AgNP exposure using NMR metabolomics.

References

Aderem, A., Underhill, D.M., 1999. Mechanisms of phagocytosis in macrophages. Annu. Rev.Immunol. 17, 593–623. doi:10.1146/annurev.immunol.17.1.593

Aggarwal, P., Hall, J.B., McLeland, C.B., Dobrovolskaia, M.A., McNeil, S.E., 2009. Nanoparticle interaction with plasma proteins as it relates to particle biodistribution, biocompatibility and therapeutic efficacy. Adv. Drug Deliv. Rev. 61, 428–437.

Ahamed, M., Karns, M., Goodson, M., Rowe, J., Hussain, S.M., Schlager, J.J., Hong, Y., 2008. DNA damage response to different surface chemistry of silver nanoparticles in mammalian cells. Toxicol. Appl. Pharmacol. 233, 404–10. doi:10.1016/j.taap.2008.09.015

Ahlberg, A., Carlsson, A.S., Lindberg, L., 1978. Hematogenous infection in total joint replacement. Clin. Orthop. Relat. Res. 69–75.

Albanese, A., Chan, W.C.W., 2011. Effect of Gold Nanoparticle Aggregation on Cell Uptake and Toxicity. ACS Nano 5, 5478–5489. doi:10.1021/nn2007496

Albers, C.E., Hofstetter, W., Siebenrock, K.A., Landmann, R., Klenke, F.M., 2013. *In vitro* cytotoxicity of silver nanoparticles on osteoblasts and osteoclasts at antibacterial concentrations. Nanotoxicology 7, 30–36. doi:10.3109/17435390.2011.626538

Alivisatos, A.P., Gu, W., Larabell, C., 2005. Quantum Dots as Cellular Probes. Annu. Rev.Biomed. Eng. 7, 55–76. doi:10.1146/annurev.bioeng.7.060804.100432

Almofti, M.R., Ichikawa, T., Yamashita, K., Terada, H., Shinohara, Y., 2003. Silver ion induces a cyclosporine a-insensitive permeability transition in rat liver mitochondria and release of apoptogenic cytochrome C. J. Biochem. 134, 43–9.

Alt, V., Bechert, T., Steinrücke, P., Wagener, M., Seidel, P., Dingeldein, E., Domann, E., Schnettler, R., 2004. An in vitro assessment of the antibacterial properties and cytotoxicity of nanoparticulate silver bone cement. Biomaterials 25, 4383–91.

Andergassen, S., Meden, V., Schoeller, H., Splettstoesser, J., Wegewijs, M.R., 2010. Charge transport through single molecules, quantum dots, and quantum wires.

Arora, S., Rajwade, J.M., Paknikar, K.M., 2012. Nanotoxicology and in vitro studies: the need of the hour. Toxicol. Appl. Pharmacol. 258, 151–65. doi:10.1016/j.taap.2011.11.010

Arvizo, R.R., Bhattacharyya, S., Kudgus, R.A., Giri, K., Bhattacharya, R., Mukherjee, P., 2012. Intrinsic therapeutic applications of noble metal nanoparticles: past, present and future. Chem. Soc. Rev. 41, 2943. doi:10.1039/c2cs15355f

AshaRani, P. V., Low Kah Mun, G., Hande, M.P., Valiyaveettil, S., 2009. Cytotoxicity and Genotoxicity of Silver nanoparticles in human cells. ACS Nano 3, 279–290.

Asharani, P. V, Hande, M.P., Valiyaveettil, S., 2009. Anti-proliferative activity of silver nanoparticles. BMC Cell Biol. 10, 65. doi:10.1186/1471-2121-10-65

Auffan, M., Bottero, J.-Y., Chaneac, C., Rose, J., 2010. Inorganic manufactured nanoparticles:

how their physicochemical properties influence their biological effects in aqueous environments. Nanomedicine 5, 999–1007. doi:10.2217/nnm.10.61

Bachler, G., Hungerbühler, K., 2013. A physiologically based pharmacokinetic model forionic silver and silver nanoparticles. Int. J. Nanomedicine 8, 3365–3382.

Bae, J.-E., Huh, M.-I., Ryu, B.-K., Do, J.-Y., Jin, S.-U., Moon, M.-J., Jung, J.-C., Chang, Y.,

Kim, E., Chi, S.-G., Lee, G.-H., Chae, K.-S., 2011. The effect of static magnetic fields on the aggregation and cytotoxicity of magnetic nanoparticles. Biomaterials 32, 9401–14.

Bakke, A.M., Glover, C., Krogdahl, Å., 2010. Feeding, digestion and absorption of nutrients. pp. 57–110. doi:10.1016/S1546-5098(10)03002-5

Balogh, L., Douglas R. Swanson, Donald A. Tomalia, Hagnauer, G.L., Manus, A.T., 2000. Dendrimer−Silver Complexes and Nanocomposites as Antimicrobial Agents.

Bastos, V., Ferreira de Oliveira, J.M.P., Brown, D., Jonhston, H., Malheiro, E., Daniel-da-Silva, A.L., Duarte, I.F., Santos, C., Oliveira, H., 2016. The influence of Citrate or PEG coating on silver nanoparticle toxicity to a human keratinocyte cell line. Toxicol. Lett. 249, 29–41.

Benmerah, A., Lamaze, C., 2007. Clathrin-Coated Pits: Vive La Différence? Traffic 8, 970–982. doi:10.1111/j.1600-0854.2007.00585.x

Bilbe, G., Roberts, E., Birch, M., Evans, D.B., 1996. PCR phenotyping of cytokines, growth factors and their receptors and bone matrix proteins in human osteoblast-like cell lines. Bone 19, 437–45.

Bingol, K., Bruschweiler-Li, L., Li, D., Zhang, B., Xie, M., Brüschweiler, R., 2016. Emerging new strategies for successful metabolite identification in metabolomics. Bioanalysis 8, 557–573. doi:10.4155/bio-2015-0004

Biskos, G., Schmidt-Ott, A., 2012. Airborne Engineered Nanoparticles: Potential Risks and Monitoring Challenges for Assessing their Impacts on Children. Paediatr. Respir. Rev. 13, 79–83. doi:10.1016/j.prrv.2011.05.011

Biswas, P., Wu, C.-Y., 2005. Nanoparticles and the Environment. J. Air Waste Manage. Assoc. 55, 708–746. doi:10.1080/10473289.2005.10464656

Borm, P., Robbins, D., Haubold, S., Kuhlbusch, T., Donaldson, K., Schins, R., Stone, V., Kreyling, W., Lademann, J., Krutmann, J., Warheit, D., Oberdorster, E., 2006. The potential risks of nanomaterials: a review carried out for ECETOC. Part. Fibre Toxicol. 3, 11. doi:10.1186/1743-8977-3-11

Braakhuis, H.M., Gosens, I., Krystek, P., Boere, J., Cassee, F., Fokkens, P., Post, J., Loveren, H., Park, M., 2014. Particle size dependent deposition and pulmonary inflammation after short-term inhalation of silver nanoparticles. Part. Fibre Toxicol. 11, 49.

Braydich-Stolle, L.K., Lucas, B., Schrand, A., Murdock, R.C., Lee, T., Schlager, J.J., Hussain, S.M., Hofmann, M.-C., 2010. Silver Nanoparticles Disrupt GDNF/Fyn kinase Signaling in

Spermatogonial Stem Cells. Toxicol. Sci. 116, 577–589. doi:10.1093/toxsci/kfq148

Buzea, C., Pacheco, I.I., Robbie, K., 2007. Nanomaterials and nanoparticles: sources and toxicity. Biointerphases 2, MR17-71.

Cao, H., Liu, X., Meng, F., Chu, P.K., 2011. Biological actions of silver nanoparticles embedded in titanium controlled by micro-galvanic effects. Biomaterials 32, 693–705.

Capanna, R., Morris, H.G., Campanacci, D., Del Ben, M., Campanacci, M., 1994. Modular uncemented prosthetic reconstruction after resection of tumours of the distal femur. J. Bone Joint Surg. Br. 76, 178–86.

Carlson, C., Hussain, S.M., Schrand, a M., Braydich-Stolle, L.K., Hess, K.L., Jones, R.L., Schlager, J.J., 2008. Unique cellular interaction of silver nanoparticles: size-dependent generation of reactive oxygen species. J. Phys. Chem. B 112, 13608–19.

Cha, K., Hong, H.-W., Choi, Y.-G., Lee, M.J., Park, J.H., Chae, H.-K., Ryu, G., Myung, H., 2008. Comparison of acute responses of mice livers to short-term exposure to nano-sized or micro-sized silver particles. Biotechnol. Lett. 30, 1893–9. doi:10.1007/s10529-008-9786-2

Champion, J.A., Mitragotri, S., 2006. Role of target geometry in phagocytosis. Proc. Natl. Acad. Sci. U. S. A. 103, 4930–4. doi:10.1073/pnas.0600997103

Chen, C., Deng, L., Wei, S., Nagana Gowda, G.A., Gu, H., Chiorean, E.G., Abu Zaid, M.,

Harrison, M.L., Pekny, J.F., Loehrer, P.J., Zhang, D., Zhang, M., Raftery, D., 2015. Exploring Metabolic Profile Differences between Colorectal Polyp Patients and Controls Using Seemingly Unrelated Regression. J. Proteome Res. 14, 2492–2499.

Chen, J., Han, C., Lin, X., Tang, Z., Su, S., 2006. [Effect of silver nanoparticle dressing on second degree burn wound]. Zhonghua Wai Ke Za Zhi 44, 50–2.

Chen, L.Q., Fang, L., Ling, J., Ding, C.Z., Kang, B., Huang, C.Z., 2015. Nanotoxicity of Silver Nanoparticles to Red Blood Cells: Size Dependent Adsorption, Uptake, and Hemolytic Activity. Chem. Res. Toxicol. 28, 501–509. doi:10.1021/tx500479m

Chithrani, B.D., Ghazani, A.A., Chan, W.C.W., 2006. Determining the Size and Shape Dependence of Gold Nanoparticle Uptake into Mammalian Cells. Nano Lett. 6.

Cho, E.C., Xie, J., Wurm, P.A., Xia, Y., 2009. Understanding the Role of Surface Charges in Cellular Adsorption versus Internalization by Selectively Removing Gold Nanoparticles on the Cell Surface with a I_2/KI Etchant. Nano Lett. 9, 1080–1084. doi:10.1021/nl803487r

Cho, H., Sung, J., Song, K., Kim, J., Ji, J., Lee, J., Ryu, H., Ahn, K., Yu, I., 2013. Genotoxicity of Silver Nanoparticles in Lung Cells of Sprague Dawley Rats after 12 Weeks of Inhalation Exposure. Toxics 1, 36–45. doi:10.3390/toxics1010036

Conner, S.D., Schmid, S.L., 2003. Regulated portals of entry into the cell. Nature 422, 37–44.

Cronholm, P., Karlsson, H.L., Hedberg, J., Lowe, T.A., Winnberg, L., Elihn, K., Wallinder,

I.O., Möller, L., 2013. Intracellular Uptake and Toxicity of Ag and CuO Nanoparticles: A Comparison Between Nanoparticles and their Corresponding Metal Ions. Small 9, 970–982. doi:10.1002/smll.201201069

Cross, S.E., Innes, B., Roberts, M.S., Suzuki, T., Robertson, T.A., McCormick, P., 2007. Human Skin Penetration of Sunscreen Nanoparticles: In-vitro Assessment of a Novel Micronized Zinc Oxide Formulation. Skin Pharmacol. Physiol. 20, 148–154.

De Giglio, E., Cafagna, D., Cometa, S., Allegretta, A., Pedico, A., Giannossa, L.C., Sabbatini, L., Mattioli-Belmonte, M., Iatta, R., 2013. An innovative, easily fabricated, silver nanoparticle-based titanium implant coating: development and analytical characterization. Anal. Bioanal. Chem. 405, 805–16. doi:10.1007/s00216-012-6293-z

Di Palma, F., Douet, M., Boachon, C., Guignandon, A., Peyroche, S., Forest, B., Alexandre, C., Chamson, A., Rattner, A., 2003. Physiological strains induce differentiation in human osteoblasts cultured on orthopaedic biomaterial. Biomaterials 24, 3139–51.

DiRienzo, M., 2006. New Applications for Silver. LBMA Precious Met. Conf. 85–90.

Dobrovolskaia, M.A., McNeil, S.E., 2007. Immunological properties of engineered nanomaterials. Nat. Nanotechnol. 2, 469–478. doi:10.1038/nnano.2007.223

Donaldson, K., Stone, V., Tran, C.L., Kreyling, W., Borm, P.J.A., 2004. Nanotoxicology. Occup. Environ. Med. 61, 727–8. doi:10.1136/oem.2004.013243

Drake, P.L., Hazelwood, K.J., 2005. Exposure-Related Health Effects of Silver and Silver Compounds: A Review. Ann. Occup. Hyg. 49, 575–85. doi:10.1093/annhyg/mei019

Ebabe Elle, R., Gaillet, S., Vidé, J., Romain, C., Lauret, C., Rugani, N., Cristol, J.P., Rouanet, J.M., 2013. Dietary exposure to silver nanoparticles in Sprague–Dawley rats: Effects on oxidative stress and inflammation. Food Chem. Toxicol. 60, 297–301.

Eby, D.M., Luckarift, H.R., Johnson, G.R., 2009. Hybrid Antimicrobial Enzyme and Silver Nanoparticle Coatings for Medical Instruments. ACS Appl. Mater. Interfaces 1, 1553–1560. doi:10.1021/am9002155

El Badawy, A.M., Luxton, T.P., Silva, R.G., Scheckel, K.G., Suidan, M.T., Tolaymat, T.M., 2010. Impact of environmental conditions (pH, ionic strength, and electrolyte type) on the surface charge and aggregation of silver nanoparticles suspensions. Environ. Sci. Technol. 44, 1260–6. doi:10.1021/es902240k

El Badawy, A.M., Scheckel, K.G., Suidan, M., Tolaymat, T., 2012. The impact of stabilization mechanism on the aggregation kinetics of silver nanoparticles. Sci. Total Environ. 429, 325–31. doi:10.1016/j.scitotenv.2012.03.041

Elder C., A., Gelein, R., N. Finkelstein, J., Cox, C., Oberdörster, G., 2000. Pulmonary inflammatory response to inhaled ultrafine particles is modified by age, ozone exposure, and bacterial toxin. Inhal. Toxicol. 12, 227–246. doi:10.1080/089583700750019585

Elder, A., Gelein, R., Azadniv, M., Frampton, M., Finkelstein, J., Oberdörster, E., 2002. Systemic Interactions between Inhaled Ultrafine\rParticles and Endotoxin. Ann. Occup. Hyg. 46, 231–234. doi:10.1093/annhyg/mef677

Fabrega, J., Fawcett, S.R., Renshaw, J.C., Lead, J.R., 2009. Silver Nanoparticle Impact on Bacterial Growth: Effect of pH, Concentration, and Organic Matter. Environ. Sci. Technol. 43, 7285–7290. doi:10.1021/es803259g

Fabrega, J., Luoma, S.N., Tyler, C.R., Galloway, T.S., Lead, J.R., 2011. Silver nanoparticles: behaviour and effects in the aquatic environment. Environ. Int. 37, 517–31.

Fan, T.W.-M., Lane, A.N., 2016. Applications of NMR spectroscopy to systems biochemistry. Prog. Nucl. Magn. Reson. Spectrosc. 92, 18–53. doi:10.1016/j.pnmrs.2016.01.005

Farré, M., Sanchís, J., Barceló, D., 2011. Analysis and assessment of the occurrence, the fate and the behavior of nanomaterials in the environment. TrAC Trends Anal. Chem. 30, 517–527. doi:10.1016/j.trac.2010.11.014

Flahaut, E., 2010. Introduction to the special focus issue: environmental toxicity of nanoparticles. Nanomedicine 5, 949–950. doi:10.2217/nnm.10.56

Foldbjerg, R., Dang, D.A., Autrup, H., 2011. Cytotoxicity and genotoxicity of silver nanoparticles in the human lung cancer cell line, A549. Arch. Toxicol. 85, 743–50.

Fong, J., Wood, F., 2006. Nanocrystalline silver dressings in wound management: a review. Int. J. Nanomedicine 1, 441–9.

Forgue, P., Halouska, S., Werth, M., Xu, K., Harris, S., Powers, R., 2006. NMR Metabolic Profiling of Aspergillus nidulans to Monitor Drug and Protein Activity.

França, A., Aggarwal, P., Barsov, E. V, Kozlov, S. V, Dobrovolskaia, M.A., González-Fernández, Á., 2011. Macrophage scavenger receptor A mediates the uptake of gold colloids by macrophages *in vitro*. Nanomedicine 6, 1175–1188. doi:10.2217/nnm.11.41

Furno, F., Morley, K.S., Wong, B., Sharp, B., Arnold, P.L., Howdle, S.M., Bayston, R., Brown, P.D., Winship, P.D., Reid, H.J., 2004. Silver nanoparticles and polymeric medical devices: a new approach to prevention of infection? J. Antimicrob. Chemother. 54, 1019–24.

Ge, L., Li, Q., Wang, M., Ouyang, J., Li, X., Xing, M.M., 2014. Nanosilver particles in medical applications: synthesis, performance, and toxicity. Int. J. Nanomedicine 9, 2399–2407.

Gliga, A.R., Skoglund, S., Wallinder, I.O., Fadeel, B., Karlsson, H.L., 2014. Size-dependent cytotoxicity of silver nanoparticles in human lung cells: the role of cellular uptake, agglomeration and Ag release. Part. Fibre Toxicol. 11, 11. doi:10.1186/1743-8977-11-11

Gopinath, P., Gogoi, S.K., Chattopadhyay, A., Ghosh, S.S., 2008. Implications of silver nanoparticle induced cell apoptosis for in vitro gene therapy. Nanotechnology 19, 75104.

Grosse, S., Evje, L., Syversen, T., 2013. Silver nanoparticle-induced cytotoxicity in rat brain endothelial cell culture. Toxicol. Vitr. 27, 305–313. doi:10.1016/j.tiv.2012.08.024

Gurunathan, S., Han, J.W., Eppakayala, V., Jeyaraj, M., Kim, J.-H., 2013. Cytotoxicity of biologically synthesized silver nanoparticles in MDA-MB-231 human breast cancer cells. Biomed Res. Int. 2013, 535796. doi:10.1155/2013/535796

Gurunathan, S., Lee, K.-J., Kalishwaralal, K., Sheikpranbabu, S., Vaidyanathan, R., Eom, S.H., 2009. Antiangiogenic properties of silver nanoparticles. Biomaterials 30, 6341–6350. doi:10.1016/j.biomaterials.2009.08.008

Haase, a, Tentschert, J., Jungnickel, H., Graf, P., Mantion, a, Draude, F., Plendl, J., Goetz, M.E., Galla, S., Mašić, a, Thuenemann, a F., Taubert, a, Arlinghaus, H.F., Luch, a, 2011. Toxicity of silver nanoparticles in human macrophages: uptake, intracellular distribution and cellular responses. J. Phys. Conf. Ser. 304, 12030.

Handy, R.D., Owen, R., Valsami-Jones, E., 2008a. The ecotoxicology of nanoparticles and nanomaterials: current status, knowledge gaps, challenges, and future needs. Ecotoxicology 17, 315–325. doi:10.1007/s10646-008-0206-0

Handy, R.D., von der Kammer, F., Lead, J.R., Hassellöv, M., Owen, R., Crane, M., 2008b. The ecotoxicology and chemistry of manufactured nanoparticles. Ecotoxicology 17, 287–314. doi:10.1007/s10646-008-0199-8

Hardes, J., von Eiff, C., Streitbuerger, A., Balke, M., Budny, T., Henrichs, M.P., Hauschild, G., Ahrens, H., 2010. Reduction of periprosthetic infection with silver-coated megaprostheses in patients with bone sarcoma. J. Surg. Oncol. 101, n/a-n/a. doi:10.1002/jso.21498

Hardman, R., 2006. A toxicologic review of quantum dots: toxicity depends on physicochemical and environmental factors. Environ. Health Perspect. 114, 165–72. doi:10.1289/EHP.8284

Harush-Frenkel, O., Rozentur, E., Benita, S., Altschuler, Y., 2008. Surface Charge of Nanoparticles Determines Their Endocytic and Transcytotic Pathway in Polarized MDCK Cells. Biomacromolecules 9, 435–443. doi:10.1021/bm700535p

He, D., Bligh, M.W., Waite, T.D., 2013. Effects of aggregate structure on the dissolution kinetics of citrate-stabilized silver nanoparticles. Environ. Sci. Technol. 47, 9148–56.

He, W., Zhou, Y.-T., Wamer, W.G., Boudreau, M.D., Yin, J.-J., 2012. Mechanisms of the pH dependent generation of hydroxyl radicals and oxygen induced by Ag nanoparticles. Biomaterials 33, 7547–7555. doi:10.1016/j.biomaterials.2012.06.076

Helmlinger, J., Sengstock, C., Groß-Heitfeld, C., Mayer, C., Schildhauer, T.A., Köller, M., Epple, M., 2016. Silver nanoparticles with different size and shape: equal cytotoxicity, but different antibacterial effects. RSC Adv. 6, 18490–18501. doi:10.1039/C5RA27836H

Hervé, F., Ghinea, N., Scherrmann, J.-M., 2008. CNS Delivery Via Adsorptive Transcytosis. AAPS J. 10, 455–472. doi:10.1208/s12248-008-9055-2

Hillaireau, H., Couvreur, P., 2009. Nanocarriers' entry into the cell: relevance to drug delivery. Cell. Mol. Life Sci. 66, 2873–2896. doi:10.1007/s00018-009-0053-z

Hillyer, J.F., Albrecht, R.M., 2001. Gastrointestinal persorption and tissue distribution of differently sized colloidal gold nanoparticles. J. Pharm. Sci. 90, 1927–36.

Howes, M.T., Kirkham, M., Riches, J., Cortese, K., Walser, P.J., Simpson, F., Hill, M.M., Jones, A., Lundmark, R., Lindsay, M.R., Hernandez-Deviez, D.J., Hadzic, G., McCluskey, A., Bashir, R., Liu, L., Pilch, P., McMahon, H., Robinson, P.J., Hancock, J.F., Mayor, S., Parton, R.G., 2010. Clathrin-independent carriers form a high capacity endocytic sorting system at the leading edge of migrating cells. J. Cell Biol. 190, 675–691.

Hsiao, I.-L., Hsieh, Y.-K., Wang, C.-F., Chen, I.-C., Huang, Y.-J., 2015. Trojan-Horse Mechanism in the Cellular Uptake of Silver Nanoparticles Verified by Direct Intra- and Extracellular Silver Speciation Analysis. Environ. Sci. Technol. 49, 3813–3821.

Huynh, K.A., Chen, K.L., 2011. Aggregation kinetics of citrate and polyvinylpyrrolidone coated silver nanoparticles in monovalent and divalent electrolyte solutions. Environ. Sci. Technol. 45, 5564–71. doi:10.1021/es200157h

Ian A. Lewis, Seth C. Schommer, Brendan Hodis, Kate A. Robb, Marco Tonelli, William M. Westler, Michael R. Sussman, and, Markley, J.L., 2007. Method for Determining Molar Concentrations of Metabolites in Complex Solutions from Two-Dimensional 1H−13C NMR Spectra. doi:10.1021/AC071583Z

Jarak, I., Carrola, J., Onio, A., Barros, S., Gil, A.M., De, M., Pereira, L., Corvo, M.L., Duarte, I.F., 2017. Metabolism Modulation in Different Organs by Silver Nanoparticles: An NMR Metabolomics Study of a Mouse Model 1–14. doi:10.1093/toxsci/kfx142

Jegatheeswaran, S., Selvam, S., Sri Ramkumar, V., Sundrarajan, M., 2016. Novel strategy for f-HAp/PVP/Ag nanocomposite synthesis from fluoro based ionic liquid assistance: Systematic investigations on its antibacterial and cytotoxicity behaviors. Mater. Sci. Eng. C 67, 8–19. doi:10.1016/j.msec.2016.04.097

Ji, J.H., Jung, J.H., Kim, S.S., Yoon, J.-U., Park, J.D., Choi, B.S., Chung, Y.H., Kwon, I.H.,

Jeong, J., Han, B.S., Shin, J.H., Sung, J.H., Song, K.S., Yu, I.J., 2008. Twenty-Eight-Day Inhalation Toxicity Study of Silver Nanoparticles in Sprague-Dawley Rats.

Joseph, T.N., Chen, A.L., Di Cesare, P.E., 2003. Use of antibiotic-impregnated cement in total joint arthroplasty. J. Am. Acad. Orthop. Surg. 11, 38–47.

Kasamatsu, H., Nakanishi, A., 1998. How do animal dna viruses get to the nucleus? Annu. Rev. Microbiol. 52, 627–686. doi:10.1146/annurev.micro.52.1.627

Kaur, J., Tikoo, K., 2013. Evaluating cell specific cytotoxicity of differentially charged silver nanoparticles. Food Chem. Toxicol. 51, 1–14. doi:10.1016/j.fct.2012.08.044

Kausar, A., Rafique, I., Muhammad, B., 2017. Aerospace Application of Polymer Nanocomposite with Carbon Nanotube, Graphite, Graphene Oxide, and Nanoclay. Polym. Plast. Technol. Eng. 1–19. doi:10.1080/03602559.2016.1276594

Kawata, K., Osawa, M., Okabe, S., 2009. In vitro toxicity of silver nanoparticles at noncytotoxic

doses to HepG2 human hepatoma cells. Environ. Sci. Technol. 43, 6046–51.Kettiger, H., Schipanski, A., Wick, P., Huwyler, J., 2013. Engineered nanomaterial uptake and tissue distribution: from cell to organism. Int. J. Nanomedicine 8, 3255–69.

Khalil, I.A., Kogure, K., Akita, H., Harashima, H., 2006. Uptake Pathways and Subsequent Intracellular Trafficking in Nonviral Gene Delivery. Pharmacol. Rev. 58, 32–45. doi:10.1124/pr.58.1.8

Khang, D., Lee, Y.K., Choi, E., Webster, T.J., Kim, S., 2014. Effect of the protein corona on nanoparticles for modulating cytotoxicity and immunotoxicity. Int. J. Nanomedicine Volume 10, 97. doi:10.2147/IJN.S72998

Kim, H.R., Kim, M.J., Lee, S.Y., Oh, S.M., Chung, K.H., 2011. Genotoxic effects of silver nanoparticles stimulated by oxidative stress in human normal bronchial epithelial (BEAS-2B) cells. Mutat. Res. 726, 129–135. doi:10.1016/j.mrgentox.2011.08.008

Kim, J.S., Kuk, E., Yu, K.N., Kim, J.H., Park, S.J., Lee, H.J., 2007. Antimicrobial effects of silver nanoparticles. Nanomedicine Nanotechnology, Biol. Med. 3.

Kim, J.S., Sung, J.H., Ji, J.H., Song, K.S., Lee, J.H., Kang, C.S., Yu, I.J., 2011. In vivo Genotoxicity of Silver Nanoparticles after 90-day Silver Nanoparticle Inhalation Exposure. Saf. Health Work 2, 34–8. doi:10.5491/SHAW.2011.2.1.34

Kim, S., Choi, J., Choi, J., Chung, K.-H., Park, K., Ryu, D.-Y., 2009. Oxidative stress-dependent toxicity of silver nanoparticles in human hepatoma cells. Toxicol. In Vitro 23, 1076–84.

Kim, T.-H., Kim, M., Park, H.-S., Shin, U.S., Gong, M.-S., Kim, H.-W., 2012. Size-dependent cellular toxicity of silver nanoparticles. J. Biomed. Mater. Res. Part A 100A, 1033–1043.

Kim, Y.S., Kim, J.S., Cho, H.S., Rha, D.S., Kim, J.M., Park, J.D., Choi, B.S., Lim, R., Chang,

H.K., Chung, Y.H., Kwon, I.H., Jeong, J., Han, B.S., Yu, I.J., 2008. Twenty-eight-day oral toxicity, genotoxicity, and gender-related tissue distribution of silver nanoparticles in Sprague-Dawley rats. Inhal. Toxicol. 20, 575–83. doi:10.1080/08958370701874663

Kingston, C., Zepp, R., Andrady, A., Boverhof, D., Fehir, R., Hawkins, D., Roberts, J., Sayre, P., Shelton, B., Sultan, Y., Vejins, V., Wohlleben, W., 2014. Release characteristics of selected carbon nanotube polymer composites. Carbon N. Y. 68, 33–57.

Kittler, S., Greulich, C., Diendorf, J., Köller, M., Epple, M., 2010. Toxicity of Silver Nanoparticles Increases during Storage Because of Slow Dissolution under Release of Silver Ions. Chem. Mater. 22, 4548–4554. doi:10.1021/cm100023p

Klaassen, C.D., 1979. Biliary excretion of silver in the rat, rabbit, and dog. Toxicol. Appl. Pharmacol. 50. doi:10.1016/0041-008X(79)90491-5

Klaine, S.., Alvarez, P.J.J., Batley, G.E., Fernandes, T.F., Handy, R.D., Lyon, D.Y., Mahendra, S., McLaughlin, M.J., Lead, J.R., 2008. Nanomaterials in the environment: behaviour, fate, bioavailability and effects. Environ. Toxicol. Chem. 27, 1825–1851.

Kou, L., Sun, J., Zhai, Y., He, Z., 2013. The endocytosis and intracellular fate of nanomedicines: Implication for rational design. Asian J. Pharm. Sci. 8, 1–8. doi:10.1016/j.ajps.2013.07.001

Kreyling, W.G., Semmler, M., Erbe, F., Mayer, P., Takenaka, S., Schulz, H., Oberdörster, G., Ziesenis, A., 2002. Translocation of ultrafine insoluble iridium particles from lung epithelium to extrapulmonary organs is size dependent but very low. J. Toxicol. Environ. Heal. Part A 65, 1513–1530. doi:10.1080/00984100290071649

Kroto, H.W., Heath, J.R., O'brien, S.C., Curl, R.F., Smalley, E.R. (1985) Nature 318, 162.-163.

Kuempel, E.D., Tran, C.L., Castranova, V., Bailer, A.J., 2006. Lung Dosimetry and Risk Assessment of Nanoparticles: Evaluating and Extending Current Models in Rats and Humans. Inhal. Toxicol. 18, 717–724. doi:10.1080/08958370600747887

Kumar, A., Kumar, P., Anandan, A., Fernandes, T.F., Ayoko, G.A., Biskos, G., 2014. Engineered nanomaterials: Knowledge gaps in fate, exposure, toxicity, and future directions. J. Nanomater. 2014. doi:10.1155/2014/130198

Lam, C.-W., James, J.T., McCluskey, R., Arepalli, S., Hunter, R.L., 2006. A review of carbon nanotube toxicity and assessment of potential occupational and environmental health risks. Crit. Rev. Toxicol. 36, 189–217.

Lam, P.K., Chan, E.S.Y., Ho, W.S., Liew, C.T., 2004. In vitro cytotoxicity testing of a nanocrystalline silver dressing (Acticoat) on cultured keratinocytes. Br. J. Biomed. Sci. 61, 125–7.

Lankoff, A., Sandberg, W.J., Wegierek-Ciuk, A., Lisowska, H., Refsnes, M., Sartowska, B., Schwarze, P.E., Meczynska-Wielgosz, S., Wojewodzka, M., Kruszewski, M., 2012. The effect of agglomeration state of silver and titanium dioxide nanoparticles on cellular response of HepG2, A549 and THP-1 cells. Toxicol. Lett. 208, 197–213.

Lankveld, D.P.K., Oomen, a G., Krystek, P., Neigh, A., Troost-de Jong, A., Noorlander, C.W., Van Eijkeren, J.C.H., Geertsma, R.E., De Jong, W.H., 2010. The kinetics of the tissue distribution of silver nanoparticles of different sizes. Biomaterials 31, 8350–61.

Lansdown, A.B.G., 2007. Critical Observations on the Neurotoxicity of Silver. Crit. Rev. Toxicol. 37, 237–250. doi:10.1080/10408440601177665

Lesniak, A., Campbell, A., Monopoli, M.P., Lynch, I., Salvati, A., Dawson, K.A., 2010. Serum heat inactivation affects protein corona composition and nanoparticle uptake. Biomaterials 31, 9511–9518. doi:10.1016/j.biomaterials.2010.09.049

Levard, C., Hotze, E.M., Lowry, G. V, Brown, G.E., 2012. Environmental transformations of silver nanoparticles: impact on stability and toxicity. Environ. Sci. Technol. 46, 6900–14.

Lieber, M., Smith, B., Szakal, A., Nelson-Rees, W., Todaro, G., 1976. A continuous tumor-cell line from a human lung carcinoma with properties of type II alveolar epithelial cells. Int. J. cancer 17, 62–70.

Linse, S., Cabaleiro-Lago, C., Xue, W.-F., Lynch, I., Lindman, S., Thulin, E., Radford, S.E., Dawson, K.A., 2007. Nucleation of protein fibrillation by nanoparticles. Proc. Natl. Acad. Sci. 104, 8691–8696. doi:10.1073/pnas.0701250104

Liu, J., Hurt, R.H., 2010. Ion release kinetics and particle persistence in aqueous nano-silver colloids. Environ. Sci. Technol. 44, 2169–75. doi:10.1021/es9035557

Liu, W., Wu, Y., Wang, C., Li, H.C., Wang, T., Liao, C.Y., Cui, L., Zhou, Q.F., Yan, B., Jiang, G.B., 2010. Impact of silver nanoparticles on human cells: effect of particle size. Nanotoxicology 4, 319–30. doi:10.3109/17435390.2010.483745

Loeschner, K., Hadrup, N., Qvortrup, K., Larsen, A., Gao, X., Vogel, U., Mortensen, A., Lam, H.R., Larsen, E.H., 2011. Distribution of silver in rats following 28 days of repeated oral exposure to silver nanoparticles or silver acetate. Part. Fibre Toxicol. 8, 1–14.

Love, S.A., Liu, Z., Haynes, C.L., Kawagoe, K., Schroeder, T., Leszczyszyn, D., Near, J., Diliberto, E., Viveros, O., Janshoff, A., 2012. Examining changes in cellular communication in neuroendocrine cells after noble metal nanoparticle exposure. Analyst 137, 3004. doi:10.1039/c2an00034b

Lu, L., Fu, R., Li, C., Yu, C., Li, Z., Guan, H., Hu, D., Zhao, D., 2013. Silver nanoparticle/chitosan oligosaccharide/poly(vinyl alcohol) nanofibers as wound dressings: a preclinical study. Int. J. Nanomedicine 8, 4131. doi:10.2147/IJN.S51679

Lühmann, T., Rimann, M., Bittermann, A.G., Hall, H., 2008. Cellular Uptake and Intracellular Pathways of PLL-g-PEG-DNA Nanoparticles. Bioconjug. Chem. 19, 1907–1916.

Lunov, O., Syrovets, T., Loos, C., Beil, J., Delacher, M., Tron, K., Nienhaus, G.U., Musyanovych, A., Mailänder, V., Landfester, K., Simmet, T., 2011. Differential Uptake of Functionalized Polystyrene Nanoparticles by Human Macrophages and a Monocytic Cell Line. ACS Nano 5, 1657–1669. doi:10.1021/nn2000756

Luoma, S.N., 2008. Silver nanotechnologies and the environment: Old problems or new challenges? Proj. Emerg. Nanotechnologies, Woodrow Wilson Centre, Wa, DC, USA 72.

Luther, E.M., Koehler, Y., Diendorf, J., Epple, M., Dringen, R., 2011. Accumulation of silver nanoparticles by cultured primary brain astrocytes. Nanotechnology 22, 375101. doi:10.1088/0957-4484/22/37/375101

Luyts, K., Napierska, D., Nemery, B., Hoet, P.H.M., 2013. How physico-chemical characteristics of nanoparticles cause their toxicity: complex and unresolved interrelations. Environ. Sci. Process. Impacts 15, 23–38. doi:10.1039/C2EM30237C

Mailinder, V., Landfester, K., 2009. Interaction of Nanoparticles with Cells. Biomacromolecules 10, 2379–2400. doi:10.1021/bm900266r

Markley, J.L., Brüschweiler, R., Edison, A.S., Eghbalnia, H.R., Powers, R., Raftery, D., Wishart, D.S., 2017. The future of NMR-based metabolomics. Curr. Opin. Biotechnol. 43, 34–40. doi:10.1016/j.copbio.2016.08.001

Marques, M.R.C., Loebenberg, R., Almukainzi, M., 2011. Simulated Biological Fluids with Possible Application in Dissolution Testing. Dissolution Technol. 18(3), 15–28.

Martínez-Gutierrez, F., Thi, E., Silverman, J.M., Oliveira, C.C., Svensson, S.L., Vanden Hoek, A., Sánchez, E.M., Reiner, N.E., Gaynor, E.C., Pryzdial, E.L.G., Conway, E.M., Orrantia, E., Ruiz, F., Av-Gay, Y., Bach, H., 2012. Antibacterial activity, inflammatory response, coagulation and cytotoxicity effects of silver nanoparticles. Nanomedicine 8, 328–36.

Matorin, D.N., Karateyeva, A. V., Osipov, V.A., Lukashev, E.P., Seifullina, N.K., Rubin, A.B., 2010. Influence of carbon nanotubes on chlorophyll fluorescence parameters of green algae Chlamydomonas reinhardtii. Nanotechnologies Russ. 5, 320–327.

Mayor, S., Pagano, R.E., 2007. Pathways of clathrin-independent endocytosis. Nat. Rev. Mol. Cell Biol. 8, 603–612. doi:10.1038/nrm2216

Medina-Kauwe, L.K., 2007. "Alternative" endocytic mechanisms exploited by pathogens: New avenues for therapeutic delivery? Adv. Drug Deliv. Rev. 59, 798–809.

Mercer, J., Helenius, A., 2009. Virus entry by macropinocytosis. Nat. Cell Biol. 11, 510–520. Miclăuş, T., Bochenkov, V.E., Ogaki, R., Howard, K.A., Sutherland, D.S., 2014. Spatial Mapping and Quantification of Soft and Hard Protein Coronas at Silver Nanocubes. NanoLett. 14, 2086–2093. doi:10.1021/nl500277c

Milić, M., Leitinger, G., Pavičić, I., Zebić Avdičević, M., Dobrović, S., Goessler, W., Vinković Vrček, I., 2015. Cellular uptake and toxicity effects of silver nanoparticles in mammalian kidney cells. J. Appl. Toxicol. 35, 581–592. doi:10.1002/jat.3081

Mittermayer, F., Krepler, P., Dominkus, M., Schwameis, E., Sluga, M., Heinzl, H., Kotz, R., 2001. Long-term followup of uncemented tumor endoprostheses for the lower extremity. Clin. Orthop. Relat. Res. 167–77.

Mohan Kumar, K., Sinha, M., Mandal, B.K., Ghosh, A.R., Siva Kumar, K., Sreedhara Reddy, P., 2012. Green synthesis of silver nanoparticles using Terminalia chebula extract at room temperature and their antimicrobial studies. Spectrochim. Acta Part A Mol. Biomol. Spectrosc. 91, 228–233. doi:10.1016/j.saa.2012.02.001

Morimoto, Y., Kobayashi, N., Shinohara, N., Myojo, T., Tanaka, I., Nakanishi, J., 2010. Hazard assessments of manufactured nanomaterials. J. Occup. Health 52, 325–34.

Morones, J.R., Elechiguerra, J.L., Camacho, A., Holt, K., Kouri, J.B., Ramírez, J.T., Yacaman, M.J., 2005. The bactericidal effect of silver nanoparticles. Nanotechnology 16, 2346–53.

Muangman, P., Chuntrasakul, C., Silthram, S., Suvanchote, S., Benjathanung, R., Kittidacha, S., Rueksomtawin, S., 2006. Comparison of efficacy of 1% silver sulfadiazine and Acticoat for treatment of partial-thickness burn wounds. J. Med. Assoc. Thai. 89, 953–8.

Munger, M.A., Radwanski, P., Hadlock, G.C., Stoddard, G., Shaaban, A., Falconer, J., Grainger, D.W., Deering-Rice, C.E., 2014. In vivo human time-exposure study of orally dosed commercial silver nanoparticles. Nanomedicine Nanotechnology, Biol. Med. 10, 1–9. doi:10.1016/j.nano.2013.06.010

Mwilu, S.K., El Badawy, A.M., Bradham, K., Nelson, C., Thomas, D., Scheckel, K.G., Tolaymat, T., Ma, L., Rogers, K.R., 2013. Changes in silver nanoparticles exposed to human synthetic stomach fluid: Effects of particle size and surface chemistry. Sci. Total Environ. 447, 90–98.

Nadworny, P.L., Wang, J., Tredget, E.E., Burrell, R.E., 2010. Anti-inflammatory activity of nanocrystalline silver-derived solutions in porcine contact dermatitis. J. Inflamm. (Lond). 7, 13. doi:10.1186/1476-9255-7-13

Navarro, E., Baun, A., Behra, R., Hartmann, N.B., Filser, J., Miao, A.-J., Quigg, A., Santschi, P.H., Sigg, L., Baun, Æ.A., Behra, Æ.R., Hartmann, Æ.N.B., Filser, J., Antonietta, Æ.A.M.Æ., Peter, Q.Æ., 2008. Environmental behavior and ecotoxicity of engineered nanoparticles to algae, plants, and fungi. Ecotoxicology 17, 372–86. doi:10.1007/s10646-008-0214-0

Nayak, D., Ashe, S., Rauta, P.R., Kumari, M., Nayak, B., 2016. Bark extract mediated green synthesis of silver nanoparticles: Evaluation of antimicrobial activity and antiproliferative response against osteosarcoma. Mater. Sci. Eng. C 58, 44–52. doi:10.1016/j.msec.2015.08.022

Necula, B.S., 2013. Silver-based antibacterial surfaces for bone implants. doi:10.4233/uuid:f2523458-cb32-4c69-963e-da7b1e89ddd5

Nel, A., Xia, T., Mädler, L., Li, N., 2006. Toxic potential of materials at the nanolevel. Science 311, 622–7. doi:10.1126/science.1114397

Nel, A.E., Mädler, L., Velegol, D., Xia, T., Hoek, E.M. V., Somasundaran, P., Klaessig, F., Castranova, V., Thompson, M., 2009. Understanding biophysicochemical interactions at the nano–bio interface. Nat. Mater. 8, 543–557. doi:10.1038/nmat2442

Nemmar, A., Hoet, P.H.M., Vanquickenborne, B., Dinsdale, D., Thomeer, M., Hoylaerts, M.F., Vanbilloen, H., Mortelmans, L., Nemery, B., 2002. Passage of inhaled particles into the blood circulation in humans. Circulation 105, 411–4.

Nguyen, K.C., Seligy, V.L., Massarsky, a, Moon, T.W., Rippstein, P., Tan, J., Tayabali, a F., 2013. Comparison of toxicity of uncoated and coated silver nanoparticles. J. Phys. Conf. Ser. 429, 12025. doi:10.1088/1742-6596/429/1/012025

Nitin, C., Padmakar, D.K, Rodney A., Bruce JH., 2002. Control of Multiwalled Carbon Nanotube Diameter by Selective Growth on the Exposed Edge of a Thin Film Multilayer Structure. doi:10.1021/NL0257061

Nowack, B., Bucheli, T.D., 2007. Occurrence, behavior and effects of nanoparticles in the environment. Environ. Pollut. 150, 5–22. doi:10.1016/j.envpol.2007.06.006

Oberdörster, G., 2005. Nanomaterials, in: Inhaled Nano-Sized Particles: Potential Effects and Mechanisms. p. p 65-71.

Oberdörster, G., Maynard, A., Donaldson, K., Castranova, V., Fitzpatrick, J., Ausman, K., Carter, J., Karn, B., Kreyling, W., Lai, D., Olin, S., Monteiro-Riviere, N., Warheit, D.,

Yang, H., ILSI Research Foundation/Risk Science Institute Nanomaterial Toxicity Screening Working Group, 2005a. Principles for characterizing the potential human health effects from exposure to nanomaterials: elements of a screening strategy. Part. Fibre Toxicol. 2, 8. doi:10.1186/1743-8977-2-8

Oberdörster, G., Oberdörster, E., Oberdörster, J., 2005b. Nanotoxicology: an emerging discipline evolving from studies of ultrafine particles. Environ. Health Perspect. 113, 823–39.

Okpala, C.C., 2013. Nanocomposites – An Overview. Int. J. Eng. Res. Dev. 8, 2278–67.

Ostiguy, C., Cloutier, Y., Boutin, M., 2006. Nanoparticles, Actual knowledge about occupational health and safety risks and prevention measures.

Paddle-Ledinek, J.E., Nasa, Z., Cleland, H.J., 2006. Effect of different wound dressings on cell viability and proliferation. Plast. Reconstr. Surg. 117, 110S–118S; discussion 119S–120S. doi:10.1097/01.prs.0000225439.39352.ce

Pal, S., Tak, Y.K., Song, J.M., 2007. Does the antibacterial activity of silver nanoparticles depend on the shape of the nanoparticle? A study of the Gram-negative bacterium Escherichia coli. Appl. Environ. Microbiol. 73, 1712–20. doi:10.1128/AEM.02218-06

Paluri, S.L.A., 2011. Synthesis , Characterization and Manipulation of Creighton Silver Nanoparticles for Future Cytotoxicity Studies. B. Phamacy, Shri Vishnu Coll. Pharmacy, Pradesh, India 2009, Wright State Univ. 2011.

Panacek, A., Kvítek, L., Prucek, R., Kolář, M., Večeřová, R., Pizúrová, N., Sharma, V.K., Nevěčná, T., Zbořil, R., 2006. Silver Colloid Nanoparticles: Synthesis, Characterization, and Their Antibacterial Activity. J. Phys. Chem. B 110, 16248–16253. doi:10.1021/jp063826h

Park, E.J., Bae, E., Yi, J., Kim, Y., Choi, K., Lee, S.H., Yoon, J., Lee, B.C., Park, K., 2010.

Repeated-dose toxicity and inflammatory responses in mice by oral administration of silver nanoparticles. Env. Toxicol Pharmacol 30. doi:10.1016/j.etap.2010.05.004

Park, K., 2013. Toxicokinetic differences and toxicities of silver nanoparticles and silver ions in rats after single oral administration. J. Toxicol. Environ. Health. A 76, 1246–60. doi:10.1080/15287394.2013.849635

Park, K., Park, E.-J., Chun, I.K., Choi, K., Lee, S.H., Yoon, J., Lee, B.C., 2011. Bioavailability and toxicokinetics of citrate-coated silver nanoparticles in rats. Arch. Pharm. Res. 34, 153–8. doi:10.1007/s12272-011-0118-z

Pautke, C., Schieker, M., Tischer, T., Kolk, A., Neth, P., Mutschler, W., Milz, S., 2004. Characterization of osteosarcoma cell lines MG-63, Saos-2 and U-2OS in comparison to human osteoblasts. Anticancer Res. 24, 3743–8.

Pelkmans, L., Püntener, D., Helenius, A., 2002. Local Actin Polymerization and Dynamin Recruitment in SV40-Induced Internalization of Caveolae. Science (80). 296, 535–539.

doi:10.1126/science.1069784

Peralta-Videa, J.R., Zhao, L., Lopez-Moreno, M.L., de la Rosa, G., Hong, J., Gardea-Torresdey, J.L., 2011. Nanomaterials and the environment: a review for the biennium 2008-2010. J. Hazard. Mater. 186, 1–15. doi:10.1016/j.jhazmat.2010.11.020

Percival, S.L., Bowler, P.G., Dolman, J., 2007. Antimicrobial activity of silver-containing dressings on wound microorganisms using an in vitro biofilm model. Int. Wound J. 4, 186–191. doi:10.1111/j.1742-481X.2007.00296.x

Philip, D., 2010. Green synthesis of gold and silver nanoparticles using Hibiscus rosa sinensis. Phys. E Low-dimensional Syst. Nanostructures 42, 1417–1424. doi:10.1016/j.physe.2009.11.081

Phogat, N., Khan, S.A., Shankar, S., Ansary, A.A., Uddin, I., 2016. Fate of inorganic nanoparticles in agriculture. Adv. Mater. Lett. Adv. Mater. Lett 7, 3–12. doi:10.5185/amlett.2016.6048

Piao, M.J., Kang, K.A., Lee, I.K., Kim, H.S., Kim, S., Choi, J.Y., Choi, J., Hyun, J.W., 2011. Silver nanoparticles induce oxidative cell damage in human liver cells through inhibition of reduced glutathione and induction of mitochondria-involved apoptosis. Toxicol. Lett. 201, 92–100. doi:10.1016/j.toxlet.2010.12.010

Pishbin, F., Mouriño, V., Gilchrist, J.B., McComb, D.W., Kreppel, S., Salih, V., Ryan, M.P., Boccaccini, A.R., 2013. Single-step electrochemical deposition of antimicrobial orthopaedic coatings based on a bioactive glass/chitosan/nano-silver composite system. Acta Biomater. 9, 7469–7479. doi:10.1016/j.actbio.2013.03.006

Powers, R., 2014. The current state of drug discovery and a potential role for NMR metabolomics. J. Med. Chem. 57, 5860–70. doi:10.1021/jm401803b

Prokopovich, P., Perni, R., Leech, R., Carmalt, I.P., Parkin, S., 2013. A novel bone cement impregnated with silver–tiopronin nanoparticles: its antimicrobial, cytotoxic, and mechanical properties. Int. J. Nanomedicine 8, 2227. doi:10.2147/IJN.S42822

Pucadyil, T.J., Schmid, S.L., 2009. Conserved Functions of Membrane Active GTPases in Coated Vesicle Formation. Science (80). 325, 1217–1220. doi:10.1126/science.1171004

Rappoport, J.Z., 2008. Focusing on clathrin-mediated endocytosis. Biochem. J. 412, 415–423. doi:10.1042/BJ20080474

Ray, P.C., Yu, H., Fu, P.P., 2009. Toxicity and Environmental Risks of Nanomaterials: Challenges and Future Needs. J. Environ. Sci. Heal. Part C 27, 1–35. doi:10.1080/10590500802708267

Reidy, B., Haase, A., Luch, A., Dawson, K., Lynch, I., 2013. Mechanisms of Silver Nanoparticle Release, Transformation and Toxicity: A Critical Review of Current Knowledge and Recommendations for Future Studies and Applications. Materials (Basel). 6, 2295–2350. doi:10.3390/ma6062295

Rejman, J., Oberle, V., Zuhorn, I.S., Hoekstra, D., 2004. Size-dependent internalization of particles via the pathways of clathrin- and caveolae-mediated endocytosis. Biochem. J. 377, 159–69. doi:10.1042/BJ20031253

Roberts, J.R., McKinney, W., Kan, H., Krajnak, K., Frazer, D.G., Thomas, T. a, Waugh, S., Kenyon, A., MacCuspie, R.I., Hackley, V. a, Castranova, V., 2013. Pulmonary and cardiovascular responses of rats to inhalation of silver nanoparticles. J. Toxicol. Environ. Health. A 76, 651–68. doi:10.1080/15287394.2013.792024

Salvati, A., Åberg, C., dos Santos, T., Varela, J., Pinto, P., Lynch, I., Dawson, K.A., 2011. Experimental and theoretical comparison of intracellular import of polymeric nanoparticles and small molecules: toward models of uptake kinetics. Nanomedicine Nanotechnology, Biol. Med. 7, 818–826. doi:10.1016/j.nano.2011.03.005

Sanford, J., Venkatapathy, R., 2010. State of the Science Literature Review: Everything Nanosilver. U.s.enviromental Prot. Agency.

Takenaka, E.K., 2001. Pulmonary and systemic distribution of inhaled ultrafine silver particles in rats. Environ. Health Perspect. 109 Suppl, 547–51.

Sathyanarayana, S., Hübner, C., 2013. Structural Nanocomposites, Structural Nanocomposites. doi:10.1007/978-3-642-40322-4

Semmler, M., Seitz, J., Erbe, F., Mayer, P., Heyder, J., Oberdörster, G., Kreyling, W.G., 2004. Long-Term Clearance Kinetics of Inhaled Ultrafine Insoluble Iridium Particles from the Rat Lung, Including Transient Translocation into Secondary Organs. Inhal. Toxicol. 16, 453–459. doi:10.1080/08958370490439650

Shavandi, Z., Ghazanfari, T., Moghaddam, K.N., 2011. In vitro toxicity of silver nanoparticles on murine peritoneal macrophages. Immunopharmacol. Immunotoxicol. 33, 135–40. doi:10.3109/08923973.2010.487489

Sibbald, R.G., Browne, A.C., Coutts, P., Queen, D., 2001. Screening evaluation of an ionized nanocrystalline silver dressing in chronic wound care. Ostomy. Wound. Manage. 47, 38–43.

Slane, J., Vivanco, J., Rose, W., Ploeg, H.-L., Squire, M., 2015. Mechanical, material, and antimicrobial properties of acrylic bone cement impregnated with silver nanoparticles. Mater. Sci. Eng. C 48, 188–196. doi:10.1016/J.MSEC.2014.11.068

Smijs, T.G., Pavel, S., 2011. Titanium dioxide and zinc oxide nanoparticles in sunscreens: focus on their safety and effectiveness. Nanotechnol. Sci. Appl. 4, 95–112. doi:10.2147/NSA.S19419

Stern, S.T., McNeil, S.E., 2008. Nanotechnology Safety Concerns Revisited. Toxicol. Sci. 101, 4–21. doi:10.1093/toxsci/kfm169

Stoehr, L.C., Gonzalez, E., Stampfl, A., Casals, E., Duschl, A., Puntes, V., Oostingh, G.J., 2011. Shape matters: effects of silver nanospheres and wires on human alveolar epithelial cells. Part. Fibre Toxicol. 8, 36. doi:10.1186/1743-8977-8-36

Sun, R.W.-Y., Chen, R., Chung, N.P.-Y., Ho, C.-M., Lin, C.-L.S., Che, C.-M., 2005. Silver nanoparticles fabricated in Hepes buffer exhibit cytoprotective activities toward HIV-1 infected cells. Chem. Commun. 5059. doi:10.1039/b510984a

Sung, J.H., Ji, J.H., Park, J.D., Yoon, J.U., Kim, D.S., Jeon, K.S., Song, M.Y., Jeong, J., Han, B.S., Han, J.H., Chung, Y.H., Chang, H.K., Lee, J.H., Cho, M.H., Kelman, B.J., Yu, I.J., 2009. Subchronic inhalation toxicity of silver nanoparticles. Toxicol Sci 108. doi:10.1093/toxsci/kfn246

Sung, J.H., Jun Ho Ji, J.H., Kyung Seuk Song, K.S., Ji Hyun Lee, J.H., Kyung Hee Choi, K.H., Sang Hee Lee, S.H., Il Je Yu, I.J., 2011. Acute inhalation toxicity of silver nanoparticles. Toxicol. Ind. Health 27, 149–154. doi:10.1177/0748233710382540

Suresh, A.K., Pelletier, D.A., Wang, W., Morrell-Falvey, J.L., Gu, B., Doktycz, M.J., 2012. Cytotoxicity Induced by Engineered Silver Nanocrystallites Is Dependent on Surface Coatings and Cell Types. Langmuir 28, 2727–2735. doi:10.1021/la2042058

Taniguchi N. On the Basic Concept of Nano-Technology. Proc. Intl. Conf. Prod. Eng. Tokyo, Part II. Japan Society of Precision Engineering; 1974.

Tejamaya, M., Römer, I., Merrifield, R.C., Lead, J.R., 2012. Stability of Citrate, PVP, and PEG Coated Silver Nanoparticles in Ecotoxicology Media. Environ. Sci. Technol. 46, 7011–7017. doi:10.1021/es2038596

Teow, Y., Asharani, P. V, Hande, M.P., Valiyaveettil, S., 2011. Health impact and safety of engineered nanomaterials. Chem. Commun. (Camb). 47, 7025–38. doi:10.1039/c0cc05271j

Tervonen, T., Linkov, I., Figueira, J.R., Steevens, J., Chappell, M., Merad, M., 2009. Risk-based classification system of nanomaterials. J. Nanoparticle Res. 11, 757–766. doi:10.1007/s11051-008-9546-1

Thomsen, L.B., Lichota, J., Eskehave, T.N., Linemann, T., Mortensen, J.H., du Jardin, K.G., Moos, T., 2012. Brain delivery systems via mechanism independent of receptor-mediated endocytosis and adsorptive-mediated endocytosis. Curr. Pharm. Biotechnol. 13, 2349–54.

Tinkle, S.S., Antonini, J.M., Rich, B.A., Roberts, J.R., Salmen, R., DePree, K., Adkins, E.J., 2003. Skin as a route of exposure and sensitization in chronic beryllium disease. Environ. Health Perspect. 111, 1202–8.

Tolaymat, T.M., El Badawy, A.M., Genaidy, A., Scheckel, K.G., Luxton, T.P., Suidan, M., 2010. An evidence-based environmental perspective of manufactured silver nanoparticle in syntheses and applications: A systematic review and critical appraisal of peer-reviewed scientific papers. Sci. Total Environ. 408, 999–1006. doi:10.1016/j.scitotenv.2009.11.003

Toll, R., Jacobi, U., Richter, H., Lademann, J., Schaefer, H., Blume-Peytavi, U., 2004. Penetration profile of microspheres in follicular targeting of terminal hair follicles. J. Invest. Dermatol. 123, 168–76. doi:10.1111/j.0022-202X.2004.22717.x

Tolochko, N.K., 2009. History of nanotechnology, in: Nanosci. Nanotechnologies, Enciclopedia for Life Support Sysntems, Oxford. http://www.eolss.net.

Trickler, W.J., Lantz, S.M., Murdock, R.C., Schrand, A.M., Robinson, B.L., Newport, G.D., Schlager, J.J., Oldenburg, S.J., Paule, M.G., Slikker, W., Hussain, S.M., Ali, S.F., 2010. Silver Nanoparticle Induced Blood-Brain Barrier Inflammation and Increased Permeability in Primary Rat Brain Microvessel Endothelial Cells. Toxicol. Sci. 118, 160–170. doi:10.1093/toxsci/kfq244

Trop, M., Novak, M., Rodl, S., Hellbom, B., Kroell, W., Goessler, W., 2006. Silver-coated dressing acticoat caused raised liver enzymes and argyria-like symptoms in burn patient. J. Trauma 60, 648–52. doi:10.1097/01.ta.0000208126.22089.b6

Vlachou, E., Chipp, E., Shale, E., Wilson, Y., Papini, R., Moiemen, N.S., 2007. The safety of nanocrystalline silver dressings on burns: a study of systemic silver absorption. Burns 33, 979–85. doi:10.1016/j.burns.2007.07.014

Walczyk, D., Bombelli, F.B., Monopoli, M.P., Lynch, I., Dawson, K.A., 2010. What the Cell "Sees" in Bionanoscience. J. Am. Chem. Soc. 132, 5761–5768. doi:10.1021/ja910675v

Wang, C.-B., Zhang, W., 1997. Synthesizing Nanoscale Iron Particles for Rapid and Complete Dechlorination of TCE and PCBs. doi:10.1021/ES970039C

Wang, H., Wu, L., Reinhard, B.M., 2012. Scavenger Receptor Mediated Endocytosis of Silver Nanoparticles into J774A.1 Macrophages Is Heterogeneous. ACS Nano 6, 7122–7132.

Wang, X., Xia, T., Addo Ntim, S., Ji, Z., Lin, S., Meng, H., Chung, C.-H., George, S., Zhang, H., Wang, M., Li, N., Yang, Y., Castranova, V., Mitra, S., Bonner, J.C., Nel, A.E., 2011. Dispersal State of Multiwalled Carbon Nanotubes Elicits Profibrogenic Cellular Responses That Correlate with Fibrogenesis Biomarkers and Fibrosis in the Murine Lung. ACS Nano 5, 9772–9787. doi:10.1021/nn2033055

Wang, Z., Tiruppathi, C., Minshall, R.D., Malik, A.B., 2009. Size and Dynamics of Caveolae Studied Using Nanoparticles in Living Endothelial Cells. ACS Nano 3, 4110–4116.

Wijnhoven, S.W.P., Peijnenburg, W.J.G.M., Herberts, C.A., Hagens, W.I., Oomen, A.G., Heugens, E.H.W., Roszek, B., Bisschops, J., Gosens, I., Van De Meent, D., Dekkers, S., De Jong, W.H., Van Zijverden, M., Sips, A.J.A.M., Geertsma, R.E., 2009. Nano-silver: a review of available data and knowledge gaps in human and environmental risk assessment. Nanotoxicology 3. doi:10.1080/17435390902725914

Wilcox, M., Kite, P., Dobbins, B., 1998. Antimicrobial intravascular catheters—which surface to coat? J. Hosp. Infect. 38, 322–324. doi:10.1016/S0195-6701(98)90084-6

Wishart, D., Knox, C., Guo, A.C., Eisner, R., Young, N., Gautam, B., Hau, D., Psychogios, N., Dong, E., Bouatra, S., Mandal, R., Sinelnikov, I., Xia, J., Jia, L., Cruz, J.A., Lim, E., Sobsey, C, Shrivastava, S., Huang, P., Liu, P., Fang, L., Peng, J., Fradette, R., Cheng, D., Tzur, D., Clements, M., Lewis, A., De Souza, A., Zuniga, A., Dawe, M., Xiong, Y., Clive,

D., Greiner, R., Nazyrova, A., Shaykhutdinov, R., Li, L., Vogel,J., Forsythe, I., 2009. HMDB: a knowledgebase for the human metabolome. Nucleic Acids Res. 37, D603–D610.

Wright, J.B., Lam, K., Buret, A.G., Olson, M.E., Burrell, R.E., 2012. Early healing events in a porcine model of contaminated wounds: effects of nanocrystalline silver on matrix metalloproteinases, cell apoptosis, and healing. Wound Repair Regen. 10, 141–51.

Wright, J.B., Lam, K., Hansen, D., Burrell, R.E., 1999. Efficacy of topical silver against fungal burn wound pathogens. Am. J. Infect. Control 27, 344–50.

Xiu, Z., Zhang, Q., Puppala, H.L., Colvin, V.L., Alvarez, P.J.J., 2012. Negligible Particle-Specific Antibacterial Activity of Silver Nanoparticles. Nano Lett. 12, 4271–4275. doi:10.1021/nl301934w

Yang, E.-J., Kim, S., Kim, J.S., Choi, I.-H., 2012. Inflammasome formation and IL-1β release by human blood monocytes in response to silver nanoparticles. Biomaterials 33, 6858–6867. doi:10.1016/j.biomaterials.2012.06.016

Yang, X., Gondikas, A.P., Marinakos, S.M., Auffan, M., Liu, J., Hsu-Kim, H., Meyer, J.N., 2012. Mechanism of Silver Nanoparticle Toxicity Is Dependent on Dissolved Silver and Surface Coating in *Caenorhabditis elegans*. Environ. Sci. Technol. 46, 1119–1127. doi:10.1021/es202417t

Ye, J., Yao, Q., Mo, A., Nie, J., Liu, W., Ye, C., Chen, X., 2011. Effects of an antibacterial membrane on osteoblast-like cells in vitro. Int. J. Nanomedicine 6, 1853–61. doi:10.2147/IJN.S17749

Yen, H.-J., Hsu, S., Tsai, C.-L., 2009. Cytotoxicity and Immunological Response of Gold and Silver Nanoparticles of Different Sizes. Small 5, 1553–1561. doi:10.1002/smll.200900126

Yilma, A.N., Singh, S.R., Dixit, S., Dennis, V.A., 2013. Anti-inflammatory effects of silver-polyvinyl pyrrolidone (Ag-PVP) nanoparticles in mouse macrophages infected with live Chlamydia trachomatis. Int. J. Nanomedicine 8, 2421–32. doi:10.2147/IJN.S44090

Yin, H.Q., Langford, R., Burrell, R.E., 1999. Comparative evaluation of the antimicrobial activity of ACTICOAT antimicrobial barrier dressing. J. Burn Care Rehabil. 20,195–200.

Zhang, T., Wang, L., Chen, Q., Chen, C., 2014. Cytotoxic potential of silver nanoparticles. Yonsei Med. J. 55, 283–91. doi:10.3349/ymj.2014.55.2.283

Zhu, M.-T., Feng, W.-Y., Wang, Y., Wang, B., Wang, M., Ouyang, H., Zhao, Y.-L., Chai, Z.-F., 2009. Particokinetics and Extrapulmonary Translocation of Intratracheally Instilled Ferric Oxide Nanoparticles in Rats and the Potential Health Risk Assessment. Toxicol. Sci. 107, 342–351. doi:10.1093/toxsci/kfn245

Chapter II

Death and cell cycle progression are differently conditioned by the AgNP size in osteoblast-like cells

Part of this chapter was already published as:

Rosário F., Hoet P., Santos C., Oliveira H. (2016) Death and cell cycle progression are differently conditioned by the AgNP size in osteoblast-like cells. *Toxicology. 368, 103-115.* doi: 10.1016/j.tox.2016.08.020

Death and cell cycle progression is differently conditioned by the AgNP size in osteoblast- like cells

Rosário F [a,I], Hoet P [b], Santos C, Oliveira H [a]

[a] *CESAM & Laboratory of Biotechnology and Cytomics, Department of Biology, University of Aveiro, 3810-193 Aveiro, Portugal*

[b] *Occupational and environmental Toxicology, KU Leuven, Leuven, Belgium*
[c] *Department of Biology, Faculty of Sciences, University of Porto, Rua do Campo Alegre, Porto*

[I] *Corresponding author. E-mail address:* fe.rosario@ua.pt

Abstract

Silver nanoparticles (AgNPs) are useful to a wide range of consumer's and medical products, due to their antimicrobial and anti-inflammatory activities. AgNPs have been used to prevent the microbial colonization, therefore decreasing the risk of infection, on implantable devices, tumor prostheses, bone cement and surgical instruments. However, the putative toxicity of AgNPs to bone cells is still poorly understood. Therefore, this study aimed to contribute to enlighten the role of Ag^+ release of small sized NPs on the biological outcomes of bone cells, in particular to what concerns to induction of cytotoxic and genotoxic effects. To achieve that goal osteoblast-like MG-63 cells were exposed to well characterized PVP coated AgNPs of two different primary sizes (10 nm and 20 nm) and evaluated after 24 and 48h. Our results showed that, the smaller sized AgNPs (10 nm) are more reactive and prone to form large aggregates, being therefore mandatory to provide a careful characterization of the particles, before the toxicity assessment. We also demonstrate that for short period exposures (up to 48h) Ag^+ (from $AgNO_3$) is more toxic than the corresponding dose of AgNP. However, when assessing longer term exposures by the clonogenic assay, we demonstrated the inverse effect, the AgNPs turn out being more toxic, completely inhibiting plate efficiency. Therefore, AgNPs toxicity cannot be attributed to the dissociated Ag^+ alone. Also, when comparing size-dependent effects, we

demonstrate that AgNP20 were found to induce a cell cycle arrest at G_0/G_1 and apoptosis, while AgNP10 did not induce a cytostatic effect, but rather induced necrosis. Finally, combining the chemical and toxicological profiles of both AgNP sizes, we hypothesize that the size dependent AgNP toxicity may be associated in part with the NPs interference with the cell membranes and consequent uptake/adsorption processes.

Keywords: Silver nanoparticles, PVP-coating, Apoptosis, Necrosis, Cell cycle, Clonogenic assay

1. Introduction

Nanomaterials have at least one dimension with a length ranging from 1 to 100 nm, which provides a high surface/volume ratio, that leads to specific characteristics (e.g., Electrical and optical properties), compared to bulk materials (Chaloupka et al., 2010; Lewinski et al., 2008). These unique properties make MNPs useful to a wide range of fields and consequently being increasingly produced and released to the environment. Along with the constant discovery of new applications of MNPs, it was estimated that their production will increase to 58,000 metric tons per year until 2020 (Lewinski et al., 2008; Maynard, 2006) and the estimated global annual production of AgNPs is ~55 tons (Piccinno et al., 2012). So far, silver nanoparticles (AgNPs) are the most frequently used nanomaterial in consumers' products (435 products, or 24%) and also the most advertised nanomaterial component (207 products, or 14.5%), mostly due to their antimicrobial (Rai et al., 2009) and anti-inflammatory activities (Vance et al., 2015); see the Woodrow Wilson consumer products inventory (www.nanotechproject.org/cpi). For example, AgNPs are used in wound dressings and topical creams, acting as a potent anti-inflammatory agent which provided a major breakthrough for treatment of burns and various infections (Chaloupka et al., 2010; Feng et al., 2000; Sibbald et al., 2007; Tian et al., 2007). In addition, most medical devices are prone to bacterial adhesion and biofilm formation. Therefore, to protect and prevent from infections, these nanoparticles have been receiving much interest in the field of orthopedics, used as coating for implantable devices, (e.g., catheters, joint replacement prostheses) (Wilcox et al., 1998; Sibbald et al., 2001; Furno et al., 2004; Necula

2013), as coating of surgical instruments (Li et al., 2013a,b) and as additive compound in bone cement (Joseph et al., 2003). The use of AgNPs as additives in bone cements or prostheses has reduced the infection rates and also decreasing the joint replacement initial mortality of 2.7%–18% (Ahlberg et al., 1978; Alt et al., 2004; Joseph et al., 2003; Saravanan et al., 2011). In spite of the wide usage of AgNPs in the medical field, there is a distinct lack of information on the amount of silver ions (Ag^+) released from the products and it is not clear if their toxicity is attributed to NPs intrinsic toxicity and/or from the released ions (Kawata et al., 2009; Navarro et al., 2008). *In vivo* toxicity studies in rats demonstrated a distribution of AgNPs among lungs, liver, heart, kidney, spleen and brain after oral and blood administration of these NPs (Lankveld et al., 2010; Lee et al., 2013; Park et al., 2010a, 2011b). Few other studies described pulmonary toxicity after AgNPs up to 4 mg/m^3, inhalation and argyria-like symptoms after wound dressing usage on different organisms (Samberg et al., 2010; Stebounova et al., 2011; Sung et al., 2009; Trop et al., 2006). In addition, (Kim et al., 2008) found no genotoxicity after 28 days of oral administration up to 1 mg/kg of AgNP, despite a gender dependency in the accumulation of Ag in rat tissues. Moreover, Kim et al. (2011) found that after 28 days of inhalation up to $1.32x10^6$ AgNP particles/cm^3, there were no significant changes in the hematology and blood biochemical values in either the male or female rats. *In vitro* exposure to AgNPs also induced toxicity in several human cell lines. For example, it was observed a decrease of cell viability and cell proliferation in human liver cells (Piao et al., 2011) and keratinocyte cell line HaCaT (Zanette et al., 2011) after exposure up to 10 µg/mL and 333 µM, respectively. Also, AshaRani et al. (2009) found an increase in apoptosis and changes in cell cycle dynamics in normal human lung fibroblasts (IMR-90 cell line) and glioblastoma cells (U251) upon exposure to AgNPs. It was also documented an AgNP size-dependent toxicity effect, independently of the cell line (Gliga et al., 2014; Kim et al., 2012; Liu et al., 2010; Park et al., 2011a,b). For example, Kim et al. (2012) reported that the AgNPs cytotoxicity was size-dependent, stimulating apoptosis in the mice osteoblastic cell line MC3T3-E, but induced necrosis in mice adrenal medulla cells PC12. Liu et al. (2010) reported a decreased cytotoxicity (e.g., morphology, viability, membrane integrity) with increased AgNPs size (5, 20 and 50 nm) in four human cell models (A549, SGC-7901, HepG2 and MCF-7). Similarly, AgNPs (20, 80 and 113 nm) showed different toxicity (e.g., membrane damage) in mice L929 fibroblasts and in murine RAW264.7 macrophages

(Park et al., 2011a,b). Studies correlating AgNPs size with cytotoxicity used large size ranges with expectable different effects in the cell. It remains therefore unclear if AgNPs with smaller differences in size also differ in their toxicity levels and trigger different or similar pathways in the cell.

Despite metal and non-metal nanoparticles toxicity, has been widely studied *in vitro*, few studies focused on bone cells, including osteoblasts (human CRL-11372 cell line) exposed to alumina and TiNPs (Gutwein & Webster 2002), pre-osteoblasts (mice L929 and MC-373 cell lines) exposed to TiO_2 (Bernier et al., 2012) and osteoblast-like (human MG-63) exposed to TiO_2 (Bacakova et al., 2007; Niu et al., 2012). Also, a cell line retaining osteosarcoma behavior (mice UMR 106) were exposed to TiO_2 and Al_2O_3 (Virgilio et al., 2010; Gerhardt et al., 2007).

However, despite its importance to prosthesis and dental surgery, AgNP cytotoxicity has not been addressed in bone cells. The few available studies (Cao et al., 2011; De Giglio et al., 2013; Ye et al., 2011) used embedded AgNPs, which therefore masks the putative toxicities due to AgNPs alone, as well as the effective release of Ag^+ from these NPs. To our knowledge, until now, there are no studies reporting the toxic potential of different-sized AgNP to bone cells and the role of subsequent Ag^+ dissociation on their toxicity. In the current work we hypothesize that even minimal differences on AgNPs size are sufficient to induce different toxicity profiles and may differently condition the pathways involved in cell death response. For that, we exposed the osteoblast-like cell line MG-63 to small size AgNPs (10 and 20 nm) and to $AgNO_3$ (control for Ag^+). Different cell parameters were investigated: uptake of AgNP, cell viability and proliferation, cell-cycle dynamic, micronuclei induction and apoptosis and necrosis. Also, we aimed to determine the contribution of Ag^+ (due to AgNP dissociation) on the toxicity of AgNPs.

2. Materials and Methods

Silver nanoparticles and physicochemical characterization

Sterile, purified and endotoxin-free AgNPs (Biopure AgNPs 1.0 mg/mL) with polyvinylpyrrolidone (PVP) coating and nominal size of 10 nm and 20 nm (here designated as AgNP10 and AgNP20, respectively), were obtained by NanoComposix Europe (Prague, Czech Republic). Morphology and size were analyzed by scanning electron microscopy (SEM -

Hitachi, model SU-70, Japan). Approximately 10µL of each stock solution was added to a carbon sheet and let dry, on atmospheric conditions. After the samples were dry, the SEM images were taken. Later, analyzed with *KLONK* Image Measurement software (https://www.imagemeasurement.com/en/). The hydrodynamic diameter of nanoparticles in culture medium 1h and 24h after preparation were measured by Dynamic light scattering (DLS) using a Malvern Zetasizer Nano ZS (Malvern I, UK). Hydrodynamic size from samples with heterogenic sizes, where presented by the mean size of the peak with the highest percentage.

Putative dissociation of silver ions from AgNPs with time was measured. For that, AgNP10 and AgNP20 suspensions in culture medium (0, 50, 100 µg/mL) were prepared and incubated for 1h, 24h and 48h in culture conditions (controlled humid atmosphere at 37 °C and 5% CO_2). After each time point, the samples were collected and ultracentrifuged (40000g for AgNP10 and 25000g for AgNP20) in order to separate the nanoparticles from the supernatant that contains the dissociated Ag^+. The supernatant (300µL) was diluted in 2700mL of ultra-pure water and it was digested with *aqua regia* solution (HNO_3 (68%): HCL (37%)). The Ag^+ content in solution was determined by inductively coupled plasma mass spectrometry (ICP-MS Thermo X Series)

Cell Culture

The human osteosarcoma MG-63 cell line (ATCC, Manassas, VA, USA) was cultured in complete growth medium (α-Minimum Essential Medium supplemented with 10% (v/v) fetal bovine serum (FBS), 2.5 µg/mL penicillin-streptomycin and 2.5µg/mL fungizone) (all medium components from Life Technologies, Carlsbad, CA, USA) at 37 °C, 5% CO_2, in a humidified atmosphere. Cell confluence and morphology were daily observed under an inverted phase contrast microscope Nikon Eclipse TS100 (Japan). Cells were subcultured when confluence reached 80% using 0.25% trypsin/1 mM EDTA (Life Technologies, Carlsbad, CA, USA). Depending on the assay, cells were seeded in 96, or 6 well plates and left 24h for adhesion. After that the culture medium was replaced with fresh medium containing AgNP solutions. MG-63 cells were cultured in the referred conditions for 24h and 48h.

AgNP and $AgNO_3$ treatments

Cells were seeded (10^5cells/mL) in 6-well plates (or in 96-well microplates for the MTT assay) and incubated for 24h to adhere under the culture conditions described above. After that period, the medium was removed and replaced by the same amount of complete medium containing AgNP (0µg/mL to 100µg/mL) or $AgNO_3$ (0µg/mL to 20µg/mL). The dose of $AgNO_3$ was calculated based on Ag^+ mass and expressed as $AgNO_3$. AgNPs dilutions in complete α-MEM medium were sonicated for 20 minutes before cell exposure. MG-63 cells were exposed for 24h and 48h, in the conditions described above. Cells were daily checked with an inverted microscope (Nikon Eclipse TS100, Tokyo, Japan).

Uptake potential by flow cytometry

Uptake potential of AgNP10 and AgNP20 by the cells was assessed by flow cytometry (FCM), according to Suzuki et al. (2007). MG-63 cells were seeded in 6-well plates for 24h and 48h exposure to AgNPs cells were trypsinized, collected to FCM tubes and analyzed in a Coulter XL Flow Cytometer (Beckman Coulter, Hialeah, FL-USA) equipped with an argon laser (15 mW, 488 nm). Acquisitions were made using SYSTEM II software v. 3.0 (Beckman Coulter, Hialeah, FL). For each sample, 10000–20000 cells were analyzed. The uptake of AgNPs was measured by the side-scatter (SS) analysis which gives information on the cell complexity.

Cell viability

Cell viability was determined using the MTT assay, according to Lévesque et al. (2008) with some modifications. This assay measures mitochondrial dehydrogenase activity of viable cells activity by the reduction of 3-(4,5-dimethylthiazol-2-yl)-2,5-diphenyltetrazolium bromide to water-insoluble blue formazan crystals. After AgNP exposure (24h and 48h), 50 mL of MTT (1 mg/mL in PBS pH 7.2) (Sigma Aldrich, USA) was added to each well and incubated for 4 h at normal culture conditions. After that, the medium was replaced by 150 mL of dimethyl sulfoxide (DMSO) and plates were placed on a shaking plate for two hours in the dark to solubilize the formazan crystals. Then the optical density of reduced MTT was measured at 570 nm in a microtiter plate reader (Synergy HT Multi-Mode, BioTek Instruments, Winooski, VT) with blank correction. Also, the background absorbance of AgNP solutions was assessed in order to

correct possible assay interferences. The 50% inhibition concentration (IC50) of AgNPs exposed to MG-63 cells for 24h and 48h, was estimated based on the MTT assay results.

Clonogenic Assay

A colony formation assay (i.e., clonogenic assay) was performed as described previously (Franken et al., 2006). Briefly, MG-63 cells were seeded at 50 cells/mL in 6-well plates and after 24h for cell adhesion they were treated for 7 and 14 days with Ag equivalent doses (ranging between 5 and 50 µg/mL) supplied in $AgNO_3$ and AgNP10 and AgNP20. To assay the putative toxicity of dissociated Ag^+ released from AgNPs (from now on denominated "dissociated Ag"), cells were also exposed to supernatant containing the dissociated Ag prepared as described above. Cells were washed with PBS, fixed and stained with a mixture of 0.5% crystal violet (Sigma, USA) in 70% ethanol. Colonies with more than 30 cells were counted. Also, plating efficiency (PE) and surviving factor (SF) were calculated. PE is the average of three independent countings for each dilution A and B, divided by the number of cells plated; SF is expressed as percentage and it is determined by dividing the PE of the treated cells by the PE of the controls, and then multiplying by 100.

Cell Cycle Analysis – Flow Cytometry

Cell cycle analysis was performed according to Oliveira et al. (2014). Cells were seeded in 6-well plates and exposed to AgNPs at 0, 50, 100 µg/mL for 24h and 48h. For each concentration, tree replicates were used. At the end of treatments, cells were trypsinized and centrifuged at 300g for 5 min. The supernatant was discarded, and the cultures were washed with PBS pH 7.2. Cells were then resuspended in cold 85% ethanol for fixation and stored at -20ºC until further analysis. At the time of analysis, cells were centrifuged at 300g for 5 min, resuspended in 1 mL PBS, and filtered through a 55 µm nylon mesh to remove big clusters. Then, 50 µg/mL of propidium iodide (PI) (Sigma Aldrich, St. Louis, MO, USA) and 50 mg/mL of RNAse were added (Sigma Aldrich, St. Louis, MO, USA) to stain nuclear DNA and remove RNA from the samples, respectively. Samples were incubated for 20 min in the dark. Relative fluorescence intensity was measured in a Coulter Epic XL flow cytometer (Beckman Coulter, Hialeah, FL) equipped with an argon laser – 15 mW, 488 nm. The fluorescence peak sample of G_0/G_1 cells

adjusted to channel 200. Acquisitions were made using SYSTEM II software (Beckman Coulter, Hialeah, FL). For each sample, the number of events reached approximately 5000. Debris and doublets were excluded by the definition of the specific region (Area vs. FL peak height). For each sample approximately 5000 nuclei were analyzed. Cell cycle analysis was then conducted based on the histogram outputs (Oliveira et al., 2006). The percentage of nuclei in each phase of the cell cycle (G_0/G_1, S and G_2 phases) was analyzed using the FlowJo software (Tree Star Inc., Ashland, Oregon, USA).

Apoptosis – Annexin V Assay

Apoptosis was measured by flow cytometry using the FITC Annexin V Apoptosis Detection Kit, from BD Pharmingen™ (BD Pharmingen, San Diego, CA, USA) following the manufacturer instructions. The double staining allows the differentiation from early-stage apoptotic cells (Annexin V-FITC (+)/PI (-) cells), from late-stage apoptotic/necrotic cells (Annexin V-FITC (+)/PI (+)) and live cells (Annexin V-FITC (-)/PI (-)). At the end of exposure, cells were trypsinized and transferred to 15mL tubes. Afterwards, cells were centrifuged twice in cold PBS and resuspended in binding buffer provided by the kit. Then, $1x10^5$cells were incubated in the dark for 15 min after addition of 5µl Annexin V-FITC and 5µl PI. Afterwards, 400µL of binding buffer were added and samples immediately analyzed in a Coulter XL Flow Cytometer (Beckman Coulter, Hialeah, FL-USA). Acquisitions were made using SYSTEM II software (v. 3.0, Beckman Coulter, USA). For each sample, 10000 events were analyzed, and the percentages were calculated from the number of cells in each quadrant divided by the total number of cells.

Cytokinesis-block micronucleus (CBMN) assay

CBMN assay was performed as described in (Fenech 2005), with some modification. Briefly, $1x10^6$ per well were seeded on coverslips onside 6 well plates. Cells were then exposed to AgNPs as described above. A positive control was performed with methyl methanesulfonate (MMS) at a final concentration of 20 g mL^{-1}. After 24h exposure, cytochalasin B (AppliChem, Darmstadt, Germany) was added to each well with further 35 h incubation. At the end of treatment, cells were washed with PBS, and subsequently 1 mL of absolute methanol at 4ºC was

added to fix the cells. Coverslips were air dried and stained with acridine orange (Merck, USA). Cells were observed and analyzed under a fluorescence microscope Nikon Eclipse 80i (Nikon, Tokyo, Japan) equipped with an acridine orange-compatible filter. Fluorescence images were captured with a Digital Sight camera, software NIS-Elements F 3.00 SP7 (Nikon, Tokyo, Japan). Samples were then scored for nuclear division index (NDI), presence of nucleoplasmic bridges (NPBs), micronuclei (MN) and cells under apoptosis and necrosis. NDI provides a measure of viable cells' proliferative status and also enables the detection of cytostatic effects. It was calculated by scoring at least 500 cells for the presence of one, two, three or four nuclei. NPBs and MN were scored in at least 1000 binucleated cells. The apoptosis and necrosis assessment were conducted on the slides by scoring at least 500 cells.

Statistical Analysis

For all experiments, at least 3 replicates, and 3 independent assays were performed. Data analysis was performed in the software SigmaPlot version 11, by one-way ANOVA analysis of variance (One-way ANOVA) ($p < 0.05$), using Dunn's-test or Dunnett-test, respectively, for non-parametric or parametric data, to evaluate the significance of differences in the parameters. Correlations between results from different assays, where analyzed by Pearson's correlation.

3. Results

Stability of AgNPs in culture medium

Morphology and size were analyzed by scanning electron microscopy. SEM images from the stock of AgNP10 showed the primary particle size of 10 nm ±1, with a unimodal size distribution (Fig.1 - B). SEM analysis of AgNP20 showed a heterogeneous size distribution (Fig.1 - C), which present the peaks are approximately at 10 and 20 nm and the particle size mean of the population is 15±5 nm (Fig.1 - D). Hydrodynamic size from AgNPs was analyzed using Zetasizer Nano ZS and presented in Table 1. Table 1 shows the hydrodynamic diameter of AgNPs dispersed in culture medium and incubated for 1 h and 24h. Data show that the AgNPs exhibit an agglomeration behavior dependent on NP size, concentration and time point. AgNP20 showed a less tendencyto aggregate at t = 1 and t = 24h (Table 1) than AgNP10. AgNP10 after

1 h for 50 µg/mL showed 53.02 nm and in the higher concentration showed a 136.8 nm size. After 24h, at the higher concentration AgNP10 increased to 378.9 nm size. For AgNP20 for both times, the medium size was 44 nm for both 50 µg/mL and 100 µg/mL. The Ag dissociation from AgNPs to the medium was measured by ICP-MS.

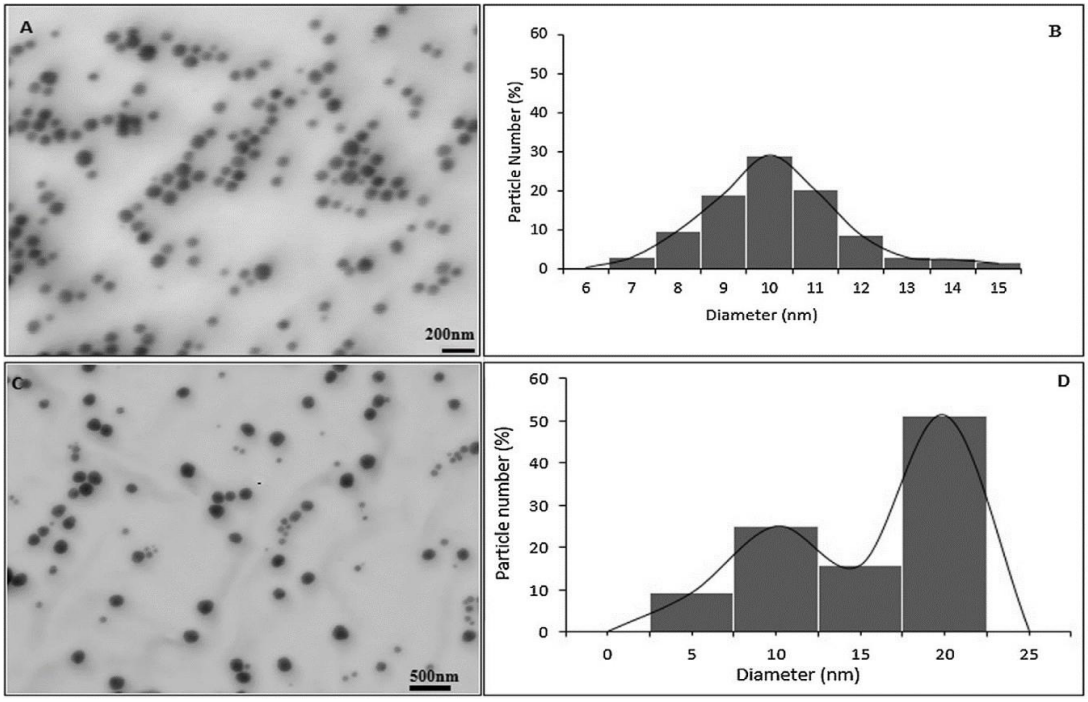

Figure 1 – SEM results for primary size and population distribution size, of AgNP10 and AgNP20 nm dispersed in (Ultra-pure) water. A) Representative image of AgNP10 stock, B) Particle size distribution, determined via image analysis with ImageJ, for AgNP10, C) Representative image of AgNP20 stock, D) Particle size distribution, determined via image analysis with ImageJ, AgNP20.

Table 1 – DLS measurements of hydrodynamic diameter (nm) of AgNP10 and AgNP20 in culture medium, 1 and 24h after preparation (t = 1 and t = 24h) of the following solutions: 10, 50 and 100 µg/mL. Solutions were prepared by dilution with complete growth media – F-12K – 10% FBS. In the presence of more than one peak of size distribution, the peak of highest percentage (and the respective percentage) is shown.

	Average size[a]	**Hydrodynamic diameter (nm) in α-MEM medium**		
		10µg/mL	50µg/mL	100µg/mL
1h	**10 nm**	45.66 (62%)	53.02	136.8
24h	**10 nm**	40.39 (48%)	51.83	378.9
1h	**20 nm**	49.77 (85%)	51.04	49.55
24h	**20 nm**	46.41	44.64	44.93

[a] According to the manufacturer nanoComposix (Biopure)

Fig.2 show the Ag^+ quantification in culture medium after 0 h, 24h and 48h cell-free incubation. An increase in the release of ionic silver was seen after 24h, at 48h the amount of free Ag^+ was lower except for the highest AgNP10 (100 µg/mL) which showed a time dependent increase in the release of Ag^+.

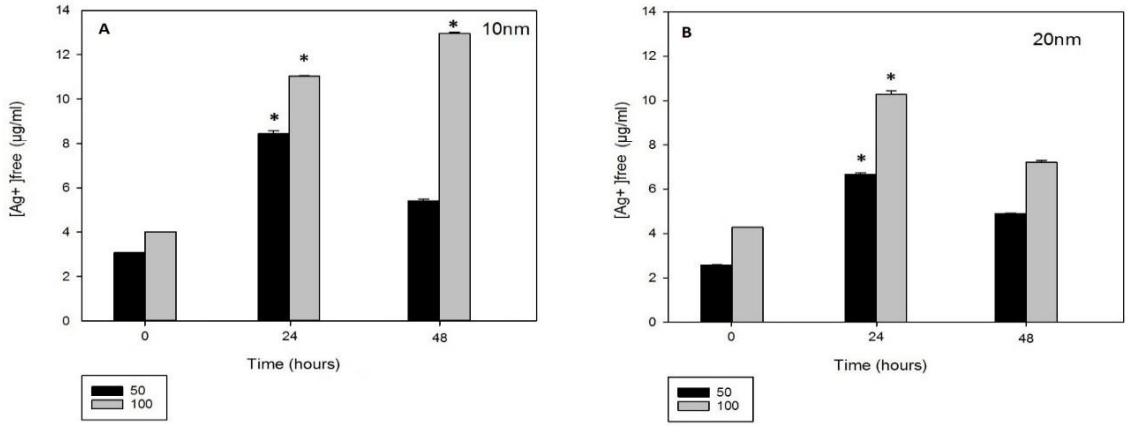

Figure 2 – Amount of free dissociated Ag^+ for 50 µg/mL and 100 µg/mL, obtained by ICP-MS, at different time points for both AgNP10 (A) and AgNP20 (B). * Indicate significant differences between time 0 and 24h and 48h.

MTT Assay

Fig.3 shows the dose-response for cell viability for MG-63 for 24 and 48h, measure by the MTT assay. Upon exposure to AgNP10 there was a significant decrease on cell viability for 50 µg/mL and at 100 µg/mL, at both time points. For AgNP20 there was only a decrease at 100 µg/mL after 24h and a four-fold decrease after 48h (Fig.3 - B). The IC50 values obtained by Sigmaplot analysis for 48h, were 58.3 µg/mL for AgNP10 and 93.9 µg/mL for AgNP20. $AgNO_3$ data revealed more severe toxic effects, comparatively to those obtained for AgNPs, despite the trend is similar to the one observed for AgNP20, with an abrupt decrease in viability observed for both conditions at around 80 µg/mL and around 17 µg/mL for AgNP20 and $AgNO_3$, respectively (Fig.3 & 4). For $AgNO_3$, the IC50 value was 18.54 µg/mL. Based on the IC50 values for 24h, 50 µg/mL and 100 µg/mL were chosen to perform the other assays (clonogenic, Annexin-V, uptake, cell cycle profile). Both 50 and 100 µg/mL correspond to the doses closer to the IC50 values found, respectively, for AgNP10 (IC50 = 58.3 µg/mL) and AgNP20 (IC50 = 93.9 µg/mL).

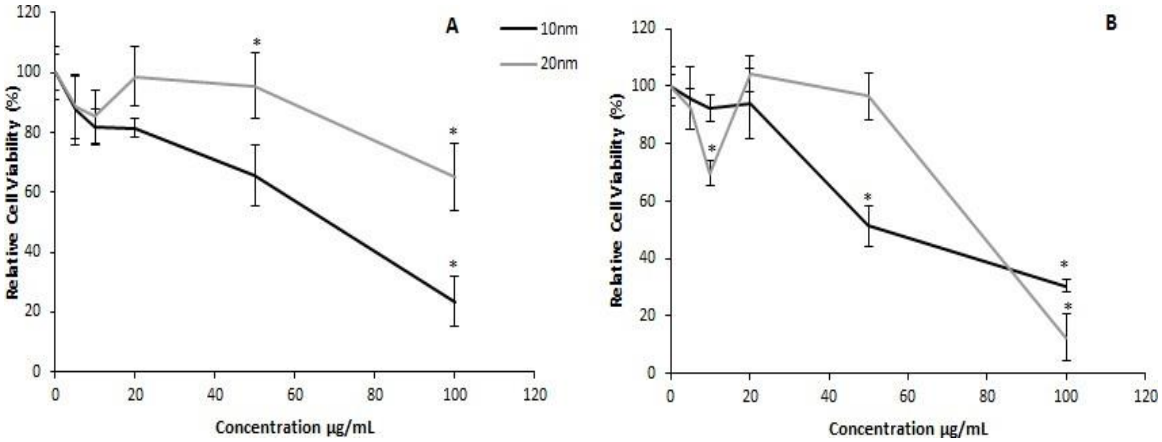

Figure 3 – Results of cell viability from MTT assay for AgNP10 and AgNP20 exposures of MG-63 cell line, after withdraw of background nanoparticles absorbance's, for A) 24h and B) 48h. * Indicate significant differences between control and AgNP concentrations ($p < 0.05$).

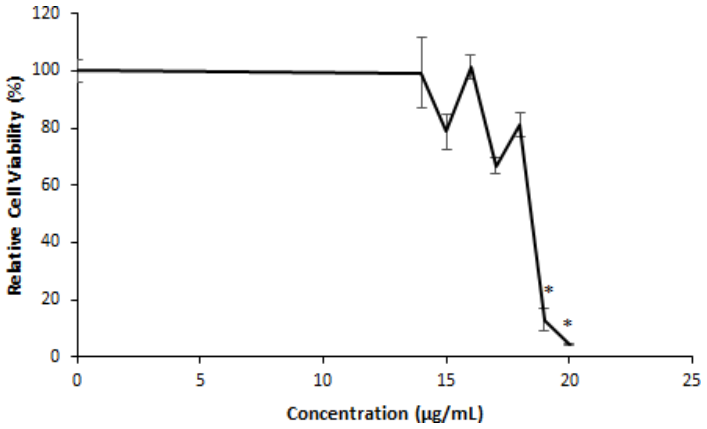

Figure 4 – Effects $AgNO_3$, in MG-63 cell viability (mean ± SD) for 24h exposure, evaluated by three independent MTT assays. *Indicates significant differences between Ag concentrations and control ($p < 0.05$).

Clonogenic assay

To investigate the proliferative capacity of cells for longer periods we used the clonogenic assay. Due to the nature of this assay, we used lower cell seeding density and lower doses of AgNPs (ranging from 5 to 50 µg/mL). Data showed a complete inhibition on colony formation for both time points (7 and 14 days) under exposure to 5–50 µg/mL, and for that only data for 7 days is

shown (Fig.5). Our results indicate that upon exposure to AgNPs there was no colony forming capacity.

The effects of $AgNO_3$ on the proliferative capacity of MG-63 cells was also evaluated at 5 µg/mL and 20 µg/mL. After 7 days of exposure to 5 µg/mL $AgNO_3$, the PE significantly decreased to around 11%, being fully inhibited at 20 µg/mL (Fig.5). The clonogenic assay as also been tested for the dissociated Ag^+ in the supernatant (from AgNPs at 50 µg/mL and 100 µg/mL) obtained from both AgNP10 AgNP20. PE was determined after 1, 24 and 48h, with evident decrease on the proliferative capacity especially after 24h for both AgNP10 and AgNP20 (Fig.6). While the control showed a linear trend to increase, the cells exposed to all ultracentrifuged solutions showed a polynomial trend with minimum values at 24h.

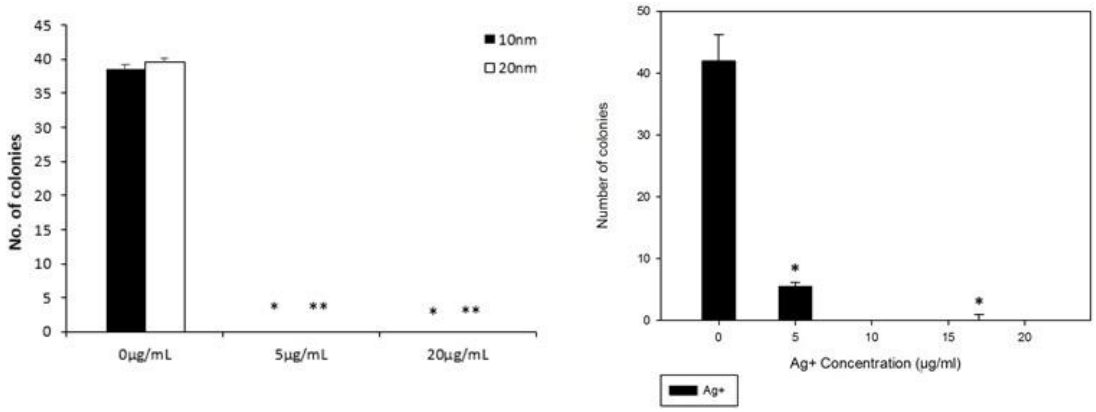

Figure 5 – Cytotoxicity of AgNP exposures determined by the Clonogenic assay in MG-63 cells, after 7 days of exposure. * and ** indicates significant differences between control and AgNP concentrations.

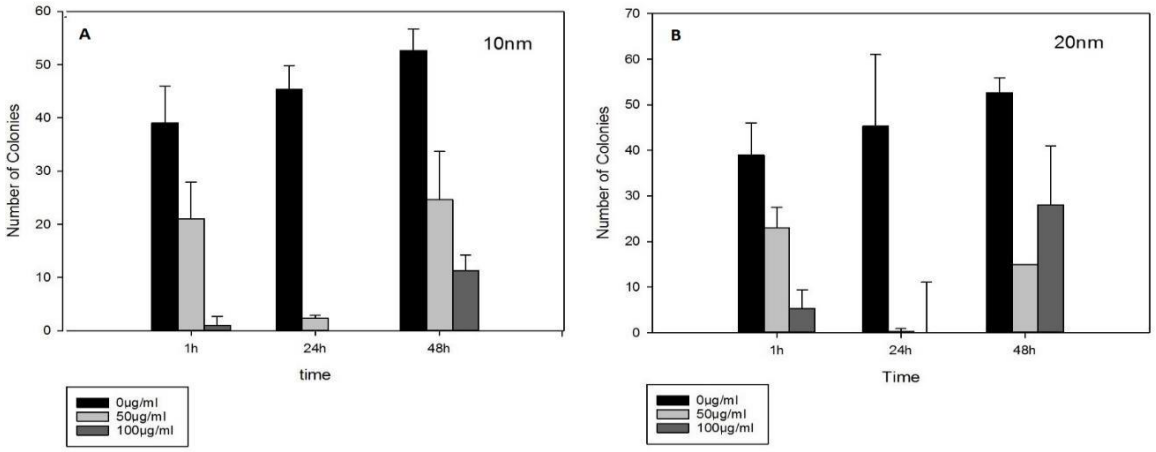

Figure 6 – Cytotoxicity of ICP-MS dissociated Ag^{+} supernatant from 1h, 24h and 48h incubation, determined by Clonogenic assay in MG-63 cell line. (A) AgNP10 and (B) AgNP20.

AgNP uptake

Uptake potential of AgNP10 and AgNP20 by MG-63 cells was assessed by flow cytometry (FCM). Flow cytometry data showed a significant increase on side scatter signal intensity (SS), which corresponds to an increase in the uptake of AgNP by MG-63 after 24h and 48h for both AgNP sizes (Fig.7). Except for AgNP10 at 100 µg/mL for 24h exposure, the SS of all treatments were significantly higher than the control.

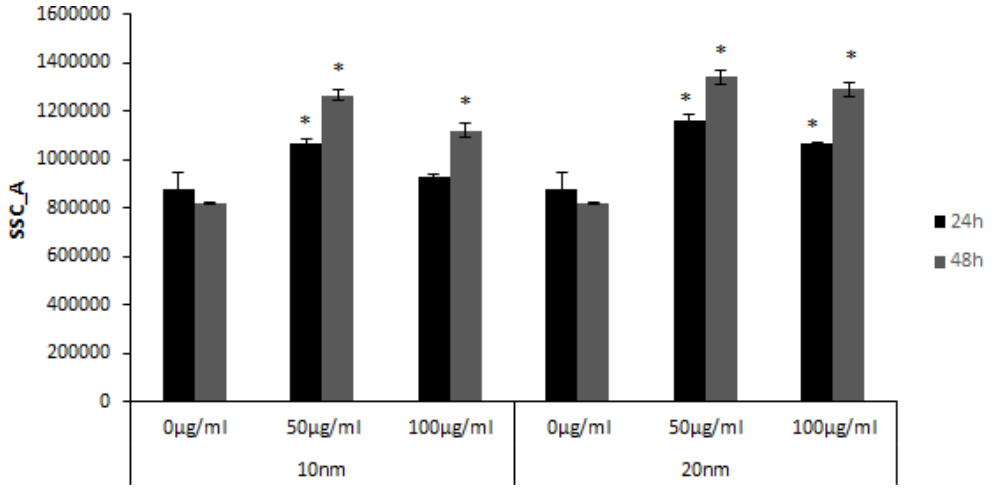

Figure 7 – Uptake of AgNP by MG-63 cell line, obtained by flow cytometry, after exposure for 24h and 48h to AgNP10 and AgNP20. * Indicate significant differences between control and AgNP concentrations ($p < 0.05$).

Cell cycle analysis

Cell cycle changes after AgNPs exposure, were investigated by FCM (Fig.8). Fig.9 (A) shows the influence of AgNP10 and AgNP20 on MG-63 cells cycle dynamics after 24h of exposure. Control cells show a typical profile of proliferation at the time point with most dominant subpopulations at G_0/G_1 (47%) and at G_2 (30%) together with a high rate of cells at S-phase. After 24h, both NPs sizes induced a significant increase on sub-G_1 cell population at 50 and 100 µg/mL. After 48h, AgNP10 only increased the sub-G_1 population, while AgNP20 also increased the percentage of cells arrested at G_0/G_1 at expenses of the two other phases, particularly S phase (Fig.9 - B).

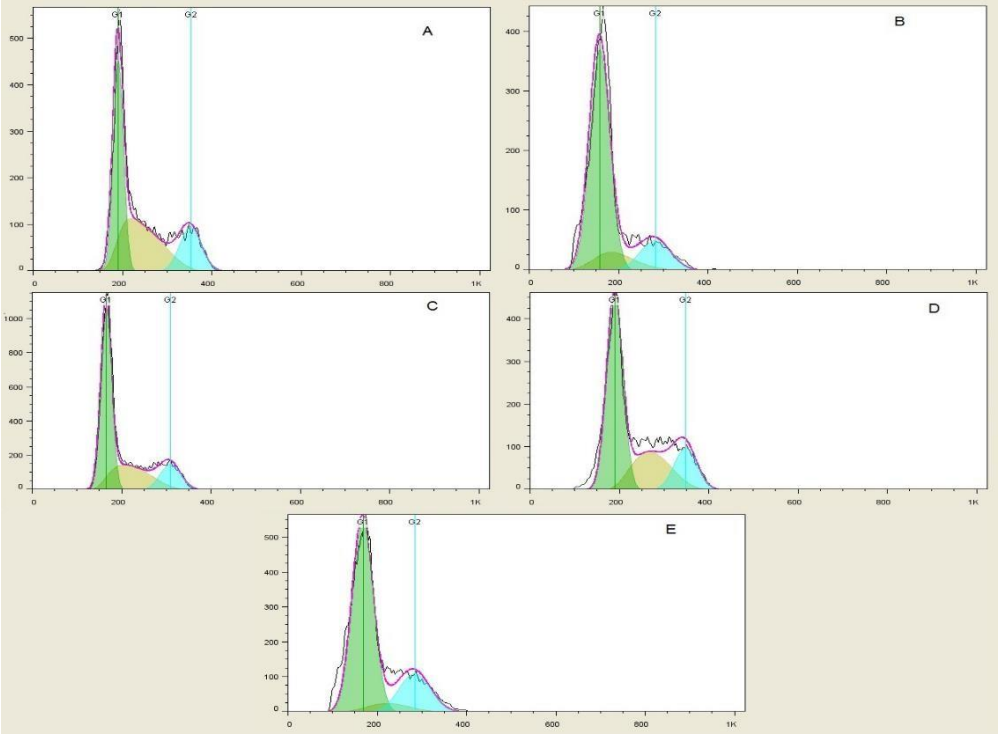

Figure 8 – Representative histograms of MG-63 cells DNA content after exposure to AgNP10 and AgNP20 for 24h and 48h. (A) 24h control, (B) 24h exposure to 100 µg/mL AgNP20, (C) 48h control, (D) 48h exposure to 50 µg/mL AgNP10 and (E) 48h exposure to 50 µg/mL AgNP 20. Colors show areas of curve corresponding to, green – G_0/G_1, yellow – S, and Blue – G_2/M.

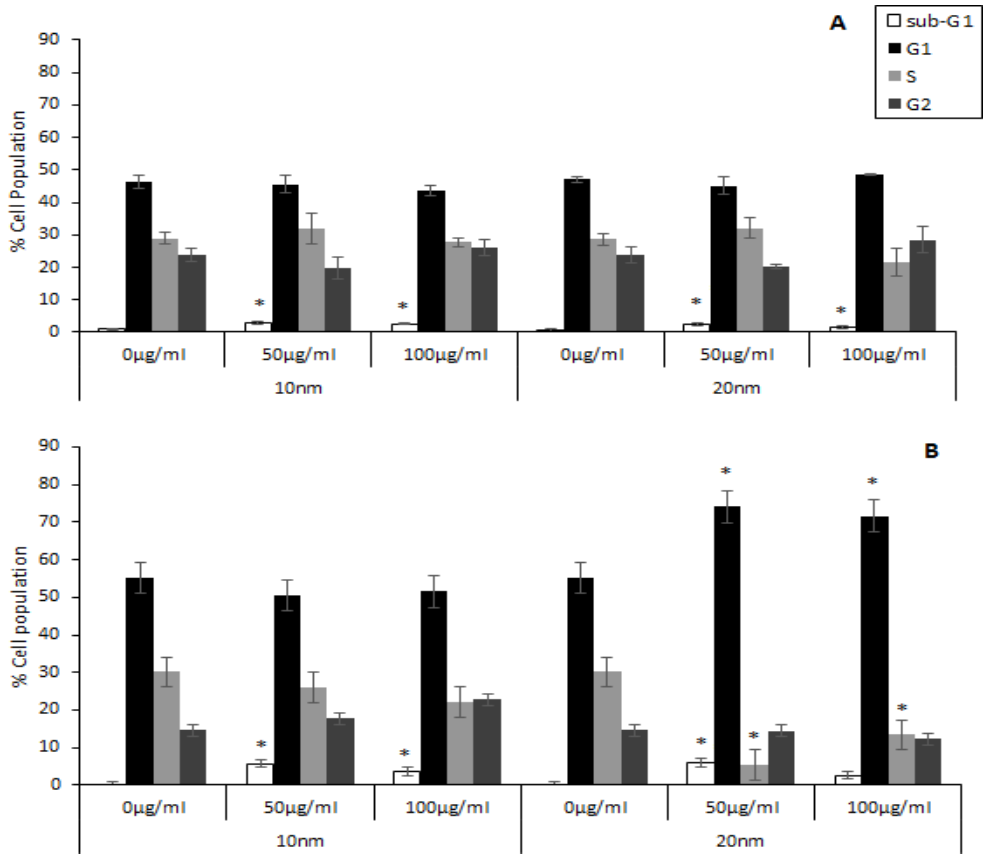

Figure 9 – Cell cycle results of MG-63 cells exposed to AgNP10 and AgNP20 for A) 24h and B) 48h. The given values are the mean % of cell population (± standard deviation) along cell cycle stages of at least 3 replicates. * Indicates differences between control and concentrations at $p < 0.05$.

ANNEXIN V Assay

We investigated the cell death by flow cytometry using the FITC Annexin V assay. After 24h exposure, the annexin-V assay data showed no significant differences in the percentage of cells under apoptosis or necrosis for both AgNP sizes, comparatively to the control (Fig.10 - A). After 48h, there was an increase in the percentage of necrotic cells for the highest concentration of AgNP10, while apoptosis was no affected (Fig.10 - B). For AgNP20, the late apoptosis was increase for 50 µg/mL along with a decrease on the number of cells on early apoptosis (Fig.10 – D). No significant changes were found for necrosis at this AgNP size.

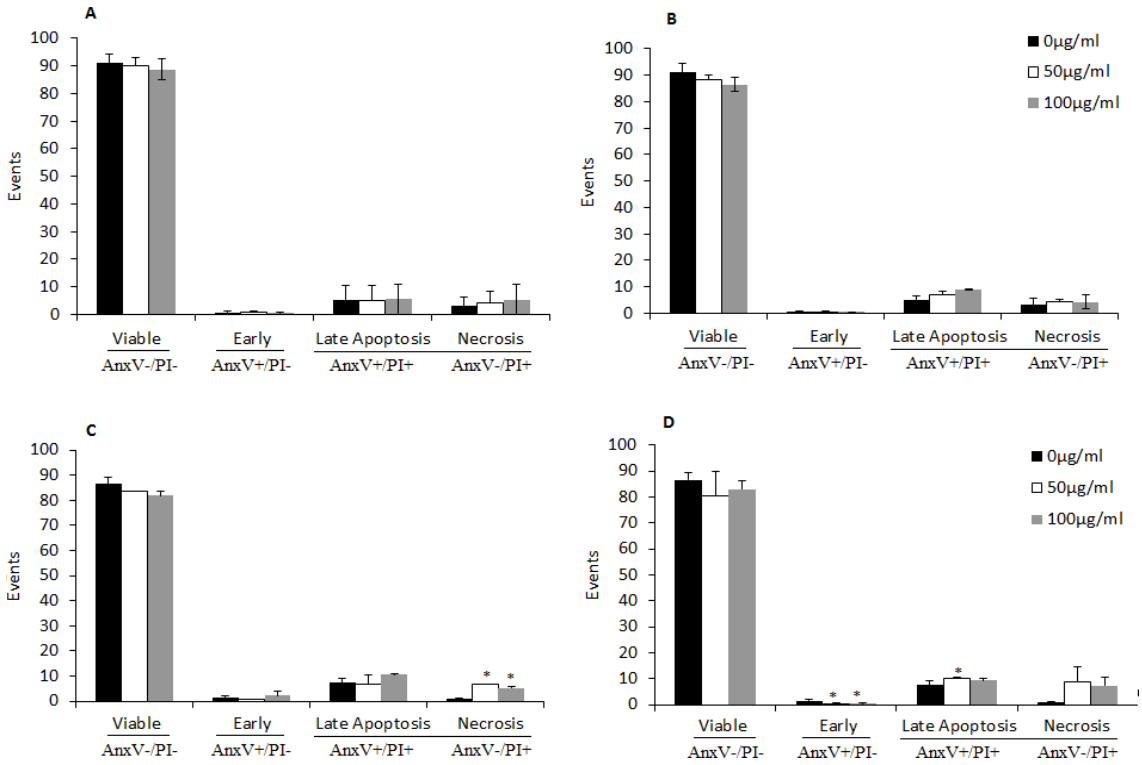

Figure 10 – Annexin V-FITC assay for apoptosis assessment of MG-63 cell line. Results for A) AgNP10 24h, B) AgNP20 24h, C) AgNP10 48h and D) AgNP20 48h, exposures with 3 replicates. ± SD. *p < 0.05.

CBMN Assay

CBMN results of MG-63 cells exposed to 50 µg/mL and 100 µg/mL are represented in Fig.11. A significant increase of the number of necrotic cells was observed after the exposure with AgNP10. Compared to untreated cells, exposure to AgNP10 also increased the number of micronucleus for 50 µg/mL and 100 µg/mL. Contrarily, in AgNP20 exposed cells micronuclei were only visible at 50 µg/mL, while for both concentrations low rates of cell death was observed. Also Fig.11 – D, show for AgNP20 a concentration-dependent decrease on nuclear division index of exposed cells.

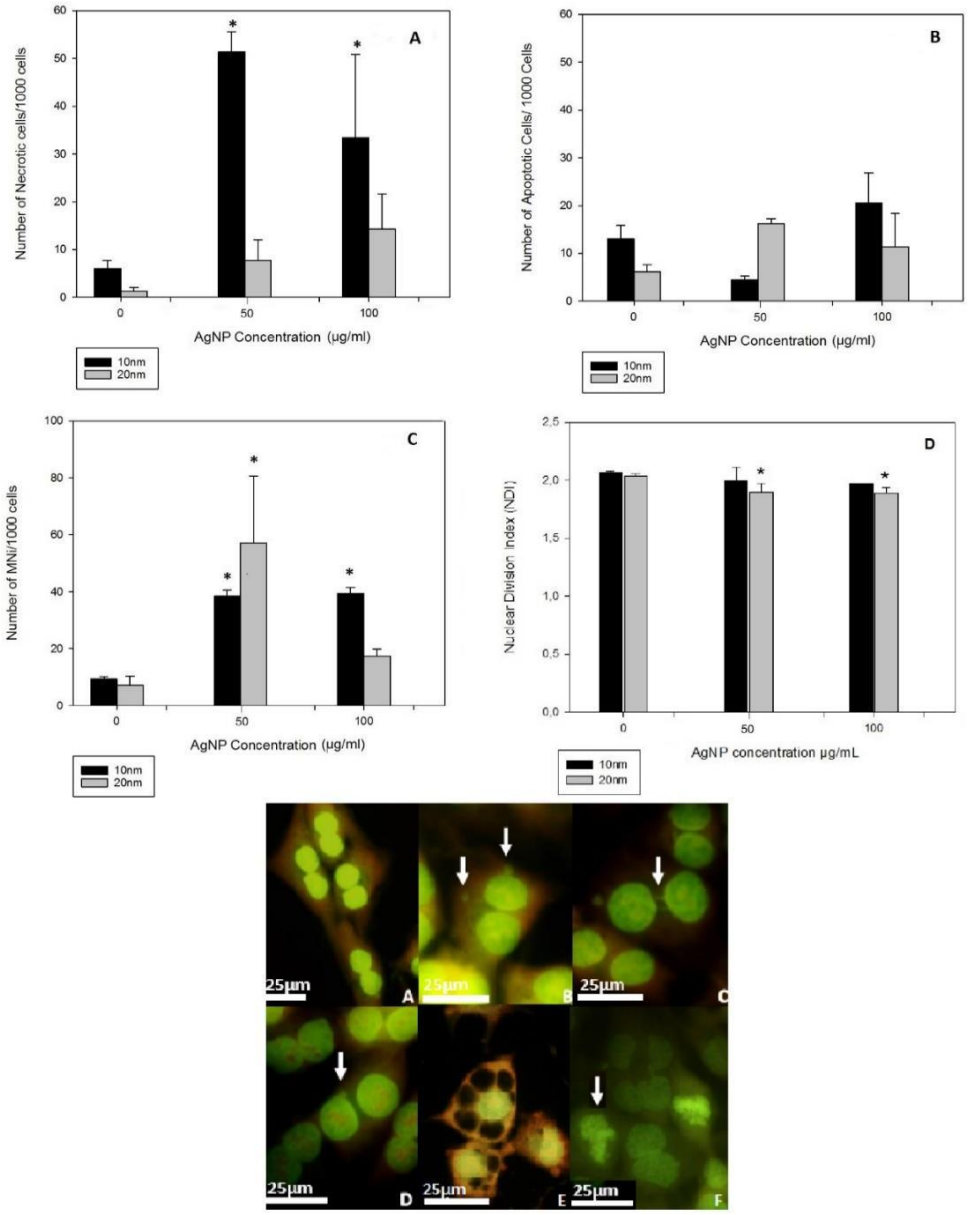

Figure 11 – The total number of necrotic/apoptotic cells (A & B) and micronucleus (C), obtained per 1000 cells, after exposure to AgNP10 and AgNP20. * Represents differences between control and concentrations. (D) Nuclear division index of MG-63 after exposure. The image at the bottom it is the representative images obtained by fluorescence microscopy of the cytokinesis-block micronucleus cytome assay in MG-63 cells for AgNP 20: A) binucleated cells (control), B) binucleated cell with two micronuclei (50 µg/mL), C) binucleated cell with two nucleoplasmic bridges (50 µg/mL), D) binucleated cell with one nuclear bud (50 µg/mL), E) Necrotic cell (100 µg/mL) and F) Apoptotic cell (50 µg/mL).

4. Discussion

The information regarding the effects of AgNPs on bone cells is still scarce. The few toxicological studies using the bone cells used AgNPs embedded in titanium (Cao et al., 2011) or derived from implant devices (Ye et al., 2011; De Giglio et al., 2013), and their focus was mainly on assessing antimicrobial effects rather than a throughout study on the potential toxicity to bone cells.

In our work two sizes of AgNPs were used, in order to evaluate size-dependent toxic effects on MG-63. DLS data support that the agglomeration/aggregation behavior (1 h and 24h after the solution preparation in the culture medium) was dependent on NPs size and concentration, as higher aggregation values were found for smaller sizes and higher concentrations. NPs aggregation in culture media is expectable due to the medium high ionic strength, and richness in proteins. It was previously demonstrated that charged nanoparticles had a high profile of binding to a range of proteins whereas neutral nanoparticles tend to bind less (Deng et al., 2012), and that the PVP-capped AgNP are negatively charged (Ahlberg et al., 2014). These interactions with the medium and/or salts, may change NPs primary physiochemical characteristic (El Badawy et al., 2010; Gliga et al., 2014). Huynh and Chen (2011) reported that the PVP-coated AgNPs were significantly more stable than citrate-coated, likely due to steric repulsion imparted by the large, noncharged polymers, in agreement with the predictions based on Derjaguin–Landau–Verwey–Overbeek (DLVO) theory.

Our results show that PVP-AgNPs tend to agglomerate in a size dependent way which is in accordance with DLVO theory (Huynh and Chen, 2011). Moreover, we demonstrate that the DLVO theory is particularly evident when, for the same coating, we deal with smaller size AgNPs. For example, AgNP10 were more reactive over time and concentration than AgNP20, which may be explained by higher specific surface area which generate a high reactivity (Carlson et al., 2008; Zhang et al., 2014).

Curiously, the electron microscopy analysis confirmed a higher uniformity of the manufacturer primary size of the AgNP10, contrarily to AgNP20 that presented a bimodal size distribution (10 and 20 nm), and the influence of this increased heterogeneity on AgNP20 specific toxicity remains under debate. Silver ion dissolution from AgNPs was dependent on the concentration and time. Maximum values of free Ag^{+} were found at 24h, decreasing or stabilizing (for the

highest concentration) thereafter. This apparent decrease may be explained by the complexation ability of several compounds in the α-MEM medium, which can bind to the free dissolved Ag^+ forming ammonia-silver complexes, interfering with the detectable amounts of free Ag^+. This kind of interference was already demonstrated by Maurer-Jones et al. (2013) who evaluated the complexation of the growth medium chemical compounds with free Ag^+. The authors demonstrated that, from an initial percentage of free Ag^+ of 28% over time this value decreases to around 3%, being the rest complexed in soluble ions of $Ag(NH_3)_2^+$ and $AgNH_3^+$ (Maurer-Jones et al., 2013). The cellular uptake of AgNPs was evaluated by flow cytometry by correlation of the increase in side scatter (SS) intensity with an increase in intracellular AgNPs, as we recently described for HaCaT cells (Bastos et al., 2016). The obtained data suggested that both AgNPs sizes were taken up by MG-63 cells at similar levels. Exception for the 100 µg/mL AgNP10 at 24h, where a significant increase in SS was not detected. AgNP10 at 100 µg/L showed more NPs aggregation at 24h, which may not only reduce the NPs surface area available to cells, but also reduce AgNPs bioavailability and therefore decrease particle internalization (El Badawy et al., 2012; Gliga et al., 2014). Internalization of NPs has been associated with a decrease of relative viability/mitochondrial function (Foldbjerg et al., 2011; Xia et al., 2008). Our MTT data show IC50 values of approximately 18, 58 and 94 µg/mL for Ag^+, AgNP10 and AgNP20 respectively. Results on the literature show that IC50 for AgNPs are strongly dependent on the cell line, the size and the coating of the NP. In the study of Arora et al. (2009) the IC50 for AgNP (7–20 nm) values for primary rat liver and primary fibroblasts were 449 and 61 µg/mL respectively. Haase et al. (2011) found that the viability of THP-1 cells decreased 50% after 24h of exposure to 20 nm AgNP and 40 nm AgNP at 110 and 140 µg/mL respectively. Gopinath et al. (2008) found an IC50 value of 27 µg/mL for 10–15 nm AgNP in BHK21 and HT29 cells. The degree of contribution of Ag^+ to the toxicity of AgNP has also been discussed in the literature. Piao et al. (2011) found an IC50 of 4 µg/mL after 24h of exposure to AgNP and an IC50 of 8 µg/mL after exposure to $AgNO_3$. AgNPs were, in general less toxic that the equimolar concentrations of $AgNO_3$, supporting that the toxicity of these NPs must be due, at least partly, to the dissolved ion. Similar results were also found by Kawata et al. (2009) and Foldbjerg et al. (2011) for HepG2 and A549 cell lines, respectively. Comparing the MTT data

as a function of NP size, we show that AgNP10 is in general more toxic that AgNP20. The higher toxicity of the smaller NPs was already reported by other studies in other cell lines (Asharani et al., 2012; Singh and Ramarao, 2012). For example, Gliga et al. (2014) reported that 10 nm particles induced cytotoxicity, independent of surface coating, after exposing cell to citrate and PVP coated and uncoated AgNPs of different sizes (10, 40, 50 and 75 nm). Also, Singh and Ramarao (2012) demonstrated a cell type-dependent toxicity of AgNP concentration until 100 µg/mL on six cell lines as a function of both culture time and AgNP concentration.

When dealing with AgNPs used in bone cements or prosthesis coatings, as they will remain in the body for long periods (Kittler et al., 2010; Singh and Ramarao, 2012), *in vitro* toxicity assessment with bone cells must be also performed for long periods of exposure, due to risk Ag^+ release with time. The clonogenic assay provides such information and has the advantage of having no/little risk of interferences between the assay compounds and the NPs (Dusinska et al., 2013; Guadagnini et al., 2015). Curiously, and contrarily to the results from MTT of the short-term assays, clonogenic data demonstrated that in longer term exposures, AgNPs become more cytotoxic than equimolar doses of $AgNO_3$ (0 and 11% of PE, respectively). This high toxicity was attributed to a progressive release of free silver from NPs into the medium over time. Kittler et al. (2010) studied the Ag^+ release from AgNPs suspensions over time and demonstrated that these NPs slowly dissolved into ions on a time scale of several days. In some cases, the nanoparticles could release up to 90% of their weight (Kittler et al., 2010). In order to evaluate the potential contribution of dissociated Ag^+ on the inhibition of colony formation we repeated the clonogenic assay using the NP-free supernatant of the ultracentrifuged AgNP-solutions. These clonogenic assays showed some cell proliferation (11% the PE of the control), supporting that the complete inhibition of colony formation/cell proliferation in AgNP-exposed cells cannot be attributed only to the dissolved ion. Another hypothesis is based on the fact that in fresh medium with AgNPs, the Ag^+ ion can be delivered into the cells by the NPs Trojan-horse- like, increasing the toxicity of the medium (Park et al., 2010).

The cell cycle analyses of AgNP exposed cells did not reveal any ploidy changes, apart from the increase of the cell subpopulation in sub-G_1. The presence of a sub-G_1 peak in the fluorescent signal is often interpreted as a loss of DNA due to its fragmentation associated with cell death (Mao et al., 2004). Our results show a positive correlation between sub-G_1 peak and apoptosis

for the AgNP20 exposure, and also a positive correlation between the sub-G_1 peak and necrosis induction for AgNP10. However, such correlation must be carefully considered as this sub-G_1 phase may also include cells that have lost DNA for other reason than undergoing apoptosis (Kajstura et al., 2007; Zhu et al., 2016). This increase of sub-G_1 for MG-63 cells exposed to AgNPs could be connected with the increase of mitotic abnormalities including chromosomic bridges and micronuclei that we obtained on CBMN assay, as we did not obtained an increase on sub-G_1 cell population for 100 µg/mL AgNP20 neither MN for the same condition.

Regarding the effects on the cell cycle progression for 48h, our data show that AgNPs size is determinant on inducing a cytostatic effect, as only AgNP20 increased an arrest at G_0/G_1 peak, leading to a decrease of the subpopulation in the S phase The blockage of the AgNP20-exposed cells at G_0/G_1 imply an inhibition of DNA synthesis and a reduction on cell proliferation (Li et al., 2013; Mao et al., 2004). This blockage was also supported by the decrease of NDI for this size obtained by CBMN assay. Contrarily, and regarding the same parameters, AgNP10 do not interfere with the cell cycle progression and, overall increased cell death by necrosis while AgNP20 induced late apoptosis but not necrosis. Moreover, combining cell cycle and CBMN data it was evident that AgNP-exposed cells that enter G_2/M show an increase of mitotic disorders (e.g., micronuclei, chromosome bridges). These results are also in line with the observed decrease of MTT reduction to formazan in the AgNP20-exposed cells. This reaction is catalyzed by cellular oxidoreductases, therefore, dependent on the cellular metabolic activity. So, the observed decrease may be explained by the decrease of cell division/proliferation together with a decrease of metabolic activity, rather than cell death observed in AgNP10-exposed cells.

The reason why size is so determinant to condition cell fate regarding cell cycle progression and death remains unknown, but may be dependent on the way NPs aggregate, and/or contact the cell membrane and enter. It was demonstrated by Kim et al. (2012a) that NPs with a diameter smaller than 50nm can easily enter in the cells by endocytic pathway and particles with a diameter bigger than 50nm have a slower rate of uptake. Liu et al. (2010) reported that AgNPs with a diameter of ~5 to 20 nm increased the ROS level and induced apoptosis in different human cells (A549, SGC-7901, HepG2 and MCF-7), while those with diameters greater than 50 nm could not do so. Two factors have to be considered: the higher instability and aggregation

of AgNP10 and the bimodal profile of the AgNP20. AgNP10 formed larger clusters, up to 100nm, probably decreased the uptake by the cells, (but the cell membrane adsorption/and direct membrane damage must not be excluded). Contrarily AgNP20 presents a maximum cluster diameter of 45nm making it easier to cross cell and/or nuclear membranes and interfere at the cytostatic and apoptotic levels.

5. Conclusions

In conclusion, our results confirm that for the same coating AgNPs size conditions NPs characteristics, being those smaller more reactive and more prone to form large aggregates, being therefore mandatory to provide a careful characterization of the particles, before their use on toxicity assessment. We also demonstrate for short period exposures (up to 48h) ionic Ag^+ is more toxic than the corresponding dose in the form of AgNP and that among AgNPs, the smaller the size, the higher the toxicity. However longer-term exposures using the clonogenic assay, demonstrate that with time, the same AgNP doses completely inhibit PE, which cannot be attributed to the dissociated Ag^+ alone. Also, when comparing size-dependent effects, we demonstrate that AgNP20 induces a more severe blockage of cells at G_0/G_1, and apoptotic cells, while AgNP10 do not have a cytostatic effect but rather induce necrosis. Finally, combining the chemical and toxicological profiles of both sizes, we concluded that this size dependent AgNP toxicity may be associated in part with the NPs interference with the cell membranes and consequent uptake/adsorption processes and to the Ag^+ delivery.

Acknowledgments:

This work was supported by national funds through the Portuguese Foundation for Science and Technology (FCT) through the fellows of Fernanda Rosário (SFRH/BD/91270/2012) and Helena Oliveira (SFRH/BPD/48853/2008) and are greatly acknowledged.

References

Ahlberg, A., Carlsson, A.S., Lindberg, L., 1978. Hematogenous infection in total joint replacement. Clin. Orthop. Relat. Res. 69–75.

Alt, V., Bechert, T., Steinrücke, P., Wagener, M., Seidel, P., Dingeldein, E., Domann, E., Schnettler, R., 2004. An in vitro assessment of the antibacterial properties and cytotoxicity of nanoparticulate silver bone cement. Biomaterials 25, 4383–91. doi:10.1016/j.biomaterials.2003.10.078

Asharani, P., Sethu, S., Lim, H.K., Balaji, G., Valiyaveettil, S., Hande, M.P., 2012. Differential regulation of intracellular factors mediating cell cycle, DNA repair and inflammation following exposure to silver nanoparticles in human cells. Genome Integr. 3, 2. doi:10.1186/2041-9414-3-2

AshaRani, P. V., Low Kah Mun, G., Hande, M.P., Valiyaveettil, S., Low, G., Mun, K., Hande, M.P., Valiyaveettil, S., 2009. Cytotoxicity and Genotoxicity of Silver nanoparticles in human cells. ACS Nano 3, 279–290. doi:10.1021/nn800596w

Bacakova, L., Grausova, L., Vacik, J., Fraczek, A., Blazewicz, S., Kromka, A., Vanecek, M.,Svorcik, V., 2007. Improved adhesion and growth of human osteoblast-like MG 63 cells on biomaterials modified with carbon nanoparticles. Diam. Relat. Mater. 16, 2133–2140. doi:10.1016/j.diamond.2007.07.015

Bastos, V., Ferreira de Oliveira, J.M.P., Brown, D., Jonhston, H., Malheiro, E., Daniel-da-Silva, A.L., Duarte, I.F., Santos, C., Oliveira, H., 2016. The influence of Citrate or PEG coating on silver nanoparticle toxicity to a human keratinocyte cell line. Toxicol. Lett. 249, 29–41. doi:10.1016/j.toxlet.2016.03.005

Bernier, MC., El Kirat, K., Besse, M., Morandat, S., Vayssade, M., 2012. Preosteoblasts and fibroblasts respond differently to anatase titanium dioxide nanoparticles: a cytotoxicity and inflammation study. Colloids Surf. B. Biointerfaces 90, 68–74. doi:10.1016/j.colsurfb.2011.09.044

Cao, H., Liu, X., Meng, F., Chu, P.K., 2011. Biological actions of silver nanoparticles embedded in titanium controlled by micro-galvanic effects. Biomaterials 32, 693–705. doi:10.1016/j.biomaterials.2010.09.066

Carlson, C., Hussain, S.M., Schrand, a M., Braydich-Stolle, L.K., Hess, K.L., Jones, R.L., Schlager, J.J., 2008. Unique cellular interaction of silver nanoparticles: size-dependent generation of reactive oxygen species. J. Phys. Chem. B 112, 13608–19. doi:10.1021/jp712087m

Chaloupka, K., Malam, Y., Seifalian, A.M., 2010. Nanosilver as a new generation of nanoproduct in biomedical applications. Trends Biotechnol. 28, 580–8. doi:10.1016/j.tibtech.2010.07.006

De Giglio, E., Cafagna, D., Cometa, S., Allegretta, A., Pedico, A., Giannossa, L.C., Sabbatini, L., Mattioli-Belmonte, M., Iatta, R., 2013. An innovative, easily fabricated, silver

nanoparticle-based titanium implant coating: development and analytical characterizationAnal. Bioanal. Chem. 405, 805–16. doi:10.1007/s00216-012-6293-z

Deng, Z.J., Liang, M., Toth, I., Monteiro, M., Minchin, R.F., 2012. Plasma protein binding of positively and negatively charged polymer-coated gold nanoparticles elicits different biological responses. Nanotoxicology 7, 314–322. doi:10.3109/17435390.2012.655342

Di Virgilio, A.L., Reigosa, M., de Mele, M.F.L., 2010. Response of UMR 106 cells exposed to titanium oxide and aluminum oxide nanoparticles. J. Biomed. Mater. Res. A 92, 80–6. doi:10.1002/jbm.a.32339

Dusinska, M., Magdolenova, Z., Fjellsbø, L.M., 2013. Toxicological aspects for nanomaterial in humans. Methods Mol. Biol. 948, 1–12. doi:10.1007/978-1-62703-140-0_1

El Badawy, A.M., Luxton, T.P., Silva, R.G., Scheckel, K.G., Suidan, M.T., Tolaymat, T.M., 2010. Impact of environmental conditions (pH, ionic strength, and electrolyte type) on the surface charge and aggregation of silver nanoparticles suspensions. Environ. Sci. Technol. 44, 1260–6. doi:10.1021/es902240k

El Badawy, A.M., Scheckel, K.G., Suidan, M., Tolaymat, T., 2012. The impact of stabilization mechanism on the aggregation kinetics of silver nanoparticles. Sci. Total Environ. 429, 325–31. doi:10.1016/j.scitotenv.2012.03.041

Fenech, M., 2000. The in vitro micronucleus technique. Mutat. Res. 455, 81–95.

Feng, Q.L., Wu, J., Chen, G.Q., Cui, F.Z., Kim, T.N., Kim, J.O., 2000. A mechanistic study of the antibacterial effect of silver ions on Escherichia coli and Staphylococcus aureus. J. Biomed. Mater. Res. 52, 662–8.

Foldbjerg, R., Dang, D.A., Autrup, H., 2011. Cytotoxicity and genotoxicity of silver nanoparticles in the human lung cancer cell line, A549. Arch. Toxicol. 85, 743–50. doi:10.1007/s00204-010-0545-5

Franken, N.A.P., Rodermond, H.M., Stap, J., Haveman, J., van Bree, C., 2006. Clonogenic assay of cells in vitro. Nat. Protoc. 1, 2315–2319.

Furno, F., Morley, K.S., Wong, B., Sharp, B.L., Arnold, P.L., Howdle, S.M., Bayston, R., Brown, P.D., Winship, P.D., Reid, H.J., 2004. Silver nanoparticles and polymeric medical devices: a new approach to prevention of infection? J. Antimicrob. Chemother. 54, 1019–24. doi:10.1093/jac/dkh478

Gerhardt, L.-C., Jell, G.M.R., Boccaccini, a R., 2007. Titanium dioxide (TiO(2)) nanoparticles filled poly(D,L lactid acid) (PDLLA) matrix composites for bone tissue engineering. J. Mater. Sci. Mater. Med. 18, 1287–98. doi:10.1007/s10856-006-0062-5

Gliga, A.R., Skoglund, S., Wallinder, I.O., Fadeel, B., Karlsson, H.L., 2014. Size-dependent cytotoxicity of silver nanoparticles in human lung cells: the role of cellular uptake, agglomeration and Ag release. Part. Fibre Toxicol. 11, 11. doi:10.1186/1743-8977-11-11

Guadagnini, R., Halamoda Kenzaoui, B., Walker, L., Pojana, G., Magdolenova, Z., Bilanicova,

D., Saunders, M., Juillerat-Jeanneret, L., Marcomini, A., Huk, A., Dusinska, M., Fjellsbø, L.M., Marano, F., Boland, S., 2015. Toxicity screenings of nanomaterials: challenges due to interference with assay processes and components of classic in vitro tests. Nanotoxicology 9 Suppl 1, 13–24. doi:10.3109/17435390.2013.829590

Gutwein, L.G., Webster, T.J., 2002. Osteoblast and Chrondrocyte Proliferation in the Presence of Alumina And Titania Nanoparticles. J. Nanoparticle Res. 4, 231–238. doi:10.1023/A:1019920105207

Hovis, C.E., Hilliard, J.K., Taylor, J.B., Yun, Y.H., Carolyn, L., Youngs, W.J., 2010. The antimicrobial efficacy of sustained release silver-carbene complex-loaded-tyrosine polyphosphate nanoparticles: charecterization, in vitro and in vivo studies 30, 3771–3779. doi:10.1016/j.biomaterials.2009.03.044.

Huynh, K.A., Chen, K.L., 2011. Aggregation kinetics of citrate and polyvinylpyrrolidone coated silver nanoparticles in monovalent and divalent electrolyte solutions. Environ. Sci. Technol. 45, 5564–71. doi:10.1021/es200157h

Joseph, T.N., Chen, A.L., Di Cesare, P.E., 2003. Use of antibiotic-impregnated cement in total joint arthroplasty. J. Am. Acad. Orthop. Surg. 11, 38–47.

Kajstura, M., Halicka, H.D., Pryjma, J., Darzynkiewicz, Z., 2007. Discontinuous fragmentation of nuclear DNA during apoptosis revealed by discrete "sub-G1" peaks on DNA content histograms. Cytom. Part A 71A, 125–131. doi:10.1002/cyto.a.20357

Kawata, K., Osawa, M., Okabe, S., 2009. In vitro toxicity of silver nanoparticles at noncytotoxic doses to HepG2 human hepatoma cells. Environ. Sci. Technol. 43, 6046–51.

Kim, T.H., Kim, M., Park, H.S., Shin, U.S., Gong, M.S., Kim, H.W., 2012. Size-dependent cellular toxicity of silver nanoparticles. J. Biomed. Mater. Res. - Part A 100 A, 1033–1043. doi:10.1002/jbm.a.34053

Kim, Y.S., Kim, J.S., Cho, H.S., Rha, D.S., Kim, J.M., Park, J.D., Choi, B.S., Lim, R., Chang, H.K., Chung, Y.H., Kwon, I.H., Jeong, J., Han, B.S., Yu, I.J., 2008. Twenty-eight-day oral toxicity, genotoxicity, and gender-related tissue distribution of silver nanoparticles in Sprague-Dawley rats. Inhal. Toxicol. 20, 575–83. doi:10.1080/08958370701874663

Kittler, S., Greulich, C., Diendorf, J., Köller, M., Epple, M., 2010. Toxicity of Silver Nanoparticles Increases during Storage Because of Slow Dissolution under Release of Silver Ions. Chem. Mater. 22, 4548–4554. doi:10.1021/cm100023p

Lankveld, D.P.K., Oomen, a G., Krystek, P., Neigh, A., Troost-de Jong, A., Noorlander, C.W., Van Eijkeren, J.C.H., Geertsma, R.E., De Jong, W.H., 2010. The kinetics of the tissue distribution of silver nanoparticles of different sizes. Biomaterials 31, 8350–61. doi:10.1016/j.biomaterials.2010.07.045

Lee, J.H., Kim, Y.S., Song, K.S., Ryu, H.R., Sung, J.H., Park, J.D., Park, H.M., Song, N.W., Shin, B.S., Marshak, D., Ahn, K., Lee, J.E., Yu, I.J., 2013. Biopersistence of silver nanoparticles in tissues from Sprague-Dawley rats. Part. Fibre Toxicol. 10, 36.

doi:10.1186/1743-8977-10-36

Lévesque, M., Martineau, C., Jumarie, C., Moreau, R., 2008. Characterization of cadmium uptake and cytotoxicity in human osteoblast-like MG-63 cells. Toxicol. Appl. Pharmacol. 231, 308–17. doi:10.1016/j.taap.2008.04.016

Lewinski, N., Colvin, V., Drezek, R., 2008. Cytotoxicity of nanoparticles. Small 4, 26–49. doi:10.1002/smll.200700595

Li, C., Fu, R., Yu, C., Li, Z., Guan, H., Hu, D., Zhao, D., Lu, L., 2013. Silver nanoparticle/chitosan oligosaccharide/poly(vinyl alcohol) nanofibers as wound dressings: a preclinical study. Int. J. Nanomedicine 8, 4131–45. doi:10.2147/IJN.S51679

Li, X., Xu, L., Shao, A., Wu, G., Hanagata, N., 2013. Cytotoxic and genotoxic effects of silver nanoparticles on primary Syrian hamster embryo (SHE) cells. J. Nanosci. Nanotechnol. 13, 161–70.

Liu, W., Wu, Y., Wang, C., Li, H.C., Wang, T., Liao, C.Y., Cui, L., Zhou, Q.F., Yan, B., Jiang, G.B., 2010. Impact of silver nanoparticles on human cells: effect of particle size. Nanotoxicology 4, 319–30. doi:10.3109/17435390.2010.483745

Mao, X., Seidlitz, E., Truant, R., Hitt, M., Ghosh, H.P., 2004. Re-expression of TSLC1 in a non-small-cell lung cancer cell line induces apoptosis and inhibits tumor growth. Oncogene 23, 5632–5642. doi:10.1038/sj.onc.1207756

Maurer-Jones, M.A., Mousavi, M.P.S., Chen, L.D., Buhlmann, P., Haynes, C.L., 2013. Characterization of silver ion dissolution from silver nanoparticles using fluorous-phase ion-selective electrodes and assessment of resultant toxicity to Shewanella oneidensis. Chem. Sci. 4, 2564–2572. doi:10.1039/C3SC50320H

Maynard, A.D., 2006. Nanotechnology: A Research Strategy for Addressing Risk • All Publications • Nanotechnology Project. Woodrow Wilson Int. Cent. Sch. URL http://www.nanotechproject.org/publications/archive/nanotechnology_research_strategy_for/ (accessed 11.27.14).

Navarro, E., Baun, A., Behra, R., Hartmann, N.B., Filser, J., Miao, A.-J., Quigg, A., Santschi, P.H., Sigg, L., Baun, Æ.A., Behra, Æ.R., Hartmann, Æ.N.B., Filser, J., Antonietta, Æ.A.M.Æ., Peter, Q.Æ., 2008. Environmental behavior and ecotoxicity of engineered nanoparticles to algae, plants, and fungi. Ecotoxicology 17, 372–86. doi:10.1007/s10646-008-0214-0

Necula, B.S., 2013. Silver-based antibacterial surfaces for bone implants. doi:10.4233/uuid:f2523458-cb32-4c69-963e-da7b1e89ddd5

Niu, L., Li, Y., Li, X., Gao, X., Su, X., 2012. Study the cytotoxicity of different kinds of water-soluble nanoparticles in human osteoblast-like MG-63 cells. Mater. Res. Bull. 47, 3654–3659. doi:10.1016/j.materresbull.2012.06.045

Oliveira, H., Monteiro, C., Pinho, F., Pinho, S., Ferreira de Oliveira, J.M.P., Santos, C., 2014. Cadmium-induced genotoxicity in human osteoblast-like cells. Mutat. Res. Genet. Toxicol.

Environ. Mutagen. 775-776, 38–47. doi:10.1016/j.mrgentox.2014.10.002

Park, E.-J., Bae, E., Yi, J., Kim, Y., Choi, K., Lee, S.H., Yoon, J., Lee, B.C., Park, K., 2010a.

Repeated-dose toxicity and inflammatory responses in mice by oral administration of silver nanoparticles. Environ. Toxicol. Pharmacol. 30, 162–8. doi:10.1016/j.etap.2010.05.004

Park, E.-J., Yi, J., Kim, Y., Choi, K., Park, K., 2010b. Silver nanoparticles induce cytotoxicity by a Trojan-horse type mechanism. Toxicol. In Vitro 24, 872–8. doi:10.1016/j.tiv.2009.12.001

Park, K., Park, E.-J., Chun, I.K., Choi, K., Lee, S.H., Yoon, J., Lee, B.C., 2011. Bioavailability and toxicokinetics of citrate-coated silver nanoparticles in rats. Arch. Pharm. Res. 34, 153–8. doi:10.1007/s12272-011-0118-z

Park, M.V.D.Z., Neigh, A.M., Vermeulen, J.P., de la Fonteyne, L.J.J., Verharen, H.W., Briedé, J.J., van Loveren, H., de Jong, W.H., 2011. The effect of particle size on the cytotoxicity, inflammation, developmental toxicity and genotoxicity of silver nanoparticles. Biomaterials 32, 9810–7. doi:10.1016/j.biomaterials.2011.08.085

Piao, M.J., Kang, K.A., Lee, I.K., Kim, H.S., Kim, S., Choi, J.Y., Choi, J., Hyun, J.W., 2011. Silver nanoparticles induce oxidative cell damage in human liver cells through inhibition of reduced glutathione and induction of mitochondria-involved apoptosis. Toxicol. Lett. 201, 92–100. doi:10.1016/j.toxlet.2010.12.010

Piccinno, F., Gottschalk, F., Seeger, S., Nowack, B., 2012. Industrial production quantities and uses of ten engineered nanomaterials in Europe and the world. J. Nanoparticle Res. 14, 1109. doi:10.1007/s11051-012-1109-9

Rai, M., Yadav, A., Gade, A., 2009. Silver nanoparticles as a new generation of antimicrobials. Biotechnol. Adv. 27, 76–83. doi:10.1016/j.biotechadv.2008.09.002

Samberg, M.E., Oldenburg, S.J., Monteiro-Riviere, N. a, 2010. Evaluation of silver nanoparticle toxicity in skin in vivo and keratinocytes in vitro. Environ. Health Perspect. 118, 407–13. doi:10.1289/ehp.0901398

Saravanan, S., Nethala, S., Pattnaik, S., Tripathi, A., Moorthi, A., Selvamurugan, N., 2011. Preparation, characterization and antimicrobial activity of a bio-composite scaffold containing chitosan/nano-hydroxyapatite/nano-silver for bone tissue engineering. Int. J. Biol. Macromol. 49, 188–93. doi:10.1016/j.ijbiomac.2011.04.010

Sibbald, R.G., Browne, A.C., Coutts, P., Queen, D., 2001. Screening evaluation of an ionized nanocrystalline silver dressing in chronic wound care. Ostomy. Wound. Manage. 47, 38–43.

Sibbald, R.G., Contreras-Ruiz, J., Coutts, P., Fierheller, M., Rothman, A., Woo, K., 2007. Bacteriology, inflammation, and healing: a study of nanocrystalline silver dressings in chronic venous leg ulcers. Adv. Skin Wound Care 20, 549–58. doi:10.1097/01.ASW.0000294757.05049.85

Singh, R.P., Ramarao, P., 2012. Cellular uptake, intracellular trafficking and cytotoxicity of silver nanoparticles. Toxicol. Lett. 213, 249–59. doi:10.1016/j.toxlet.2012.07.009

Stebounova, L. V, Adamcakova-Dodd, A., Kim, J.S., Park, H., O'Shaughnessy, P.T., Grassian, V.H., Thorne, P.S., 2011. Nanosilver induces minimal lung toxicity or inflammation in a subacute murine inhalation model. Part. Fibre Toxicol. 8, 5. doi:10.1186/1743-8977-8-5

Sung, J.H., Ji, J.H., Park, J.D., Yoon, J.U., Kim, D.S., Jeon, K.S., Song, M.Y., Jeong, J., Han, B.S., Han, J.H., Chung, Y.H., Chang, H.K., Lee, J.H., Cho, M.H., Kelman, B.J., Yu, I.J., 2009. Subchronic inhalation toxicity of silver nanoparticles. Toxicol. Sci. 108, 452–61. doi:10.1093/toxsci/kfn246

Suzuki, H., Toyooka, T., Ibuki, Y., 2007. Simple and easy method to evaluate uptake potential of nanoparticles in mammalian cells using a flow cytometric light scatter analysis. Environ. Sci. Technol. 41, 3018–24

Tian, J., Wong, K.K.Y., Ho, C.-M., Lok, C.-N., Yu, W.-Y., Che, C.-M., Chiu, J.-F., Tam, P.K.H., 2007. Topical delivery of silver nanoparticles promotes wound healing. ChemMedChem 2, 129–36. doi:10.1002/cmdc.200600171

Trop, M., Novak, M., Rodl, S., Hellbom, B., Kroell, W., Goessler, W., 2006. Silver-coated dressing acticoat caused raised liver enzymes and argyria-like symptoms in burn patient. J. Trauma 60, 648–52. doi:10.1097/01.ta.0000208126.22089.b6

Vance, M.E., Kuiken, T., Vejerano, E.P., McGinnis, S.P., Hochella Jr., M.F., Rejeski, D., Hull, M.S., 2015. Nanotechnology in the real world: Redeveloping the nanomaterial consumer products inventory. Beilstein J. Nanotechnol. 6, 1769–1780.

Wilcox, M., Kite, P., Dobbins, B., 1998. Antimicrobial intravascular catheters—which surface to coat? J. Hosp. Infect. 38, 322–324. doi:10.1016/S0195-6701(98)90084-6

Xia, T., Kovochich, M., Liong, M., Mädler, L., Gilbert, B., Shi, H., Yeh, J.I., Zink, J.I., Nel, A.E., 2008. Comparison of the mechanism of toxicity of zinc oxide and cerium oxide nanoparticles based on dissolution and oxidative stress properties. ACS Nano 2, 2121–34. doi:10.1021/nn800511k

Ye, J., Yao, Q., Mo, A., Nie, J., Liu, W., Ye, C., Chen, X., 2011. Effects of an antibacterial membrane on osteoblast-like cells in vitro. Int. J. Nanomedicine 6, 1853–61. doi:10.2147/IJN.S17749

Zanette, C., Pelin, M., Crosera, M., Adami, G., Bovenzi, M., Larese, F.F., Florio, C., 2011. Silver nanoparticles exert a long-lasting antiproliferative effect on human keratinocyte HaCaT cell line. Toxicol. In Vitro 25, 1053–60. doi:10.1016/j.tiv.2011.04.005

Zhang, T., Wang, L., Chen, Q., Chen, C., 2014. Cytotoxic potential of silver nanoparticles. Yonsei Med. J. 55, 283–91. doi:10.3349/ymj.2014.55.2.283

Zhu, B., Li, Y., Lin, Z., Zhao, M., Xu, T., Wang, C., Deng, N., 2016. Silver Nanoparticles Induce HePG-2 Cells Apoptosis Through ROS-Mediated Signaling Pathways. Nanoscale Res. Lett. 11, 198. doi:10.1186/s11671-016-1419-4

Chapter III

Small sized AgNPs modulate differently the cytotoxicity and genotoxicity in lung cells

Part of this chapter was published as:

Rosário F., Hoet P., Nogueira AJA., Santos C., Oliveira H. (2018) Differential pulmonary *in vitro* toxicity of two small-sized polyvinylpyrrolidone-coated silver nanoparticles. Journal of Toxicology and Environmental Health, Part A. https://doi.org/10.1080/15287394.2018.1468837

Small sized AgNPs modulate differently the cytotoxicity and genotoxicity in lung cells

Rosário F [a], Hoet P [b], Nogueira AJA [a] Santos C [c,I], Oliveira H [a,d,II]

[a] *Department of Biology & CESAM, University of Aveiro, 3810-193 Aveiro, Portugal*

[b] *Occupational and environmental Toxicology, KU Leuven, ON1Campus Gasthuisberg, Herestraat 49, 3000 Leuven, Belgium*

[c] *Department of Biology, Faculty of Sciences, University of Porto, Rua do Campo Alegre, Porto*

[d] *CICECO - Aveiro Institute of Materials, University of Aveiro, 3810-193 Aveiro, Portugal*

[I] *Corresponding author. E-mail address: csantos@fc.up.pt*

[II] *Corresponding author. E-mail address: holiveira@ua.pt*

Abstract

Silver nanoparticles (AgNP), with their important properties, are being used in a range of sectors from industry to medicine, leading to increased human exposure. Hence, their toxicity potential needs to be comprehensively evaluated. It was postulated that within small sized (≤20 nm) polyvinylpyrrolidone coated silver nanoparticles (PVP-AgNP), minor size differences may induce different toxicity profiles and involve varying cellular pathways. Therefore, the aim of this study was to examine the influence of differing size AgNP 10 nm (AgNP10) and 20 nm (AgNP20) (up to 100 μg/mL), as well as to Ag^+ as $AgNO_3$ for 24 and 48h using the human lung cell line A549. The effects on cell viability, proliferation, apoptosis, DNA damage and cell cycle dynamics were assessed. Results for both time periods showed that for low concentrations (<5 μg/mL), AgNP20 were more cytotoxic than AgNP10, however, at higher doses, AgNP10 exhibited higher toxicity. For concentrations >50 μg/mL, AgNP10 induced severe DNA damage (comet class 3–4), cell cycle arrest at G_2 phase, and late-stage apoptosis, while AgNP20 induced cell cycle arrest at S phase and an increase in the percentage sub-G_1, which did not recover after

48h and late-stage apoptosis/necrosis. In longer-term exposures, the greater impairment in colony formation due to AgNP exposure than to silver ion supports that nanotoxicity is not exclusively due to the released ion. Data suggest that toxicity mediated by small AgNP (≤20 nm) in lung cells is not only dependent of the level of particle internalization, but also ion size which may involve varying pathways as targets.

Keywords: Silver nanoparticles, PVP-coating, Cell cycle, Apoptosis, Clonogenic assay, DNA damage

1. Introduction

Nanoscience and nanotechnology play an increasingly crucial role in many key technologies of the new millennium (e.g., Bunderson-Schelvan, Holian, and Hamilton 2017). Due to their known antimicrobial activity, silver nanoparticles (AgNPs) are used in a wide range of applications, leading to a substantial growth of their production and number products containing AgNPs, namely in medical devices (Vance et al., 2015; Kermanizadeh et al., 2016; Kaweeteerawat et al., 2017). Intentional and unintentional exposure to AgNPs mainly occurs via inhalation, skin contact and ingestion. Lung is considered the least protected organ and the main portal of entry of inhaled NPs that can gain access to the alveoli, the deepest part of the respiratory tract where they can be translocated to other tissues (Oberdörster, Oberdörster, and Oberdörster, 2005; Nel et al., 2006). The Occupational Safety and Health Administration (OSHA) and the National Institute of Occupational Safety and Health (NIOSH) limit silver in workplace air to 0.01 mg/m^3 and the time of exposure to 40h per week (Drake and Hazelwood 2005), however more data on the levels of exposure of humans to AgNPs on real scenarios (e.g., concentrations and routes) are still required. Several reports have addressed the toxicity of AgNPs towards lung cells. Lee et al. (2011) found that AgNPs induced strong toxicity and G_2/M cell cycle arrest by a mechanism involving PKCζ downregulation in A549 lung cells. Kaur and Tikoo (2013) showed that the cytotoxicity of AgNPs is highly determined by the surface potential of nanoparticles and is cell type dependent. By comparing the sensitivity of A431, A549 and RAW264 cell lines, the following ranking was established A431> A549 > RAW264

(Kaur and Tikoo 2013). Also, Chairuangkitti et al. (2013) proposed that the toxic effects of AgNPs (<100nm) on A549 cells are mediated by ROS-dependent (cytotoxicity) and ROS-independent (cell cycle arrest) pathways. In A549 and HepG2 cells, a dose-dependent cytotoxicity induced by AgNPs (20-50nm) related to oxidative stress, DNA damage and mitochondrial injury was described (Xin et al., 2015). However, no such oxidative stress (e.g., ROS production) was reported in other studies (Gliga et al., 2014; Sahu et al., 2014).

Despite its widespread use and the existent data on the possible adverse health effects, it is difficult to build a consensual mechanism of AgNP toxicity towards lung cells, maybe because it is problematic to compare biological data from different studies with a great variety in NP sizes, coatings or shapes. Nevertheless, AgNPs toxicity has been attributed to the amount of Ag^+ ion released (dissolution) by the NP during exposure (Kawata, Osawa, and Okabe 2009). AgNPs are usually stabilized with surface coatings to prevent oxidation and dissolution of Ag^+. PVP is a common surface coating, rendering NPs a negative surface charge, and providing more effective re-dispersion and diminished propensity towards aggregations by steric hindrance (Tejamaya et al., 2012; Kvítek et al., 2008). Anderson et al. (2015) showed that PVP is a stronger capping agent than citrate (another common stabilizer) and that PVP-coated AgNPs are more efficiently cleared from the lungs than citrate-coated. We have shown that AgNPs toxicity depends on the coating material and that the capping agent has a major role in the internalization of the AgNPs (Bastos et al., 2016). However, internalization and toxicity may not be directly correlated, with PVP, citrate and tannic acid-AgNPs being differently internalized by A549 cells, but inducing similar toxicity (Zhang et al., 2015). The size of the NPs also influences their toxicity, being the smaller sized AgNPs more toxic (Guo et al., 2016; Gliga et al., 2014). We have found that AgNPs size influences the mechanisms of cell death in osteoblast like cells (Rosário et al., 2016). Smaller AgNPs penetrate cell membrane more efficiently than larger ones and also the high surface area to volume ratio of smaller AgNPs compared to higher sized may contribute to the release of Ag^+ from their surface. Previous *in vitro* and *in vivo* studies on the toxicity of PVP-AgNPs have considered mostly larger sized NPs: moderate pulmonary toxicity was found in rats intratracheally instilled with 70nm PVP-AgNP (Haberl et al., 2013). Foldbjerg and co-workers have reported the toxicity of 69nm PVP-AgNPs towards A549 cells at concentrations <15µg/mL (Foldbjerg, Dang, and Autrup 2011). Furthermore, Nymark et al.

(2013) detected induction of DNA damage in BEAS 2B cells upon exposure to PVP-AgNPs with 42.5nm. Considering that the toxicity is highly dependent on the combined properties of the AgNPs, evaluating its biological effects requires a detailed physicochemical characterization of the particles and a set of *in vitro* assays that allow the screening of the NP variants.

In this work we hypothesize that small differences on AgNPs size are enough to induce different toxicity profiles in lung cells and may differently condition the pathways involved in cell death response. The A549 cell line was selected as a lung cell model for this study as it presents many important biological properties of the alveolar epithelial type II cells (Shapiro et al., 1978). It has been also used in the study of the toxicity of substances like nanomaterial (Reshma, Syama, and Mohanan 2016; Foldbjerg, Dang, and Autrup 2011; Kermanizadeh et al., 2016). A549 cells were exposed to PVP-AgNPs (10 and 20nm). To better understand the role of ionic silver in AgNPs toxicity, cells were also exposed to Ag^+ added as $AgNO_3$. Different cell parameters were investigated: AgNPs uptake, cell viability and proliferation, cell-cycle dynamics, micronuclei, induction of apoptosis and necrosis and DNA damage by the comet assay. Also, we aimed to predict the long-term (7 days) effects of *in vitro* AgNPs exposure.

2. Materials and Methods

Silver nanoparticles and physicochemical characterization

Sterile, purified and endotoxin-free AgNPs (1.0 mg/mL) with PVP surface layer and nominal size of 10 and 20 nm, were purchased to nanoComposix Europe (CZ). Samples for SEM analysis were prepared by placing 10µL of each AgNP stock solution on a carbon sheet and dried at room temperature. AgNPs morphology and size were analyzed by a Hitachi SU-70 microscope (Hitachi High-Technologies Europe GmbH, Germany). SEM images were analyzed with *ImageJ (open platform for scientific image analysis).* The hydrodynamic diameter (Dh) was measured by Dynamic light scattering (DLS) using a Zetasizer Nano ZS (Malvern Instruments, UK) in AgNPs dispersed in ultra-pure water and in culture medium to final concentrations of 10, 50 and 100 µg/mL (after sonication for 20 minutes to disperse NP agglomerates and aggregates). In the latter, prior to analysis samples were incubated at 37ºC for 1 and 24h.

Cell Culture

The pulmonary adenocarcinoma cell line A549 was obtained from European Collection of Authenticated Cell Cultures (ECACC) and (Sigma Aldrich, St. Louis, MO, USA).

Cells were cultured in 75 cm^2 culture flasks with Kaighn's Modification of Ham's F-12 Medium supplemented with 10% (v/v) fetal bovine serum (FBS), with 2.5 µg/mL penicillin-streptomycin and 2.5 µg/mL fungizone. All medium components used were purchased from Life Technologies, Carlsbad, CA, USA. Cells were grown at 37°C, 5% CO_2, in a humidified atmosphere. Cell confluence and morphology were daily observed under an inverted phase contrast microscope Nikon Eclipse TS100 (Japan). Cells were subcultured when confluence reached 80% using 0.25% trypsin/1mM EDTA (Life Technologies, Carlsbad, CA, USA). Depending on the assay, cells were seeded in 96, or 6-well plates and left 24h for adhesion. After that, the culture medium was replaced with fresh medium containing AgNP solutions and cells were kept in the referred conditions for 24h and 48h.

AgNPs and Ag^+ treatments

Cells were seeded (10^5cells/mL) in 6-well plates (or in 96-well microplates for the MTT assay) and incubated for 24h to adhere under the culture conditions described above. After that period, the medium was removed and replaced by the same amount of new complete medium containing AgNPs (0-100 µg/mL) or Ag^+, added as $AgNO_3$ (0-20 µg/mL). The stock solution of AgNPs (BioPure - 1.0 mg/ml) was diluted in culture medium to obtain the desired concentrations and sonicated for 20 minutes for NP dispersion. The concentrations were chosen after preliminary assays to optimize the concentration range, in order to obtain a dose-response curve that would show the effect of the compound and would allow us to determine the half maximal inhibitory concentration (IC50). The dose of $AgNO_3$ was calculated based on silver mass and expressed as $AgNO_3$. Cells were exposed for 24h and 48h under the culture conditions described above. Cultures were daily checked with an inverted microscope (Nikon Eclipse TS100, Tokyo, Japan).

Cell viability

Cell viability was determined using the MTT assay, according to (Lévesque et al., 2008) with some modifications. After AgNP or Ag^+ exposure (24h and 48h), 50µl of MTT (1 mg/mL in

PBS) were added to each well and incubated for 4h at normal culture conditions. After that, the medium was removed and 150µl of dimethyl sulfoxide (DMSO) were added to each well to solubilize the formazan crystals. Finally, the samples absorbance was measured by a microplate reader (BioTek ®– Gen5™ software) at 570 nm with blank correction.

Clonogenic Assay

For the colony formation assay (CF), A549 cells were seeded at 50 cells per mL in triplicate and treated for 7 days with Ag^+ 5-17 µg/mL and AgNP 20-100 µg/mL. Cells were washed with PBS, fixed and stained with a mixture of 0.5% crystal violet (Sigma-Aldrich, St. Louis, MO, USA) in 70% ethanol (Franken et al., 2006). Colonies with >30 cells were counted and the surviving factor (SF) was calculated. CF is the average of three independent counting's for each dilution A and B, divided by the number of cells plated; SF is expressed as percentage and is determined by dividing the CF of the treated cells by the CF of the controls, and then multiplying by 100.

Uptake potential of AgNP by flow cytometry

Uptake potential of AgNP10 and AgNP20 by A549 cells was assessed by flow cytometry (FCM), as previously described by (Suzuki et al., 2007). Briefly, A549 cells were seeded in 6-well plates and after 24h an 48h exposure they were trypsinized, collected and analyzed in an Attune Acoustic Focusing Cytometer (Thermo Fisher Scientific, Waltham, MA, USA) equipped with a 488 nm laser. For each sample, 10000–20000 cells were analyzed. Both forward scatter (FS, which gives information on particles' size) and side scatter (SS, which gives information on cell complexity) were scored. The uptake of AgNPs was measured by the shift in SS signal.

Cell Cycle Analysis – Flow Cytometry

Cell cycle analysis was performed according to Oliveira et al. (2014). Cells were seeded in 6-well plates and exposed to AgNPs 50, 100 µg/mL for 24h and 48h (and only medium as control). For each concentration, three replicates were used. Treated cells were trypsinized and washed with PBS pH 7.2. Cells were fixed with 85% ethanol and stored at -20°C. Fixed cells were washed with PBS and filtered by a 55µm nylon mesh. Then 50µl PI (Fluka, USA) (1mg/ mL) and 50µl of RNAse (Sigma, USA) (1 mg/mL) were added. Samples were then incubated for 20

min in the dark. PI relative fluorescence was measured in a flow cytometer Epics coulter XL (Beckman Coulter) equipped with an argon laser - 15mW, 488 nm. For each sample, the number of events reached approximately 5000. Acquisitions were made using SYSTEM II software (v. 3.0, Beckman Coulter, USA). Debris and doublets were excluded by the definition of specific regions (FL peak area vs. FL peak height). The percentage of nuclei in each phase of the cell cycle (G_0/G_1, S and G_2 phases) was analyzed using the FlowJo software (Tree Star Inc., Ashland, Oregon, USA).

Apoptosis – Annexin V Assay

The apoptotic/necrotic cells ratio was measured by flow cytometry using the FITC Annexin V Apoptosis Detection Kit, from BD Pharmingen™, by double staining with Annexin V-FITC and PI. The double staining allows the differentiation from early-stage apoptotic cells (Annexin V-FITC (+)/PI (-) cells), from late-stage apoptotic/necrotic cells (Annexin V-FITC (+)/PI (+)), and live cells (Annexin V-FITC (-)/PI (-)).

Cells were seeded in 6-well plates and exposed to 0, 50, 100 µg/mL, AgNP concentrations. At the end of 24h and 48h exposure, cells were trypsinized and transferred to 15ml tubes. Afterwards, cells were washed twice in cold PBS and resuspended in "1x binding buffer*"* (Detection Kit from BD Pharmingem™) ($1x10^5$cells/ml). To stain the cell suspension, 5µL of FITC-Annexin V and 5µL of PI were added and cells were incubated for 15 min at room temperature in the dark, then 400µL of "1x binding buffer" were added and samples analyzed by an Epics coulter XL flow cytometer. For each sample, 10000 cells were analyzed, and results were expressed as percentages of cells in each quadrant.

Comet Assay

DNA damage was measured by the comet assay, as described by Singh et al. (2009) and Tice et al. (2000) with minor modifications. After AgNP exposure (see above), cells were harvested and washed in PBS. Positive controls were resuspended in 100µM H_2O_2 for 10 min. The cell suspension (50µL) was mixed with 50µL of 1% low melting point agarose (LMPA) and placed on microscope slides coated with normal melting point agarose (NPMA). Cells were then treated with lysis solution (2.5M NaCl, 100mM EDTA, 10mM Tris, 1% Triton X-100 and 10% DMSO,

pH 10) for 2h in the dark. DNA was allowed to unwind for 20 min in cold electrophoretic buffer (300mM NaOH and 1mM EDTA, pH 13). Electrophoresis was conducted at 0.74 V cm−1 and 300 mA for 30 min at 4ºC. Slides were then neutralized with 0.4 M Tris buffer, pH 7.5, and washed with distilled water. Nucleoids were stained with ethidium bromide (Sigma–Aldrich, St. Louis, MO) and observed under a fluorescence microscope Nikon Eclipse 80i (Nikon, Tokyo, Japan) equipped with an ethidium bromide compatible filter (excitation filter: 510–560 nm; dichroic mirror: 572; absorption filter: 590 nm). Fluorescence images of each nucleoid were captured with a Digital Sight camera, software NIS-Elements F 3.00 SP7 (Nikon, Tokyo, Japan). For each sample, two gels were analyzed by visual scoring of 100 comets, quantified by visual classification of nucleoids into five comet classes, according to the tail intensity and length. The total score was calculated on a scale of 0-400 arbitrary units according to Collins (2004) by multiplying the percentage of nucleoids in each class by the corresponding factor, according to the following formula: GDI (genetic damage indicator) = [(%nucleoids class 0)x0] + [(%nucleoids class 1)x1] + [(%nucleoids class 2)x2] + [(%nucleoids class 3)x3] + [(%nucleoids class 4)x4].

CBMN Assay

Cytochalasin B-blocked micronucleus (CBMN) assay was performed as described by Fenech, (2007), with some modification. Briefly, cells were seeded in glass coverslips and exposed to AgNPs as described above. A positive control was performed with methyl methanesulfonate (MMS). After 24h exposure, cytochalasin B (AppliChem, Darmstadt, German) was added to each well and incubated for further 29h to inhibit cytokinesis. At the end of treatment, cells were washed with PBS, and subsequently 1mL of absolute methanol at 4°C was added for cell fixation. To analyze micronuclei, cells were stained with acridine orange (Merck, Darmstadt, Germany) and slides were analyzed at 400× magnification using a fluorescence microscope (Nikon Eclipse 80i, Japan). At least three slides were analyzed per condition, and at least 1,000 cells were scored per slide. Nuclear division cytotoxicity index (NDCI), micronuclei formation (MN), apoptosis and necrosis were recorded (Fenech, 2000).

Statistical Analysis

For all experiments, at least 3 replicates and three independent assays were performed. Statistical significance of the data was analyzed by one-way ANOVA followed by Dunn's or Dunnett-test, for non-parametric or parametric data, respectively, using the SigmaPlot version 11 software. The differences were considered statistically significant for $p < 0.05$. When necessary, data were transformed to achieve normality and equality of variances.

3. Results

Physicochemical characterization of AgNPs

AgNPs primary size was characterized by SEM as described in our previous publication (Rosário et al., 2016)**.** Briefly**,** AgNP10 showed a unimodal size distribution and a particle diameter mean of 10±1.40nm. On other hand, AgNP20 population showed a visible heterogeneous size with a bimodal size distribution (two peaks at 10±0.86 nm and 20±1.06 nm and a particle size mean of 15±4.94 nm).

The DLS measurements obtained 1h and 24h after the AgNPs dispersion in culture medium, provide information on the hydrodynamic size distribution and stability of AgNPs from the time the solution is prepared until the end of a 24h exposure. The dispersion medium was determinant for the NP behavior, as both AgNPs increased their hydrodynamic size when in F-12K complete medium. Data in Table 1 shows that AgNP10 exhibit an agglomeration behavior which increase with concentrations and decrease with time, possible due to Ag dissolution, while, AgNP20 hydrodynamic size was stable within time but changed between concentrations. AgNP10 presented the maximum size of 84.66 nm at the highest concentration, 100 µg/mL, while AgNP20 showed the highest size of 95.8 nm at the concentration of 50 µg/mL, both after 1h.

Table 1 – DLS measurements of hydrodynamic diameter (nm) of AgNP10 and AgNP20 in culture medium, 1 and 24h after preparation (t = 1 and t = 24h) of the following solutions: 10, 50 and 100 µg/mL. Solutions were prepared by dilution with complete growth media – F-12K – 10% FBS. In the presence of more than one peak of size distribution, the peak of highest percentage (and the respective percentage) is shown.

	Average size[a]	**Hydrodynamic diameter (nm) in F12K medium**		
		10µg/mL	50µg/mL	100µg/mL
1h	**10 nm**	49.92 (55%)	75.22	84.66
24h	**10 nm**	17.19 (77%)	47.85	81.05
1h	**20 nm**	78.15 (79%)	95.80	52.13
24h	**20 nm**	79.78 (78%)	93.93	48.04

[a] According to the manufacturer nanoComposix (Biopure)

Confluence and Morphology

A549 cells presented typical cuboidal epithelial aspect, indicative of type II pulmonary morphology and their morphology and confluence was checked daily under microscope.

After 24h exposure to AgNP10 and AgNP20, cell confluence was lower than the one of control cells (Fig.1 – b, b', c and c'). Despite the visible agglomeration of AgNPs, the 100 µg/mL treatment showed a higher confluence loss (Fig.1 – c and c'). A visible scattered background due to AgNPs was visible for higher concentrations, and after 48h compromised the visibility of cells (images not shown).

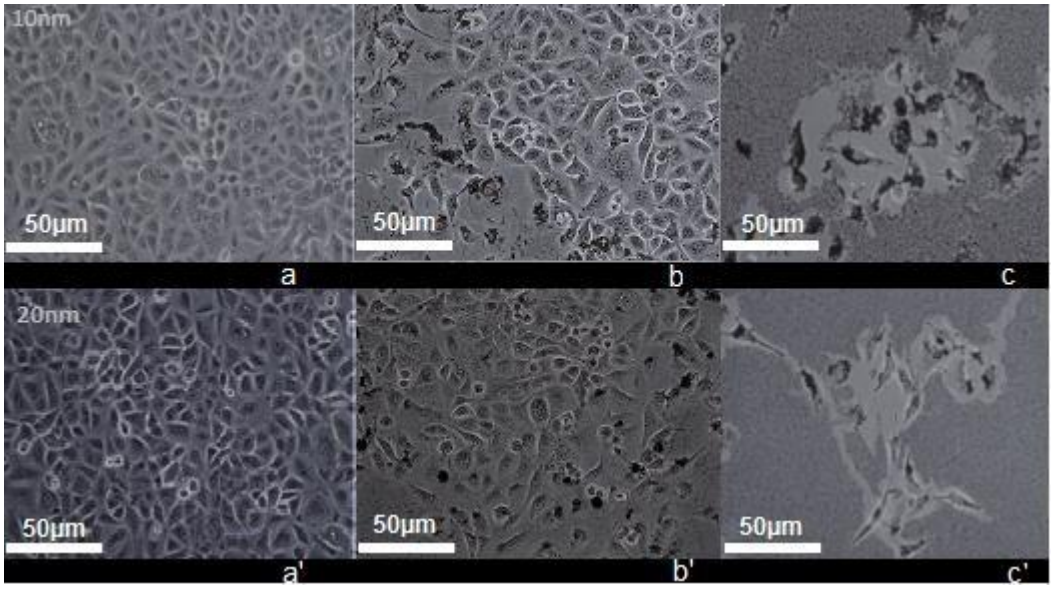

Figure 1 – Light microscopy images of A549 cells exposed to AgNP10 (a - c) and AgNP20 (a´- c´) for 24h. Control (a, a´); 50µg/mL (b, b´), 100µg/mL (c, c´). 100X.

Cell viability

The MTT Assay was used to assess cell relative viability, upon exposure to AgNPs, after 24h and 48h exposure. After 24h and 48h, AgNP10 decreased the viability of A549 cells only for the highest concentrations (>50 µg/mL). While, all the AgNP20 doses reduced the cell viability. Remarkably, at 48h, AgNP10 at higher doses (>50 µg/mL) presented the same degree of toxicity as the same doses of AgNP20 (Fig.2 - b).

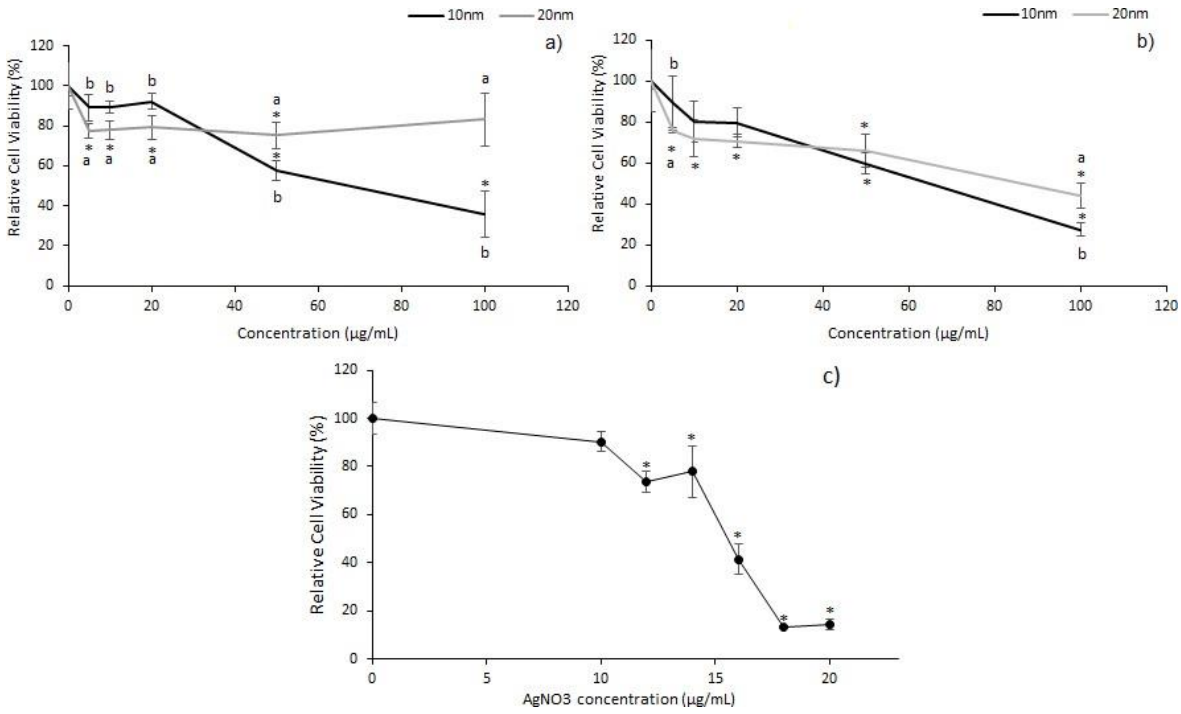

Figure 2 – Results of cell viability from MTT assay for A549 cell line exposed to AgNP10 and AgNP20 (after withdraw of background nanoparticles absorbance's). a) 24h and b) 48h. c) Effects of $AgNO_3$ (Ag^+) in A549 cell line. * means significant differences between control and AgNP concentrations. Different letters (a; b) mean significant differences between AgNP sizes ($p < 0.05$).

Cell exposure to Ag^+ (from $AgNO_3$) revealed, after 24h a sharp decrease in cell viability at levels ≥14 µg/mL (Fig.2 - C). Based on MTT results for the 24h exposure, the estimated IC30 and IC50 were calculated using Sigmaplot 11.0. The estimated IC30 value for Ag^+ was 14.6 µg/mL and the IC50 value was 15.84 µg/mL. The calculated IC30 values for AgNP10 and AgNP20 were 38 µg/mL and 7 µg/mL, respectively. The IC50 value for AgNP10 was 56.4 µg/mL, while

for AgNP20 the calculated IC50 value was out the dose range selected (>100 µg/mL). Therefore, for cell exposures to both AgNP10 and AgNP20 in the subsequent assays (clonogenic assay, apoptosis by the Annexin-V assay, nanoparticle uptake and cell cycle profile) the doses of 50 and 100 µg/mL were selected.

Clonogenic Assay

To investigate the proliferative capacity of cells under exposure to AgNPs or Ag^+ for longer periods, the clonogenic assay was used. For AgNPs, data showed a complete inhibition of colony formation for both time points (7 and 14 days) under exposure to 20-100 µg/mL, and therefore only the data for 7 days is presented (Fig 3 - a). The results indicate that upon exposure to both sizes of AgNPs there was no colony forming capacity.

The effects of Ag^+ on the proliferative capacity of A549 cells were also evaluated at 5 µg/mL and 17 µg/mL. After 7 days of exposure to 5 µg/mL and 17 µg/mL Ag^+, the proliferative capacity significantly decreased to around 9% and 4%, when compared to control (Fig 3 - b).

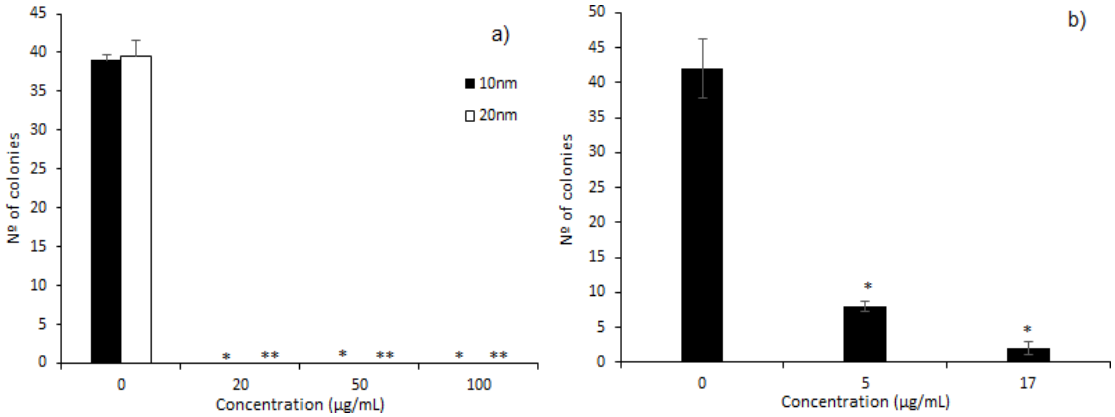

Figure 3 – Cytotoxicity of A549 cells exposed to AgNP for 7 days, determined by the Clonogenic assay. a) AgNP10 and AgNP20, b) Ag^+. * and ** indicates differences between control and AgNP concentrations at $p < 0.05$.

Uptake potential of AgNP

The uptake potential of AgNP10 and AgNP20 by A549 cells was assessed by changes in flow cytometric SS. Flow cytometry data showed a significant increase on the SS signal, which indicates an increase in the uptake of both AgNPs by the cells after 24h and 48h exposure (Fig 4).

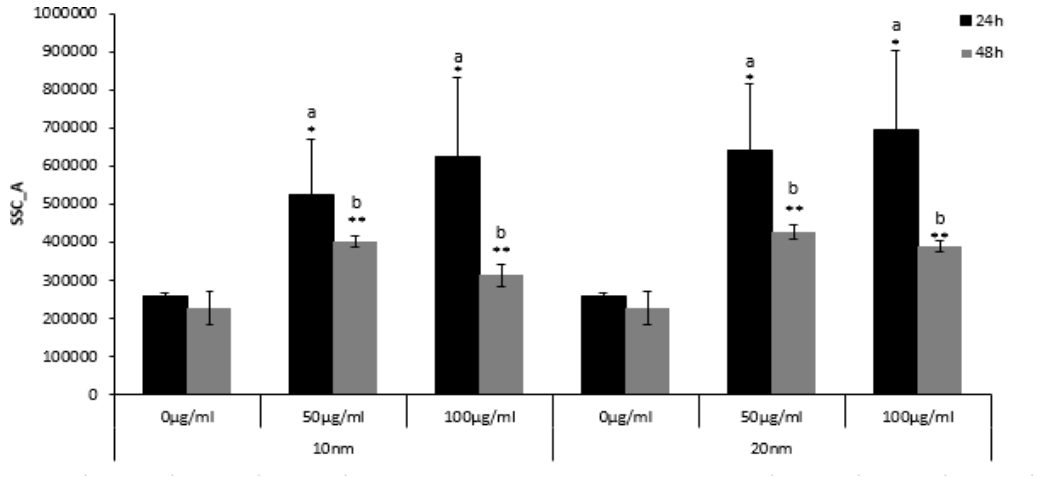

Figure 4 – Uptake of AgNP by A549 cell line exposed to AgNP10 and AgNP20 for 24h and 48h, obtained by flow cytometry. * and ** indicates differences between control and AgNP concentrations at $p < 0.05$. Different letters (a; b) mean significant differences between AgNP sizes ($p < 0.05$).

Cell Cycle

Figure 5 shows the effect of AgNP10 and AgNP20 on the cell cycle dynamics of A549 cells assessed by FCM. As expected, at both 24h and 48h the controls had most of its cells at G_0/G_1 (Fig.5). At 24h, AgNPs increased the S-phase subpopulation, mostly at expenses of G_0/G_1 and G_2 subpopulations while for higher concentrations (particularly evident for 100 µg/mL AgNP20) the increase of cells at sub-G_1 (often associated to cells with DNA break/damaged) increased dramatically (Fig.5 - a). After 48h, in cells exposed to AgNP10 the reduction of the G_0/G_1 subpopulation was aggravated, while the G_2 subpopulation increased (Fig.5 – b). For the same period, exposure to AgNP20 intensified the decrease in G_0/G_1 subpopulation and increased the number of cells at S phase. For this period (48h), while still present, the % of sub-G_1 cells decreased compared to 24h.

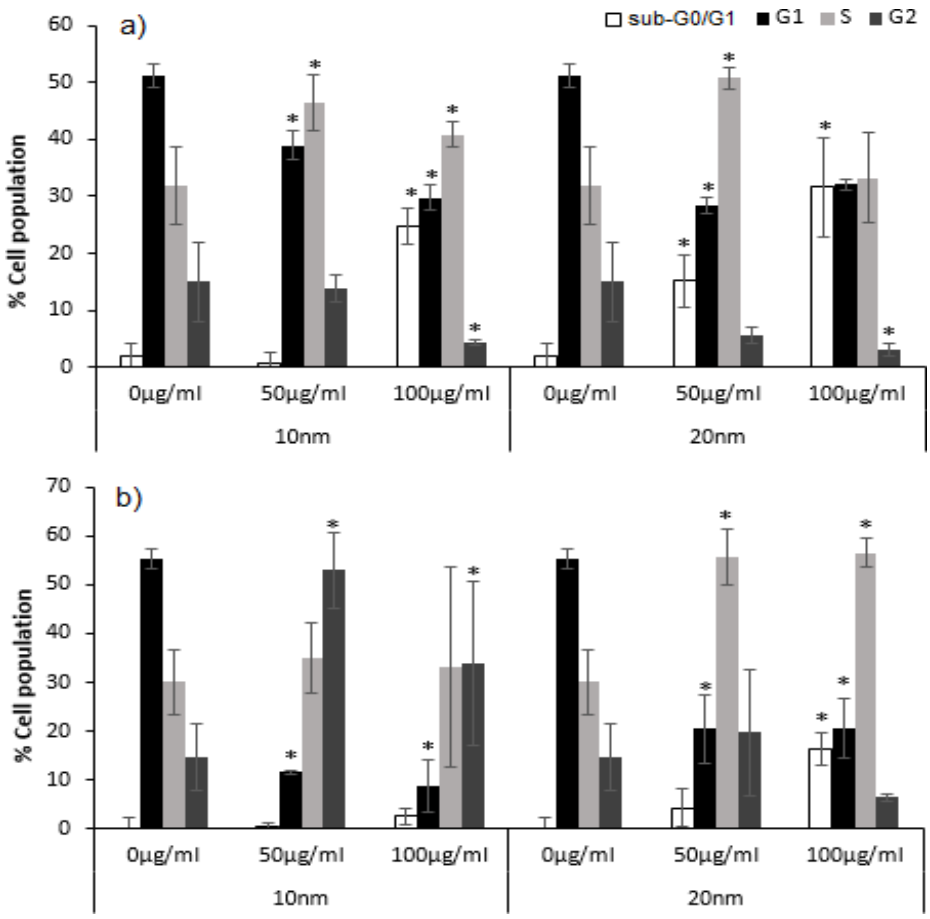

Figure 5 – Cell cycle results of A549 cells exposed to AgNP10 and AgNP20 for a) 24h and b) 48h. The given values are the mean % of cell population (± SD) along cell cycle stages of at least 3 replicates. * indicates differences between control and AgNP concentrations at $p < 0.05$.

Apoptosis by Annexin-V assay

The potential of PVP-coated AgNPs to induce apoptosis in A549 cells was assessed by the Annexin V-FITC/PI assay. After 24h, no significant differences in the percentage of cells under apoptosis or necrosis were found in both AgNP sizes, comparatively to the controls (Fig.6 – a and b). However, after 48h, both concentrations of AgNP10 decreased the number of viable cells and increased the number of late-apoptotic cells (Fig 6– c). AgNP20 also decreased the number of viable cells and increased the number of late-apoptotic and necrotic cells for 100 µg/mL (Fig.6 – d).

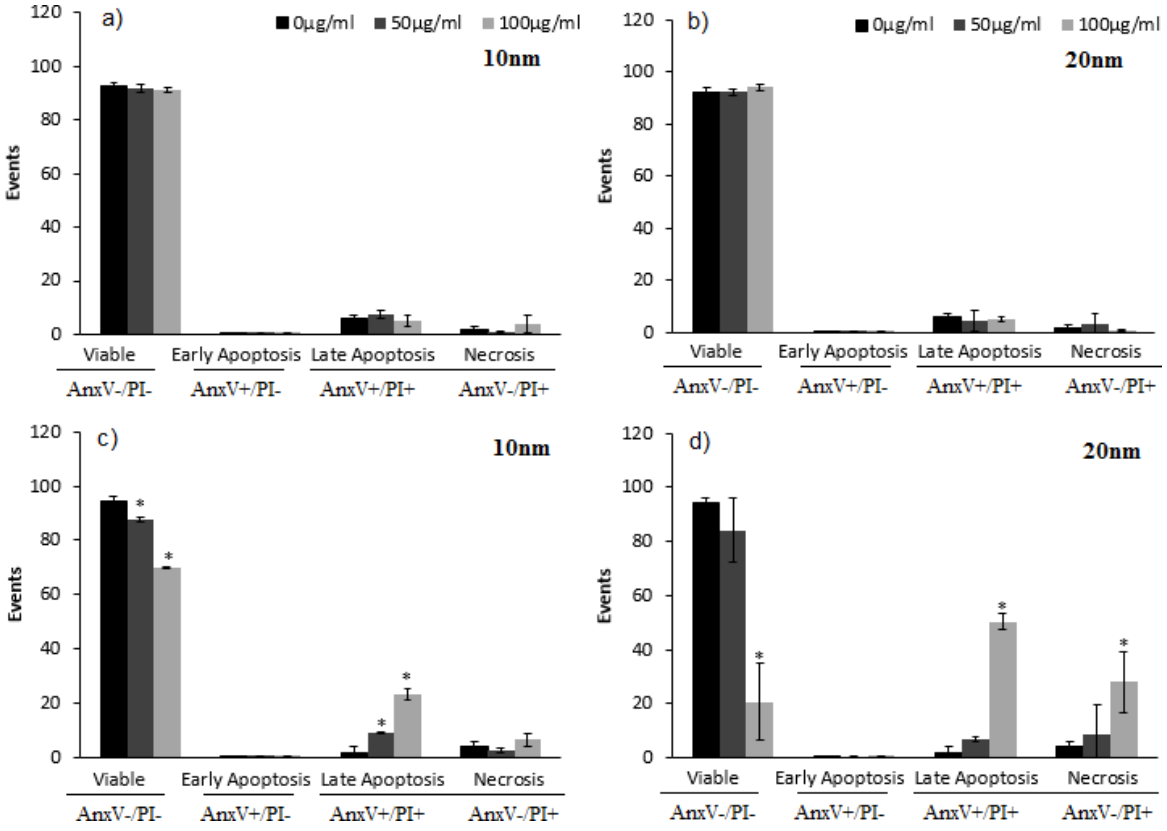

Figure 6 – Annexin V-FITC assay for cell death assessment of A549 cell line exposed to AgNP10 and AgNP20 for 24h and 48h. a) 24h AgNP10, b) 24h AgNP20, c) 48h AgNP10 and d) 48h AgNP20, with 3 replicates. ± SD. * indicates differences between control and AgNP concentrations at $p < 0.05$.

CBMN assay

The CBMN assay was used to measure AgNPs induced MN, cytostasis (the proportion of mono, bi-, and multinucleated cells; NDCI) and cytotoxicity (necrosis and apoptosis) in A549 cells (Fig.7). After 24h, most of the cells exposed to AgNP10 and AgNP20 were mononucleated, contrarily the control cells which were binucleated (Fig.7 - I). For both AgNPs, the NDCI index was always close to 1.0, indicating a high cytostatic effect. (Fig.7 - I). Despite this low NDCI, MN were found in all the binucleated cells found. As the selected doses of AgNPs induced a high cytostatic effect, CBMN assay was also performed with a lower AgNP concentration (20 µg/mL). For both AgNP sizes, the concentration of 50 µg/mL led to an increase in MN frequency. For the highest dose (100 µg/mL) both the rate of dead cells and non-dividing cells

were highly increased and were accompanied by a decrease of the number of MN (Fig.7 – II).

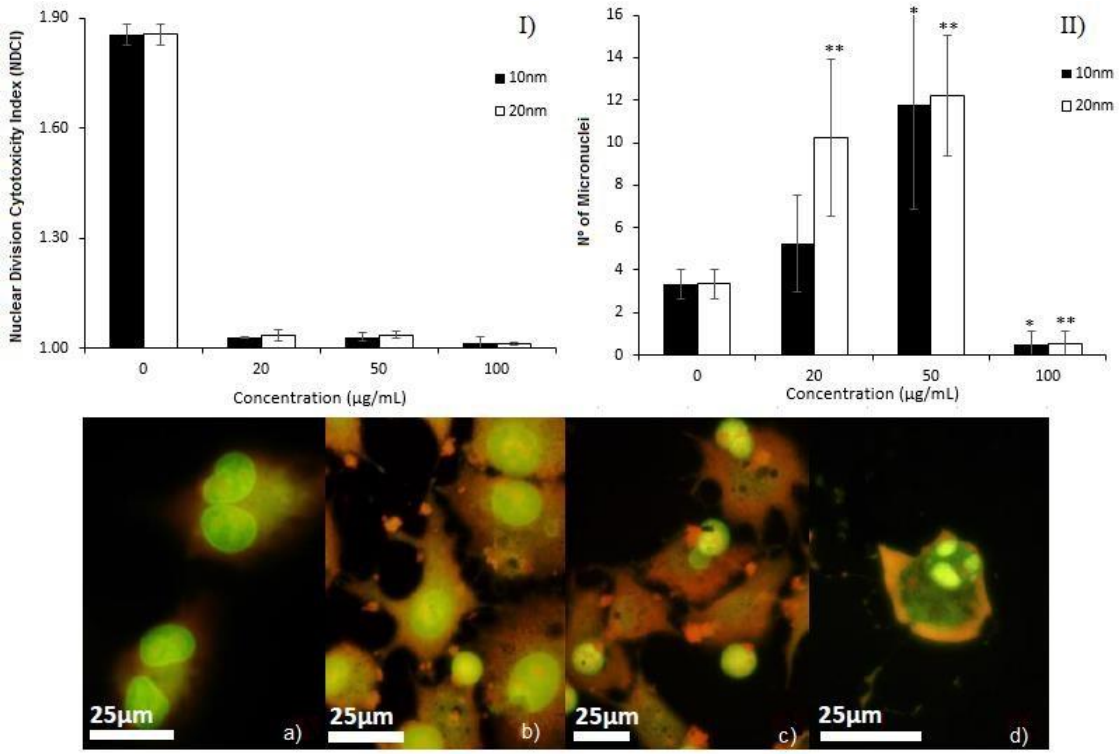

Figure 7 – CBMN assay results of A549 cells exposed to AgNP10 and AgNP20. The graphs represent I) NDCI and II) number of micronuclei obtained after the exposure. *and ** indicates differences between control and concentrations at $p < 0.05$. Down part is the representative images of the cytokinesis-block micronucleus cytome assay in A549 cells, obtained by fluorescence microscopy. a) binucleated cells (control), b) mononucleated cells (100µg/mL - AgNP20), c) necrotic cells (50µg/mL - AgNP20) and d) apoptotic cell (50µg/mL – AgNP10).

Comet assay

To investigate the effects of AgNPs on DNA fragmentation, the comet assay was performed in cells exposed to 50 µg/mL and 100 µg/mL of AgNP10 and AgNP20 for 24h.

In AgNP-exposed cells, the genetic damage indicator (GDI) significantly increased ($p < 0.05$) for both AgNP sizes and concentrations of exposure, the effects being more pronounced for AgNP10 (Fig.8).

Controls showed a predominance of cells in class 0 (“no tail”) (~90%), while AgNP-exposed cells showed overall a tendency to decrease the number of cells in class 0, increasing the % of classes 1-3 (Fig.9). AgNP10 exposure induced, at 50 µg/mL, comets classified as class 1 (~22%),

2 (~10%) and 3 (~10%). For the highest concentration, 100 µg/mL, there was an increase in class 1 (~48%) and 2 (~37%), while the class 3 remained the same (~10%) as at 50 µg/mL. As representative example, Fig.9 (down) illustrates the increase of the comet tail with the increase of AgNP10 concentration (from 0 to 100 µg/mL). On the other hand, AgNP20 exposure increased particularly the percentage of cells in class 1 (~50% and ~58% respectively for 50 and 100 µg/mL) (Fig.9 – b). Interestingly, it should be noted the higher frequency of classes 2/3 in the cells exposed to AgNP10 (Fig.9 – a) than in cells exposed to AgNP20, which could mean a more severe fragmentation of the DNA.

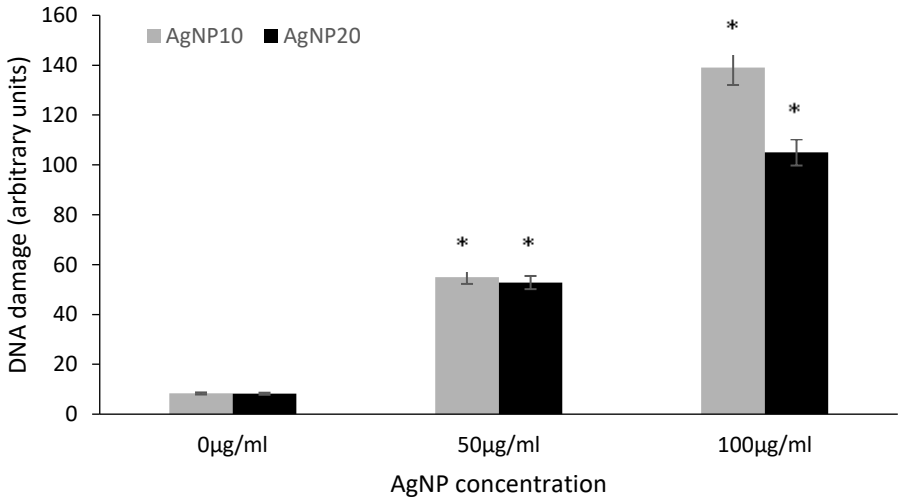

Figure 8 - Mean values of genetic damage indicator (GDI) measured by the standard (alkaline) comet assay of A549 cells after exposure to 50 and 100µg/mL AgNP10 and AgNP20. The results were expressed as the mean +/- SD versus control. * indicate significant differences between control at $p < 0.05$.

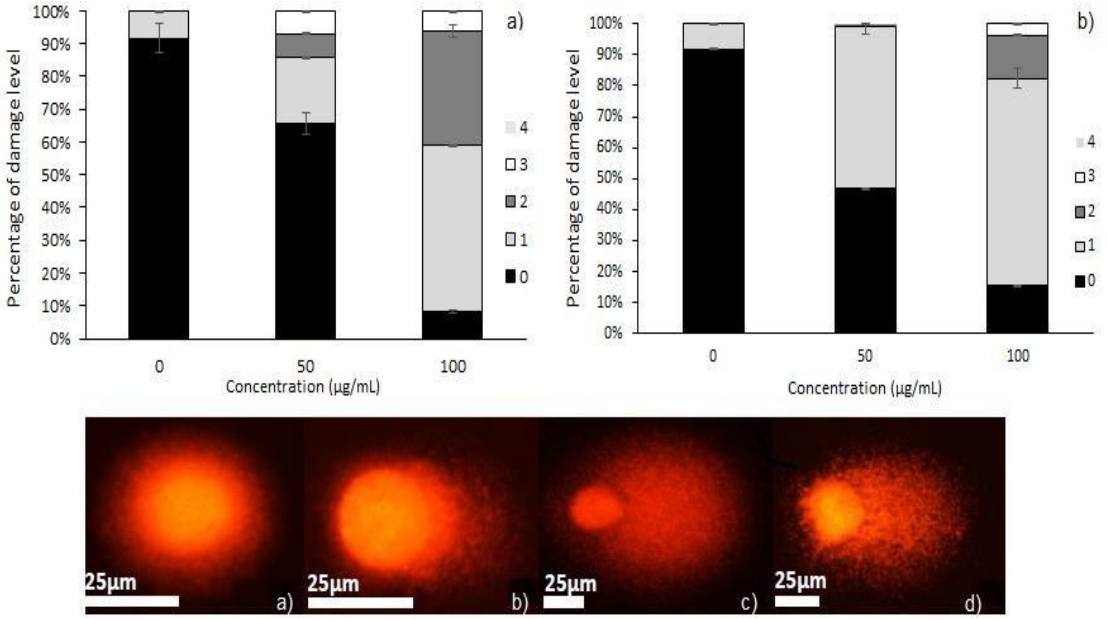

Figure 9 – DNA damage of A549 after exposure to AgNP10 and AgNP20, expressed as % DNA in tail. I) AgNP10 and II) AgNP20. Down part of the figure is the representative images obtained by fluorescence microscopy of the comet assay, for AgNP10: a) control, b) 50µg/mL, c) 100µg/mL and d) positive control.

4. Discussion

In this work, we have investigated the cellular effects of well characterized AgNPs coated with PVP with two small nominal diameters (10 and 20 nm), in order to address if small differences in the NPs size may condition the biological responses in lungs cells, and if/how these responses depend on the dose.

The DLS results show that the hydrodynamic diameter of both AgNPs increased immediately after suspension in F12K culture medium with 10% FBS, which is likely to be due to the formation of a protein corona (Khang et al., 2014). Also, some aggregation induced by the high ionic strength of the culture medium may have occurred (El Badawy et al., 2012; Li et al., 2012; Liu and Hurt, 2010). However, both AgNPs showed a different time-course behavior, where AgNP10 hydrodynamic diameter decreased over time, which could be an indication of Ag dissociation/dissolution leading to an overall of smaller sizes of the particles in suspension. Contrarily, AgNP20 hydrodynamic size was stable over time indicating a low propensity towards aggregations by steric hindrance (Kvítek et al., 2008). Most likely, a rich medium and

the addition of FBS facilitates protein corona formation, which contributes to colloidal stability on the suspended AgNP (Treuel et al., 2015).

Studies have shown that the physicochemical characteristics of AgNPs will influence cellular uptake, intracellular fate and, consequently, their toxicity. Concerning nanoparticle cell uptake, a size-dependent uptake of AgNPs has been observed in different cell lines, with small NPs being internalized more easily than larger ones (e.g., Liu et al., 2010). In the present work the cellular uptake was similar for both AgNP10 and AgNP20, indicating that this difference in size was not enough to significantly change the uptake rate by A549 cells. Bastos et al. (2016a; 2016b) reported that citrate or PEG coated AgNPs modulate similarly the cellular uptake by HepG2 cell line, while PEG coated AgNPs are taken up by HaCaT cells in a lower extent than citrate coated AgNPs. Previous studies indicate that A549 cell line is more sensitive to different metal-NPs than other cells lines/tissues. For example, A549 cell line was more sensitive to 0.5μg/mL CeO_2NP than colon (CaCo2) and liver (HepG2) cell lines (De Marzi et al., 2013).

We also demonstrated previously (Rosário et al., 2016) that for the same AgNPs, osteosarcoma cells (MG-63) had, for 24h, an IC50 value of 58.3μg/mL and of 93.9μg/mL for AgNP10 and AgNP20 respectively. Our results demonstrated that A549 cells are more sensitive to AgNP20 at lower concentrations (up to 5μg/mL) presenting an IC30 of ~7μg/mL. Contrarily, AgNP10 toxicity seems to be concentration-dependent, with less toxicity at lower doses (IC30 ~38μg/mL) and increased toxicity at higher concentrations (IC50 ~56μg/mL), when compared to AgNP20 (IC50>100μg/mL). Therefore, the toxicity profiles of both AgNPs to A549 cells cannot be solely explained based on the NP internalization. The analysis of AgNP10 and AgNP20 dissolution in culture medium showed for 24h a similar release of Ag^+ for AgNP10 and AgNP20, but at 48h there was a concentration-dependent release of Ag^+ into the medium, with the higher amount of Ag^+ release for 100μg/mL for AgNP10, when compared to AgNP20 (Rosário et al., 2016). This result suggests a significant contribution of Ag^+ in the AgNP10 toxicity and may explain the high toxicity obtained at 48h to 100 μg/ml of AgNP10 in the MTT assay compared to AgNP20. However, the non-classical dose-response curve obtained for AgNP20 at MTT - 24h is not due to low Ag^+ release but in fact it may be due to the bimodal size distribution obtained for AgNP20. The effects of AgNPs towards cell viability are often compared to those of Ag^+. Liu et al. (2010) compared the effects of 5, 20 and 50nm AgNP and

Ag^+ in the cell viability of several cell models (A549, SGC-7901, HepG2, and MCF-7) and established the following toxicity ranking: AgNP 5nm > Ag^+ > AgNP 20nm > AgNP 50nm detected by the MTT assay. In present work, we found that in small doses, AgNP20 is more toxic to A549 cells than Ag^+, as they present IC30 of 7 and 14.16 µg/mL, respectively. With increase in concentration, both AgNP show a similar toxicity, which was lower than the obtained for Ag^+. After a long-term exposure of 7 days, both AgNP10 and AgNP20 showed higher toxicity than Ag^+, which was not expected according to their respective IC50 (MTT) values (AgNP20 >100µg/mL; AgNP10=56.4µg/mL; $AgNO_3$=15.84µg/mL). It seems therefore, that the difference between the cytotoxicity of AgNP10 and AgNP20 is related to core size, which influences the AgNP reactivity. The concentrations selected for our study are within those recommended by Gangwal et al. (2011) for *in vitro* assays, based on the calculations of the mass of nanoparticle retained in the alveolar region of the lung per alveolar surface area size in exposure scenarios of 24h and 45 years. Alveolar retention per surface area for Ag spherical NPs was ~ 48.9µg/cm^2 for a full working lifetime (considering 20nm diameter particles, and an exposure aerosol concentration of 1 mg/m^3) (Gangway et al., 2011). Considering the area of a 96-well plate the peak lung surface concentration equates to 78.2µg/mL, thus within the range of tested in our work.

In general, toxic substances interfering with the cell cycle progression may induce DNA damage and/or interfere with the structural elements from the mitotic apparatus and, eventually, may lead to cell death. In particular, A549 cells exposed to AgNPs>100nm and IMR-90 and U251 cells exposed to both 6 and 20nm AgNPs, showed an accumulation of cells at G_2/M and sub-G_1 phases, with a concurrent decrease in cells at G_1 (AshaRani et al., 2009; Lee et al., 2011). In the present work, the two small sizes of AgNPs interfered differently with the cell cycle of A549 cells. AgNP10 cytostatic effects differed with duration of exposure, with an increase on the number of cells at S and sub-G_1 phases after 24h, and an increase in the G_2 subpopulation together with a decrease of sub-G_1 after 48h. Lim et al. (2012) reported an increase in active ATM protein after 48h exposure to AgNPs at 100µg/mL in different mammalian cells types. ATM phosphorylates several proteins involved in the DNA-damage response, including p53. After DNA damage, p53 leads to cell cycle arrest via activation of p21, promoting DNA repair processes or the induction of apoptosis. We assume that when A549 cells are exposed to the

smaller size AgNPs (AgNP10) the repair process is easily activated, which explains the decrease of the sub-G_1 phase and increase on the number of cells at G_2 phase, from 24h to 48h exposure. Thus, supporting the hypothesis that AgNP10 exposed cells at the G_2/M checkpoint/transition, may have an extra time to repair DNA damage prior segregation of chromosomes, which was described by AshaRani et al. (2009). Cells exposed to AgNP20, showed also an increase in the number of cells at S phase and sub-G_1 phase, at 24h. However, after 48h more than 55% of the cell population was still arrested at S phase indicating that DNA repair mechanisms are not the same as those proposed for AgNP10. Beer et al. (2012) found that PVP-coated AgNPs significantly increased the percentage of A549 cells at G_2/M and S phases. S phase delay was also observed by Liu et al. (2010) in HepG2 cells exposed to PVP-coated AgNPs and by Foldbjerg et al. (2012) in A549 cells exposed to citrate coated AgNPs.

The mechanisms behind the different pathways of DNA damage and cell death induced by small sized AgNPs remains unknown. The lack of binucleated cells in the CBMN assay, and the evident reduction of the NDCI after treatment with the higher doses of AgNPs (50 and 100 µg/mL) are in good agreement with the cell cycle results. To overcome this AgNP cytostatic effect, cells were exposed to a lower AgNP concentration (20 µg/mL) and the number of MN were also scored. Our data showed that both NPs induced DNA damage with an increase in the presence of MN at 50µg/mL for AgNP10 for both 20 and 50µg/mL for AgNP20. Once again, as obtained by MTT assay, a lower dose of AgNP induced higher damage to the exposed cells, when compared to AgNP10. Despite the observed MN increase and NDCI decrease, presence of nucleoplasmic bridges (NPBs) was not detected. Genotoxicity may also be evaluated by the DNA fragmentation assessment using the comet assay (Martins et al., 2017). The comet assay showed once more a size-dependent toxicity, as the AgNP10 exposed cells presented a slightly lower number of damaged cells when compared to AgNP20 exposed cells, however the level of damage of AgNP10 exposed cells was more severe (class 3). Brzóska et al. (2015) reported that AgNPs with 20 and 200 nm (up to 100µg/mL) induced for A549 cells, a minor decrease in viability and increase in the extent of DNA breakage after 24h for both sizes by comet assay, while for HepG2 a massive induction of DNA breakage at a short-term exposure was observed. The increase in sub-G_1 population upon exposure to both AgNP10 and AgNP20 detected in DNA content frequency histograms may be an indicator of apoptosis, as reported in the

literature. The annexin V/PI assay can distinguish between viable, early apoptotic and late apoptotic/necrotic cells. Late apoptotic cells and necrotic cells are difficult to distinguish with this assay as in both the integrity of the plasma and nuclear membranes decreases, allowing PI to pass through the membranes leading to subsequent nuclei intercalation. Foldbjerg, Dang, and Autrup (2011) exposed A549 cells to PVP-coated AgNPs with 69nm and found an increase in late apoptosis/necrosis and slight increases in early apoptosis. Our results show increase in late apoptosis/necrosis after 48h exposure for both AgNP20 and increase in late apoptosis for AgNP10. These clastogenic and apoptotic/necrotic data may indicate a severe and irreparable damage, or a failure of repair pathways present in the cells exposed AgNP20, when compared to AgNP10 exposed cells. Finally, the lack of visible early-apoptosis expected, may be justified with the fact that A549 cells have a constitutively high expression of the heme oxygenase-1, which might render them less susceptible to ROS-induced cell death – early-apoptosis (Foldbjerg et al., 2011; Kweon et al., 2006).

5. Conclusions

In sum, the toxicological activities of small sized PVP-coated AgNPs (10 and 20 nm) were found to be size-dependent at all endpoints tested. For lower concentrations ($\leq$5 µg/mL) AgNP20 induced higher mortality than AgNP10. A behavior that was inverted at higher doses where AgNP10 showed higher toxicity. For doses >50 µg/mL AgNP10 induced severe damages in DNA (class 3 and 4 of comet assay), cell cycle disturbance (arrest at G_2) with an active DNA repair process and induction of late-apoptosis. Contrarily, AgNP20 induced arrest at S phase and increase in the sub-G_1 that was not recovered after 48h. This size also induced more expressive late apoptosis/ necrosis than AgNP10. In long term exposures, clonogenic assay showed that both AgNPs sizes impaired the A549 colony formation and were found much more toxic than Ag^+.

Overall, this study contributes to the understanding of the cytotoxicity mechanisms of small sized PVP-coated AgNPs to lung cells. Our data demonstrate that for small AgNP sizes ($\leq$20 nm), the cyto and genotoxic effects are dependent in a nonlinear way of both size x concentration, targeting different cell pathways, namely in regarding programmed cell death.

Finally, we contribute to clarify that the toxicity of AgNPs is related with their core size (which influences the AgNP reactivity) and not only conditioned by the Ag^+ ion dissolution, nor by their internalization, since both sizes were internalized at equivalent levels by these cells.

Acknowledgments:

Thanks are due, for the financial support, to CESAM (UID/AMB/50017), to FCT/MEC through national funds and the co-funding by the FEDER, within the PT2020 Partnership Agreement and COMPETE. Funding to the project PTDC/AAC-AMB/113649 by FEDER through COMPETE and by national funds through FCT (Fundação para a Ciência e a Tecnologia). FCT-awarded grants to Fernanda Rosário (SFRH/BD/91270/2012) and Helena Oliveira (SFRH/BPD/111736/2015) are greatly acknowledged.

References

Anderson, D.S., Patchin, E., Silva, R.M., Uyeminami, D., Sharmah, A., Guo, T., Das, G., Brown, J., Shannahan, J., Gordon, T., Chen, L., Pinkerton, K., Van Winkle, L., 2015. Influence of particle size on persistence and clearance of aerosolized silver nanoparticles in the rat lung. Toxicol. Sci. 144, 366–81. doi:10.1093/toxsci/kfv005

AshaRani, P. V., Low Kah Mun, G., Hande, M.P., Valiyaveettil, S., 2009. Cytotoxicity and Genotoxicity of Silver nanoparticles in human cells. ACS Nano 3, 279–290. doi:10.1021/nn800596w

Bastos, V., Brown, D., Johnston, H., Daniel-da-Silva, A.L., Duarte, I.F., Santos, C., Oliveira, H., 2016a. Inflammatory responses of a human keratinocyte cell line to 10 nm citrate- and PEG-coated silver nanoparticles. J. Nanoparticle Res. 18, 205. doi:10.1007/s11051-016-3515-x

Bastos, V., Ferreira de Oliveira, J.M.P., Brown, D., Jonhston, H., Malheiro, E., Daniel-da-Silva, A.L., Duarte, I.F., Santos, C., Oliveira, H., 2016b. The influence of Citrate or PEG coating on silver nanoparticle toxicity to a human keratinocyte cell line. Toxicol. Lett. 249, 29–41.

Beer, C., Foldbjerg, R., Hayashi, Y., Sutherland, D.S., Autrup, H., 2012. Toxicity of silver nanoparticles - nanoparticle or silver ion? Toxicol. Lett. 208, 286–92. doi:10.1016/j.toxlet.2011.11.002

Brzóska, K., Męczyńska-Wielgosz, S., Stępkowski, T.M., Kruszewski, M., 2015. Adaptation of HepG2 cells to silver nanoparticles-induced stress is based on the pro-proliferative and anti-apoptotic changes in gene expression. Mutagenesis 30, 431–439. doi:10.1093/mutage/gev001

Bunderson-Schelvan, M., Holian, A., Hamilton, R., 2017. Engineered nanomaterial-induced lysosomal membrane permeabilization and anti-cathepsin agents. J. Toxicol. Environ. Heal. Part B 20, 230– 248. doi:10.1080/10937404.2017.1305924

Chairuangkitti, P., Lawanprasert, S., Roytrakul, S., Aueviriyavit, S., Phummiratch, D., Kulthong, K., Chanvorachote, P., Maniratanachote, R., 2013. Silver nanoparticles induce toxicity in A549 cells via ROS-dependent and ROS-independent pathways. Toxicol. In Vitro 27, 330–8.

Collins, A., Dušinská, M., Franklin, M., Somorovská, M., Petrovská, H., Duthie, S., Fillion, L., Panayiotidis, M., Rašlová, K., Vaughan, N., 1997. Comet assay in human biomonitoring studies: Reliability, validation, and applications. Environ. Mol. Mutagen. 30, 139–146.

Collins, A., Ma, A., Duthie, S., 1995. The kinetics of repair of oxidative DNA damage (strand breaks and oxidised pyrimidines) in human cells. Mutat. Res. Repair 336, 69–77.

De Marzi, L., Monaco, A., De Lapuente, J., Ramos, D., Borras, M., Di Gioacchino, M., Santucci, S., Poma, A., 2013. Cytotoxicity and Genotoxicity of Ceria Nanoparticles on Different Cell Lines in Vitro. Int. J. Mol. Sci. 14, 3065–3077. doi:10.3390/ijms14023065

Drake, P.L., Hazelwood, K.J., 2005. Exposure-Related Health Effects of Silver and Silver

Compounds: A Review. Ann. Occup. Hyg. 49, 575–85. doi:10.1093/annhyg/mei019

El Badawy, A.M., Scheckel, K.G., Suidan, M., Tolaymat, T., 2012. The impact of stabilization mechanism on the aggregation kinetics of silver nanoparticles. Sci. Total Environ. 429, 325–31.

Fenech, M., 2007. Cytokinesis-block micronucleus cytome assay. Nat. Protoc. 2, 1084–1104. Fenech, M., 2000. The in vitro micronucleus technique. Mutat. Res. 455, 81–95.

Foldbjerg, R., Dang, D.A., Autrup, H., 2011. Cytotoxicity and genotoxicity of silver nanoparticles in the human lung cancer cell line, A549. Arch. Toxicol. 85, 743–50. doi:10.1007/s00204-010-0545-5

Foldbjerg, R., Hayashi, Y., Sutherland, D., Autrup, H., Beer, C., 2012. Global gene expression profiling of human lung epithelial cells after exposure to nanosilver. Toxicol. Sci. 130, 145–157.

Foster, K., Oster, C., Mayer, M., Avery, M., Audus, K.L., 1998. Characterization of the A549 Cell Line as a Type II Pulmonary Epithelial Cell Model for Drug Metabolism. Exp. Cell Res. 243, 359–366.

Franken, N.A.P., Rodermond, H.M., Stap, J., Haveman, J., van Bree, C., 2006. Clonogenic assay of cells in vitro. Nat. Protoc. 1, 2315–2319.

Gangwal, S., Brown, J.S., Wang, A., Houck, K.A., Dix, D.J., Kavlock, R.J., 2011. Informing Selection of Nanomaterial Concentrations for ToxCast in Vitro Testing Based on Occupational Exposure Potential 1539–1546.

Gliga, A.R., Skoglund, S., Wallinder, I.O., Fadeel, B., Karlsson, H.L., 2014. Size-dependent cytotoxicity of silver nanoparticles in human lung cells: the role of cellular uptake, agglomeration and Ag release. Part. Fibre Toxicol. 11, 11. doi:10.1186/1743-8977-11-11

Guo, X., Li, Y., Yan, J., Ingle, T., Jones, M.Y., Mei, N., Boudreau, M.D., Cunningham, C.K., Abbas, M., Paredes, A.M., Zhou, T., Moore, M.M., Howard, P.C., Chen, T., 2016. Size- and coating- dependent cytotoxicity and genotoxicity of silver nanoparticles evaluated using in vitro standard assays. Nanotoxicology 10, 1373–1384. doi:10.1080/17435390.2016.1214764

Haberl, N., Hirn, S., Wenk, A., Diendorf, J., Epple, M., Johnston, B.D., Krombach, F., Kreyling, W.G., Schleh, C., 2013. Cytotoxic and proinflammatory effects of PVP-coated silver nanoparticles after intratracheal instillation in rats. Beilstein J. Nanotechnol. 4, 933–940. doi:10.3762/bjnano.4.105

Herzog, F., Loza, K., Balog, S., Clift, M.J.D., Epple, M., Gehr, P., Petri-Fink, A., Rothen-Rutishauser, B., 2014. Mimicking exposures to acute and lifetime concentrations of inhaled silver nanoparticles by two different in vitro approaches. Beilstein J. Nanotechnol. 5, 1357–1370.

Kaur, J., Tikoo, K., 2013. Evaluating cell specific cytotoxicity of differentially charged silver nanoparticles. Food Chem. Toxicol. 51, 1–14. doi:10.1016/j.fct.2012.08.044

Kawata, K., Osawa, M., Okabe, S., 2009. In Vitro Toxicity of Silver Nanoparticles at Noncytotoxic Doses to HepG2 Human Hepatoma Cells. Environ. Sci. Technol. 43, 6046–6051.

Kaweeteerawat, C., Na Ubol, P., Sangmuang, S., Aueviriyavit, S., Maniratanachote, R., 2017. Mechanisms of antibiotic resistance in bacteria mediated by silver nanoparticles. J. Toxicol. Environ. Heal. Part A 80, 1276–1289. doi:10.1080/15287394.2017.1376727

Kermanizadeh, A., Gosens, I., MacCalman, L., Johnston, H., Danielsen, P., Lenz, A., Fernandes, T., Wallin, H., Kreyling, W., Loft, S., Møller, P., 2016. A Multilaboratory Toxicological Assessment of a Panel of 10 Engineered Nanomaterials to Human Health—ENPRA Project—The Highlights, Limitations, and Current and Future Challenges. J. Toxicol. Environ. Heal. Part B 19, 1–28.

Khang, D., Lee, Y.K., Choi, E., Webster, T.J., Kim, S., 2014. Effect of the protein corona on nanoparticles for modulating cytotoxicity and immunotoxicity. Int. J. Nanomedicine Volume 10, 97. doi:10.2147/IJN.S72998

Kvítek, L., Panáček, A., Soukupová, J., Kolář, M., Večeřová, R., Prucek, R., Holecová, M., Radek, Z., 2008. Effect of Surfactants and Polymers on Stability and Antibacterial Activity of Silver Nanoparticles (NPs). J Phys. Chem C 112(15), 5825-5834 doi:10.1021/JP711616V

Kweon, M., Adhami, V.M., Lee, J., Mukhtar, H., 2006. Constitutive overexpression of Nrf2-dependent heme oxygenase-1 in A549 cells contributes to resistance to apoptosis induced by epigallocatechin 3-gallate. J. Biol. Chem. 281, 33761–72. doi:10.1074/jbc.M604748200

Lee, Y.S., Kim, D.W., Lee, Y.H., Oh, J.H., Yoon, S., Choi, M.S., Lee, S.K., Kim, J.W., Lee, K., Song, C., 2011. Silver nanoparticles induce apoptosis and G2/M arrest via PKCζ-dependent signaling in A549 lung cells. Arch. Toxicol. 85, 1529–40. doi:10.1007/s00204-011-0714-1

Lévesque, M., Martineau, C., Jumarie, C., Moreau, R., 2008. Characterization of cadmium uptake and cytotoxicity in human osteoblast-like MG-63 cells. Toxicol. Appl. Pharmacol. 231, 308–17.

Li, J., Zuo, Y., Man, Y., Mo, A., Huang, C., Liu, M., Jansen, J.A., Li, Y., 2012. Fabrication and biocompatibility of an antimicrobial composite membrane with an asymmetric porous structure. J. Biomater. Sci. Polym. Ed. 23, 81–96. doi:10.1163/092050610X543159

Lim, H.K., Asharani, P. V., Hande, M.P., 2012. Enhanced genotoxicity of silver nanoparticles in DNA repair deficient Mammalian cells. Front. Genet. 3, 104. doi:10.3389/fgene.2012.00104

Liu, J., Hurt, R.H., 2010. Ion release kinetics and particle persistence in aqueous nano-silver colloids. Environ. Sci. Technol. 44, 2169–75. doi:10.1021/es9035557

Liu, W., Wu, Y., Wang, C., Li, H.C., Wang, T., Liao, Y., Cui, L., Zhou, Q.F., Yan, B., Jiang, G.B., 2010. Impact of silver nanoparticles on human cells: effect of particle size.

Nanotoxicology 4, 319–30.

Martins, A.J., Azevedo, L.F., de Souza Rocha, C., Carneiro, M.F.H., Venancio, V.P., de Almeida, M.R., Antunes, ., De Carvalho, H., Rodrigues, J.L., Ogunjimi, A.T., Adeyemi, J.A., Barbosa, F., 2017. Evaluation of distribution, redox parameters, and genotoxicity in Wistar rats co-exposed to silver and titanium dioxide nanoparticles. J. Toxicol. Environ. Heal. - Part A Curr. Issues 80, 1156–1165.

Nel, A., Xia, T., Li, N., 2006. Toxic potential of materials at the nanolevel. Science 311, 622–7. Nymark, P., Catalán, J., Suhonen, S., Järventaus, H., Birkedal, R., Clausen, P.A., Jensen, K.A., Vippola, M., Savolainen, K., Norppa, H., 2013. Genotoxicity of polyvinylpyrrolidone-coated silver nanoparticles in BEAS 2B cells. Toxicology 313, 38–48. doi:10.1016/j.tox.2012.09.014

Oberdörster, G., Oberdörster, E., Oberdörster, J., 2005. Nanotoxicology: an emerging discipline evolving from studies of ultrafine particles. Environ. Health Perspect. 113, 823–39. doi:10.1289/EHP.7339

Oliveira, H., Monteiro, C., Pinho, F., Pinho, S., Ferreira de Oliveira, J.M.P., Santos, C., 2014. Cadmium- induced genotoxicity in human osteoblast-like cells. Mutat. Res. - Genet. Toxicol. Environ. Mutagen. 775–776, 38–47. doi:10.1016/j.mrgentox.2014.10.002

Reshma, S.C., Syama, S., Mohanan, P. V., 2016. Nano-biointeractions of PEGylated and bare reduced graphene oxide on lung alveolar epithelial cells: A comparative in vitro study. Colloids Surfaces B Biointerfaces 140, 104–116. doi:10.1016/j.colsurfb.2015.12.030

Rosário, F., Hoet, P., Santos, C., Oliveira, H., 2016. Death and cell cycle progression are differently conditioned by the AgNP size in osteoblast-like cells. Toxicology 368–369, 103–115.

Sahu, S.C., Zheng, J., Graham, L., Chen, L., Ihrie, J., Yourick, J.J., Sprando, R.L., 2014. Comparative cytotoxicity of nanosilver in human liver HepG2 and colon Caco2 cells in culture. J. Appl. Toxicol. 34, 1155–1166. doi:10.1002/jat.2994

Shapiro, D.L., Nardone, L.L., Rooney, S.A., Motoyama, E.K., Munoz, J.L., 1978. Phospholipid biosynthesis and secretion by a cell line (A549) which resembles type II aleveolar epithelial cells. Biochim. Biophys. Acta 530, 197–207.

Singh, N., Manshian, B., Jenkins, G.J.S., Griffiths, S.M., Williams, P.M., Maffeis, T.G.G., Wright, C.J., Doak, S.H., 2009. NanoGenotoxicology: The DNA damaging potential of engineered nanomaterials. Biomaterials 30, 3891–3914. doi:10.1016/j.biomaterials.2009.04.009

Suzuki, H., Toyooka, T., Ibuki, Y., 2007. Simple and easy method to evaluate uptake potential of nanoparticles in mammalian cells using a flow cytometric light scatter analysis. Environ. Sci. Technol. 41, 3018–24.

Tejamaya, M., Römer, I., Merrifield, R.C., Lead, J.R., 2012. Stability of Citrate, PVP, and PEG Coated Silver Nanoparticles in Ecotoxicology Media. Environ. Sci. Technol. 46, 7011–

7017.

Tice, R.R., Agurell, E., Anderson, D., Burlinson, B., Hartmann, A., Kobayashi, H., Miyamae, Y., Rojas, E., Ryu, J.C., Sasaki, Y.F., 2000. Single cell gel/comet assay: Guidelines for in vitro and in vivo genetic toxicology testing. Environ. Mol. Mutagen. 35, 206–221.

Treuel, L., Docter, D., Maskos, M., Stauber, R.H., 2015. Protein corona - from molecular adsorption to physiological complexity. Beilstein J. Nanotechnol. 6, 857–873. doi:10.3762/bjnano.6.88

U.S EPA, 2010. Emerging Contaminants - Nanomaterials, U.S. Environmental Protection Agency (EPA). Washington, DC. doi:10.1016/B978-0-12-374849-2.00004-6

Vance, M.E., Kuiken, T., Vejerano, E.P., McGinnis, S.P., Hochella Jr., M.F., Rejeski, D., Hull, M.S., 2015. Nanotechnology in the real world: Redeveloping the nanomaterial consumer products inventory. Beilstein J. Nanotechnol. 6, 1769–1780.

Williams, D., 2006. The appropriateness of existing methodologies to assess the potential risks associated with engineered and adventitious products of nanotechnologies. Toxicology 246, 79.

Xin, L., Wang, J., Fan, G., Che, B., Wu, Y., Guo, S., Tong, J., 2015. Oxidative stress and mitochondrial injury-mediated cytotoxicity induced by silver nanoparticles in human A549 and HepG2 cells. Environ. Toxicol. n/a-n/a. doi:10.1002/tox.22171

Zhang, F., Durham, P., Sayes, C.M., Lau, B.L.T., Bruce, E.D., 2015. Particle uptake efficiency is significantly affected by type of capping agent and cell line. J. Appl. Toxicol. 35, 1114–1121.

Chapter IV

Impact of particle size on toxicity, tissue distribution and excretion kinetics of chronic intratracheal instilled AgNPs in a mouse model

Part of this chapter was submitted as:

Rosário F., Creylman J., Verheyen G., Van Miert S., Santos C., Hoet P., Oliveira H (2018) Impact of particle size on toxicity, tissue distribution and excretion kinetics of chronic intratracheal instilled silver nanoparticles in mice

Impact of particle size on toxicity, tissue distribution and excretion kinetics of chronic intratracheal instilled silver nanoparticles in mice

Rosário F [a], Creylman J [b], Verheyen G [b], Van Miert S [b], Santos C [C], Hoet P [d II] Oliveira H [a,e I]

[a] *Department of Biology & CESAM, University of Aveiro, Campus Universitário, 3810-193 Aveiro, Portugal*

[b] *RADIUS Group, Thomas More University College, Campus Kempen, Kleinhoefstraat 4, 2440, Geel, Belgium*

[c] *Department of Biology, Faculty of Sciences, University of Porto, Rua do Campo Alegre, 4169-007, Porto*

[d] *Occupational and environmental Toxicology, KU Leuven, ON1Campus Gasthuisberg, Herestraat 49, 3000 Leuven, Belgium*

[e] *CICECO - Aveiro Institute of Materials, University of Aveiro, 3810-193 Aveiro, Portugal*

[I] *Corresponding author. E-mail address:* holiveira@ua.pt

[II] *Corresponding author. E-mail address:* peter.hoet@kuleuven.be

Abstract

The unique physicochemical properties of silver nanoparticles (AgNPs) make them useful in a wide range of sectors, increasing their propensity for human exposure, as well as the need for thorough toxicological assessment. In this study mice were intratracheally exposed to AgNP (5 and 50nm) and Ag^{+}, once a week for 5 weeks and were allowed to recover for up to 28 days after the last instillation (dpi). Biodistribution profile of AgNPs and ionic silver were studied together with hematological parameters and GSH/GSSG levels in lung and liver. Data was gathered to build a PBPK model after the entry of AgNPs into the lungs. Hematology results show that AgNP5 induced toxicity to RBC, neutrophils and basophils which may indicate inflammation. AgNP50 showed eosinophilia and possible blockage in the monocyte-macrophage differentiation. The organ redox state was affected, specially by the AgNPs treatments. Overall, the GSSG:Total GSH ratio was increased in the lung for 14 and 21 dpi,

while in the liver there was an increase in the GSSG:Total GSH ratio shortly after 1 and 2 dpi for AgNPs, followed by a decrease at 14 and 21 dpi, for all treatments. Silver levels decreased over time in all organs of animals treated with AgNP50, while for AgNP5 treated mice, silver levels were lowest at 7 dpi and highest at 28 dpi in lung, spleen, kidney, liver and blood. The major route for excretion was through the urine, despite a high concentration of AgNP5 was also found in feces. The PBPK model from 7 specific tissues proved to be successful for the heart, liver and kidney.

Keywords: Instillation, pulmonary, *in vivo,* PBPK, silver distribution, excretion

1. Introduction

AgNPs are fast-acting fungicides (Wright et al., 1999) and effective agents against antibiotic-resistant bacteria, inhibiting biofilms formation (Wright et al., 1999; Wijnhoven et al., 2009; Percival et al., 2007). In addition, AgNPs showed antiviral activity (Sun et al., 2005) and anti-inflammatory properties (Nadworny et al., 2010).

The applications of silver nanomaterials are numerous and can be mainly classified under three categories: scientific, industrial, and consumer products. The increased manufacture and use of AgNP leads to an inevitable increase in the release of these particles into the environment from its production to the disposal. The wide variety of uses of silver allows the exposure through various routes including inhalation, ingestion and dermal contact. The exposure to dust or fume of metallic silver and soluble silver was established to 100 $\mu g/m^3$ for AgNPs inhalation by the ACGIH (ACGIH, 2007), however, data on human effects under realistic levels and exposure scenarios are still lacking. Studies of the toxic effects of AgNPs in animals have mainly assessed the effects of oral or systemic exposure (Lankveld et al., 2010; Loeschner et al., 2011), with a limited number reporting the effects of inhalation and intratracheal instillation. Diverse outcomes for AgNP exposure were reported, for instance, some inhalation studies show that AgNPs can induce pulmonary inflammation and decrease lung function, depending on the exposure time and dosage. For instance, Silva et al. (2015) found an increase in polymorphonuclear cells in bronchoalveolar lavage fluid at 0.5 and/or 1 mg/kg body weight

(bw), after intratracheal instillation of 20 and 110 nm AgNPs stabilized with citrate or PVP. Furthermore, neutrophils, macrophages, and monocytes were also found in the airway submucosa and perivascular regions at days 1 and 7 post instillation and with 110 nm AgNPs producing lasting effects past 21 days (Silva et al., 2015). Regarding the tissue distribution of the AgNPs, a dose-dependent increase in the silver concentration in the lungs and liver after a single oral or intravenous (i.v.) administration was reported (Park et al., 2011). In Sprague–Dawley rats exposed to 15 nm AgNPs by inhalation, higher concentration of Ag was found in the lungs and blood and very low concentration in the liver, kidneys, spleen, brain and heart. Also, the amounts of Ag in the lungs decreased rapidly with time, and by day 7 only 4% of the initial burden remained (Takenaka et al., 2001). Furthermore, Sung et al. (2009) found that the upper nasal deposition of 18 nm AgNPs into Sprague–Dawley rats caused olfactory bulb accumulation, as well as a dose-dependent deposition of silver within the brain, blood, lungs, kidney and liver. Despite the number of studies on tissue distribution of AgNPs there is still lacking information about tissue distribution of AgNPs smaller than 15 nm (Bachler et al., 2013).

The comparison of static and isolated data is difficult between different studies, especially when different study designs were used (i.e., nanoparticle doses, animal models, administration routes, and time points). Physiologically based pharmacokinetic (PBPK) modelling could provide an insight into the relationships between an external dose and internal organ, blood or excretion dose (IPCS, 2010). Yet, for NPs only a handful of published PBPK models are available in the literature. Lankveld et al. (2010) developed a PBPK model to compare the kinetics of AgNPs 20, 80, and 110 nm. The model simulated the experimental data and the authors suggested that the kinetics was determined not only by size but also by other NPs properties, such as surface charge, particle number and coating. Some of these models have been extrapolated to humans and proved to be helpful in risk assessment (Bachler et al., 2013; Bachler et al., 2015). Bachler et al. (2013) model could successfully predict the biodistribution of silver and uncoated 15–150 nm AgNPs. The authors state that particle size and coating had a minor influence on biodistribution and that *in vivo*, is more likely that AgNPs are directly stored as insoluble salt particles than dissolve into silver ion.

In the present work we aimed at characterizing the toxicity and kinetics of distribution and

excretion of AgNPs (5 and 50nm) and Ag^+ ($AgNO_3$) after the entry into the lungs, fitting the data in a PBPK model. To fulfil our goals, we (I) analyzed the effect of AgNP size on tissue distribution at different time points; (II) determined the accumulation of AgNPs in target organs; (III) evaluated the excretion of AgNPs; (IV) examined hematological effects; and finally (V) analyzed the GSH and GSSG in mice lung and liver.

2. Materials and methods AgNP and $AgNO_3$ treatments

Sterile, purified and endotoxin-free AgNPs (Econix 5.0 mg/mL) with polyvinylpyrrolidone (PVP) coating and nominal size of 5 nm and 50 nm (here designated as AgNP5 and AgNP50, respectively), were obtained by NanoComposix Europe (Prague, Czech Republic). The AgNP5 have a diameter of 5.2 ± 0.7nm (TEM) and the stock solution contained 6.9^{15} particles/mL, the AgNP50 have a diameter of 54.8 ± 10.1nm (TEM) and the stock solution contained 5.2^{12} particles /ml. The treatment solutions were prepared by dilution of AgNPs and $AgNO_3$ in NaCl (0.9%) to obtain 0.075mg for AgNPs (3 mg/kg) and 0.025mg for $AgNO_3$ (1 mg/kg). The dose of $AgNO_3$ was calculated based on silver ion mass and expressed as $AgNO_3$.

Mice

Male BALB/c OlaHsd mice (6 weeks old – 20g) were obtained from Harlan (Horst, The Netherlands). The mice were housed in a conventional animal house with 12h dark/light cycles. They were housed in filter top cages and received lightly acidified water and pelleted food (Trouw Nutrition, Ghent, Belgium) *ad libitum*. Individual animal weights were recorded every week pre-dosing and at the time of death or euthanasia**.** All experimental procedures were approved by the local Ethical Committee for Animal Experiments (License KU Leuven 054/2015).

Study groups and dosing regimen

The experimental protocol was divided in two main time windows, 28 days of exposure and 28 days of recovery with a total of 56 days. Ninety-six mice were divided into 3 experimental groups (AgNP5/AgNP50/$AgNO_3$) and 1 control group (0.9% NaCl) per each recovery time

point (1, 2, 7, 14, 21, and 28 days post instillation), 4 mice in each. On days 0, 2, 7, 14, 21 and 28 of the exposure time, mice were intratracheally instilled with treatment solutions (150µl of air + 50µl of NaCl/AgNP5/AgNP50/$AgNO_3$ solutions), 1 once a week for a period of 5 weeks. The solution was administrated using 24-gauge catheters under intraperitoneal anesthesia of a mixture of xylazine + ketalar in 0.9% NaCl (150µl/25g of body weight). The recovery period began at the end of the last exposure. The mice were checked for normal behavior and placed back in the cages. On days 1, 2, 7, 14, 21 and 28 post the last instillation (dpi) mice were weighted and sacrificed by an intraperitoneal injection of 200 µl of Nembutal. A schematic overview of the experimental protocol is shown in Fig.1.

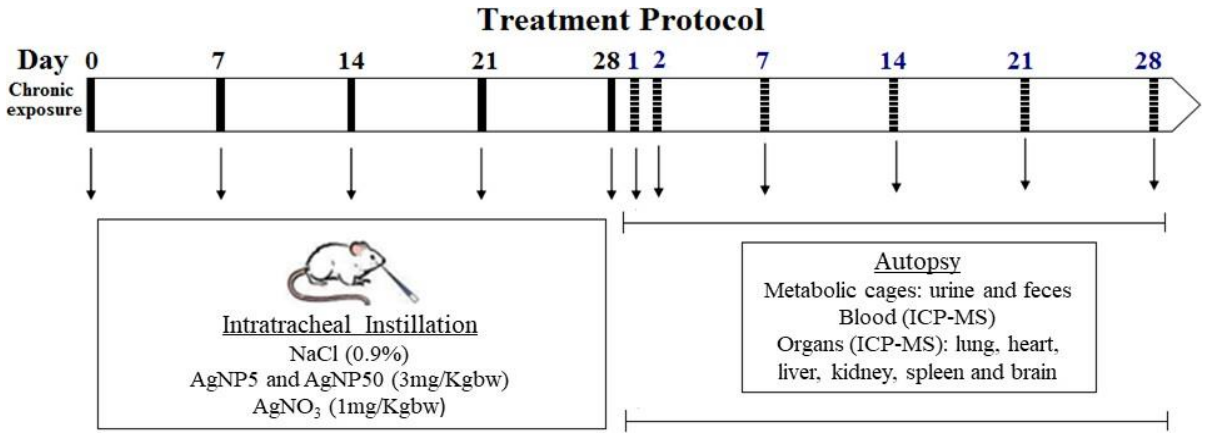

Figure 1 – Schematic overview of the experimental protocol. Black lines mean exposure time and dashed lines mean recovery time.

Blood collection and analysis

After euthanasia, blood was collected from the retro-orbital plexus. Five hundred µl of blood were collected into a microtube with 50µl of citrate (3.8%) and diluted in 200 µl of sterile saline (0.9% NaCl). Total and differential blood cell counts (white blood cells, neutrophils, monocytes, lymphocytes, eosinophils, basophils, red blood cells, platelets) and hemoglobin concentration and mean corpuscular volume were determined on a Cell-Dyn 3500R counter (Abbott Laboratories, Philippines).

Assessment of GSH and GSSG levels

The levels of oxidized (GSSG) and reduced (GSH) glutathione were determined according to

Rahman et al. (2007) with some modifications. Lung and liver samples for GSSG and GSH measurements were collected, snap-frozen and stored in -80°C until analysis. Briefly, lung and liver samples were homogenized on ice with cold 40 mM Nethylmaleimide (20 ml/g tissue, to prevent rapid oxidation of GSH) and then centrifuged at 14000 g for 15 minutes at 4°C. The supernatant was transferred to a new tube and 5% metaphosphoric acid was added (1/5th of the supernatant volume, final concentration is 1% metaphosphoric acid, for removing the proteins), mixed and again centrifuged at 14000 x g during 15 minutes at 4°C. The supernatants were stored at −80°C until measurements. Total protein levels were determined using the Bio-Rad Protein assay, according to the Bradford method. The ratio of GSSG to total glutathione was then calculated (GSSG:Total GSH). (Bio-Rad Laboratories GmbH, München, Germany using bovine serum albumin as standard).

Silver quantification by ICP-MS

On days 1, 7 and 28 dpi, samples from the following organs were collected: lung, hair, spleen, kidney, liver, brain, bone marrow and blood for silver quantification by inductively coupled plasma mass spectrometry (ICP-MS). For the same days, 4 mice from each treatment were placed in metabolic cages for 24h to collect urine and feces. Samples for ICP-MS analysis were digested in *Aqua Regia*. Briefly 1.5 ml HCl and 0.5 ml of HNO_3 were added to approximately 30 mg tissue or 100 µl urine in glass tubes and left for 24h. After 24h, samples were heated at 140°C for 90 min. Finally, samples were diluted in Milli-Q water to 10 ml and Ag concentration was measured by ICP-MS (Agilent 7700x ICP-MS). Elements were measured as ^{107}Ag using ^{103}Rh as internal standard. The detection limit was 0.015 µg Ag /L.

PBPK model

The structure of the PBPK model is based on the available knowledge on the disposition of silver and AgNP within the rat and human as described by Bachler et al. (2013). It is assumed that the mechanisms of absorption, distribution, metabolism and excretion (ADME) follow first-order kinetics which simplifies the model, but which is also common for many other PBPK models. Physiological parameter values of mice were extracted from Anger (2004) and Arms et al. (1988). The absorption of NPs through instillation is simulated based on a simplified

International Commission on Radiological Protection (ICRP) Human Respiratory Tract Model as shown in supplementary materials from (Bachler et al., 2013). It was assumed that 100% of the instilled AgNPs are deposited in the initial compartment of the lungs. Through this compartment the nanoparticles are transported into the blood and then distributed to all tissues. However, a fraction of the instilled dose will be stored in a "bound state", and other fractions will directly move to the gastrointestinal tract or will be exhaled instantaneously. Except for the 'remaining tissues' and blood compartments, each of the compartments is divided into two subcompartments. A first subcompartment represents the AgNP particles which can freely exchange between blood and tissue. The other subcompartment is assumed to store the instilled particles in the tissue. The uptake of AgNP in the mononuclear phagocyte systems (MPS) of the lungs, liver and spleen is not included in this model because the blood silver concentration will not exceed 180 ng/g (Bachler et al., 2013). The bone marrow is assumed to be a sink for all AgNPs that are neither distributed to organs in the model nor excreted. For this reason, particle release from the bone marrow to the blood is not implemented in the model. Due to lack of mouse data, uptake constants of AgNPs from blood to various tissues were used from the rat model (Bachler et al., 2013). These constants describe the membrane transport of AgNP and were assumed to be size-independent. The release rate to the blood was assumed to be the same for all tissues. The distribution of nanoparticles in the blood stream was also assumed to be size-independent. Particle dissolution into smaller particles or Ag^+ was neglected to simplify the model. The biliary and urinary excreted AgNPs are directly removed from the blood compartment. RStudio © (Version 0.98.1103) (R Core Team, 2014) was used to set up the model. The desolve-package (Soetaert et al., 2010) was used for solving differential equations. To simulate the five weekly instillations, the events parameter of the ode function was addressed.

Statistical analysis

The results are reported as means ± standard deviations (SD). Data analysis was performed in the software SigmaPlot version 11 (Systat Software Inc.), by one-way, two-way and tree-way ANOVA analysis of variance (p <0.05) followed by Holm-Sidak test or the Dunn's test for the parametric and non-parametric data, respectively. The differences were considered statistically

significant for $p < 0.05$.

3. Results

Mice behavior observations

Overall, the repeated intratracheal instillations of AgNPs and $AgNO_3$ were well-tolerated by the animals and normal feeding behavior was observed. Animals did not exhibit any signs of illness during the instillation or the recovery period. Two out of 96 animals died out of the planned sacrifices: one was euthanized for unrelated causes (abnormal abscesses found in the heart) and the other one died because of intratracheal-related injury. No unpredicted deaths were observed due to the tested substances. An interesting remark is that at last week of treatment, mice treated with AgNP50 and $AgNO_3$ specially, showed an altered sexual behavior, towards same sex. Alterations on accessory olfactory bulb or stress/anxiety could be the responsible to the same-sex attraction.

Body and Organ weights

No significant body weight (bw) change was observed during the exposure time (Fig.2). Although, from the cessation of exposure the mice bw fluttered and decreased, except for the control group. $AgNO_3$ treatment significantly decreased mice bw at 2 and 7 dpi but after that, mice seem to recover well and bw were in line with control at 14 dpi. AgNP5 showed a non-significant bw decrease at 2, 7, 14 dpi, followed by a steep significant reduction at 21 dpi. AgNP50 treatment significantly decreased mice bw at 2 dpi, recovering slowly after that time (Fig.2). No significant organ weight changes were observed in either control or treated mice after 28 dpi – or any other time-point considered - of Ag^+ and AgNPs exposure (Fig.3).

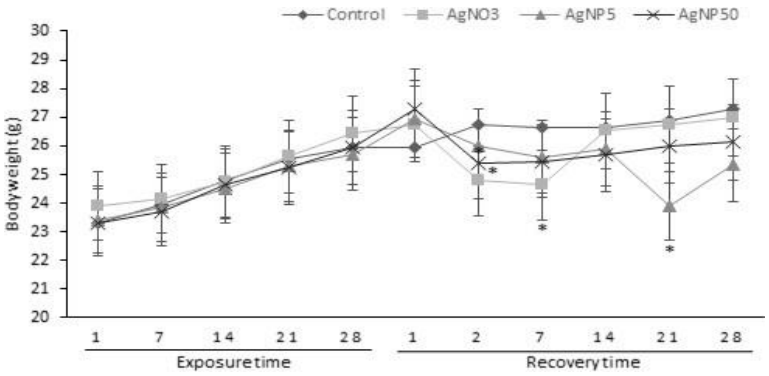

Figure 2 – Mice body weight changes during 28-day exposure by intratracheal instillation of saline (control),

$AgNO_3$, AgNP5 and AgNP50 and 28-day recovery time. * means significant difference vs. last day of exposure, $p < 0.05$ (n=4).

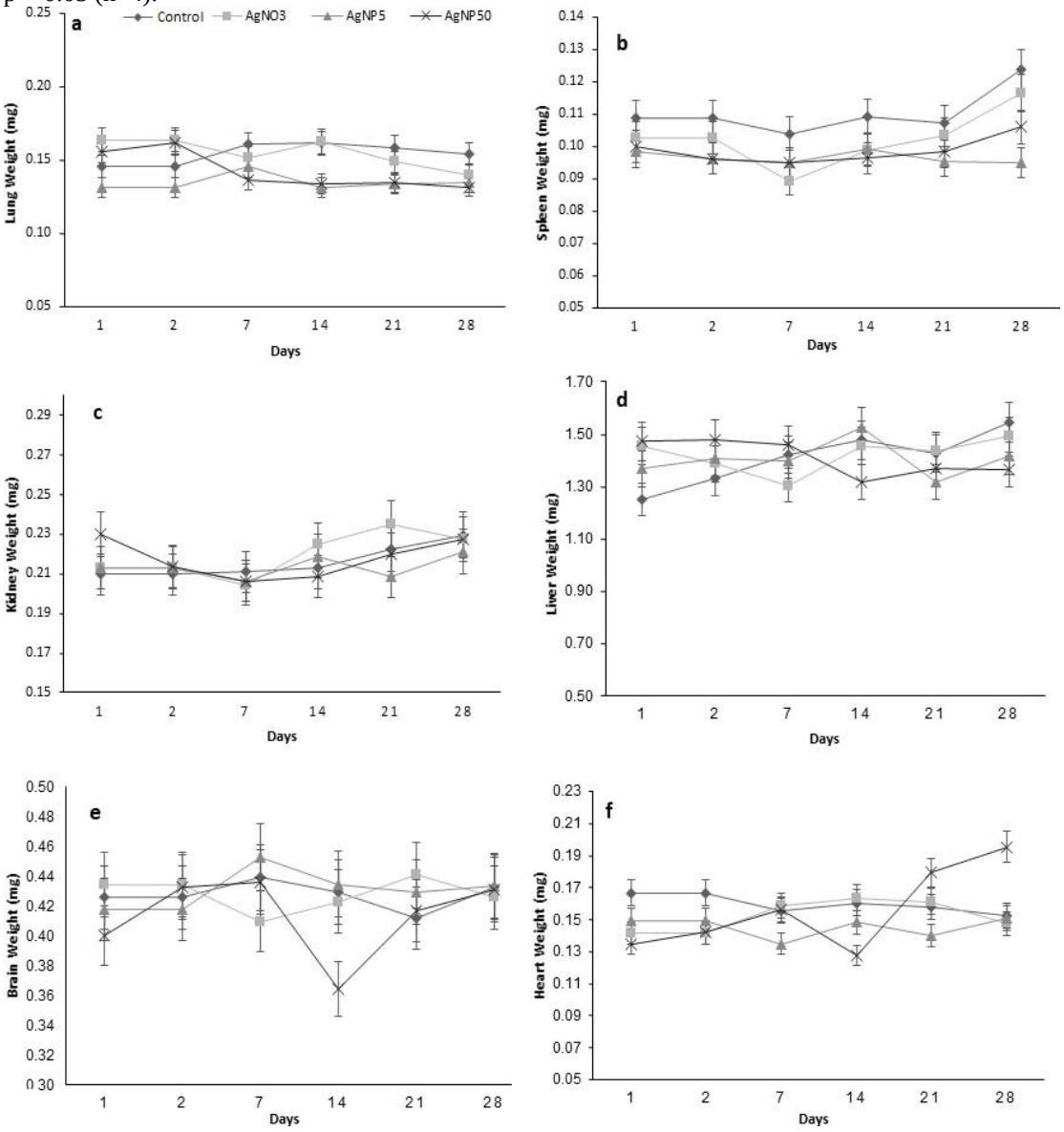

Figure 3 – Mice relative organ weights over 28-day recovery time, after repeated intratracheal instillations of saline (control), $AgNO_3$, AgNP5 and AgNP50. * means significant difference vs. last day of exposure, $p < 0.05$ (n=4).

Blood parameters

Hematology results are depicted in Fig.4 & 5. At 21 and 28 dpi for $AgNO_3$ and AgNP5 exposures, a significant increase in hemoglobin (HGB) concentration and number of red blood cells (RBC) was observed (Fig.4 – a & b). No significant statistical differences were observed for the mean corpuscular volume (MCV) for any treatment (Fig.4 – c).

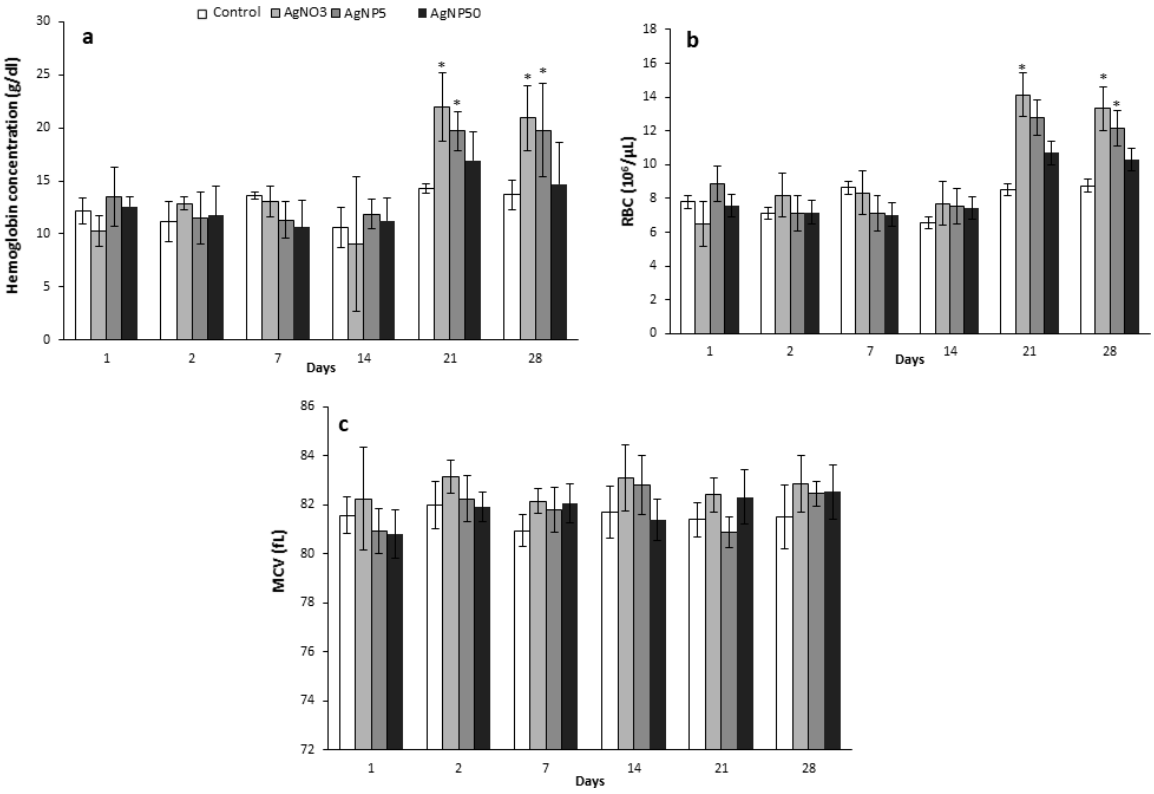

Figure 4 – Differential mice blood cell counts for hemoglobin (a), RBC (b), MCV (c) and concentration over 28-day recovery time, after repeated intratracheal instillations of saline (control), $AgNO_3$, AgNP5 and AgNP50. * mean significant differences between control and treatments. $p < 0.05$ (n=4).

AgNP50 decreased the number of basophils and monocytes at all time-points, except for 21 dpi (Fig.5 – d & f). Contrarily, a significantly increase in the number of basophils was observed for AgNP5 exposure at 1, 14, 21 and 28 dpi (Fig.5 - f). Total white blood cells (WBC) were only affected at 7 and 28 dpi by AgNP5 and $AgNO_3$ exposures, being respectively decreased and increased (Fig.5 - a). Neutrophils were significantly decreased by $AgNO_3$ at 1, 14 and 21 dpi, while AgNP5 exposure increased the number of neutrophils from 14 dpi, until the end of recovery (Fig.5 – c). The $AgNO_3$ and AgNP5 exposed groups showed a significant increase in the total number of lymphocytes at 28 dpi, while at 7 dpi to AgNP5 and AgNP50 the number of lymphocytes was decreased. The minimum number of lymphocytes was obtained at 14 dpi to AgNP50 (Fig.5 – b). At 1 dpi, the eosinophils number was increased by AgNP5 and recovered from that on, while, AgNP50 increased the number of eosinophils from 21 dpi, reaching the peak at 28 dpi (Fig.5 – e).

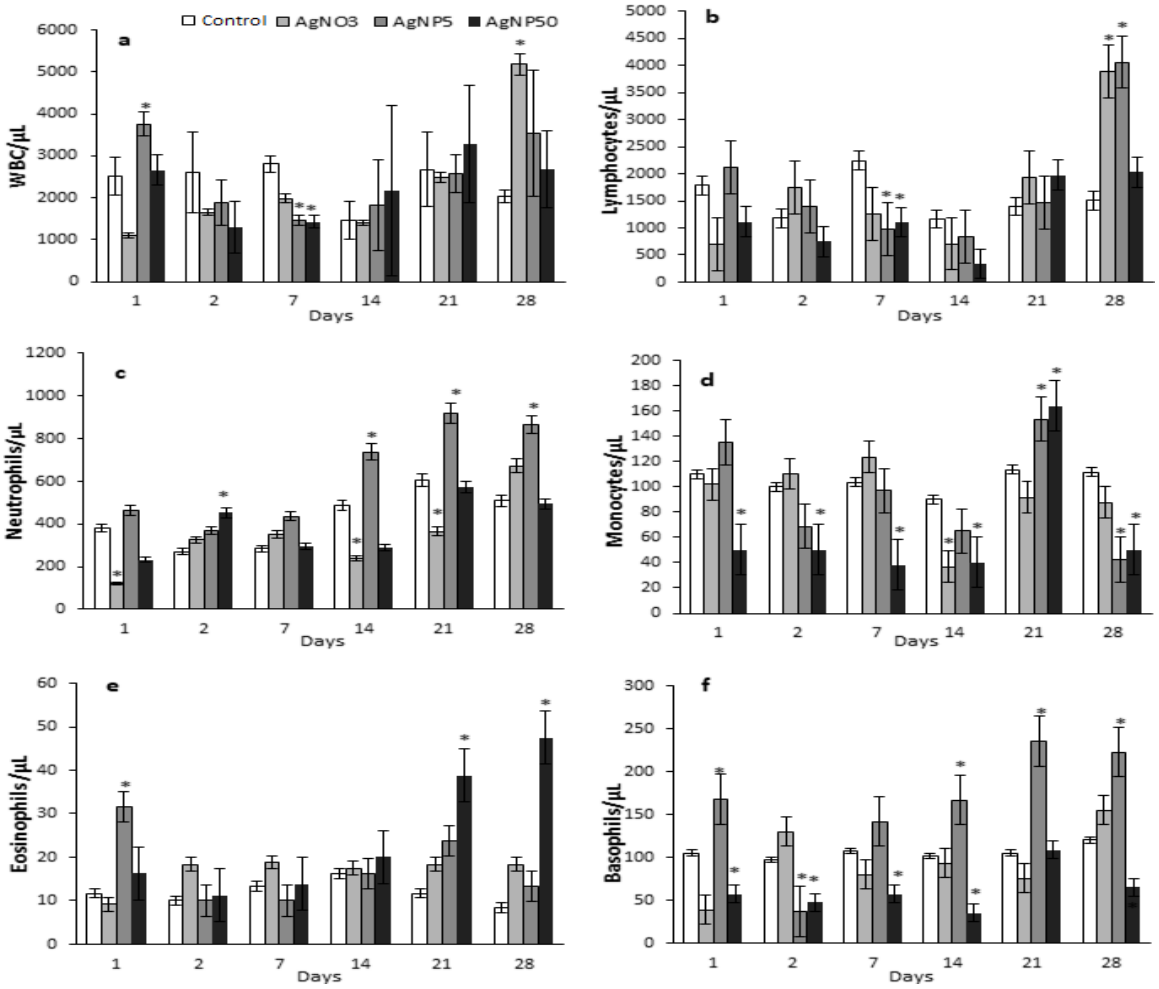

Figure 5 – Mice Hematology values during 28-day recovery time after repeated intratracheal instillations of saline (control), $AgNO_3$, AgNP5, and AgNP50. a. WBC; b. Lymphocytes; c. Neutrophils; d. Monocytes; e. Eosinophils; f. Basophils. * mean significant differences between control and treatments. $p < 0.05$ (n=4).

GSH and GSSG levels

The results of GSH and GSSG quantification in lung and liver tissues are presented in Fig.6. GSSG:Total GSH ratio was significantly increased at 14 dpi for AgNP50, along with an increase GSSG for the same period (Fig.6 – a & c), while for AgNP5 GSSG:Total GSH ratio increased at 21 dpi, at the expenses of GSH content (Fig.6 – b). Additionally, in the lung the GSH content was increased for AgNP50 at 2 dpi and both GSH and GSSG increased at 21 dpi and decrease

at the last dpi. At last, the $AgNO_3$, did not altered the redox state of the lung but increase the GSH content at 21 dpi.

Regarding the liver, the GSSG:Total GSH ratio was significantly increased for both AgNPs at the first time-point, along with an increase in the GSSG levels. The AgNP5 maintained the increase in the GSSG:Total GSH at 2 dpi. At 14 dpi, both AgNPs decreased the GSSG:Total GSH ratio and the GSSG levels (Fig.6 – f). Finally, the GSSG:Total GSH decreased at 21 dpi for all treatments (Fig.6 – d). The levels of GSH in the liver presented an increasing behavior from 21 dpi, for AgNP50, while both AgNPs increased the GSH levels at 28 dpi (Fig.6 – e).

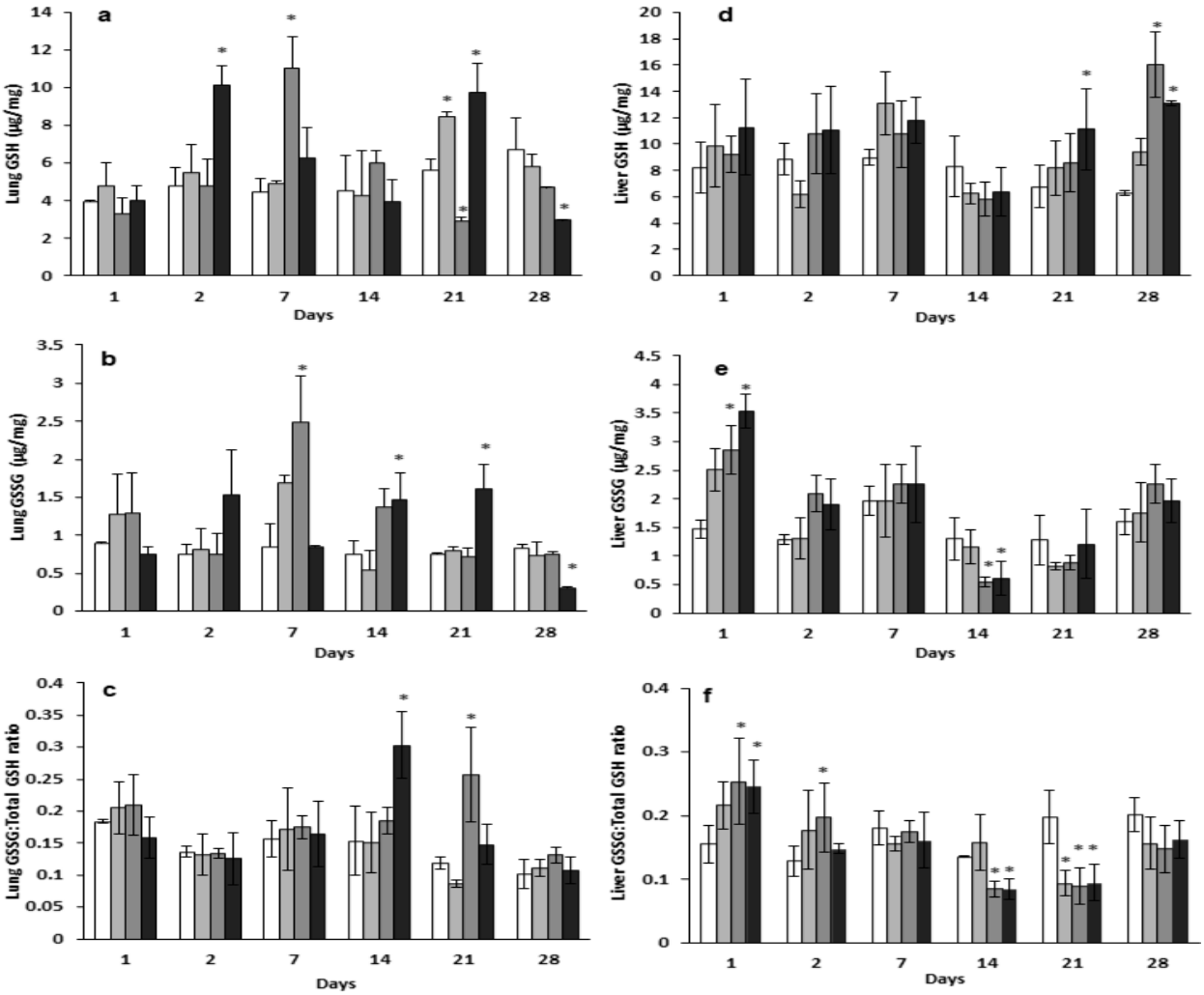

Figure 6 – GSH and GSSG levels (µg/mg protein) and GSSG:Total GSH ratio analysis during 28-day recovery time after repeated intratracheal instillations of saline (control), $AgNO_3$, AgNP5 and AgNP50. a. Lung GSH; b. Lung GSSG; c. Lung GSSG:Total GSH Ratio; d. Liver GSH; e. Liver GSSG; f. Liver GSSG:Total GSH Ratio. * significant difference between control and treatments $p < 0.05$ (n=4).

Biodistribution, accumulation and elimination of AgNPs

Total Ag contents were determined in the selected organs (lung, brain, heart, spleen, kidney, liver and bone marrow) as well as in urine, feces and blood by ICP-MS. Unfortunately, Ag concentration in bone marrow was under the detection limit of ICP-MS, due to the small amount of sample collected. The same result was obtained for control groups, therefore they were not represented in the Fig7. Fig.7 shows the mean silver levels in organs after 1, 7 and 28 dpi. The results showed that at 1 dpi, the highest levels of silver were detected in the lungs (Fig.7 - d), urine, and blood (Fig.7 - f), followed by spleen and kidney and the least accumulation was found in heart and liver. Concerning AgNPs, they were translocated from lungs to the other organs analyzed, as silver was detected in all organs evaluated, regardless of particle size. In control animals, silver was not detected in any organ or fluid analyzed (data not shown).

In the lungs, at 1 dpi the highest levels of silver were observed for AgNP50 treatments. For this treatment, the concentration of silver at 1 dpi in the lung was 2.2 ng/mg tissue and deceased after that, until almost total clearance at 28 dpi (0.04 ng/mg tissue) (Fig.7 – d). The same pattern of clearance from 1 to 28 dpi, was observed in brain, spleen, kidney, liver and blood for AgNP50 (Fig.7). The smaller particles (AgNP5), showed a somewhat opposite silver level distribution compared to AgNP50. For instance, for AgNP5 treated mice, the silver concentrations in lung, spleen, kidney and liver were lowest at 7 dpi and highest concentrations at 28 dpi, while in the heart and brain highest silver levels were noted at 7 dpi and followed by a decrease at 28 dpi (Fig.7 – a & e). For $AgNO_3$ treatment, the highest concentrations were observed in lung, blood, kidney and heart (Fig.7). Except for the heart, the concentration of silver in all organs of mice treated with $AgNO_3$ decreased until 28 dpi, but no total clearance was observed. The elimination of silver from the organs seems to be size-related. In post instillation time, silver concentration decreased faster from 1 to 28 dpi in almost all organs for treatments with AgNP50 and $AgNO_3$, however, at the end of the recovery time (28 dpi) a small concentration of silver remains (Fig.7). On the contrary, for AgNP5 treatment, the elimination seems to occur in a slower rate, being possible to observe a high concentration of silver in several organs at 28 dpi. An accumulation of silver was detected from 7 dpi to 28 dpi in kidney, liver and spleen, as the concentrations obtained increased in this period (Fig.7 - b, g & c). $AgNO_3$ and AgNP50 treatment also seem to

be accumulated in the liver. Fig.7 – g, showed similar concentrations of silver in the liver at 7 and 28 dpi in both treatments.

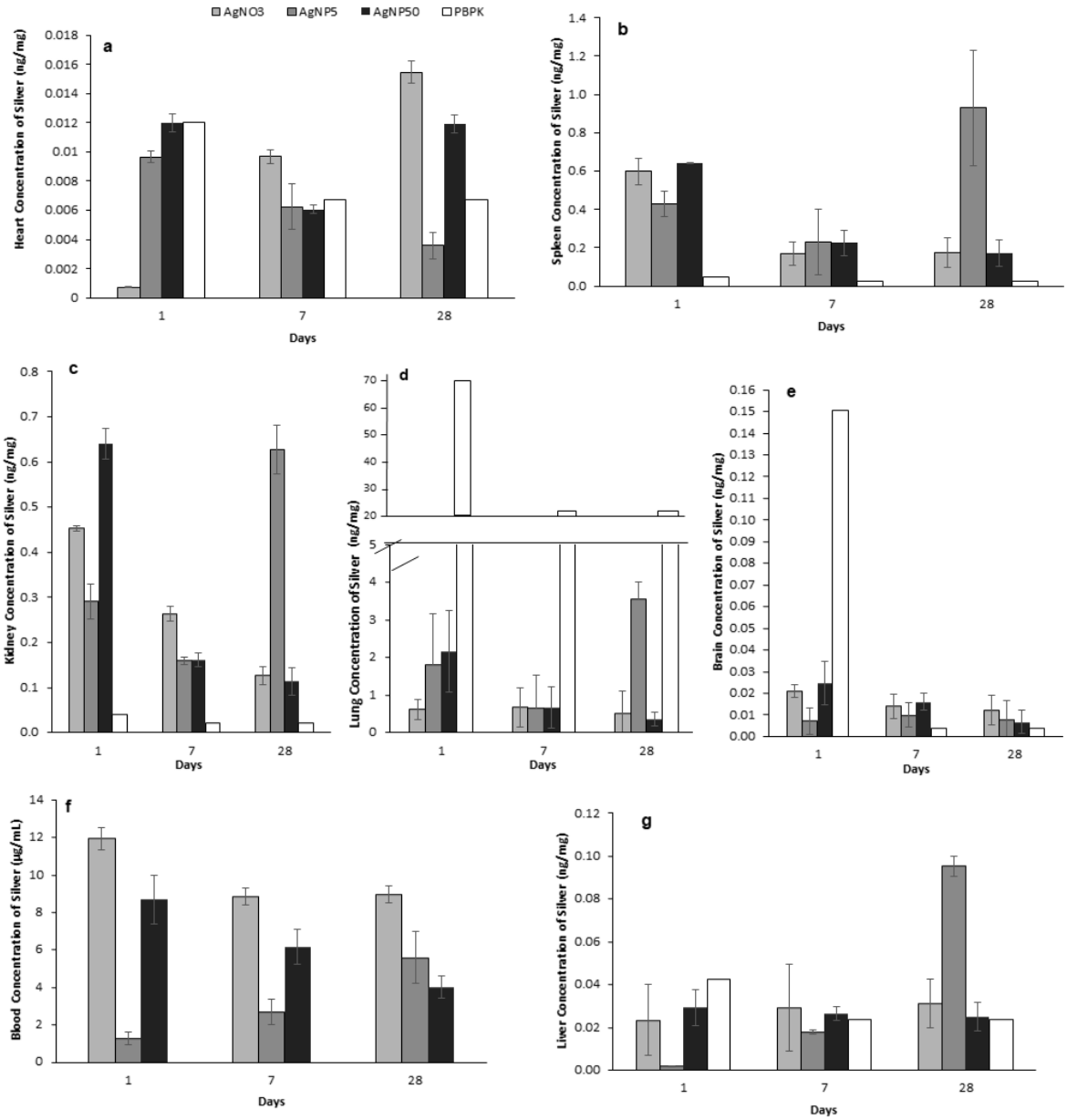

Figure 7 – Silver concentrations (ng/mg tissue fresh weight) during 28-day recovery time after repeated intratracheal instillations of saline (control), $AgNO_3$, AgNP5 and AgNP50. a. Heart; b. Spleen; c. Kidney; d. Lung; e. Brain; f. Blood; and g. Liver. Silver PBPK data is represent as the lighter bars.

Excretion of AgNPs

The kinetics of silver excretion in urine and feces was determined by measuring the silver concentration in urine and feces samples collected from animals kept in metabolic cages for 24h at 1, 7 and 28 dpi. Fig.8 (a & b), showed that the major part of silver is excreted by the urinary tract and the highest silver levels in the urine were obtained for mice exposed to AgNP50 and $AgNO_3$. The highest concentrations of silver in feces were obtained for AgNP5 and $AgNO_3$ treatments at 1 dpi (Fig.8 – b). The nanoparticles elimination rate in feces decreased steadily and reached the minimal value at 28 dpi.

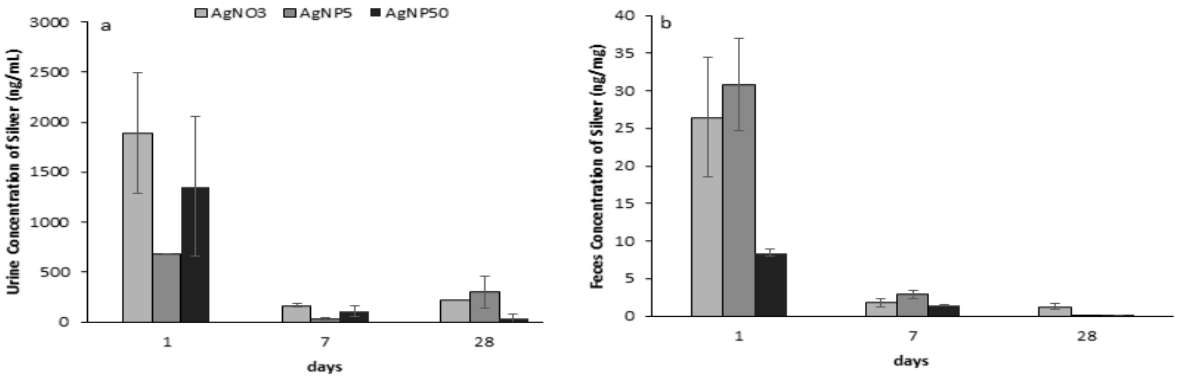

Figure 8 – Excreted Silver concentrations (ng/mL or ng/mg) during 28-day recovery time after repeated intratracheal instillations of saline (control), $AgNO_3$, AgNP5 and AgNP50. a. Urine; b. Feces.

PBPK

Figure 7 shows the results of the PBPK model compared with the experimental results of both AgNP5 and AgNP50. ADME model was created to validate and help to predict the amount of silver at each compartment (Fig.7 & 8). Modeling the ADME of AgNPs in 7 specific tissues of mice proved to be successful for the heart, liver and kidney compartments. For these compartments, the modeled silver concentrations seem to be in line with the *in vivo* data. However, the modeled silver levels in the lung compartment seem to be overestimated, as AgNPs seem to be more quickly removed from the lungs. The absorption of AgNPs through instillation may need a different approach than the simplified ICRP Human Respiratory Tract Model. *In vivo* data of silver levels in the brain showed that the concentration did not exceed 0.05ng/mg organ at 1 dpi. However, the modeled silver level was close to 0.15ng/mg organ.

This could show that actual uptake of silver in the brain is much lower or the release rate to the blood much higher than simulated. For the spleen, the opposite was true, *in vivo* data showed a much higher uptake or slower release rate, or even a higher storage capacity than the simulated spleen compartment.

4. Discussion

In the present work, the toxicity, distribution and excretion of two differently sized AgNPs (and Ag^{+}) were assessed in a mouse model after intratracheal instillation exposures. Exposure by instillation allows to study of lung toxicity of substances with the advantage of not requiring specialized facilities (as inhalation studies), decreasing also the costs of the studies. Doses of AgNPs and $AgNO_3$ administered here (3mg/kg and 1mg/kg, respectively) fall within the range previously tested on intravenously injected, oral and intranasal administered mice/rats without eliciting overt toxicity (Dziendzikowska et al., 2012; Liu et al., 2012; Shrivastava et al., 2009). Given that the workplace exposure limit for silver dust and fumes is 100µg/m^3, and the average adult working male breathes 16.8 m^3 of air per day, this would yield a daily exposure of 1.68 mg of silver/day (American Conference of Governmental Industrial Hygienists, 2001; iQ Power Tools, 2014). Our dose in this study was 3 mg/kg for AgNPs, so for a 25 g mouse, the total exposure was 0.375 mg per mice, of which is well within the range of a potential acceptable workplace exposure. Since, the burden of particulate silver is higher than the one caused by AgNPs we used a lower dose of $AgNO_3$ administered to mice (1mg/kg). Mice bw was not affected by AgNPs or $AgNO_3$ during exposure time, but during recovery, a significant flutter was observed. $AgNO_3$ induced the highest decrease in mice bw at 7 dpi, but after that time-point, mice bw recovered from, close to the bw of control group. Both AgNPs decreased the mice bw during recovery, but the higher effect was obtained for AgNP5. A decrease in bw was also obtained by Shahare and Yashpal. (2013) with Swiss-albino mice treated orally with 5 to 20 mg/kg of AgNPs (3 to 20 nm) for 21 days. Authors hypothesized that the weight loss was related to a loss of microvilli and reduced absorptive capacity of intestinal epithelium induced by AgNPs (Shahare and Yashpal, 2013). Considering the high amount of silver excreted by the

feces at 1 dpi, a possible alteration in intestinal function could have occurred upon AgNPs/$AgNO_3$ exposure.

Repeated intratracheal instillations of AgNPs affected the hematology of the treated mice. An increase on RBC and HGB was observed for $AgNO_3$ and AgNP5, which could be an indicator of polycythemia as a result of a defect on RBC maturation and HGB syntheses (De Jong et al., 2013). This also suggests a need to compensate any condition that results in low O_2 levels by a pulmonary disruption (Zhao et al., 2014). Also, increased number of neutrophils and basophils in AgNP5 exposed mice from the 14 dpi, suggest inflammatory or allergic reactions. In fact, Seiffert et al. (2015) compared AgNPs (20 and 110nm) effects in Brown-Norway and Sprague-Dawley rats and reported that the smallest size induced the highest effect on neutrophilic inflammation. Mice treated with larger particles (110nm) showed an increased toxicity for monocytes and basophils and a high degree of eosinophilia immediately after their entrance into circulation. Effects of AgNPs on the function of blood monocytes is scarcely reported, but larger AgNPs are easily taken by monocytes inducing cytotoxicity and lysosomal dysfunction, blocking the monocyte-macrophage differentiation (Ahlberg et al., 2014; Foldbjerg et al., 2009; Xu et al., 2015).

The reduced and oxidized forms of glutathione (GSH and GSSG, respectively) act in concert to regulate and maintain cellular redox status. Under oxidative stress conditions, GSH is oxidized to GSSG, thus, the GSSG:Total GSH ratio is altered (Owen and Butterfield, 2010). Therefore, an increase in GSSG:Total GSH ratio is an indication of oxidative stress. Our data show an increase in GSSG:Total GSH ratio in the lung, along with an increase in GSH content, particularly after AgNPs exposures. Lung GSSG:Total GSH ratio increase for 14 for AgNP50 and for the same treatment it was obtained and increase in the GSSG content, which can reflect a stress response from the organ. The same treatment increases the GSH content for 2 and 21 dpi, but the GSSG was also increased and therefore the organ redox state was maintained. The same effects occurred for AgNP5 treatment at 7 dpi. This increase in GSSG:Total GSH along with an increase in GSH can be related not only to an antioxidant response but also can be related to lung inflammation (Comhair et al., 1999; Rahman and MacNee, 1999). Regarding, the liver the opposite reaction was observed. Both AgNPs, increased the GSSG:Total GSH ratio at 1 dpi, followed by an increase in the GSSG level, which clearly indicate an oxidation of the

GSH as a stress response. Also, for this period, the liver showed the highest levels of silver. At 2 dpi, only the smaller size maintained the decrease in the GSSG:Total GSH. At 14 and 21 dpi, there was a remarkable decrease in the GSSG:Total GSH for AgNPs along with a decrease in GSSG levels. At last, 28 dpi showed a significant increase in the GSH level for the AgNPs treatments, these increase in the GSH level without affecting the redox state of the organ can be linked to a parallel increase in the biliary excretion of silver as Ag-GSH complex or stress tolerance and tissue regeneration. (Alexander and Aaseth, 1981; Huang et al., 2001).

Concerning AgNP tissue distribution and accumulation, some studies reported a size-dependent distribution (Lankveld et al., 2010) while, others claim that the silver distribution is irrespective of the size (Lee et al., 2012). Chuang et al. (2013) found that AgNPs accumulated predominantly in the lungs, followed in decreasing order by the heart, spleen, liver, kidneys and brain after 7 days of exposure by inhalation. In our work, the higher amount of silver was observed in the blood, followed by lung, spleen, kidney, liver, brain and heart. Hence, the former could have been overestimated, since at autopsy as much blood as possible was collected to maximize removal of residual blood from the organs, possibly increasing the content of silver in the blood (Lankveld et al., 2010). Our work showed that AgNP50 seem to have a similar distribution of silver in the lung as $AgNO_3$, since the peak of concentration in the tissue was observed at 1 dpi followed by almost total clearance 28 dpi. AgNP5, showed an opposite silver distribution pattern, with lowest levels at 7 dpi and higher at 28 dpi. This profile of distribution was observed in the lungs, spleen, kidney, liver and blood, while heart and brain were an exception, with lower values at 28 dpi. Taken our results along with the lack of information on the literature of AgNP with this size (5 nm) we purposed one hypothesis. This hypothesis lays on the capacity of AgNP form secondary NPs once inside the organism (Liu J. et al., 2012), this reaction is specially noted in AgNPs of smaller sizes and can influence and alter the distribution system. Nevertheless, this is, to our knowledge, the first study on silver biodistribution upon intratracheal instillation of AgNP5, therefore the confrontation of our results with those in literature is limited. Also, the delayed distribution of the AgNPs from 1 to 28 dpi, may be due to its internalization by the epithelial cells or its entrapment by the macrophages with slow release of silver (Fehaid et al., 2016).

Excretion of orally and i.v. administered AgNPs with 20-200 nm was found to be size-dependent

and predominantly excreted through feces, suggesting low bioavailability (Dziendzikowska et al., 2012; Park, 2013). In the present study, excretion of AgNPs trough urine or feces, seems to be dependent on the AgNP size. The highest silver excretion through urine was observed at 1 dpi, for AgNP50 and $AgNO_3$, which is consistent with higher concentration of silver observed in the kidney of mice treated with AgNP50 at 1 dpi. A faster particle dissolution into ionic silver for AgNP50, could be the reason for excretion by urine (Lankveld et al., 2010). Also, the levels of silver found in the liver after exposures to AgNP50, were similar from 1 to 28 dpi without significant excretion by feces. This could be an indicator of high accumulation of Ag at this organ or difficulty of biliary excretion of particles with this size. To our knowledge, excretion of AgNPs in inhalation or intratracheal instillation studies has been confined to one study in mice (Chuang et al., 2013) and one in humans exposed to silver (DiVincenzo et al., 1985). Chuang et al. (2013) reported trivial amounts of 33 nm AgNP excreted in urine and feces of mice, until 7 dpi after inhalation, while DiVincenzo et al. (1985) found that silver was eliminated predominantly by the feces. The highest excretion of silver through feces was verified for AgNP5 and $AgNO_3$ at 1 dpi and decreased after that. One of the possible routes for elimination of AgNPs from the alveolar region may take place through the tracheobronchial tree, with subsequent ingestion into gastrointestinal tract and excretion with the feces (Takenaka et al., 2001). At 1 dpi AgNP5 treated mice show the higher concentration of silver in feces and less in the lung when compared to AgNP50 exposed mice, which may indicate the ingestion of some of the instilled AgNP5. Additionally, $AgNO_3$ exposed mice seem to excrete silver easily and faster, since higher concentrations of silver were found in urine and feces.

A PBPK model was developed based on the model described by Bachler et al. (2013). Modeled silver levels in heart, liver and kidney compartments for particles with AgNP5 and AgNP50 were in line with the *in vivo* data, while in the lung compartment modeled silver level was much higher than the experimental values. These differences may be explained by the different administration procedures followed. Our assumption was that all instilled AgNPs were absorbed in the "initial state" compartment defined in the lungs. For future work, an exhaled fraction could be considered. The BBB plays an important role in the transport of molecules between the blood and brain compartment, however, the BBB was not considered in the model, which could explain the overestimation of silver levels in the brain compartment at 1 dpi. The spleen

compartment also plays an important role in the MPS, but the latter was not incorporated into the PBPK-model which could be an explanation of the lower modeled silver levels in spleen. Modeled uptake, release and storage rates of AgNP used are from rats (Bachler et al., 2013), thus using mice specific rates could enhance the prediction of the model. In a next stage, these can be fitted by ACSL-modeling, which is designed for modelling the behavior of continuous systems described by time-dependent, nonlinear differential equations and transfer functions. However, this implies that a more extended *in vivo* data set on an hourly base, especially within 1 dpi. Finally, decomposition of AgNP into both smaller sized NPs and silver could also explain the lower estimated levels of AgNPs in the various compartments. Similar to Lankveld et al. (2010) the model did not indicate clear relationships between AgNP size and its corresponding kinetic characteristics. Other physicochemical characteristics, besides size, may affect its kinetics such as surface charge, surface coating, number of particles, protein absorption or the tendency of aggregation/agglomeration in plasma. This implies an integrative and thus much more complex modeling algorithm.

5. Conclusions

Overall, our results indicate that AgNPs induce inflammatory responses, which are determined by the particle size. Both AgNPs induced higher cytotoxicity to blood cells than $AgNO_3$, although AgNP5 revealed a promotion of inflammatory or allergic reactions, while AgNP50 showed possible blockage in the monocyte-macrophage differentiation. The increase in GSSG:Total GSH ratio and GSH content could be a response to the cell antioxidant needs in the lung or potentially related to inflammation, while the decrease in the liver can be related to biliary excretion of silver as Ag-GSH complex or a stress tolerance. Although, different pattern of responses of GSH induced by NPs make it difficult to use it alone as a predictor of pulmonary toxicity. The distribution of both AgNPs appears to be different suggesting that they may also show a different toxicity and thus might be associated with a different health risk. Accumulation is observed after repeated intratracheal instillations, generally with a peak level at 28 dpi for AgNP5. AgNP50 presented a high retention in the liver during the entire recovery process. Although, this particle seems to be easily distributed from the lung to the remain organs and

cleared by urine excretion. $AgNO_3$ exposed mice seem to excrete silver easily and faster, since high levels of silver were detected in both urine and feces. Modeling the ADME of AgNPs in 7 specific tissues of mice proved to be successful for the heart, liver and kidney compartments. For these compartments, the modeled silver concentrations seem to be in line with the *in vivo* data. Decomposition of AgNP into both smaller sized nanoparticles and ionic silver could also explain the lower concentration estimation of AgNPs in the various compartments.

Acknowledgments:

This work was supported by CESAM (UID/AMB/50017), FCT/MEC through by FEDER. FCT/FERDER through COMPETE supported the project PTDC/AAC-AMB/113649 by FEDER through COMPETE and by national funds through FCT. FCT-awarded grants to FR (SFRH/BD/91270/2012) and HO (SFRH/BPD/111736/2015) are acknowledged. Authors thank Sofie V. D. Broucke and Hanne Vriens for their technical support.

References

Ahlberg, S., Antonopulos, A., Diendorf, J., Dringen, R., Epple, M., Flöck, R., Goedecke, W., Graf, C., Haberl, N., Helmlinger, J., Herzog, F., Heuer, F., Hirn, S., Johannes, C., Kittler, S., Köller, M., Korn, K., Kreyling, W.G., Krombach, F., Lademann, J., Loza, K., Luther, E.M., Malissek, M., Meinke, M.C., Nordmeyer, D., Pailliart, A., Raabe, J., Rancan, F., Rothen-Rutishauser, B., Rühl, E., Schleh, C., Seibel, A., Sengstock, C., Treuel, L., Vogt, A., Weber, K., Zellner, R., 2014. PVP- coated, negatively charged silver nanoparticles: A multi-center study of their physicochemical characteristics, cell culture and in vivo experiments. Beilstein J. Nanotechnol. 5, 1944–65. doi:10.3762/bjnano.5.205

Anger, C., 2014. Physiological ranges and variability in organ blood flow in laboratory animals. Swedish University of Agricultural Sciences.

Arms, A.D., Travis, C.C., 1988. Reference Physiological Parameters in Pharmacokinetic Modeling. United States Environmental Protection Agency, Office of Health and Environmental Assessment, Washington, DC.

Bachler, G., Hungerbühler, K., 2013. A physiologically based pharmacokinetic model for ionic silver and silver nanoparticles. Int. J. Nanomedicine 8, 3365–3382.

Bachler, G., von Goetz, N., Hungerbuhler, K., 2015. Using physiologically based pharmacokinetic (PBPK) modeling for dietary risk assessment of titanium dioxide (TiO_2) nanoparticles. Nanotoxicology 9, 373–380. doi:10.3109/17435390.2014.940404

Braakhuis, H.M., Gosens, I., Krystek, P., Boere, J.A.F., Cassee, F.R., Fokkens, P.H.B., Post, J.A., van Loveren, H., Park, M.V.D.Z., 2014. Particle size dependent deposition and pulmonary inflammation after short-term inhalation of silver nanoparticles. Part. Fibre Toxicol. 11, 49. doi:10.1186/s12989-014-0049-1

Chuang, H.C., Hsiao, T.C., Wu, C.K., Chang, H.H., Lee, C.H., Chang, C.C., Cheng, T.J., 2013. Allergenicity and toxicology of inhaled silver nanoparticles in allergen-provocation mice models. Int. J. Nanomedicine 8, 4495–4506. doi:10.2147/IJN.S52239

De Jong, W.H., Van Der Ven, L.T.M., Sleijffers, A., Park, M.V.D.Z., Jansen, E.H.J.M., Van Loveren, H., Vandebriel, R.J., 2013. Systemic and immunotoxicity of silver nanoparticles in an intravenous 28 days repeated dose toxicity study in rats. Biomaterials 34, 8333–43. doi:10.1016/j.biomaterials.2013.06.048

DiVincenzo, G.D., Giordano, C.J., Schriever, L.S., 1985. Biologic monitoring of workers exposed to silver. Int. Arch. Occup. Environ. Health 56, 207–15.

Drescher, D., Büchner, T., McNaughton, D., Kneipp, J., Kneipp, K., Martin, F.L., Fullwood, N.J., Artmann, A.T., Artmann, G.M., Spiro, T.G., Dekkers, S., Jong, W.H. De, Zijverden, M. Van, Sips, A., Geertsma, R.E., 2013. SERS reveals the specific interaction of silver and gold nanoparticles with hemoglobin and red blood cell components. Phys. Chem. Chem. Phys. 15, 5364. doi:10.1039/c3cp43883j

Dziendzikowska, K., Gromadzka-Ostrowska, J., Lankoff, A., Oczkowski, M., Krawczyńska,

A., Chwastowska, J., Sadowska-Bratek, M., Chajduk, E., Wojewódzka, M., Dušinská, M., Kruszewski, M., 2012. Time-dependent biodistribution and excretion of silver nanoparticles in male Wistar rats. J. Appl. Toxicol. 32, 920–928. doi:10.1002/jat.2758

Fehaid, A., Hamed, M.F., Abouelmagd, M.M., Taniguchi, A., 2016. Time-dependent Toxic Effect and Distribution of Silver Nanoparticles Compared to Silver Nitrate after Intratracheal Instillation in Rats. Am. J. Nanomater. 4, 12–19. doi:10.12691/ajn-4-1-3

Foldbjerg, R., Olesen, P., Hougaard, M., Dang, D.A., Hoffmann, H.J., Autrup, H., 2009. PVP-coated silver nanoparticles and silver ions induce reactive oxygen species, apoptosis and necrosis in THP- 1 monocytes. Toxicol. Lett. 190, 156–62. doi:10.1016/j.toxlet.2009.07.009

Huang, H., Lai, W., Cui, M., Liang, L., Lin, Y., Fang, Q., Liu, Y., Xie, L., 2016. An Evaluation of Blood Compatibility of Silver Nanoparticles. Sci. Rep. 6, 25518. doi:10.1038/srep25518.

IPCS, 2010. The harmonization project document series No. 9 – Guidance on principles of characterizing and applying PBPK models in risk assessment., World Health Organization.

Lankveld, D.P.K., Oomen, a G., Krystek, P., Neigh, A., Troost-de Jong, A., Noorlander, C.W., Van Eijkeren, J.C.H., Geertsma, R.E., De Jong, W.H., 2010. The kinetics of the tissue distribution of silver nanoparticles of different sizes. Biomaterials 31, 8350–61. doi:10.1016/j.biomaterials.2010.07.045

Lee, Y.-J., Kim, J., Oh, J., Bae, S., Lee, S., Hong, I.S., Kim, S.-H., 2012. Ion-release kinetics and ecotoxicity effects of silver nanoparticles. Environ. Toxicol. Chem. 31, 155–9. doi:10.1002/etc.717

Liu, Y., Guan, W., Ren, G., Yang, Z., 2012. The possible mechanism of silver nanoparticle impact on hippocampal synaptic plasticity and spatial cognition in rats. Toxicol. Lett. 209, 227–231. doi:10.1016/j.toxlet.2012.01.001

Loeschner, K., Hadrup, N., Qvortrup, K., Larsen, A., Gao, X., Vogel, U., Mortensen, A., Lam, H.R., Larsen, E.H., 2011. Distribution of silver in rats following 28 days of repeated oral exposure to silver nanoparticles or silver acetate. Part. Fibre Toxicol. 8, 1–14. doi:10.1186/1743-8977-8-18

Nadworny, P.L., Wang, J., Tredget, E.E., Burrell, R.E., 2010. Anti-inflammatory activity of nanocrystalline silver-derived solutions in porcine contact dermatitis. J. Inflamm. (Lond). 7, 13. doi:10.1186/1476-9255-7-13

National Institute for Occupational Safety and Health (NIOSH)., 2013. Managing the Health and Safety Concerns Associated with Engineered Nanomaterials, in: Approaches to Safe Nanotechnology. pp. 331–342.

Park, K., 2013. Toxicokinetic differences and toxicities of silver nanoparticles and silver ions in rats after single oral administration. J. Toxicol. Environ. Health. A 76, 1246–60. doi:10.1080/15287394.2013.849635

Park, K., Park, E.-J., Chun, I.K., Choi, K., Lee, S.H., Yoon, J., Lee, B.C., 2011. Bioavailability and toxicokinetics of citrate-coated silver nanoparticles in rats. Arch. Pharm. Res. 34, 153–8. doi:10.1007/s12272-011-0118-z

Percival, S.L., Bowler, P.G., Dolman, J., 2007. Antimicrobial activity of silver-containing dressings on wound microorganisms using an in vitro biofilm model. Int. Wound J. 4, 186–191. doi:10.1111/j.1742-481X.2007.00296.x

Rahman, I., Kode, A., Biswas, S.K., 2007. Assay for quantitative determination of glutathione and glutathione disulfide levels using enzymatic recycling method. Nat. Protoc. 1, 3159–3165. doi:10.1038/nprot.2006.378

Sahiner, U.M., Birben, E., Erzurum, S., Sackesen, C., Kalayci, O., 2011. Oxidative stress in asthma. World Allergy Organ. J. 4, 151–8. doi:10.1097/WOX.0b013e318232389e

Seiffert, J., Hussain, F., Wiegman, C., Li, F., Bey, L., Baker, W., Porter, A., Ryan, M.P., Chang, Y., Gow, A., Zhang, J., Zhu, J., Tetley, T.D., Chung, K.F., 2015. Pulmonary toxicity of instilled silver nanoparticles: Influence of size, coating and rat strain. PLoS One 10, 1–17. doi:10.1371/journal.pone.0119726

Shahare, B., Yashpal, M., 2013. Toxic effects of repeated oral exposure of silver nanoparticles on small intestine mucosa of mice. Toxicol. Mech. Methods 23, 161–167. doi:10.3109/15376516.2013.764950

Shrivastava, S., Bera, T., Singh, S.K., Singh, G., Ramachandrarao, P., Dash, D., 2009. Characterization of Antiplatelet Properties of Silver Nanoparticles. ACS Nano 3, 1357–1364. doi:10.1021/nn900277t

Silva, R.M., Anderson, D.S., Franzi, L.M., Peake, J.L., Edwards, P.C., Van Winkle, L.S., Pinkerton, K.E., 2015. Pulmonary effects of silver nanoparticle size, coating, and dose over time upon intratracheal instillation. Toxicol. Sci. 144, 151–162. doi:10.1093/toxsci/kfu265

Soetaert, K., Petzoldt, T., Setzer, R.W., 2010. Solving Differential Equations in R: Package deSolve. J. Stat. Softw. 33.

Sun, R.W.-Y., Chen, R., Chung, N.P.-Y., Ho, C.-M., Lin, C.-L.S., Che, C.-M., 2005. Silver nanoparticles fabricated in Hepes buffer exhibit cytoprotective activities toward HIV-1 infected cells. Chem. Commun. 5059. doi:10.1039/b510984a

Sung, J.H., Ji, J.H., Park, J.D., Yoon, J.U., Kim, D.S., Jeon, K.S., Song, M.Y., Jeong, J., Han, B.S., Han, J.H., Chung, Y.H., Chang, H.K., Lee, J.H., Cho, M.H., Kelman, B.J., Yu, I.J., 2009. Subchronic inhalation toxicity of silver nanoparticles. Toxicol Sci 108. doi:10.1093/toxsci/kfn246

Takenaka, S., Karg, E., Roth, C., Schulz, H., Ziesenis, A., Heinzmann, U., Schramel, P., Heyder, J., 2001. Pulmonary and systemic distribution of inhaled ultrafine silver particles in rats. Environ. Health Perspect. 109, 547–551.

Team, R.C., 2014. A language and environment for statistical computing. R Found. Stat. Comput. Vienna, Austria.

Wijnhoven, S.W.P., Peijnenburg, W.J.G.M., Herberts, C.A., Hagens, W.I., Oomen, A.G., Heugens, E.H.W., Roszek, B., Bisschops, J., Gosens, I., Van De Meent, D., Dekkers, S., De Jong, W.H., Van Zijverden, M., Sips, A.J.A.M., Geertsma, R.E., 2009. Nano-silver: a review of available data and knowledge gaps in human and environmental risk assessment. Nanotoxicology 3. doi:10.1080/17435390902725914

Wright, J.B., Lam, K., Hansen, D., Burrell, R.E., 1999. Efficacy of topical silver against fungal burn wound pathogens. Am. J. Infect. Control 27, 344–50.

Xu, Y., Wang, L., Bai, R., Zhang, T., Chen, C., 2015. Silver nanoparticles impede phorbol myristate acetate-induced monocyte-macrophage differentiation and autophagy. Nanoscale 0, 1–3. doi:10.1039/x0xx00000x

Yin, H.Q., Langford, R., Burrell, R.E., 1999. Comparative evaluation of the antimicrobial activity of ACTICOAT antimicrobial barrier dressing. J. Burn Care Rehabil. 20, 195–200.

Zhao, J., Magaya, R.R., Zou, B., Shi, H., Yu, H., Yue, X., Liu, K., Lin, X., Xu, J., Yang, C., Wu, A., 2014. Acute toxicity of nickel nanoparticles in rats after intravenous injection. Int. J. Nanomedicine 9, 1393. doi:10.2147/IJN.S56212

Chapter V

Biodistribution and pulmonary metabolic effects of silver nanoparticles in mice following acute intratracheal instillations

Part of this chapter was submitted as:

Rosário F., Duarte I., Santos C., Hoet P., Oliveira H (2018) Biodistribution and pulmonary metabolic effects of silver nanoparticles in mice following acute intratracheal instillations

Biodistribution and pulmonary metabolic effects of silver nanoparticles in mice following acute intratracheal instillations

Rosário F [a], Duarte IF [b,II], Santos C [c], Hoet P [d], Oliveira H [a,b,I]

[a] *Department of Biology & CESAM, University of Aveiro, Campus Universitário, 3810-193 Aveiro, Portugal.*

[b] *CICECO - Aveiro Institute of Materials, Department of Chemistry, University of Aveiro, 3810-093 Aveiro, Portugal.*

[c] *Department of Biology, LAQV/REQUIMTE, Faculty of Sciences, University of Porto, 4169-007, Porto, Portugal.*

[d] *Occupational and environmental Toxicology, KU Leuven, ON1Campus Gasthuisberg, Herestraat 49, 3000 Leuven, Belgium.*

[I] *Corresponding author. E-mail address:* holiveira@ua.pt

[II] *Corresponding author. E-mail address*: ioladuarte@ua.pt

Abstract

The respiratory tract is the route of entry for accidentally inhaled AgNPs, which can enter the lungs and redistribute to the other main organs through systemic circulation. In the present work, we aimed at evaluating silver biodistribution and biological effects after 1 or 2 intratracheal instillations (IT) of two differently sized AgNPs (5 and 50 nm – 3mg/kg) and ionic silver ($AgNO_3$ - 1mg/kg). Nuclear magnetic resonance (NMR) metabolomics was applied to unveil pulmonary metabolic variations. Overall, the effects of the instilled AgNPs were dependent on particle size and number of instillations. After 1 IT, the highest silver concentration was found in lungs, followed by spleen, kidneys and liver. AgNP5 showed faster and higher distribution to all organs, whereas larger particles remained mostly in the blood. AgNP50 showed also higher excretion, with higher silver levels in the urine and feces of AgNP50 exposed animals. The two AgNPs also differed in hematological effects, with AgNP5 producing larger variations in total WBC count and specific subpopulations like basophils and eosinophils. GSH levels hinted to oxidative stress in the lungs, after 2 IT, while liver showed good antioxidant protection. Lung

NMR profiling revealed several Ag-induced alterations in metabolites involved in different pathways, such as glycolysis and TCA cycle, amino acid metabolism, phospholipid metabolism and antioxidant defense. Notably, most of the metabolic changes observed after 1 IT were either absent or reversed in animals subjected to 2 IT, suggesting adaptation mechanisms to cope with the initial insult and recover homeostasis.

Keywords: silver nanoparticles, *in vivo*, intratracheal instillation, biodistribution, excretion, NMR metabolomics

1. Introduction

Silver nanoparticles (AgNPs) have been extensively produced and incorporated into consumer products, mainly due to their antimicrobial properties. Moreover, emergent evidence on AgNPs potent anti-inflammatory, antiviral and/or anticancer activity (Wei et al., 2015) makes it likely that the biomedical applications of these nanoparticles will expand in the future. Hence, increased production, consumer use and disposal of AgNP-containing products have raised the potential for accidental or incidental human exposure via inhalation, dermal or ingestion routes, reinforcing the need for their thorough toxicological assessment.

The respiratory tract is the route of entry for all accidentally inhaled AgNPs, which may subsequently accumulate in the lungs, enter systemic circulation and distribute to the remaining organs and tissues. Previous studies have revealed toxic effects for inhaled or instilled AgNPs in animal models, often focusing on the determination of silver lung burden and assessment of pulmonary toxicity. For instance, Anderson and co-authors investigated the persistence and clearance of aerosolized AgNPs (sized 20 or 110 nm) in the rat lung and reported pulmonary silver persistence at 56 days post-exposure and size-dependent silver burden in bronchoalveolar lavage fluid macrophages (Anderson et al., 2015). Regarding pulmonary toxicity, while some works reported minimal or no toxic effects after single, short-term (Ji and Yu 2012; Roberts et al., 2013) or repeated daily exposures (Stebounova et al., 2011) of rats or mice to AgNPs, others have observed moderate toxicity comprising lung inflammatory responses and/or

histopathological changes (Kwon et al., 2012; Haberl et al., 2013; Seiffert et al., 2015). Moreover, some studies underlined the transient nature of pulmonary inflammation, with changes gradually regressing with time (Kaewamatawong et al., 2009; Braakhuis et al., 2014). Mechanistically, pulmonary toxicity of inhaled or instilled AgNPs has been associated with MAPK signaling, local inflammatory response and pro-inflammatory cytokines production (Kwon et al., 2012; Armstead et al., 2015; Fehaid et al., 2016). The potential neurotoxic effects of inhaled AgNPs have also been reported (Hu and Gao 2010; Xu et al., 2015a). Trickler et al. (2010) isolated primary rat brain microvessel endothelial cells (rBMEC) from adult Sprague-Dawley rats for an *in vitro* blood brain barrier (BBB) model of exposure to AgNPs. The results showed that smaller AgNPs (25 and 40 nm) induced time-dependent brain pro-inflammatory responses at lower concentrations than 80 nm AgNPs. Also, 25 nm AgNPs induced tumor necrosis factor (TNF) and prostaglandin PGE (2) response, while the larger AgNPs (40 and 80 nm) also induced significant TNF but no PGE (2) response (Trickler et al., 2010).

The above-mentioned studies were mostly based on conventional toxicity readouts. At the moment, information on the *in vivo* biological effects produced by AgNPs at the metabolic and functional level is still scarce. Recently, metabolomics has emerged as a powerful approach to assess cellular or whole organism responses to nanomaterials (Duarte 2011; Lv et al., 2015). For instance, nuclear magnetic resonance (NMR) metabolomics has been recently employed to characterize multi-organ and systemic metabolic responses to AgNPs intravenously administered to mice at a dose not eliciting overt toxicity (Jarak et al., 2017). That study has shown that intermediary metabolism not only responded sensitively to the presence of AgNPs, in an organ-specific and time-dependent way, as it played vital roles in protecting cells and mitigating toxic effects.

In the present work, we aimed to characterize the biological responses to AgNPs of two different sizes (5 and 50 nm) and to Ag^+ ($AgNO_3$), after one or two intratracheal instillations, as this administration route is suitable for mimicking accidental inhalation exposure. For that purpose, the following assays have been performed: i) silver quantification in blood and organ tissues of control and exposed mice; ii) silver quantification in urine and feces, to assess excretion patterns; iii) hematological analysis, including white and red blood cell counts; iv) determination of GSH and GSSG levels in liver and lung tissues; v) NMR metabolic profiling of lung tissues.

This set of assays is expected to provide a novel, integrated view on the biological effects of inhaled AgNPs.

2. Materials and methods AgNP and $AgNO_3$ solutions

Sterile, purified and endotoxin-free AgNPs (Econix 5.0 mg/mL) with polyvinylpyrrolidone (PVP) coating and nominal sizes of 5 and 50 nm (here designated as AgNP5 and AgNP50, respectively), were obtained from NanoComposix Europe (Prague, Czech Republic). The AgNP5 had a diameter of 5.2 ± 0.7 nm (TEM) and the stock solution contained $6.9x10^{15}$ particles/mL, the AgNP50 had a diameter of 54.8 ± 10.1nm (TEM) and the stock solution contained $5.2x10^{12}$ particles /mL. The treatment solutions were prepared by dilution of AgNPs or $AgNO_3$ in NaCl (0.9%) to obtain 0.075mg for AgNPs (3 mg/kg) and 0.025mg for $AgNO_3$ (1 mg/kg) in 50 µL. The dose of $AgNO_3$ was calculated based on Ag^+ mass and expressed as $AgNO_3$.

Mice

Six-week-old male BALB/c OlaHsd mice (weighing approximately 25 g) were obtained from Harlan (Horst, The Netherlands). Mice were housed in a conventional animal house, in filter top cages with 12 h dark/light cycles and received lightly acidified water and pelleted food (Trouw Nutrition, Ghent, Belgium) *ad libitum*. Individual animal weights were recorded pre-dosing twice a week and at the time of euthanasia**.** All experimental procedures were approved by the local Ethical Committee for Animal Experiments.

Experimental protocol

Twenty-four mice were randomly assigned to one control (n = 6) and three experimental groups (AgNP5, AgNP50 and $AgNO_3$, n = 6 each), which were further divided according to the number of instillations. Twelve mice were dosed by a single intratracheal instillation (1 IT) (day 0) and allowed to recover for 7 days, while 12 other mice were dosed 2 times by intratracheal instillation (2 IT) (day 0 and day 7) and allowed to recover for additional 7 days (sample collection at day 14). The controls were instilled once or twice with saline solution (NaCl 0.9%).

In each instillation, animals were dosed with 50µl of solution/suspension. The administrations were performed using 24-gauge catheters under intraperitoneal anesthesia of a mixture of xylazine + ketalar in NaCl (150µl/25g of body weight). After each dosage, the mice were checked for normal behavior and placed back in the cages. Two animals from each treatment group were placed for 24h in metabolic cages to collect urine and feces. At the end of the testing periods, mice were weighted and sacrificed by an intraperitoneal injection of 200 µl of Nembutal. A schematic overview of the experimental protocol is shown in Fig.1.

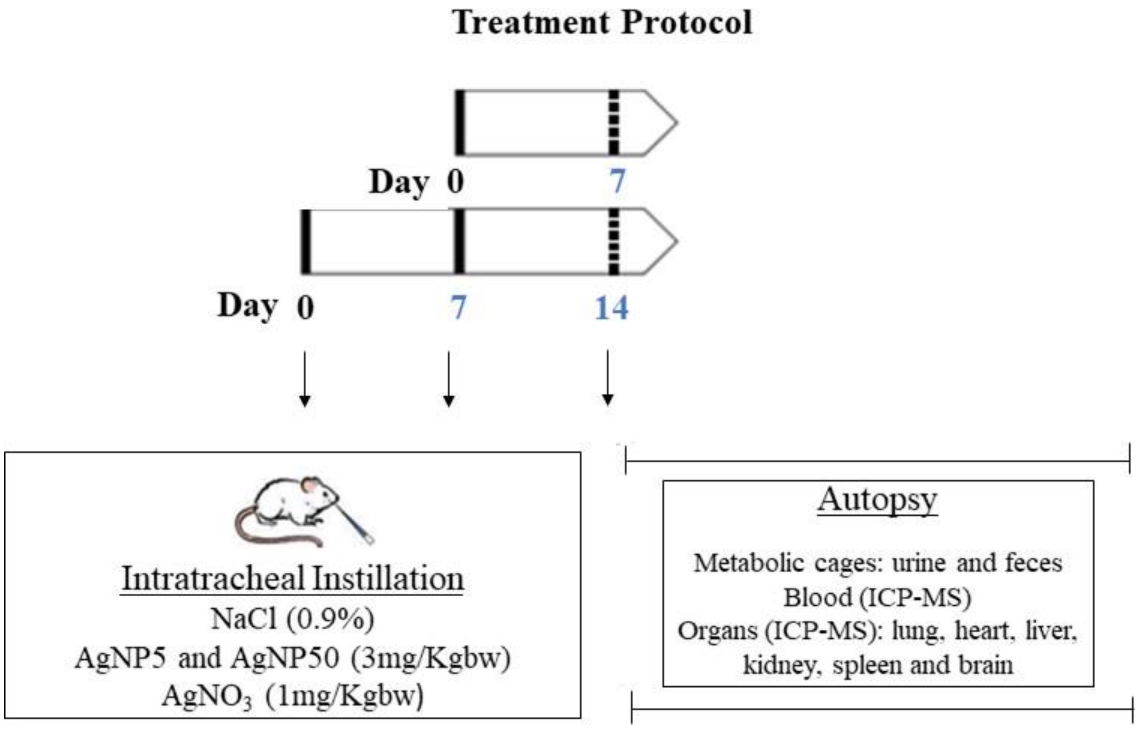

Figure 1 – Schematic overview of the experimental protocol. Black lines represent exposure time and black dashed lines represent recovery time.

Tissue sampling

Following sacrifice, tissue organs were collected and weighted. Samples were separated for ICP-MS analysis (lung, spleen, kidney, liver and bone marrow, heart and brain), GSH/GSSG measurements (lung and liver) and metabolic profiling (lung), snap-frozen in liquid nitrogen and stored at -80ºC until analysis. Hair, blood, urine and feces samples were also collected in eppendorfs and stored at -20ºC for ICP-MS measurements.

Silver quantification by ICP-MS

Aqua regia digestion of the samples was made by adding 1.5 mL HCl + 0.5 mL of HNO_3 to approximately 30 mg tissue (hair, lung, kidney, spleen, liver, brain, heart, bone marrow, blood, urine and feces) in glass tubes. After 24h, samples were heated at 140°C for 90 min on a digestion block. Finally, samples were diluted to 10 mL with Milli-Q water and metal concentration was measured by ICP-MS (Agilent 7700x ICP-MS). Elements were measured as ^{107}Ag using ^{103}Rh as internal standard. The limit of quantification from the ICP-MS, in the solutions was 0.015 µg/L (Ag).

Blood collection and analysis

After euthanasia, blood was collected from the retro-orbital plexus and 500 µL aliquots were transferred into eppendorfs with 50 µL of citrate (3.8%) and 200 µL of sterile saline (NaCl 0.9%). Total and differential blood cell counts (white blood cells, neutrophils, monocytes, lymphocytes, eosinophils, basophils, red blood cells, platelets) and hemoglobin concentration were determined on a Cell-Dyn 3500R counter (Abbott Laboratories, Philippines).

Assessment of GSH and GSSG levels

Total GSH content was determined according to Rahman et al. (2007) with some modifications. Lung and liver samples were homogenized in ice cold 40 mM Nethylmaleimide (20 mL/g tissue to prevent rapid oxidation of GSH) and centrifuged at 14000 g for 15 min at 4°C. The supernatant was then transferred to a new tube and 5% metaphosphoric acid was added (1/5th of the supernatant volume, final concentration 1% metaphosphoric acid, for protein removal), mixed and again centrifuged at 14000 g during 15 min at 4°C. The supernatants were stored at −80°C until measurements. Total protein levels were determined using the Bio-Rad Protein assay, according to the Bradford method (Bio-Rad Laboratories GmbH, München, Germany using bovine serum albumin as standard).

Nuclear magnetic resonance analysis

At the time of analysis, about 40 mg of frozen lung were washed with a few drops of D_2O saline (0.9%) to remove excess blood, and packed into 50 µL HRMAS rotors, containing 10 µL of

D_2O saline with 0.25% 3-(trimethylsilyl) propionate sodium salt (TSP)-d_4 to provide signal for lock (D_2O) and for shimming (TSP). NMR spectra were acquired at 277 K using a 4 mm HRMAS probe (4 kHz spinning rate) on a Buker Avance DRX-500 spectrometer operating at 500 MHz for ^1H observation. To attenuate broad signals of macromolecules and improve the detection of small metabolites, the T_2-edited Carr-Purcell-Meiboom-Gill spin-echo pulse sequence with water presaturation ('cpmgpr1d' in Bruker library) was employed, using a total spin echo time of 64 ms (n = 80, τ = 400 μs). 256 transients were acquired with 32 k points, spectral width of 13 ppm, relaxation delay of 4 s and acquisition time of 2.5 s. Spectra were processed with a line broadening of 0.3 Hz and a zero-filling factor of 2, manually phased and baseline corrected. Chemical shifts were referenced internally to the alanine signal phased and baseline corrected.

Additionally, 2D homonuclear (TOCSY, J-resolved) and heteronuclear (HSQC) spectra were recorded for selected samples to help spectral assignment. Spectral assignment was based on our previously reported work (Jarak et al., 2017) and confirmed by matching the recorded 1D and 2D NMR spectra to reference data available in the Buker Biorefcode database and other publicly available databases such as HMDB (Wishart et al., 2007).

Multivariate analysis and integration of NMR spectra

Spectra were normalized by probabilistic quotient normalization (PQN) using the median of controls as reference spectrum and scaled to unit variance (UV). Data matrices were built in Amix-viewer (version 3.9.14, Bruker Biospin, Rheinstetten) using all intensity values in the δ 0.5 – 8.8 ppm region (excluding suppressed water and contaminant signals). Principal Component Analysis (PCA) was performed in SIMCA-P11.5 (Umetrics, Sweden) to explore data variability and identify clusters and outliers. To assess the magnitude of metabolite variations, selected spectral peaks were integrated in Amix-viewer and normalized by the quotient computed from PQN. For each metabolite, the magnitude of variation in exposed mice relatively to respective controls was assessed by calculating the effect size (ES), adjusted for small samples numbers, and respective standard error, according to the equations provided in the literature (Berben et al., 2012). The metabolic changes with absolute ES larger than 0.8 (and with standard error < ES) were represented in a heatmap colored according to the % variation

(vs. controls), using the R-statistical software. Additionally, the difference between the means of each experimental group and the control group was assessed using the two-sample t-test (results reported at a confidence level of 95%).

Statistical analysis

All data are presented as means and standard deviations (SD). Data analysis was performed in the software SigmaPlot version 11, by one-way, two-way and tree-way ANOVA analysis of variance ($p < 0.05$), using Holm-sidak test. When the treatments group sizes were unequal, an ANOVA was performed on ranks, using Dunn's test.

3. Results

Mice behavior observations

Overall, intratracheal instillations of AgNPs or $AgNO_3$ were well-tolerated and normal feeding behavior was observed. Animals did not exhibit illness, and none died or was euthanized due to test substance-related causes, prior to the study endpoint. No significant body weight (bw) changes were observed during treatment time (Table 1), although a slight non-significant increase was observed for mice instilled twice with AgNP5 or AgNP50

Table 1 - Mice Body weight (g) following 1 or 2 intratracheal instillations (1IT and 2 IT, respectively) of saline (control), $AgNO_3$, AgNP5 or AgNP50. Both 1 and 2 IT treated mice were allowed to recover for 7 days (n=3 per group).

	1 IT	**2 IT**
Control	24.0±1.0	25.0±0.0
$AgNO_3$	24.7±1.2	25.0±0.8
AgNP5	24.3±1.2	25.9±1.6
AgNP50	25.5±1.5	26.7±1.2

Silver tissue distribution

Silver concentration in the blood, lung, heart, spleen, kidney, liver and brain of mice subjected to a single instillation with saline (control), $AgNO_3$, AgNP5 or AgNP50 was determined by ICP-MS (Fig.2). Bone marrow and hair were analyzed, but due to the small amount of sample available, the silver levels were below the detection limit of ICP-MS (data not shown).

In mice exposed to 5 nm particles (AgNP5), the highest silver levels were detected in the lungs, followed by the blood, spleen, kidneys, liver, brain and heart. Larger particles (AgNP50) accumulated mostly in the blood, with a smaller fraction being distributed to the organs. Upon instillation with $AgNO_3$, the amount of silver detected in all organs was much lower than in those instilled with AgNPs.

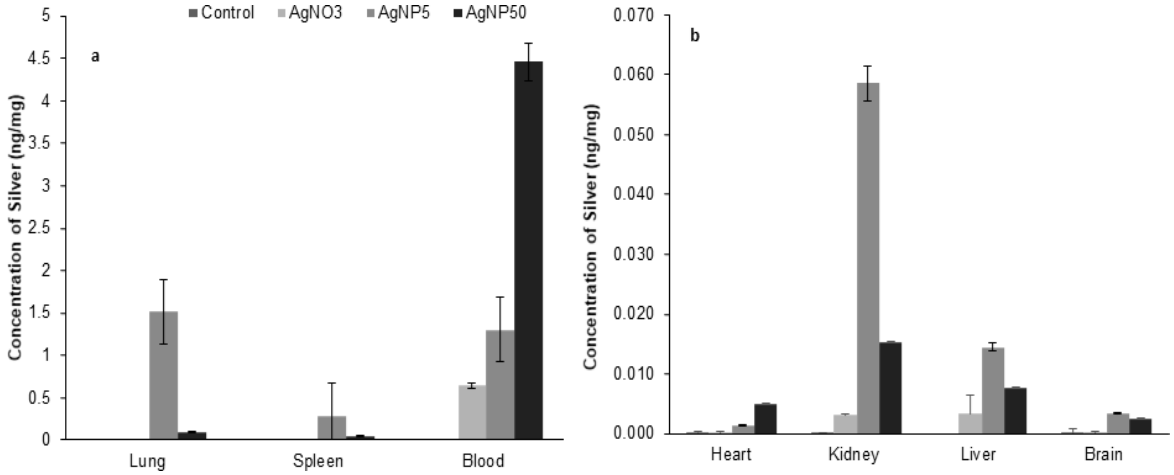

Figure 2 – Silver concentrations (ng/mg tissue fresh weight (or ng/ml for blood) after 1 intratracheal instillation of saline (control), $AgNO_3$, AgNP5 and AgNP50. $p < 0.05$ (ANOVA on all groups). a. Lung, Spleen and Blood; b. Heart, Kidney, Liver and Brain.

Silver excretion

Fig.3 shows the presence of silver in urine and feces of mice exposed to $AgNO_3$ or AgNPs (upon a single instillation). The highest amount of silver excreted was observed in both urine and feces of mice exposed to $AgNO_3$, followed by AgNP50 and AgNP5.

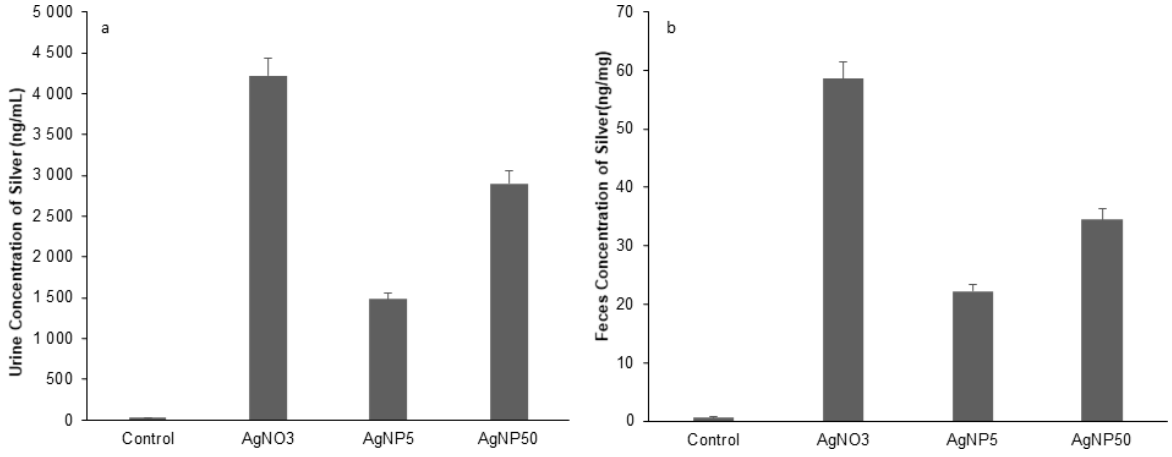

Figure 3 – Levels of excreted silver by urine and feces (ng/mL or ng/mg) after 1 intratracheal instillation of saline (control), $AgNO_3$, AgNP5 and AgNP50. a. Urine; b. Feces.

Hematological analysis

Fig.4 shows the results of blood cell counts for control and treatment groups ($AgNO_3$, AgNP5 and AgNP50), after 1 or 2 IT. The red blood cell count (RBC) and hemoglobin concentration (HBG) were not affected by any of the treatments (Fig.4 - a & b). On the other hand, platelet (PLT) numbers were significantly decreased after 1 IT with AgNP5 and AgNP50, although they recovered back to higher levels after 2 IT. (Fig.4 – c). As for the total white blood cells (WBC) count (Fig.4 – d), it decreased significantly upon instillation with $AgNO_3$, showing an opposite and cumulative increase for AgNP5. Instillation with AgNP50 produced no major changes in total WBC count. Regarding granulocytes, neutrophils showed a significant increase upon 1 IT of AgNP50 (recovering back to control levels after 2 IT), basophils increased in the blood of AgNP5 exposed mice, and also eosinophils, although only after 2 IT of both AgNPs. Eosinophils also increased after $AgNO_3$ instillation, whereas basophils showed a decrease after 1 IT and no difference to control at 2 IT (Fig.4 – g & f). As for monocytes, while $AgNO_3$ caused a transient decrease at 1 IT, significant decreases were observed upon 2 IT of both NP types. Finally, lymphocytes were decreased in the blood of mice after 1 IT of AgNP5 but showed no differences at 2 IT (Fig.4 – i).

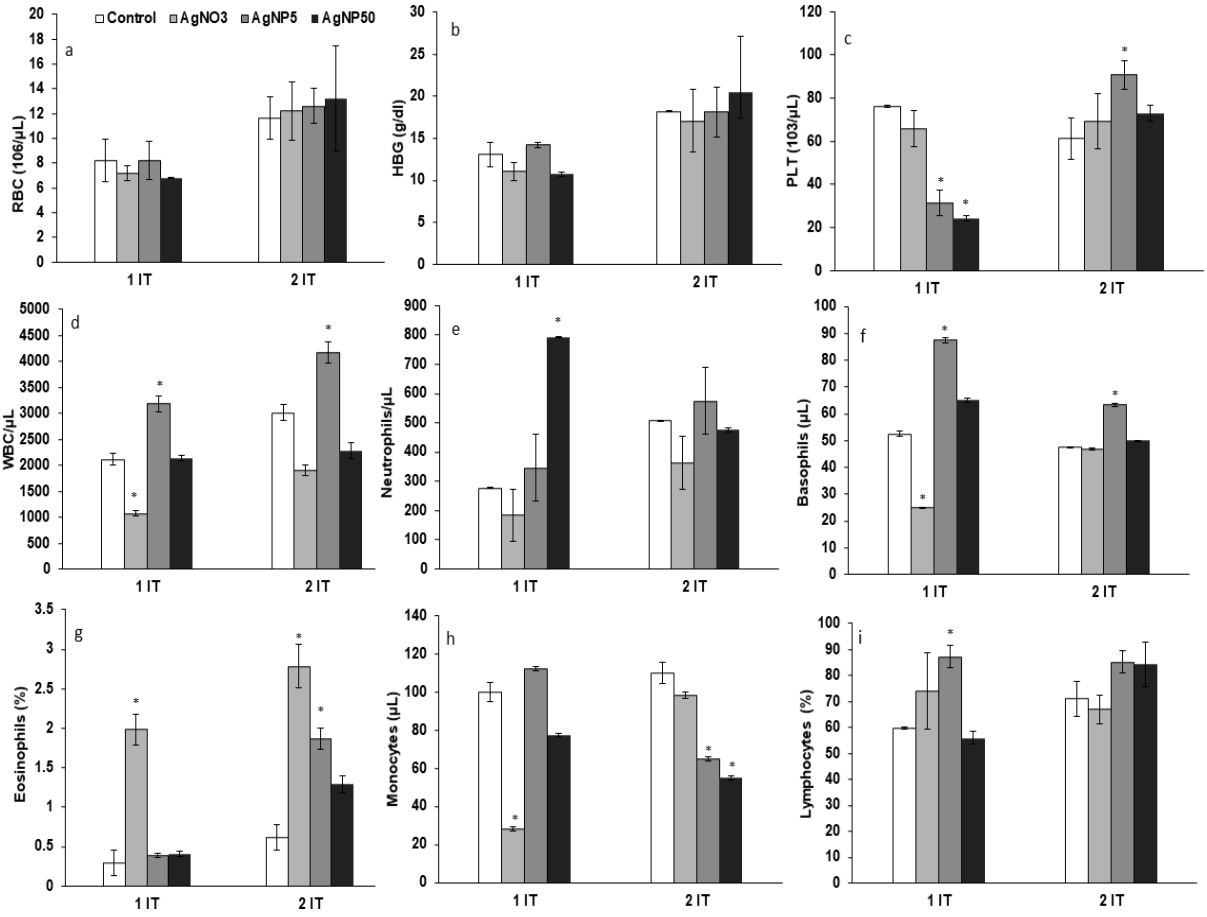

Figure 4 – Mice hematology values after 1 or 2 intratracheal instillations (1 IT and 2 IT, respectively) of saline (control), $AgNO_3$, AgNP5 and AgNP50. a. red blood cells (RBC); b. hemoglobin concentration (HGB); c. platelets (PLT); d. white blood cells (WBC); e. Neutrophils; f. Basophils; g. Eosinophils; h. Monocytes; i. Lymphocytes. * significant differences between control and treatments ($p < 0.05$).

Lung and liver GSH levels

The results of GSH and GSSG quantification in lung and liver tissues are presented in Fig.5. In the lungs, GSH showed increased levels after 1 IT of $AgNO_3$, AgNP5 or AgNP50 (although not significantly for the latter), and no difference to controls after 2 IT (Fig.5 – a). On the other hand, pulmonary GSSG levels decreased upon 1 IT for all treatments and showed an increasing trend after 2 IT, especially for AgNP50 (Fig.5 – b). In the liver, GSH levels increased upon 1 IT of $AgNO_3$ or AgNP5, returning to control levels at 2 IT (Fig.5 – c), whereas GSSG was consistently decreased in relation to controls, except after 2 IT of $AgNO_3$ (Fig.5 – d).

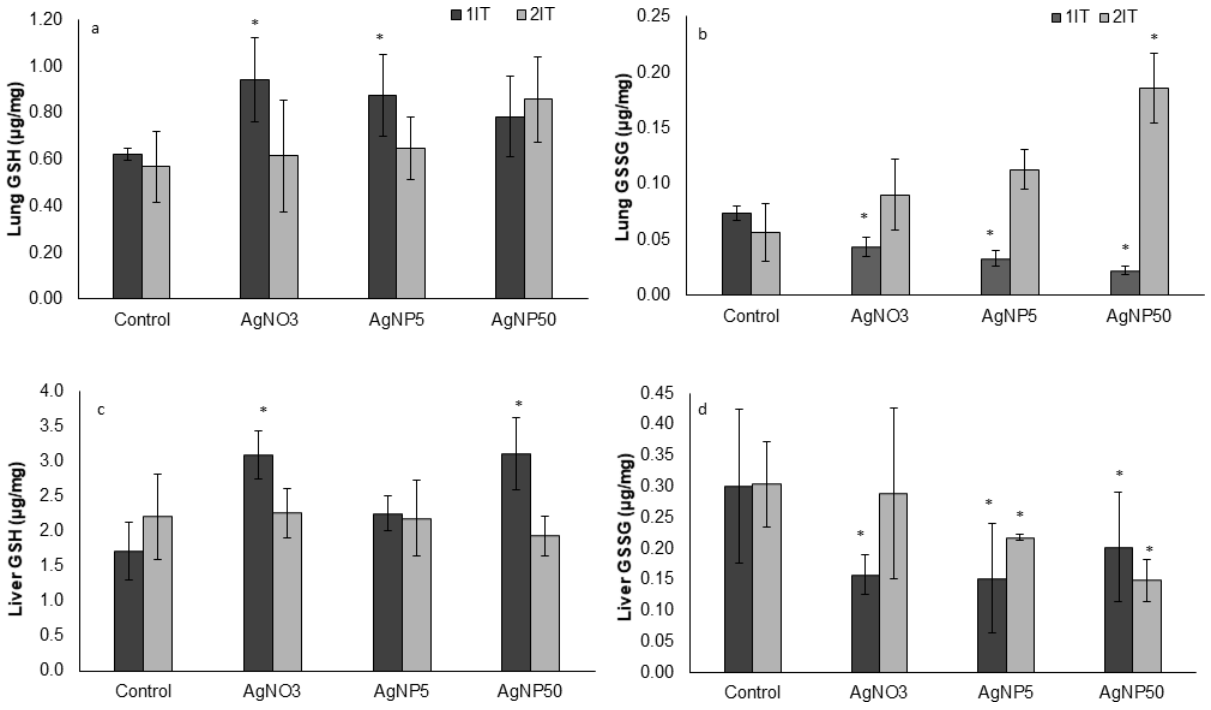

Figure 5 – GSH and GSSG levels in lungs and livers of mice upon 1 or 2 intratracheal instillations (1IT or 2IT, respectively) with saline (Control), $AgNO_3$, AgNP5 and AgNP50. Treated mice could recover for 7 days. A. Lung GSH; B. Lung GSSG; C Liver GSH. D. Liver GSSG. * significant difference between treatments and respective controls ($p < 0.05$).

Metabolic composition of lung tissues

Fig.6 – a, shows a typical ^1H NMR spectrum of lung tissue, with some metabolites annotated according to the assignment previously reported by us for mice tissues (Jarak et al., 2017). As a first approach to investigate the impact of the different treatments on lung tissue metabolic composition, Principal Component Analysis (PCA) was applied to the spectra of samples collected from the animal groups subjected to 1 or 2 instillations. The corresponding scores scatter plots are shown in Fig.6 - b & c. After 1 IT, there was a clear separation between controls, $AgNO_3$ and AgNP5 samples, along the PC2 axis (Fig.6 - b). On the other hand, lung tissues from AgNP50-treated mice, although separating from controls, were more spread in space, suggesting higher variability in the corresponding profiles. After 2 IT (Fig.6 - c), control and $AgNO_3$ samples were separated from AgNP samples along PC2, and a slight trend for size-dependent clustering was observed.

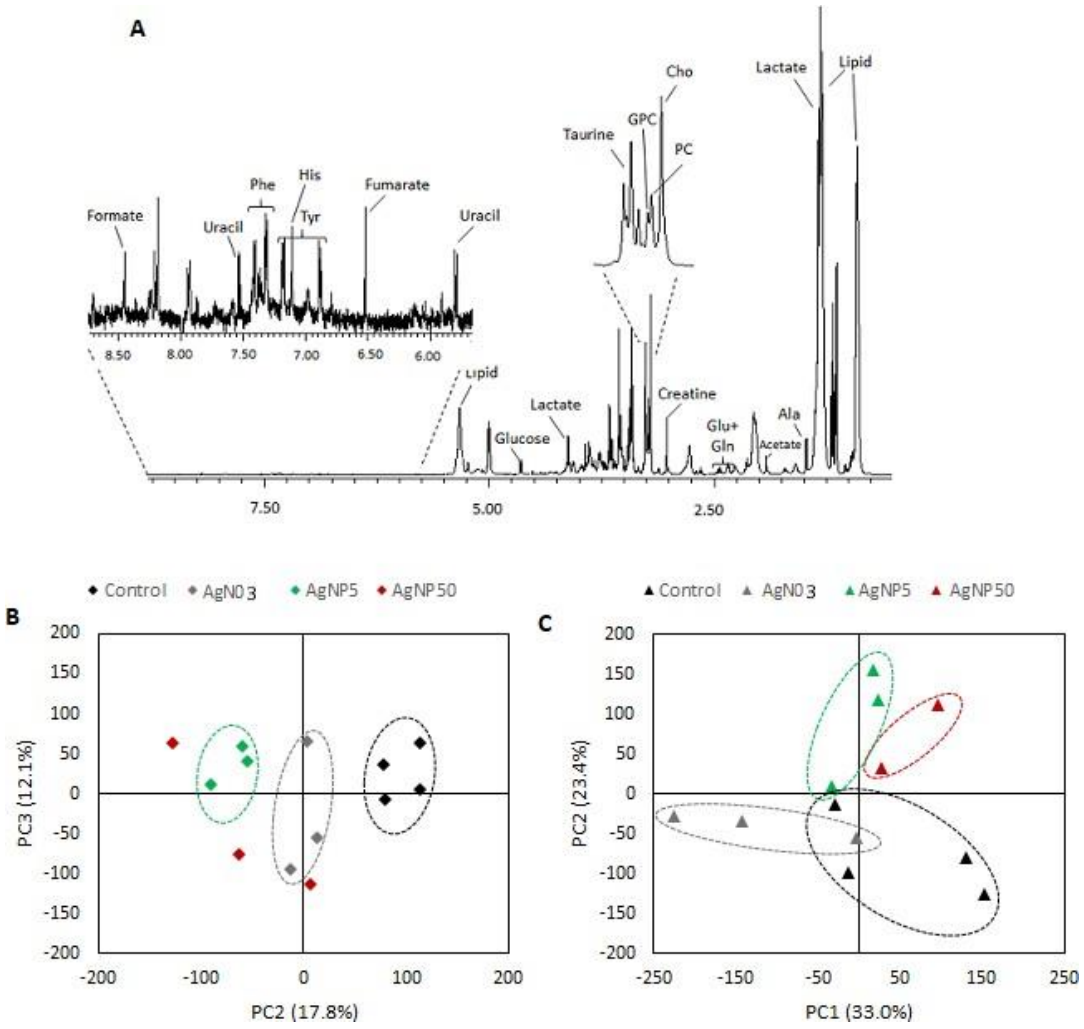

Figure 6 – Typical ^{1}H HRMAS NMR spectrum of control lung tissue A. Scores scatter resulting from PCA of ^{1}H NMR spectra of lung tissues from controls, $AgNO_3$, AgNP5 and AgNP50-treated animals; B. after 1 instillation; C. after 2 instillations.

To study group differences in more detail, individual metabolite variations were assessed through spectral integration. The results were summarized in the form of a heatmap, color-coded according to the % of variation in relation to controls (Fig.7). Only metabolites with large magnitude variations (absolute ES > 0.8), (Berben et al., 2012) were included. A total of 22 metabolites were affected upon one of the treatments ($AgNO_3$, AgNP5 or AgNP50), in a way which greatly depended on the number of instillations. In the case of $AgNO_3$, the impact on lung tissue composition was much higher in animals subjected to 1 IT, as the lungs of animals instilled twice showed very few differences in relation to their respective controls, in agreement with the

PCA results. As for the varying metabolites, glucose, succinate, malonate, some amino acids (glutamine, glutamate, glycine), phosphocholine, glycerophosphocholine, formate and ascorbate registered increases, whereas another set of amino acids (including branched chain and aromatic amino acids), choline and acetate were decreased upon $AgNO_3$ single instillation. The response profiles to AgNPs were also greatly dependent on the number of ITs, with both single and double instilled mice showing several differences in comparison to their respective controls. Regarding AgNP5, several effects were common to those observed for $AgNO_3$, while others were distinct, for instance, the variations in fumarate, some amino acids (lysine, glutamate, glycine, methionine) and uracil. As for the effects of AgNP50, although the overall qualitative impact was highly similar to AgNP5, there were some noticeable quantitative differences. Moreover, the variation in creatine (strong increase after 1 IT followed by a decrease in double instilled mice) was exclusive to AgNP50.

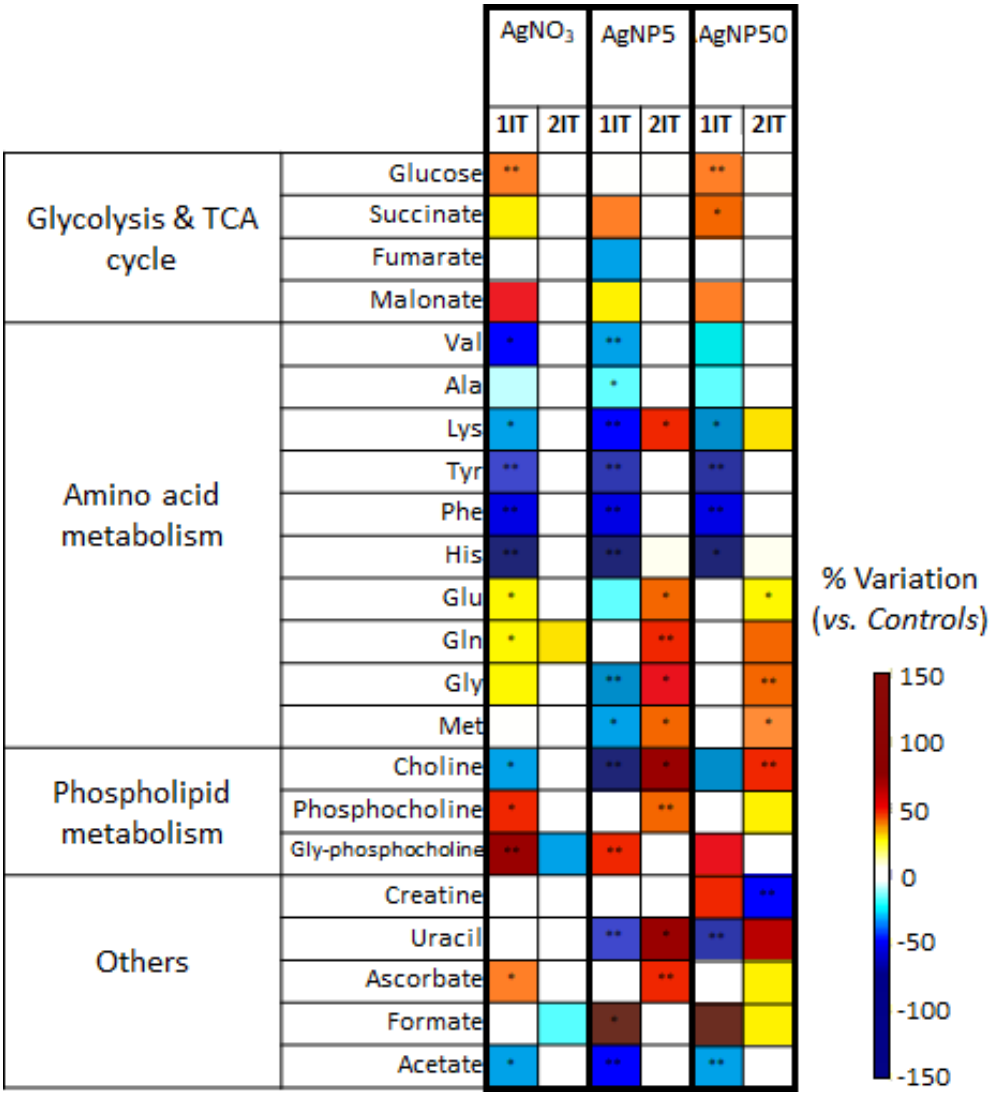

Figure 7 – Heatmap showing the metabolic variations in the lungs mice exposed to $AgNO_3$ and AgNP5 and AgNP50 by 1 or 2 intratracheal instillations (1 IT or 2 IT, respectively), in relation to controls. The scale is color- coded as a function of the % variation, from maximum decrease (dark blue) to maximum increase (dark red). The criterium for including a metabolite in the heatmap was absolute ES > 0.5 (and SE < ES). Statistically significant differences are indicated (*p < 0.05, **p < 0.01). 3 letter code used for amino acids.

4. Discussion

In this study, the distribution, excretion and metabolic effects of two differently sized AgNPs (as well as of Ag^+) have been assessed in a mouse model after one or two intratracheal instillation exposures. The doses of AgNPs and $AgNO_3$ administered to mice (3 mg/kg or 75 µg/mice and 1mg/kg or 25 µg/mice, respectively) fall within the dose range previously tested on intravenously injected, oral and intranasal administered mice/rats without eliciting overt toxicity (Shrivastava et al., 2009; Dziendzikowska et al., 2012; Liu et al., 2012). Moreover, Wiemann et al. (2017) studied the effects of PVP-coated AgNP50 after intratracheal instillation at 37.5, 75, 150, 300 µg per rat lung. The effects produced upon administration of 75 µg/rat lung were fully reversed on day 21. The escalating doses progressively increased the number of alveolar macrophages and PMN, indicating ongoing damage of the lung epithelium. Therefore, our dose range is suitable for studying the inflammation and distribution of AgNPs.

According to the silver quantification data, AgNP5 showed a faster distribution and higher accumulation in most tissue organs, compared to AgNP50, which was accompanied by reduced excretion in urine or feces. On the other hand, a higher amount of silver in blood was obtained for the AgNP50 particles, along with higher concentrations excreted in both urine and feces. For both AgNP5 and AgNP50, the lungs were the preferential organ of AgNPs accumulation, followed by the spleen, kidneys and liver. Mice exposed to $AgNO_3$ showed low silver levels in all organs, and, unlike AgNPs, the highest relative amounts were found in the liver and kidneys. High silver concentrations were found in both urine and feces. These results suggest that $AgNO_3$ was cleared from the organism at a faster rate than AgNPs. This agrees with a previous study where silver administered as $AgNO_3$ was reported to be cleared from mice lungs more rapidly than AgNPs (Choi et al., 2010), although silver excretion in urine or feces was not assessed. In fact, to our knowledge, the present work is the first to quantify silver excretion after instillation of AgNP < 5 nm.

Regarding, hematological parameters, the platelet count was significantly decreased after 1 IT of both AgNPs. Such alteration, termed thrombocytopenia, may be due to either decreased platelet production or increased platelet destruction (Wei et al., 2016). Nevertheless, after 2 IT, this effect was reversed, which could possibly reflect the triggering of a rapid procoagulant response, as reported for gold nanoparticles (AuNPs) (Gryshchuk and Galagan 2016). In that

study, small (< 20 nm) AuNPs were found to induce platelet activation, while larger (> 30 nm) particles caused no effect. White blood cell counts were also found to vary in the present study, likely reflecting a respiratory inflammatory response (Chuang et al., 2013). Different granulocytes registered increases in the blood of AgNPs-exposed mice. Moreover, upon 2 IT of AgNPs, monocytes decreased. Their count below average could reflect an increased recruitment of phagocytes in the peripheral organs (Faqi 2013). Also, other authors have reported AgNPs-induced blockage in monocytes to macrophage differentiation, ultimately leading to cell death (Xu et al., 2015b). However, most literature reports on blood cell responses to inhaled/instilled AgNPs are quite discrepant, varying from no inflammation at all, after inhalation of ±18 nm AgNPs (Ji et al., 2007; Sung et al., 2009; Gosens et al., 2015), to allergic reaction upon inhalation of 33 nm AgNP by sensitized mice (Chuang et al., 2013), or innate immune response with an increase in monocytes after acute inhalation of ~15 nm AgNPs (Roberts et al., 2013). The reduced and oxidized forms of glutathione (GSH and GSSG, respectively) act in concert to regulate and maintain cellular redox status, and a decreased GSH:GSSG ratio is considered a marker of oxidative stress (Owen and Butterfield 2010). While providing reducing equivalents to antioxidant enzymes, hydroxyl radicals and other reactive species, GSH is itself oxidized to GSSG. After 2 IT of AgNPs or $AgNO_3$, the lungs of exposed mice showed increased GSSG levels and a concomitant decrease in the GSH:GSSG ratio, suggesting an oxidative stress response. On the other hand, the liver increased GSH and decreased GSSG contents, likely reflecting an efficient antioxidant protection, as previously observed in AgNPs-injected mice (Jarak et al., 2017). Moreover, increased liver GSH has been correlated with a parallel increase in biliary excretion of silver (Alexander and Aaseth 1981). Indeed, the treatments for which higher hepatic GSH levels were observed (AgNP50 and $AgNO_3$) were also those for which higher silver excretion was observed.

As the lungs were a major target for instilled silver, we have analyzed lung tissue metabolite composition to assess the impact of the different treatments on lung cells metabolic state. After a single intratracheal instillation (1 IT), several intermediates of the TCA cycle showed altered levels in the lungs of silver-exposed mice as compared to controls. In particular, succinate and malonate were increased, while fumarate was decreased (this latter variation being seen only in AgNP5-treated animals). These changes hint to the possible inhibition of succinate

dehydrogenase (SDH) by malonate, as this metabolite is a well-known competitive inhibitor of SDH, which catalyzes the conversion of succinate into fumarate in the TCA cycle (Potter and Dubois 1943). Impairment of this cycle could also relate to the glucose increase observed in AgNP50-exposed mice, as it could possibly reflect the down-regulation of the upstream glycolytic pathway. Interestingly, glucose was also increased upon $AgNO_3$ exposure but not in the lungs of AgNP5-instilled mice. On the other hand, several amino acids were depleted after 1 IT, which may be hypothesized to reflect the anaplerotic replenishment of the TCA cycle, to counteract SDH inhibition. This effect appeared to be more pronounced for the AgNP5 exposure. Downregulation of the TCA cycle has also been suggested to occur in the lungs of mice i.v. injected with 30 nm AgNPs, likely reflecting AgNPs-induced impairment of metabolic activity in inflamed lungs (Jarak et al., 2017).

Notably, most of the effects described above, putatively related to energy metabolism, were mostly absent in the lungs of mice instilled 2 times, which showed no differences compared to controls in the levels of glucose, TCA cycle intermediates or most amino acids. There was, however, a subset of amino acids which increased significantly in the lungs of 2 IT mice, especially in the case of AgNPs exposure. These were glutamine, glutamate, glycine and methionine, and their elevated levels could reflect their reduced use and/or higher production or protein turnover. In particular, glutamate and glycine increase may be associated with the observed increases in GSH/GSSG as these amino acids are needed for de novo glutathione synthesis.

Choline metabolites were also significantly altered after silver instillation. After 1 IT, choline decreased and glycerophosphocholine increased for all treatments, while phosphocholine increased only upon $AgNO_3$ instillation. Again, the 2 IT response differed from the 1 IT and entailed a decrease in glycerophosphocholine ($AgNO_3$), together with increases in choline and phosphocholine (AgNP5 and AgNP50). These changes may possibly relate to alterations in pulmonary surfactant composition and turnover, reported to occur under the influence of cytokines released during inflammation (Akella and Deshpande 2013). Moreover, as choline-containing metabolites are important membrane structural and signaling components, their variations may also reflect membrane alterations. In particular, the increase in glycerophosphocholine, which is a major breakdown product of phosphatidylcholine, could

reflect membrane disruption in association with silver toxicity, an effect which appeared to be mitigated in doubly instilled mice.

Creatine was altered in the lungs of mice instilled with AgNP50, increasing significantly after 1 IT, while the other treatments produced no changes in this metabolite. Creatine is a key intermediate in energy transfer processes, its increase often being associated with high energy demand. Also, high creatine levels have been postulated to have cytoprotective effects toward oxidative agents (Young et al., 2010) and inflammation (Khanna and Madan 1978). A creatine increase related to inflammatory reactions has also been observed in the lungs of mice i.v. injected with AgNPs (Jarak et al., 2017). Interestingly, in the present study, creatine decreased back to levels lower than control after the second AgNP50 instillation, again possibly reflecting an adaptation to the initial insult. Uracil was another metabolite whose variation differed according to the number of instillations, suggesting disruption of pyrimidine homeostasis by AgNPs (an effect only seen for AgNPs and not for $AgNO_3$). Ascorbate increased in the lungs exposed to either $AgNO_3$ (1 IT) or AgNPs (2 IT), which could possibly relate to its antioxidant role. Indeed, increases in lung GSH and GSSG were also observed in this study, which raises the hypothesis of a protective response elicited by low levels of oxidative stress.

Overall, NMR metabolic profiling of intact lung tissues revealed unanticipated changes in a number of metabolites, hinting to possible effects on multiple pathways and highlighting the dependence of such effects on the silver form administered.

5. Conclusions

This study has provided insight into silver biodistribution and biological effects after single or double IT of $AgNO_3$ and AgNPs (5 and 50 nm). Overall, the effects of the instilled AgNPs were dependent on size and the number of instillations. Regarding the biodistribution results, smaller particles showed a faster and higher distribution to all organs, whereas larger particles remained mostly in the blood and only a small fraction was obtained in the organs. On the other hand, AgNP5 appeared to be less excreted than AgNP50, as evaluated by higher silver levels in the urine and feces of AgNP50-exposed animals, which agrees with higher tissue organ accumulation of smaller particles. The two AgNP types also differed in hematological effects,

with AgNP5 producing larger variations in total WBC count and specific subpopulations like basophils and eosinophils. Assessment of GSH levels hinted to oxidative stress in the lungs, after 2 IT, while the liver showed good antioxidant protection. NMR profiling of lung tissues additionally revealed a number of Ag-induced alterations in metabolites involved in different pathways, such as glycolysis and TCA cycle, amino acid metabolism, phospholipid metabolism, energy transfer processes or antioxidant defense. Notably, most of the metabolic changes observed after 1 IT were either absent or reversed in animals subjected to 2 IT, suggesting adaptation mechanisms to cope with the initial insult and recover homeostasis. An exception to this trend was, however, noted for a subset of amino acids, which varied more significantly in the lungs of 2 IT mice than in 1 IT animals. In particular, the increases in glutamate and glycine could potentially be associated with the observed increases in glutathione. Some size-related metabolic changes were also observed, such as a creatine increase for AgNP50, and an increase ascorbate especially prominent for AgNP5, which could possibly relate to its antioxidant role.

Acknowledgments:

This work was supported b**y** CESAM (UID/AMB/50017), to FCT/MEC through national funds and the co-funding by the FEDER, within the PT2020 Partnership Agreement and COMPETE. Funding to the project PTDC/AAC-AMB/113649 by FEDER through COMPETE and by national funds through FCT (Fundação para a Ciência e a Tecnologia). FCT-awarded grants to Fernanda Rosário (SFRH/BD/91270/2012) and Helena Oliveira (SFRH/BPD/111736/2015) are greatly acknowledged.

References

Akella, A., Deshpande, S.B., 2013. Pulmonary surfactants and their role in pathophysiology o lung disorders. Indian J. Exp. Biol. 51, 5–22.

Alexander, J., Aaseth, J., 1981. Hepatobiliary transport and organ distribution of silver in the rat as influenced by selenite. Toxicology 21, 179–186. doi:10.1016/0300-483X(81)90154-2

Anderson, D.S., Patchin, E.S., Silva, R.M., Uyeminami, D.L., Sharmah, A., Guo, T., Das, G.K., Brown, J.M., Shannahan, J., Gordon, T., Chen, L.C., Pinkerton, K.E., Van Winkle, L.S., 2015. Influence of particle size on persistence and clearance of aerosolized silver nanoparticles in the rat lung. Toxicol. Sci. 144, 366–81. doi:10.1093/toxsci/kfv005

Armstead, A.L., Minarchick, V.C., Porter, D.W., Nurkiewicz, T.R., Biomaterials, B.L., 2015. Acute inflammatory responses of nanoparticles in an intra-tracheal instillation rat model. PLoS One 10.

Berben, L., Sereika, S.M., Engberg, S., 2012. Effect size estimation: Methods and examples. Int. J. Nurs. Stud. 49, 1039–1047. doi:10.1016/j.ijnurstu.2012.01.015

Braakhuis, H.M., Gosens, I., Krystek, P., Boere, J.A.F., Cassee, F.R., Fokkens, P.H.B., Post, J.A., van Loveren, H., Park, M.V.D.Z., 2014. Particle size dependent deposition and pulmonary inflammation after short-term inhalation of silver nanoparticles. Part. Fibre Toxicol. 11, 49. doi:10.1186/s12989-014-0049-1

Choi, H.S., Ashitate, Y., Lee, J.H., Kim, S.H., Matsui, A., Insin, N., Bawendi, M.G., Semmler-Behnke, M., Frangioni, J. V, Tsuda, A., 2010. Rapid translocation of nanoparticles from the lung airspaces to the body. Nat. Biotechnol. 28, 1300–1303. doi:10.1038/nbt.1696

Chuang, H.C., Hsiao, T.C., Wu, C.K., Chang, H.H., Lee, C.H., Chang, C.C., Cheng, T.J., 2013. Allergenicity and toxicology of inhaled silver nanoparticles in allergen-provocation mice models. Int. J. Nanomedicine 8, 4495–4506. doi:10.2147/IJN.S52239

Duarte, I.F., 2011. Following dynamic biological processes through NMR-based metabonomics: A new tool in nanomedicine? J. Control. Release 153, 34–39. doi:10.1016/j.jconrel.2011.03.008

Dziendzikowska, K., Gromadzka-Ostrowska, J., Lankoff, A., Oczkowski, M., Krawczyńska, A., Chwastowska, J., Sadowska-Bratek, M., Chajduk, E., Wojewódzka, M., Dušinská, M., Kruszewski, M., 2012. Time-dependent biodistribution and excretion of silver nanoparticles in male Wistar rats. J. Appl. Toxicol. 32, 920–928. doi:10.1002/jat.2758

Faqi, A.S., 2013. A comprehensive guide to toxicology in preclinical drug development, 1st edn. ed. Academic Press.

Fehaid, A., Hamed, M.F., Abouelmagd, M.M., Taniguchi, A., 2016. Time-dependent Toxic Effect and Distribution of Silver Nanoparticles Compared to Silver Nitrate after Intratracheal Instillation in Rats. Am. J. Nanomater. 4, 12–19. doi:10.12691/ajn-4-1-3

Gosens, I., Kermanizadeh, A., Jacobsen, N.R., Lenz, A.G., Bokkers, B., De Jong, W.H., Krystek, P., Tran, L., Stone, V., Wallin, H., Stoeger, T., Cassee, F.R., 2015. Comparative hazard identification by a single dose lung exposure of zinc oxide and silver nanomaterials in mice. PLoS One 10, 1–17. doi:10.1371/journal.pone.0126934

Gryshchuk, V., Galagan, N., 2016. Silica Nanoparticles Effects on Blood Coagulation Proteins and Platelets. Biochem. Res. Int. 2016, 2959414. doi:10.1155/2016/2959414

Haberl, N., Hirn, S., Wenk, A., Diendorf, J., Epple, M., Johnston, B.D., Krombach, F., Kreyling, W.G., Schleh, C., 2013. Cytotoxic and proinflammatory effects of PVP-coated silver nanoparticles after intratracheal instillation in rats. Beilstein J. Nanotechnol. 4, 933–940. doi:10.3762/bjnano.4.105

Hu, Y.-L., Gao, J.-Q., 2010. Potential neurotoxicity of nanoparticles. Int. J. Pharm. 394, 115–21. doi:10.1016/j.ijpharm.2010.04.026

Jarak, I., Carrola, J., Onio, A., Barros, S., Gil, A.M., De, M., Pereira, L., Corvo, M.L., Duarte, I.F., 2017. Metabolism Modulation in Different Organs by Silver Nanoparticles: An NMR Metabolomics Study of a Mouse Model 1–14. doi:10.1093/toxsci/kfx142

Ji, J.H., Jung, J.H., Kim, S.S., Yoon, J.-U., Park, J.D., Choi, B.S., Chung, Y.H., Kwon, I.H., Jeong, J., Han, B.S., Shin, J.H., Sung, J.H., Song, K.S., Yu, I.J., 2007. Twenty-Eight-Day Inhalation Toxicity Study of Silver Nanoparticles in Sprague-Dawley Rats. Inhal. Toxicol. 19, 857–871. doi:10.1080/08958370701432108

Ji, J.H., Yu, I.J., 2012. Estimation of human equivalent exposure from rat inhalation toxicity study of silver nanoparticles using multi-path particle dosimetry model. Toxicol. Res. (Camb). 1, 206. doi:10.1039/c2tx20029e

Kaewamatawong, T., Banlunara, W., Ekgasit, S., Maneewattanapinyo, P., 2009. Acute Pulmonary Toxicity Caused by Single Intratracheal Instillation of Colloidal Silver Nanoparticles in Mice. Thai J. Vet. Med. 39, 442.

Khanna, N.K., Madan, B.R., 1978. Studies on the anti-inflammatory activity of creatine. Arch. Int. Pharmacodyn. Ther. 231, 340–50.

Kwon, J.T., Minai-Tehrani, A., Hwang, S.K., Kim, J.E., Shin, J.Y., Yu, K.N., Chang, S.H., Kim, D.S., Kwon, Y.T., Choi, I.J., Cheong, Y.H., Kim, J.S., Cho, M.H., 2012. Acute pulmonary toxicity and body distribution of inhaled metallic silver nanoparticles. Toxicol. Res. 28, 25–31. doi:10.5487/TR.2012.28.1.025

Liu, Y., Guan, W., Ren, G., Yang, Z., 2012. The possible mechanism of silver nanoparticle impact on hippocampal synaptic plasticity and spatial cognition in rats. Toxicol. Lett. 209, 227–231. doi:10.1016/j.toxlet.2012.01.001

Lv, M., Huang, W., Chen, Z., Jiang, H., Chen, J., Tian, Y., Zhang, Z., Xu, F., 2015. Metabolomics techniques for nanotoxicity investigations. Bioanalysis 7, 1527–1544. doi:10.4155/bio.15.83

Owen, J.B., Butterfield, D.A., 2010. Measurement of Oxidized/Reduced Glutathione Ratio, in:

Methods in Molecular Biology (Clifton, N.J.). pp. 269–277. doi:10.1007/978-1-60761-756-3_18

Potter, V.R., Dubois, K.P., 1943. Studies on the mechanism of hydrogen transport in animal tissues: VI. Inhibitor studies with succinic dehydrogenase. J. Gen. Physiol. 26, 391–404.

Rahman, I., Kode, A., Biswas, S.K., 2007. Assay for quantitative determination of glutathione and glutathione disulfide levels using enzymatic recycling method. Nat. Protoc. 1, 3159–3165. doi:10.1038/nprot.2006.378

Roberts, J.R., McKinney, W., Kan, H., Krajnak, K., Frazer, D.G., Thomas, T. a, Waugh, S., Kenyon, A., MacCuspie, R.I., Hackley, V. a, Castranova, V., 2013. Pulmonary and cardiovascular responses of rats to inhalation of silver nanoparticles. J. Toxicol. Environ. Health. A 76, 651–68.

Seiffert, J., Hussain, F., Wiegman, C., Li, F., Bey, L., Baker, W., Porter, A., Ryan, M.P., Chang, Y., Gow, A., Zhang, J., Zhu, J., Tetley, T.D., Chung, K.F., 2015. Pulmonary toxicity of instilled silver nanoparticles: Influence of size, coating and rat strain. PLoS One 10, 1–17. doi:10.1371/journal.pone.0119726

Shrivastava, S., Bera, T., Singh, S.K., Singh, G., Ramachandrarao, P., Dash, D., 2009. Characterization of Antiplatelet Properties of Silver Nanoparticles. ACS Nano 3, 1357–1364. doi:10.1021/nn900277t

Stebounova, L. V, Adamcakova-Dodd, A., Kim, J.S., Park, H., O'Shaughnessy, P.T., Grassian, V.H., Thorne, P.S., 2011. Nanosilver induces minimal lung toxicity or inflammation in a subacute murine inhalation model. Part. Fibre Toxicol. 8, 5. doi:10.1186/1743-8977-8-5

Sung, J.H., Ji, J.H., Park, J.D., Yoon, J.U., Kim, D.S., Jeon, K.S., Song, M.Y., Jeong, J., Han, B.S., Han, J.H., Chung, Y.H., Chang, H.K., Lee, J.H., Cho, M.H., Kelman, B.J., Yu, I.J., 2009. Subchronic inhalation toxicity of silver nanoparticles. Toxicol. Sci. 108, 452–61. doi:10.1093/toxsci/kfn246

Trickler, W.J., Lantz, S.M., Murdock, R.C., Schrand, A.M., Robinson, B.L., Newport, G.D., Schlager, J.J., Oldenburg, S.J., Paule, M.G., Slikker, W., Hussain, S.M., Ali, S.F., 2010. Silver Nanoparticle Induced Blood-Brain Barrier Inflammation and Increased Permeability in Primary Rat Brain Microvessel Endothelial Cells. Toxicol. Sci. 118, 160–170. doi:10.1093/toxsci/kfq244

Wei, L., Lu, J., Xu, H., Patel, A., Chen, Z.-S., Chen, G., 2015. Silver nanoparticles: synthesis, properties, and therapeutic applications HHS Public Access. Drug Discov Today 20, 595–601. doi:10.1016/j.drudis.2014.11.014

Wei, X., Gao, J., Fang, R.H., Luk, B.T., Kroll, A. V, Dehaini, D., Zhou, J., Kim, H.W., Gao, W., Lu, W., Zhang, L., 2016. Nanoparticles camouflaged in platelet membrane coating as an antibody decoy for the treatment of immune thrombocytopenia. Biomaterials 111, 116–123.

Wiemann, M., Vennemann, A., Blaske, F., Sperling, M., Karst, U., 2017. Silver Nanoparticles

in the Lung: Toxic Effects and Focal Accumulation of Silver in Remote Organs. Nanomater. (Basel, Switzerland) 7. doi:10.3390/nano7120441

Wishart, D.S., Tzur, D., Knox, C., Eisner, R., Guo, A.C., Young, N., Cheng, D., Jewell, K.,

Arndt, D., Sawhney, S., Fung, C., Nikolai, L., Lewis, M., Coutouly, M.-A., Forsythe, I., Tang, P., Shrivastava, S., Jeroncic, K., Stothard, P., Amegbey, G., Block, D., Hau, D.D., Wagner, J., Miniaci, J., Clements, M., Gebremedhin, M., Guo, N., Zhang, Y., Duggan, G.E., MacInnis, G.D., Weljie, A.M., Dowlatabadi, R., Bamforth, F., Clive, D., Greiner, R., Li, L., Marrie, T., Sykes, B.D., Vogel, H.J., Querengesser, L., 2007. HMDB: the Human Metabolome Database. Nucleic Acids Res. 35, D521–D526. doi:10.1093/nar/gkl923

Xu, L., Shao, A., Zhao, Y., Wang, Z., Zhang, C., Sun, Y., Deng, J., Chou, L.L., 2015. Neurotoxicity of Silver Nanoparticles in Rat Brain After Intragastric Exposure. J. Nanosci. Nanotechnol. 15, 4215–23.

Xu, Y., Wang, L., Bai, R., Zhang, T., Chen, C., 2015. Silver nanoparticles impede phorbol myristate acetate-induced monocyte-macrophage differentiation and autophagy. Nanoscale 0, 1–3. doi:10.1039/x0xx00000x

Young, J.F., Larsen, L.B., Malmendal, A., Nielsen, N., Straadt, I.K., Oksbjerg, N., Bertram, H.C., 2010. Creatine-induced activation of antioxidative defence in myotube cultures revealed by explorative NMR-based metabonomics and proteomics. J. Int. Soc. Sports Nutr. 7, 9. doi:10.1186/1550-2783-7-9

Chapter VI: General Conclusions

The respiratory tract is considered the least protected and the main portal entry of accidentally inhaled AgNPs that can gain access to the alveoli and then translocated to other tissues. Additionally, the organisms can be exposed to AgNPs in an intentional way. AgNPs have been used to prevent the microbial colonization, decreasing the risk of infection, on implantable devices, tumor prostheses, bone cement and surgical instruments. The assessment of the bioactivity and toxicity of these AgNPs is highly complex as it is dependent on the combination of several properties. AgNPs exposure lead to a variety of responses (e.g., induction of apoptosis, oxidative damage and generation of reactive oxygen species (ROS)). Due to the possible high exposure to AgNPs, in the present work we aimed to study the cyto and genotoxicity of AgNPs, with a main focus on the different outcomes from the exposure to AgNPs with different sizes. Also, we aimed to address the contribution of Ag^+ (due to AgNP dissociation) on the toxicity of AgNPs. Therefore, in the first part of this work we investigated the effects of two small sized AgNPs on the toxicity towards a model of lung cells (A549 cell line) and bone cells (MG-63 cell line). These cells lines were exposed to AgNPs of 10 nm (AgNP10) and 20 nm (AgNP20) (up to 100 µg/mL), as well as Ag^+ ($AgNO_3$). Despite its widespread use and the existent data on the possible adverse health effects, it is difficult to build a consentual mechanism of toxicity of the AgNP towards cell lines, maybe because it is problematic to compare biological data from different studies with a great variety in NP sizes, coatings or shapes. It remains therefore unclear if AgNPs with smaller differences in size also differ in their toxicity levels and trigger different or similar pathways in the cell.

Taken the results together, we can conclude that the small difference in size from the NPs used in this work, were not enough to interfere in the uptake rate of AgNPs from both cell lines, but it was enough to induce size-dependent toxicity.

For short period exposures (up to 48h) Ag^+ (from $AgNO_3$) induced more toxicity than the corresponding dose of AgNPs. However, when assessing longer term exposures by the clonogenic assay, we demonstrated the inverse effect, i.e. the AgNPs turn out being more toxic, completely inhibiting colony formation. This result was obtained for both cells lines. Therefore, AgNPs toxicity cannot be attributed to the dissociated silver ion alone.

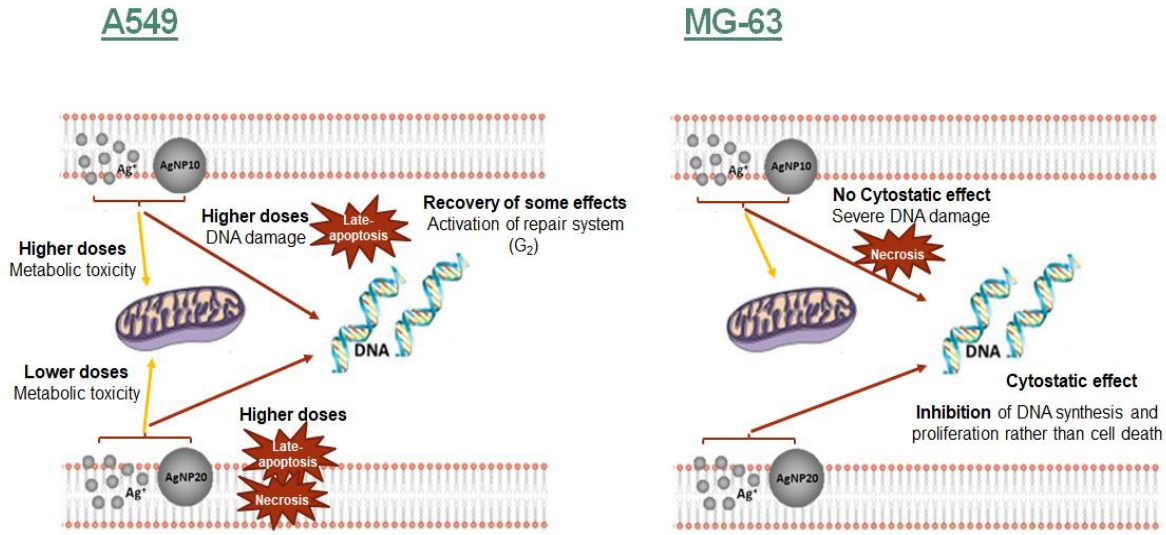

Figure 1 – Summary of the in vitro results obtained for the A549 and MG-63 cell line exposed to AgNP10 and AgNP20.

Regarding the *in vitro* exposure the summary of the results are presented in Fig.1. Exposure of A549 to AgNPs was size and dose dependent. More specifically, exposure to AgNP10 induced at higher doses metabolic toxicity, DNA damage, cell cycle arrest at G_2 and late-apoptosis. Some adverse effects were recovered for 48h, so we concluded that when A549 cells are exposed to the smaller sized AgNP (AgNP10) the repair process is easily activated, which explains the decrease of the sub-G_1 phase and increase on the number of cells at G_2 phase, from 24h to 48h exposure. These results support the hypothesis that AgNP10 exposed cells at the G_2/M checkpoint/transition may have an extra time to repair DNA damage prior segregation of chromosomes, as described by AshaRani et al. (2009). The exposure to AgNP20 was dose dependent, inducing metabolic toxicity at lower doses. While, at doses >50 µg/mL, AgNP20 induced arrest at S phase and increase in the % sub-G_1. After 48h more than 55% of the cell population was still arrested in S phase and an increase in late-apoptotic/necrotic cells were obtained. These clastogenic and apoptotic/necrotic data may indicate that DNA repair mechanisms are not the same as those proposed for AgNP10. Thus, a severe and irreparable damage or a failure of repair pathways could occur in the cells exposed AgNP20, when compared to AgNP10 exposed cells.

For MG-63 exposure, the results showed that AgNPs were toxic only at higher concentrations,

where AgNP10 induced a severe DNA damage, possibly irreparable, which ultimately lead to cell death by necrosis. The AgNP20 exposure, induced a high cytostatic effect with arrest of cell cycle at G_0/G_1, leading to a decrease of the subpopulation at S phase. The blockage of the AgNP20-exposed cells at G_0/G_1 imply an inhibition of DNA synthesis and a reduction on cell proliferation (Li et al., 2013a,b; Mao et al., 2004). These results are also in line with the observed decrease of MTT reduction to formazan in the AgNP20-exposed cells. This reaction is catalyzed by cellular oxidoreductases, therefore, dependent on the cellular metabolic activity. Therefore, the observed decrease may be explained by the decrease of cell division/proliferation together with a decrease of metabolic activity, rather than cell death observed in AgNP10-exposed cells. It is therefore evident that the cell line type was a determinant factor on the observed cyto and genotoxic effects induced by AgNPs.

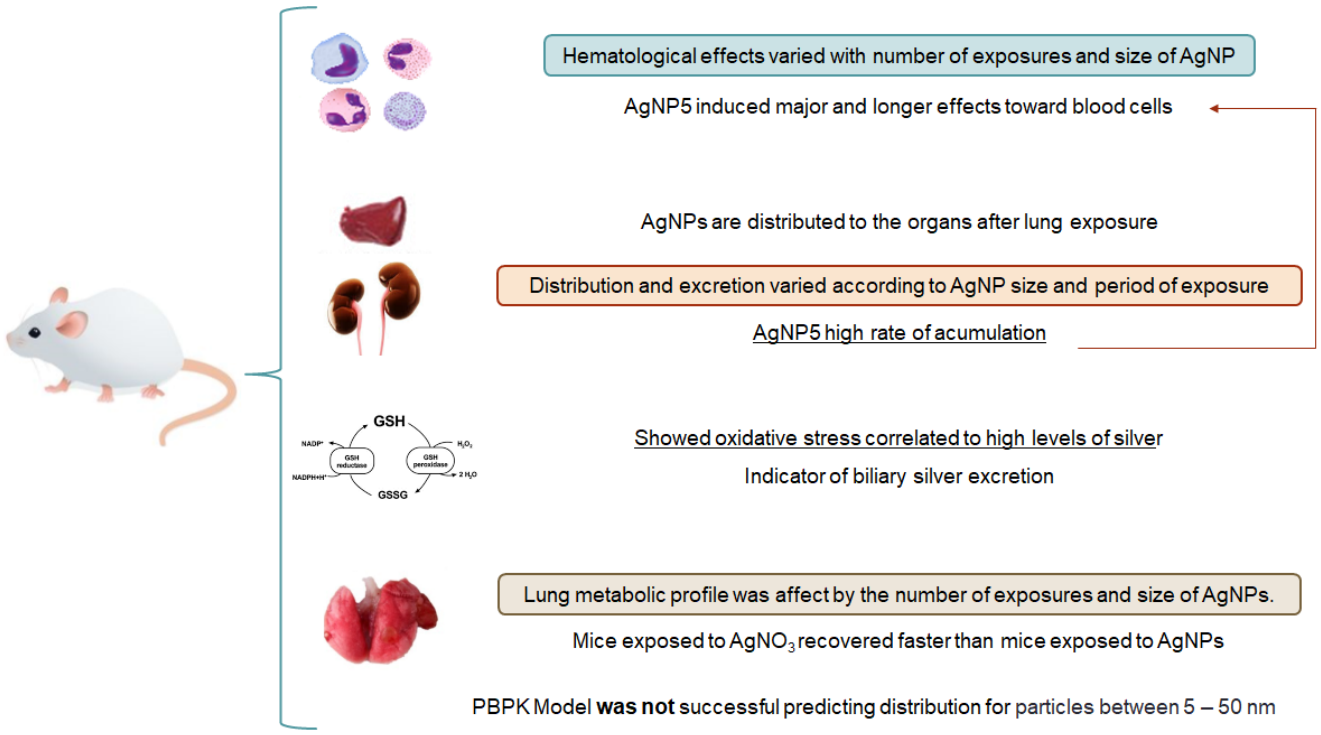

Figure 2 – Summary of the results obtained for *in vivo* exposures to AgNP5, AgNP50 and $AgNO_3$ by intratracheal instillation.

At the second part of this work, we assessed the toxicity, distribution and excretion of two

different sizes of AgNPs (5 and 50nm) and Ag^+ ($AgNO_3$) after: A) 1 or 2 intratracheal instillation (IT) (acute exposure), where mice were allowed to recover for 7 days, and B) after repeated ITs, once a week for 5 weeks (chronic exposure), where mice allowed to recover for 1, 2, 7, 14, 21 or 28 days after the last instillation (dpi). Overall Fig.2, describes the summary of the results obtained.

The hematology results showed that the effects of the instilled AgNPs were dependent on size and number of instillations. Both acute and chronic exposure to AgNP5 seem to induce major and longer effects towards blood cells and shared a similar inflammatory effect with $AgNO_3$, while AgNP50 seems to have higher influence on the innate immune system.

Regarding the distribution and excretion of silver thought the organs, it was proved that silver was distributed to all evaluated organs after lung exposure and the distribution/excretion kinetics was dependent on size and period of exposure. In general, the distribution the AgNP5 presented a high rate of accumulation, probably being the reason for the severe toxic effects obtained for mice treated with AgNP5. While mice treated with AgNP50 and $AgNO_3$ showed a faster and easier elimination of silver from the organism.

The organ's silver uptake was proposed to be proportional to the relative organ GSH concentration (Bachler and Hungerbühler, 2013). Our antioxidant data shows a correlation for both acute and chronic exposures of the oxidative stress and amount of silver obtained in the lung. Therefore, exposures to AgNP5 and $AgNO_3$ increased the GSH content in the lung and presented the higher concentration of silver in lung tissue. Additionally, GSH is known to play a major role in the excretion of silver, which happens via the biliary route as a silver-GSH complex. The analysis of GSH and GSSG levels in the liver, proved to be a great indicator of both, oxidative stress and biliary excretion of silver, where mice exposed to AgNP50 and $AgNO_3$ showed an increase in GSH in the liver along with a higher amount of silver excreted in the feces. Metabolomics showed to be a sensitive and high-throughput approach, capable of detecting alterations in cellular pathways at sub-toxic doses and to act as a complementary technique to the conventional battery of cytotoxicity assays that could link to different obtained data.

NMR profiling of lung tissues after acute exposure revealed a number of Ag-induced alterations in metabolites involved in different pathways, especially for the TCA cycle. Notably, most of

the metabolic changes observed after 1 IT were either absent or reversed in animals subjected to 2 IT, suggesting adaptation mechanisms to cope with the initial insult and recover homeostasis. Also, mice exposed to $AgNO_3$ seemed to recover faster than mice exposed to AgNPs. After 2 IT, mice exposed to AgNPs showed alterations in a different set of metabolites. In particular, glutamate and glycine increases may potentially be associated with the observed increases in GSH/GSSG as these amino acids are needed for *de novo* glutathione synthesis. Also, choline-derivatives changes could reflect membrane disruption or in association with silver toxicity or alterations in pulmonary surfactant composition and turnover. Some size-related metabolic changes were also observed, viz: a creatine increase for AgNP50 and ascorbate, which could possibly relate to its antioxidant role and uracil for AgNP5, suggesting disruption of pyrimidine homeostasis.

The comparison of static and isolated data is difficult between different studies, especially when different study designs were used (i.e., nanoparticle doses, animal models, administration routes, and time points). Physiologically based pharmacokinetic (PBPK) modelling could provide an insight into the relationships between an external dose and internal organ, blood or excretion dose (IPCS, 2010). In our data, modeling the ADME of AgNPs in 7 specific tissues of mice was not successful for predicting the distribution of silver nanoparticles with size from 5 – 50nm. In fact, from the 7 tissues modelled, only the heart and liver modelled concentrations were in line with the *in vivo* data. Decomposition of AgNP into both smaller sized nanoparticles and Ag^+ could also explain the lower concentration estimation of AgNPs in the various compartments. No clear relation between parameter values and corresponding particle diameters became apparent.

As future work, additional cytotoxic studies, including metabolomics and epigenetic assays, could be performed to better understand the mechanisms of AgNPs cell death and to make possible the clear discriminations against early or late apoptosis and late apoptosis and necrosis. Also, repair processes should be investigated to understand the cell resistance and fight system against AgNPs adverse effects. The uptake of NPs by the cells should also be investigated, since the pathway of uptake can lead to different effects and trigger different cell death responses and toxic mechanisms.

Regarding the *in vivo* assays, the lung inflammatory responses, by the BALF assay, could also be assessed providing information that could help to link the obtained inflammatory effects towards blood cells and some of the metabolic alteration observed in the lungs.

Additional time points in the exposure and recovery time (from 1 to 28 day) could be crucial to fully understand the distribution and excretion route of AgNPs, along with life time of these NPs in the organism. The analysis of the silver content in the bone marrow or also the alteration in the bone marrow metabolic profile, could give a number of significative information's, since bone marrow seem to be one of the sinks for silver distribution and also silver elimination. At last, the rebuilt of the PBPK with a different distribution algorithm, specific for the intratracheal instillation and specific for each AgNP size, could give a realistic distribution data, which would help to predict the AgNPs behavior and fate after lung exposure.